TOWARDS TERMINAL RARE EARTH IMIDO COMPLEXES

JACKSON PAUL KNOTT
Bachelor of Science, **University of Lethbridge, 2016**

A thesis submitted
in partial fulfilment of the requirements for the degree of

MASTER OF SCIENCE

in

CHEMISTRY

Department of Chemistry and Biochemistry
University of Lethbridge
LETHBRIDGE, ALBERTA, CANADA

Towards Terminal Rare Earth Imido Complexes

JACKSON PAUL KNOTT

Date of Defence: November 21, 2019

Dr. Paul G. Hayes Thesis Supervisor	Professor	Ph.D.
Dr. Stacey D. Wetmore Thesis Examination Committee Member	Professor	Ph.D.
Dr. Michael Gerken Thesis Examination Committee Member	Professor	Ph.D.
Dr. Laurel Schafer External Examiner University of British Columbia Vancouver, British Columbia	Professor	Ph.D.
Dr. Marc Roussel Chair, Thesis Examination Committee	Professor	Ph.D.

For Dad:

Mon Dénouement

Abstract

The development of rare earth complexes supported by a bisphosphinimine pyrrole-based pincer ligands is described herein. Synthesis of these species was conducted *via* alkane elimination and salt metathesis pathways. These complexes and their precursors were prepared and characterized by multi-dimensional (1-, pseudo-2-, and 2-dimensional), multi-nuclear (^{1}H, ^{2}H, ^{11}B, ^{13}C, ^{19}F, and ^{31}P) NMR spectroscopy, single-crystal X-ray diffraction analysis and elemental analysis.

Systematic modifications to the ancillary ligand and the resulting impact on complex reactivity is also presented with the ultimate goal of generating a species that bears a rare earth-nitrogen double bond. Specifically, electron withdrawing (Ph) and donating (^{i}Pr) groups were installed on the phosphinimine P atoms of the ligand and Pipp (4-^{i}PrC$_6$H$_4$) and Pm (4,6-dimethylpyrimidine) were utilized on the phosphinimine nitrogen atoms. Each iteration of the ancillary ligand led to distinct and unique reactivities upon complexation to a rare earth metal.

Acknowledgements

To my father, Paul: In the unfortunately short time you had, you bestowed me with the values which made this thesis possible. Determination, will, curiosity, confidence, and respect are all key virtues that helped carry me to this point. Your hard work and sacrifices paved me a bright future for which I will always be grateful. For setting a shining example of the man I have the potential to become I'd like to extend a special thank you.

To my mother, Samantha: I can't possibly begin to list everything you've done for me that has led me to this point. Since October 17th, 1992 you have graced me with love and a welcoming, understanding home. You dedicated a large portion of your time and energy to sculpt me a life in which I can reach my full potential. I hope you flip through these pages knowing that the stability, warmth, love, and kindness you unconditionally gave me each and every day is the main reason they exist in the first place. Thanks, mom.

To my brother, Liam: Thoughts of playing Dark Souls and building Lego in the basement with you over Christmas break are some of my fondest memories of my entire university experience. Knowing those nights were coming carried me through finals season each December. I hope, in some way, I've taught you to follow your passions and curiosities. Thanks for all the fun times.

To Phillip Liddell, Captain of the USS Enterprise NCC 1701-A: The wisdom and compassion you exude has not gone unheeded. Your unwavering support to my operations as Science Commander has unequivocally been the key to my success within the Star Fleet Academy. May your reign as Captain continue to be marked by peace and opulence. I look forward to celebrating with Romulan ale; Live long and prosper.

To my Nana: You are undoubtedly the zaniest person I have ever met. Every time I visit you I am reminded that sometimes all you need to get by is a little bit of whimsy. After each story I tell about you the list of people aching to meet you grows longer. For your laughter, love, support, and fearless use of emojis, I thank you.

To my supervisor, Paul Hayes: Allowing me to start doing research in your lab opened up an entire world of possibilities I never would have imagined for myself. Without your mentorship would not have become the scientist I am today. For guiding me along the way, opening countless doors for me, and for letting me be a part of your research group, I sincerely thank you.

To my friends: Nathan Kostiuk, Rhys Hakstol, Daniel Stuart, David McWatters, Dylan Webb, Danielle Howard, Edward Hsiang, Amanda Sequeira, Jesse Boutin, Angela Boutin, Damon Irwin, Saif Zahir, and Kathleen Ward, you all witnessed my highest highs and lowest lows over the past 10 years. Thank you all for the fun and letting me be a part of your lives.

I would like to thank my coworkers throughout my time in the Hayes Lab, Dylan, Ed, Ash, Daisy, Tara, Chris, Hudson, Kayla, Karen, Sam, Bryan, Connor, Mikko, and Breanne for the continuing discussions and assistance you provided me throughout my degree. An extra thank you goes out to Kevin R.D. Johnson, for sparking my interest in rare earth chemistry and to Matt Zamora, for being a great, patient friend. I would also like to thank my committee members Dr. Michael Gerken and Dr. Stacey D. Wetmore, as well as my external examiner Dr. Laurel Schafer.

Table of Contents

List of Tables

List of Figures

List of Schemes

List of New Compounds

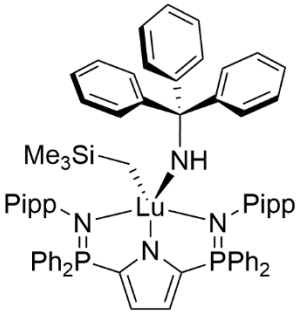

37

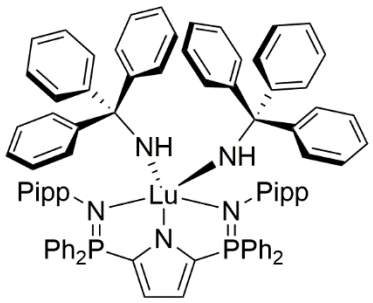

44

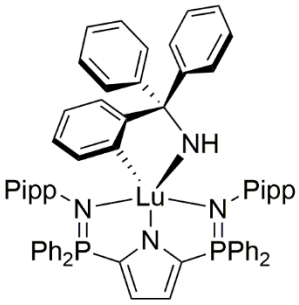

45

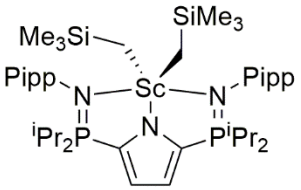

39a

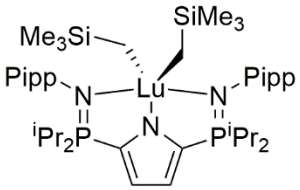

39b

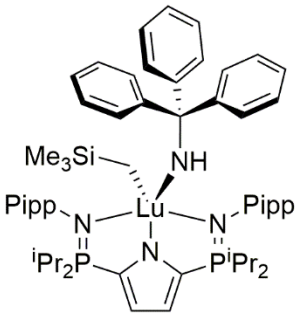

40c

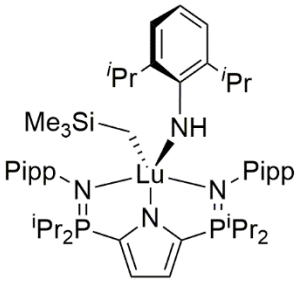

40d

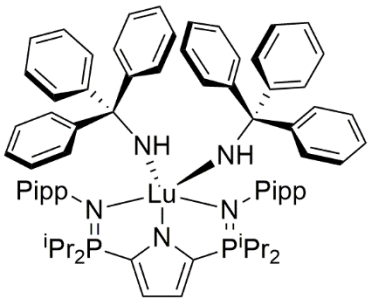

48c

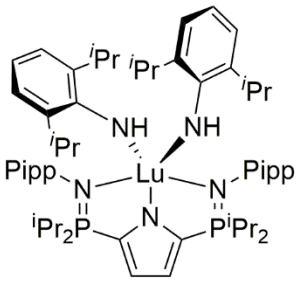

48d

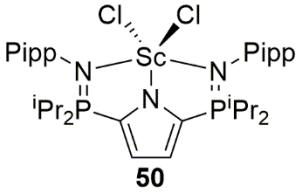

50

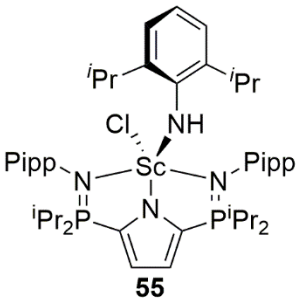

55

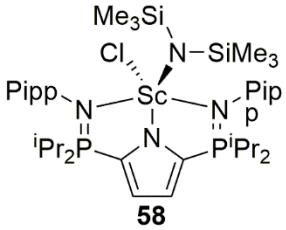

58

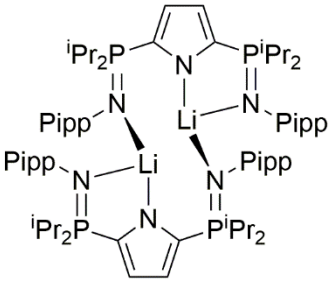

[LiL^{iPr}]$_2$

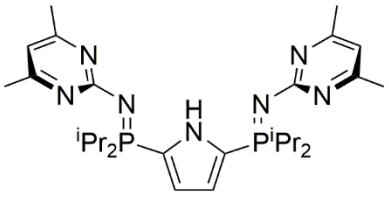

HL^{Pm}

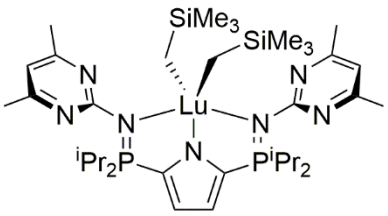

63

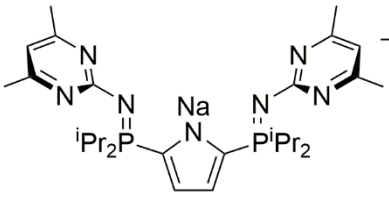

NaL^{Pm}

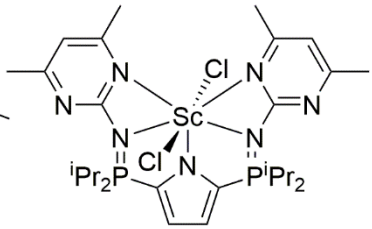

66

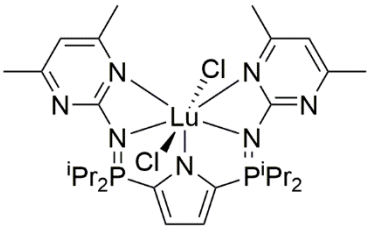

67

List of Symbols and Abbreviations

a, b, c, α, β, γ	crystallographic unit cell parameters
Ad	adamantyl
Anal. Calcd.	analysis calculated
APT	attached proton test
Ar	aryl
au	atomic units
BCF	$B(C_6F_5)_3$
br	broad
C	Celsius
Cat	catalyst
COD	1,5-cyclooctadiene
COSY	correlated spectroscopy
Cp	η^5-cyclopentadienyl (C_5H_5)
Cp*	η^5-pentamethylcyclopentadienyl (C_5Me_5)
Cy	cyclohexyl
d	doublet
dd	doublet of doublet
DAMS	dianionic atom, multiply- or singerly-bound
DEPT	distortionless enhancement by polarization transfer
DFT	density functional theory
Dipp	2,6-diisopropylphenyl
DMAP	4-dimethylaminopyridine
DOSY	diffusion oriented spectroscopy
F_c	calculated structure factor
F_o	observed structure factor
FW	formula weight
G	Gibbs free energy
g	gram(s)
GoF	goodness of fit
H	enthalpy
h	hour(s)
HMBC	heteronuclear multiple bond coupling
HOMO	highest occupied molecular orbital
HOMO –1	second highest occupied molecular orbital
HSAB	hard-soft acid-base
HSQC	heteronuclear single quantum coherence
Hz	Hertz
^{i}Pr	isopropyl
J	Joule(s)
k	reaction rate constant
K	Kelvin
kcal	kilocalorie(s)
KIE	kinetic isotope effect

L	ligand
LUMO	lowest unoccupied molecular orbital
m-	meta
M	metal
Me	methyl
Mes	mesityl
Mes*	2,4,6-^{t}BuC$_6$H$_2$
mg	milligram(s)
MHz	megahertz
min	minute(s)
mL	millilitre(s)
^{n}Bu	^{n}butyl
$^{n}J_{A–B}$	coupling constant between nuclei A and B, separated by n bonds
Nacnac	β-dikiteminato
NMR	nuclear magnetic resonance
o-	ortho
^{o}	degrees
ov	overlapping
p-	para
PES	potential energy scan
Ph	phenyl
Pipp	4-isopropylphenyl
Pm	pyrimidine
ppm	parts per million
Py	pyridine
R_1	conventional agreement index
R^2	coefficient of determination for a linear regression
RCP	ring-closing metathesis
RE	rare earth (group III or lanthanide element)
ROMP	ring-opening metathesis polymerization
ROP	ring-opening polymerization
S	entropy
s	second(s) or singlet
sp	septet
t	time or triplet
TACN	(MeNCH$_2$CH$_2$)$_3$
^{t}Bu	tertiary butyl
THF	tetrahydrofuran
wR_2	weighted agreement index
Z	number of formula units per unit cell
{^{1}H}	proton decoupled
{^{31}P}	phosphorus decoupled
9-BBN	9-borabicyclo[3.3.1]nonane
%	percent
Å	angstrom

β	beta
Δ	change in/heat
δ	chemical (ppm)
$\Delta H^{\ddagger}$	enthalpy of activation
$\Delta S^{\ddagger}$	entropy of activation
η^n	hapticity of order n
κ^n	denticity of order n
μ^n	bridging of order n
π	pi
τ^5	five-coordinate geometry index

Chapter 1 – Introduction and Relevant Literature

1.1 Overview of Organometallic Rare Earth Chemistry

1.1.1 Historical Context

The field of organometallic rare earth* (RE) chemistry has experienced slower progression than other areas of organometallic chemistry due to the strong Lewis acidity and extreme hydrophilicity of these metals requiring specialty glassware and experimental apparati such as high vacuum manifolds and Schlenk flasks.[1-2] The first rare earth compounds were synthesized by Birmingham and Wilkinson in 1954 and featured three cyclopentadienyl (Cp) ligands (Scheme 1.1).[3]

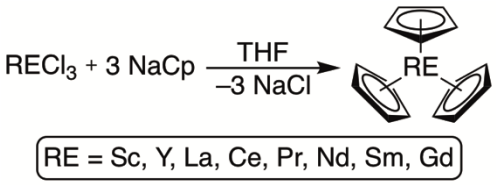

Scheme 1.1 Cp_3RE Complexes Synthesized by Birmingham and Wilkinson.

These seminal complexes revealed the metals' tendency to attain the +3 oxidation state.†[4-9] Accordingly, the two-electron transformations commonplace in transition metal chemistry, such as oxidative addition and reductive elimination, are not readily available.

---

* For the context of this thesis the term 'rare earth' encompasses group III and lanthanide elements.

† Other oxidation states including Ce^{4+}, La^{2+}, Nd^{2+}, Sm^{2+}, Eu^{2+}, Dy^{2+}, Yb^{2+}, Tm^{2+}, Sc^{2+}, and Sc^{1+} have been reported in the literature.

Additionally, exploration of rare earth chemistry elucidated the effects brought upon by the presence of 4*f*-orbitals; some of these realizations are as follows:[1, 10]

1) Despite being commonly occupied, the small size of the 4*f*-orbitals largely prevents them from participating in covalent bonding. Thus, bonding involving the lanthanide metals is predominantly ionic.
2) The electrons in the 4*f*-orbitals are poorly shielded, leading to the observed lanthanide contraction effect.‡
3) Reactivity can be strongly influenced by steric conformation.
4) Paramagnetism often hinders the use of NMR spectroscopy as a standard characterization technique.

1.1.2 Typical Reaction Pathways and Common Hindrances

Two main reaction pathways have emerged for the attachment of ligands to rare earth metals. One of these methods is protonolysis (top, Scheme 1.2), in which a metal–alkyl, –amide, or –alkoxide complex undergoes a σ-bond metathesis reaction with a protio ligand resulting in the loss of the respective alkane, amine, or alcohol.[11-12] Another ligand attachment strategy is salt metathesis (bottom, Scheme 1.2), in which a metal halide species is reacted with a salt, typically of an alkali metal, of the desired ligand.

---

‡ Lanthanide contraction describes the inverse relationship lanthanides experience between their atomic radius and atomic number arising from the poor shielding of 4*f* electrons.

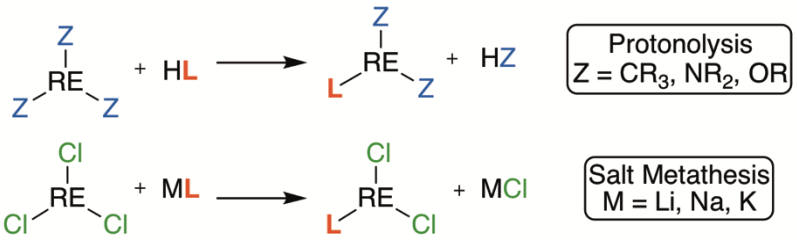

Scheme 1.2 Common Ligand Attachment Methodologies for Organometallic Rare Earth Complexes.

Salt metathesis strategies allow for a plethora of ligands which can be installed at the metal centre, as any alkali metal compound may be implemented. Additionally, the insolubility of the resulting alkali halide salts in most organic solvents allows for ease of purification *via* filtration. Conversely, protonolysis is limited by the availability of well-behaved metal starting materials. Typically, large substituents (*e.g.* CH_2SiMe_3, CH_2Ph, $N(SiMe_3)_2$) are required for steric protection to form thermally stable metal compounds.[§13]

While salt metathesis and protonolysis pathways have proven to be effective for rare earth metals, they are not without common hindrances. The alkali halide salt released in salt metathesis reactions can be retained by the metal centre, resulting in what is commonly referred to as an 'ate' complex (top, Scheme 1.3). Additionally, compounds bearing alkyl, amide, or alkoxide functionalities commonly exhibit intramolecular C–H

[§] A recent report by Anwander has shown that trimethyl scandium ($Sc(CH_3)_3(Me_3TACN)$, $Me_3TACN = (MeNCH_2CH_2)_3$) can be isolated. However, the complexity of the synthesis renders this report as a proof of concept (i.e. homoleptic rare earth trialkyl species with small alkyl ligands can be isolated).

bond activation of the ancillary ligand (bottom, Scheme 1.3). This process, commonly referred to as cyclometalation, often inhibits subsequent reactivity.[14]

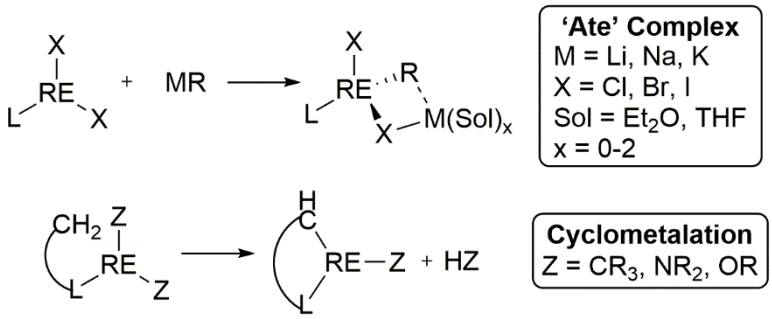

Scheme 1.3 Formation of 'ate' Complexes (top) and Ligand Cyclometalation (bottom).

1.2 Cp* Ligand – Development of Organometallic Rare Earth Chemistry

1.2.1 Overview

Use of the Cp* (Cp* = $C_5(CH_3)_5^-$) ligand in organometallic rare earth chemistry provided a myriad of reactivity and prompted further interest into this field.[15] Formation of stable rare earth complexes provided a platform in which their reactivity could be explored. This section of the thesis aims to provide the reader with a brief background of the use of the Cp* ligand to support samarium complexes, and the subsequent reaction chemistry of those species with small molecules. These examples are discussed as they provide a terse historical context for the types of typical reactions rare earth metals undergo with small molecules.

1.2.2 Cp* Ligand

Isolation of Cp^*_3Sm (**1**, Scheme 1.4) by Evans in 1991 provided an early example of a thermally stable organometallic rare earth complex capable of small molecule

activation.[16] The large steric pressure provided by the three Cp* ligands is evident in the η^1- η^5 equilibrium complex **1** exhibits with Cp^*_2Sm-η^1-$C_5(CH_3)_5$ (**1a**, Scheme 1.4).

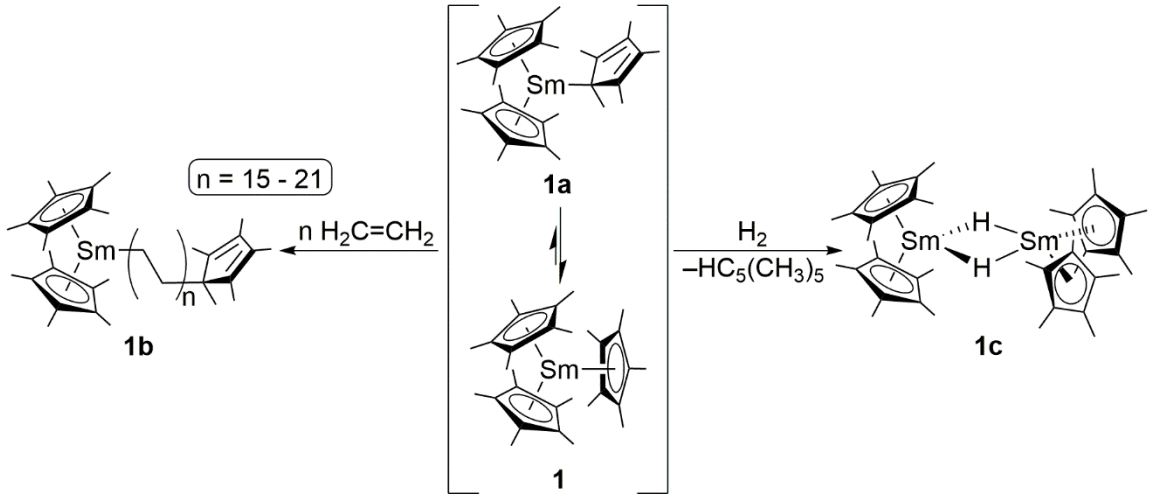

Scheme 1.4 Reactivity of Complex **1**/**1a** With H_2 and $H_2C{=}CH_2$.

Upon exposure of complex **1** to ethylene ($H_2C{=}CH_2$), insertion into the Sm–Cp* bond was observed yielding $Cp^*_2Sm(H_2CCH_2)_nC_5(CH_3)_5$ (**1b**, n = 15 - 21, Scheme 1.4). When excess ethylene was used polyethylene was produced.[16] Addition of H_2 gas to Cp^*_3Sm yielded the dimeric complex $(Cp^*_2SmH)_2$ (**1c**, Scheme 1.4).[17] Previously, the Cp* ligands in homoleptic Cp* complexes fulfilled a solely ancillary role and were not involved in reactivity.[15] However, the equilibrium compound **1** possesses with complex **1a** let the Cp* ligand behave similarly to an alkyl substituent, allowing for its involvement in reaction chemistry.

Addition of 1 atm of carbon monoxide (CO) at 1 atm to compound **1** yielded Cp^*_2Sm-κ^2-$((CO)_2C_5(CH_3)_5)$ (**1d**, Scheme 1.5) which possessed a unique cationic bicyclic

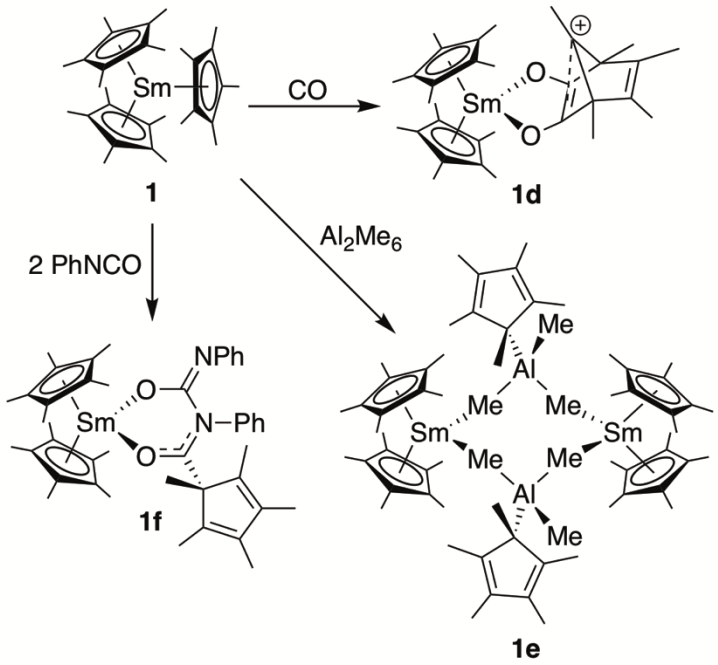

Scheme 1.5 Reactivity of Complex **1** With CO, Al_2Me_6, and PhN=C=O.

ligand.[18] The insertion of CO into the Cp* ligand had not been previously reported in the literature. Like CO, Al_2Me_6 also inserted into the Sm–Cp* bond of compound **1,** giving rise to $(C_5(CH_3)_5)_2Sm[(\mu^2\text{-}CH_3)_2Al(C_5(CH_3)_5)CH_3]_2\text{-}Sm(Cp^*)_2$ (**1e**, Scheme 1.5).[19-20] Reaction of complex **1** with 2 equivalents of PhN=C=O yielded $Cp^*_2Sm\text{-}\kappa^2\text{-}(OC(C_5(CH_3)_5)N(Ph)C(NPh)O)$ (**1f**) wherein the first equivalent of PhN=C=O inserted into the Sm–Cp* bond and the second equivalent established a 6-membered metallacycle (Scheme 1.5).

Addition of $B(C_6F_5)_3$ to compound **1** resulted in the complete loss of a Cp* ligand, in the form of tetramethylfulvene, and formation of $(C_5(CH_3)_5)_2Sm\text{-}\kappa^3\text{-}(HB(C_6F_5)_3)$ (**1g**, Scheme 1.6). This reaction, which can be described as a Lewis acid induced ß-hydride elimination, represented the first instance in which a Cp* ligand did not play an ancillary

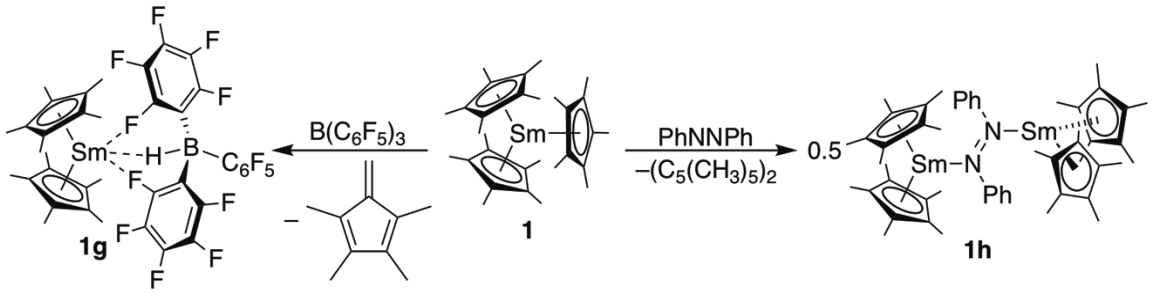

Scheme 1.6 Reactivity of Complex **1** With BCF and PhN=NPh.

role upon addition of BCF.[19] The hydride eliminated in this reaction bridges between the boron and samarium atoms. Further electron density is provided to the metal centre *via* two of the fluorine atoms which interact with samarium in both the solution and solid states. Complex **1** was also demonstrated to be capable of undergoing reduction chemistry. Addition of PhN=NPh induced a formal reduction of the samarium centre, forming the dimeric compound $(Cp^*)_2Sm(PhN{=}NPh)Sm(Cp^*)_2$ (**1h**, Scheme 1.6).[21-22]

Using the Cp* ligand in organometallic rare earth chemistry showcased intriguing transformations with small organic molecules that differed from the traditional Cp* chemistry of transition metals.[15] The development of well-defined reactions in the 1990s spurred a great deal of interest into the emerging field of synthetic rare earth chemistry. However, the relative lack of straight forward modularity of Cp* ligands, the extensive academic and industrial work done, and the large number of broad patents protecting them, led to development of new ligand systems, particularly pincer ligands, for use with these highly reactive elements.

1.3 Rare Earth Complexes Supported by Pincer Ligands

1.3.1 Overview

This section will briefly highlight pincer ligands based upon the following definition: a ligand that binds to a metal *via* three donor atoms in a meridional fashion; upon bonding to the metal five membered (or greater) chelate rings are formed (Figure 1.1).[23] These ligand frameworks boast an extensively modular design, as the donor atoms and the linking main group elements can all be easily varied. The goal of this section is to familiarize the reader with a representative sample of pincer ligands to support rare earth elements as well as the reactivity of the ensuing complexes. For a more complete review the reader is encouraged to read the book chapter in *Topics in Organometallic Chemistry*: Rare Earth Pincer Complexes: Synthesis, Reaction Chemistry and Catalysis.[23]

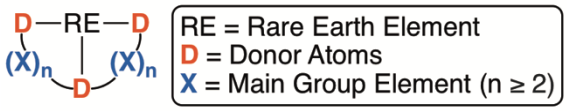

Figure 1.1 Generic Definition of a Pincer Ligand.

1.3.2 Examples of Pincer Ligands Supporting Rare Earth Complexes

An early example of a pincer ligand binding a rare earth metal was reported by Fryzuk and coworkers in 1988.[24] The chosen ligand, L^{Fryzuk} (L^{Fryzuk} = $[Me_2PCH_2SiMe_2]_2N^-$) features an anionic nitrogen donor as well as two neutral phosphines. Interestingly, no neutral phosphine ligands coordinated to a rare earth metal had been previously reported, presumably because these metals are extremely Lewis acidic and HSAB theory predicts that hard ligands (*e.g.* $^-CR_3$, $^-NR_2$, ^-OR) are preferred over soft ligands (*e.g.* PR_3). However, using pincer ligands made it possible for both hard and soft

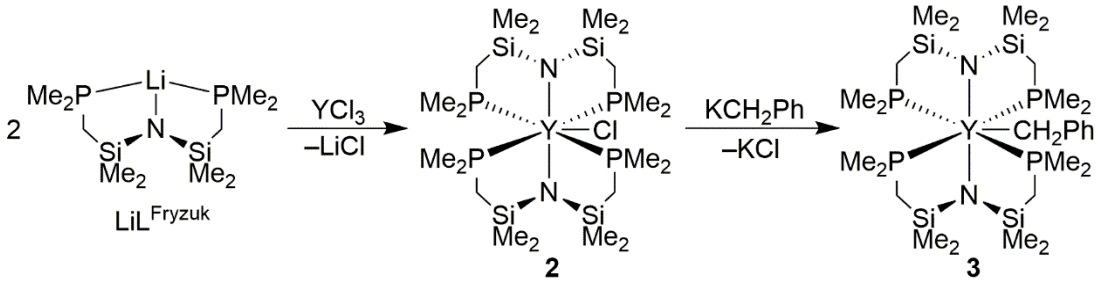

Scheme 1.7 Early Example of a Pincer Ligand Stabilizing a Rare Earth Metal.

donors to interact with the same electrophilic metal centre. Treatment of two equivalents of LiL^{Fryzuk} with anhydrous YCl_3 yielded the seven coordinate, pentagonal bipyramidal complex $L^{Fryzuk}YCl$ (**2**, Scheme 1.7). Upon reaction with benzyl potassium $L^{Fryzuk}Y(CH_2Ph)$ (**3**, Scheme 1.7) was generated with concomitant loss of KCl.

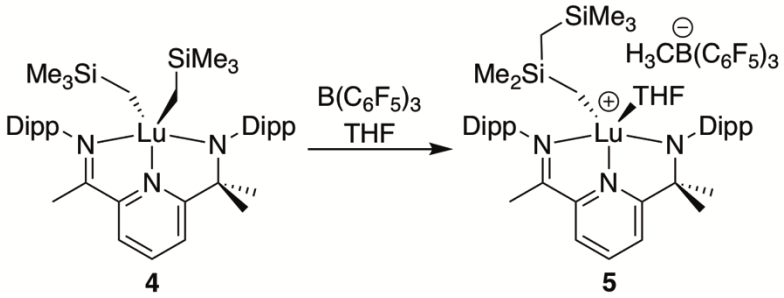

Scheme 1.8 Synthesis of Complex **5**.

Gordon and coworkers isolated $L^{Gordon}Lu(CH_2SiMe_3)_2$, L^{Gordon} = [2-(DippN=CMe)-6-(DippNCMe$_2$)]C_6H_3N, (**4**, Scheme 1.8).[25] This complex differed from Fryzuk's example in that the pyridine moiety provided a more rigid ligand scaffold, and that it is an *NNN*-pincer ligand (L^{Fryzuk} = *PNP*-pincer ligand). Addition of $B(C_6F_5)_3$ to complex **4** resulted in alkide abstraction of a Si–CH_3 group with subsequent rearrangement to

[$L^{Gordon}Lu(CH_2SiMe_2CH_2SiMe_3)(THF)][H_3CB(C_6F_5)_3]$ (**5**, Scheme 1.8). Compound **5** represents the first isolated example of a non-Cp supported cationic lanthanide complex.[25]

In a similar vein, Diaconesu isolated $L^{Diaconseu}Lu(CH_2\text{-}3,5\text{-}Me_2C_6H_3)(THF)$ and $L^{Diaconseu}Y(CH_2Ph)(THF)$, $L^{Diaconseu}$ = 2,6-[$DippNCH_2$]C_6H_3N (**6** and **7** respectively, Scheme 1.9) in 2010.[26] Like complex **4**, both of these complexes also featured a ligand with a pyridine backbone, but, unlike complex **4**, this ligand system has two symmetrical amide donors. As the ligand is dianionic, one valence remains for an alkyl group (CH_2Ph (**6**), $CH_2\text{-}3,5\text{-}Me_2C_6H_3$ (**7**)). In addition, one coordination site is available for an external Lewis base (THF) to coordinate to the metal centre. Depending on the metal, varying degrees of acridine ($C_{13}H_9N$) activation was achieved (Scheme 1.9). When compound **6** (RE =Y) and acridine were reacted with one another, alkyl migration of the CH_2Ph group and concomitant dearomatization of acridine occurred, yielding $L^{Diaconseu}Y(\text{-}6\text{-}CH_2PhNC_{13}H_{10})THF$ (**6a**, Scheme 1.9). Conversely, when the analogous reaction was carried out with the lutetium analogue, complex **7**, direct C–H bond activation of the acridine ligand and concomitant loss of mesitylene ($1,3,5\text{-}(CH_3)_3C_6H_3$) afforded $L^{Diaconseu}Lu\text{-}\kappa^2\text{-}(NC_{13}H_8)THF$ (**7a**, Scheme 1.9).

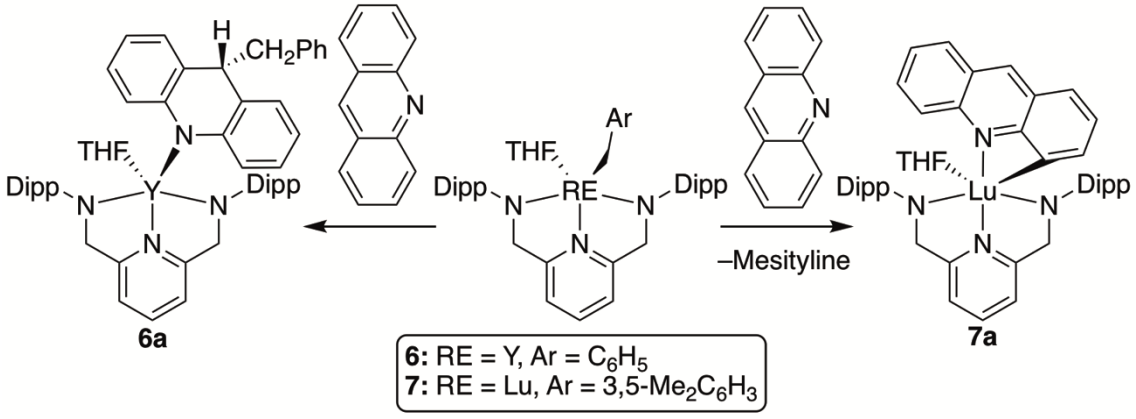

Scheme 1.9 Varying Acridine Activation of Rare Earth Metal Complexes.

Compounds **6** and **7** were shown to be capable of undergoing C–C coupling reactions upon addition of 3 equivalents of 1-methylimidazole at 70 ºC (Scheme 1.10). The reactivity of $L^{Diaconseu}Y(CH_2Ph)(THF)$ and $L^{Diaconseu}Lu(CH_2\text{-}3,5\text{-}Me_2C_6H_3)(THF)$ provided an example of unique C–C coupling, C–H bond activation, and dearomatization reactions while highlighting common and differing reaction pathways seen in rare earth metals.[26]

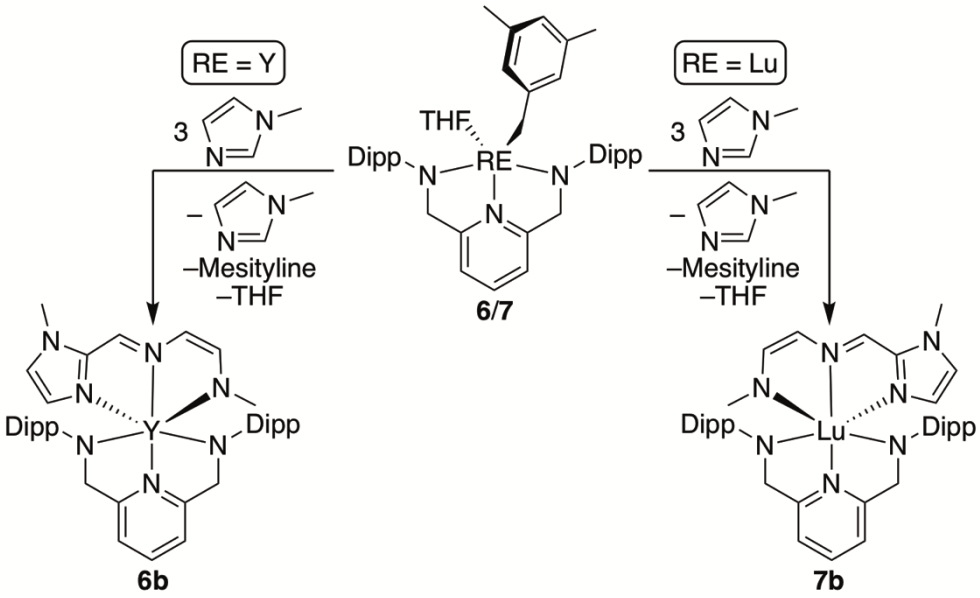

Scheme 1.10 C–C Coupling Reaction of 1-Methylimidizole.

In 2010 Chen reported numerous rare earth complexes supported by the β-diketiminato (Nacnac) derived pincer ligand HL^{Chen1} (HL^{Chen1} = (*o*-$C_5H_4N)CH_2NC(CH_3)CH_2C(CH_3)$NDipp), Scheme 1.11).[27] The thermally stable rare earth complex $L^{Chen1}Sc(CH_2SiMe_3)_2$ (**8**, Scheme 1.11) was synthesized by reacting HL^{Chen1} with a stoichiometric amount of $Sc(CH_2SiMe_3)_3THF_2$ at ambient temperature. Larger metals were shown to be supported by L^{Chen1} as addition of $La(N(SiMe_3)_2)_3$ to HL^{Chen1} yielded

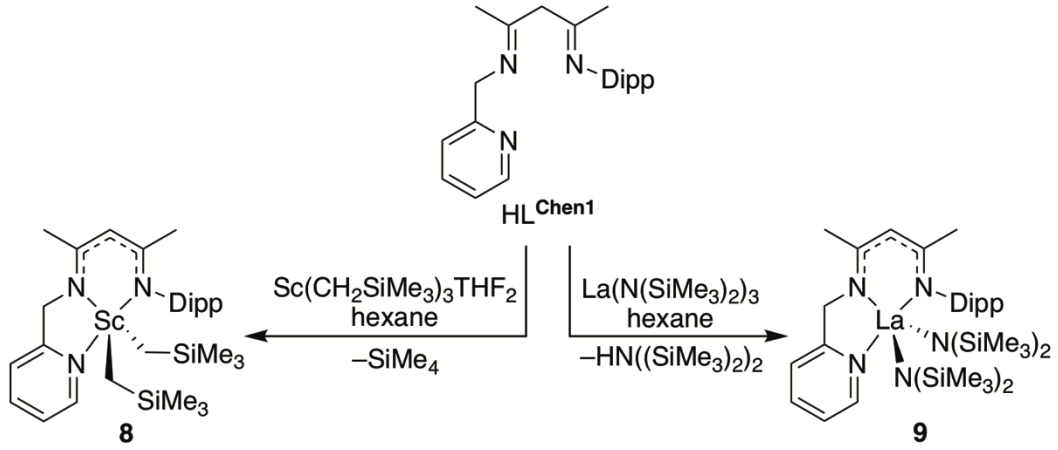

Scheme 1.11 Rare Earth Pincer Complexes Synthesized by Chen.

$L^{Chen1}La(N(SiMe_3)_2)_2$ (**9**, Figure 1.11). Unfortunately, no further reactivity for these complexes has yet been reported. Nacnac-derived pincer ligands have been shown to support a large number of rare earth metals, demonstrating pincer ligands' far reaching capabilities of supporting group 3 and lanthanide metals.[28]

1.4 Overview of Rare Earth Imido Complexes

1.4.1 Language Clarification

Sections 1.4.2 and 1.4.3 of this thesis discuss a variety of uncommon ligands. In order to provide the reader with clear and concise language, the term 'DAMS ligand' must be defined. A DAMS ligand is one which possesses a dianionic C, N, or P atom which is κ^1, μ^2, or μ^3 bound to one or more metal centres. The dianionic atom may be a part of a larger ligand system. A representative sample of the DAMS ligands discussed in this thesis are provided in Figure 1.2 and highlighted in blue.

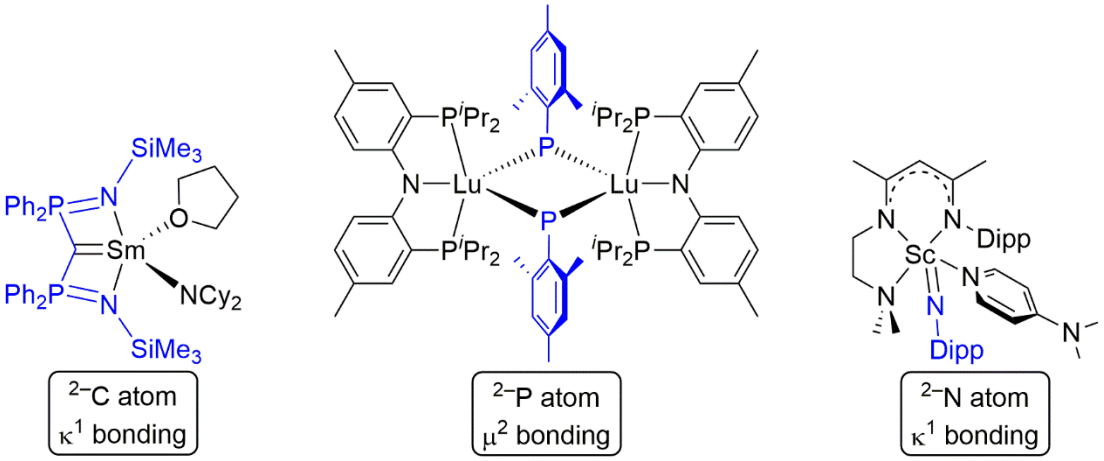

Figure 1.2 DAMS Ligands.

1.4.2 General Overview of Multiply Bound Ligands

Research into DAMS ligands bound to late transition metals led to the development of catalysts capable of mediating olefin metathesis, the impact of which led to the 2005 Nobel Prize being awarded to Richard Schrock, Robert Grubbs, and Yves Chauvin.[29-31]

These catalysts featured nitrogen (ArN^{2-}) and carbon based (R_2C^{2-}) DAMS ligands (*e.g.* Schrock Cat and Grubbs Cat, Figure 1.3). Schrock Cat and Grubbs Cat exhibited a myriad of noteworthy reactivity, including ring-closing metathesis (RCP, left, Figure 1.3) and ring-opening polymerization (ROP) and provided a convenient methodology for the formation of cyclic compounds. Furthermore, the creation of large (>10 atoms) rings is an application which is of particular interest to the pharmaceutical industry. For instance, Boehringer Ingelheim reported using a ruthenium based catalyst for the synthesis of a 15 member ring in a compound utilized in Hepatitis C treatment.[32-33] Grubbs Cat was also shown to be capable of ring-opening metathesis polymerization (ROMP) of unsaturated, cyclic monomers (right, Figure 1.3). This process allows for the synthesis of a variety of olefin-based products (e.g. polymerization of dicyclopentadiene, right, Figure 1.2).[34-35]

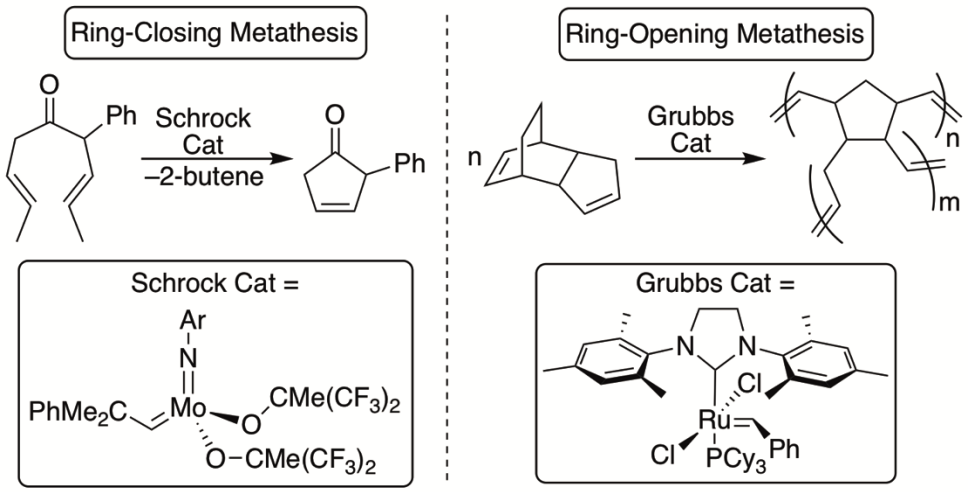

Figure 1.3 Reactivity of Transition Metals Bearing Multiply Bound Ligands.

With the large success that DAMS ligands have experienced with transition metals, efforts to synthesize analogous rare earth complexes were undertaken. However, the extreme Lewis acidity and HOMO/LUMO (HOMO = highest occupied molecular orbital, LUMO = lowest unoccupied molecular orbital) energy mismatch between the rare earth metal and the DAMS ligand makes this goal challenging.[36]

1.4.3 Non-Nitrogenous and μ^2 or μ^3 Bound Nitrogenous DAMS Ligands

The first instance of a DAMS ligand being bound to a rare earth metal was reported by Schumann and coworkers in 1991 whereupon an ytterbium napthalide complex $Yb(C_{10}H_8)(THF)$ was exposed to azobenzene (PhN=NPh).[37] The resulting complex, $Yb_4(\mu_2\text{-}\eta^2\text{:}\eta^2\text{-}Ph_2N_2)_4(\mu_3\text{-}PhN)_2(THF)_4$ (top left, **10**, Figure 1.4) was characterized by X-ray diffraction analysis and displayed 2 PhN^{2-} ligands each bound in a μ^3 fashion.

The first example of a DAMS ligand bound μ^1 to a rare earth metal came from Cavell in 2000.[38] Two methylene C–H bond activations occurred when H_2L^{Cavell} (H_2L^{Cavell} = $[Me_3SiN{=}PPh_2]_2CH_2$) was reacted with $Sm(NCy_2)_3$, releasing two equivalents of

dicyclohexamine ($HNCy_2$) and forming complex **11**, $L^{Cavell}Sm(NCy)(THF)$ which featured a Sm=C double bond (top right, Figure 1.4).

Deviating from the second period elements, Masuda and Kiplinger utilized the *PNP* pincer ligand $L^{Kiplinger}$ ($L^{Kiplinger}$ = $[2\text{-}P^{i}Pr_2\text{-}4\text{-}CH_3C_6H_3]_2N^-$) to stabilize the lutetium dialkyl complex, $L^{Kiplinger}Lu(CH_2SiMe_3)_2$ (bottom, **12**, Figure 1.3).[39] Two instances of $MesPH_2$ (Mes = 2,4,6-$(CH_3)_3C_6H_2$) P–H bond activation occurred when the compound was allowed to react with complex **12**, releasing 2 equivalents of $SiMe_4$ and yielding $[L^{Kiplinger}Lu(PMes)]_2$ (bottom, **13**, Figure 1.4). Compound **13** contains P-based DAMS

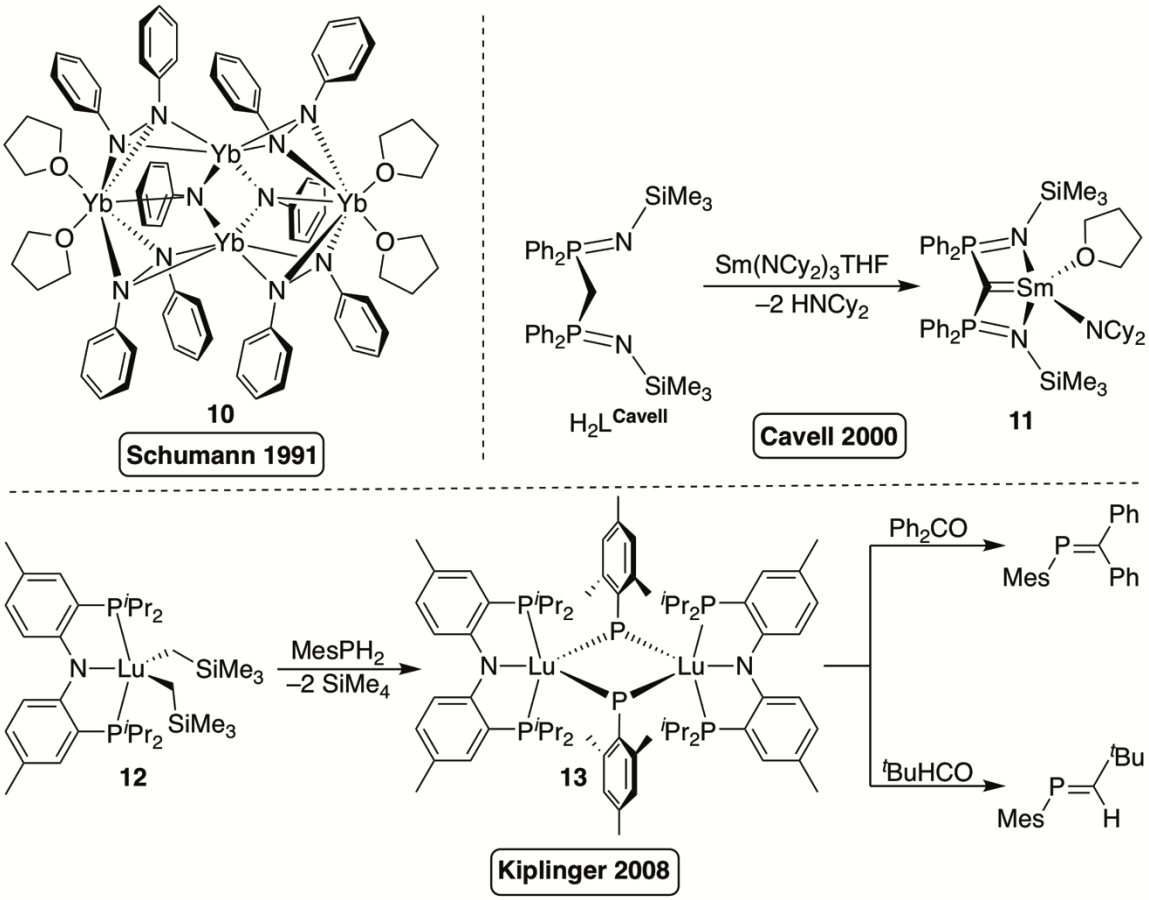

Figure 1.4 Examples of Bridging and non-Nitrogenous Dianionic Ligands on Rare Earth Metals.

ligands bound in a μ^2 fashion. Upon exposure to a stoichiometric amount of benzophenone (Ph_2CO) or pivalaldehyde (^tBuHCO), compound **13** acted as a phospha-Wittig reagent, stoichiometrically converting Ph_2CO and ^tBuHCO into Ph_2CPMes and $^tBuHCPMes$ respectively (bottom, Figure 1.4).

One of the first attempts to intentionally synthesize a rare earth complex bearing a nitrogenous, μ^1 bound, DAMS ligand was reported by Gordon in 2003.[25] The samarium triamide compound ($Sm(NHDipp)_3$) was introduced to a solution of 4 equivalents of $AlMe_3$ producing the Lewis acid stabilized product, $(AlMe_3)_2(-\mu^2\text{-}DippNH)_2(-\mu^2\text{-}DippN)_2Sm_2$ (**14**,

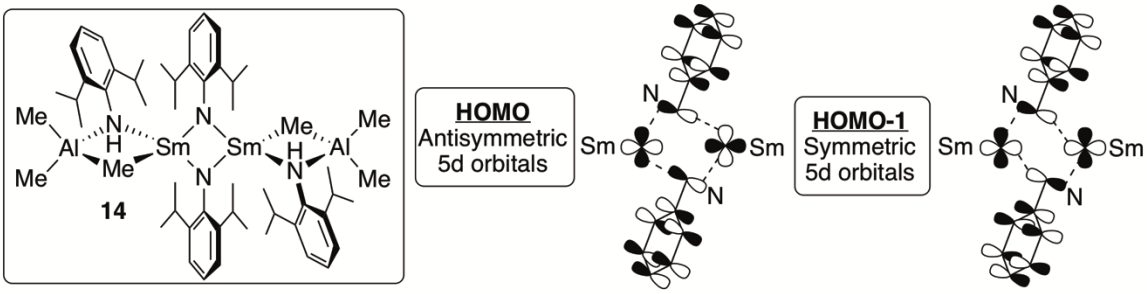

Figure 1.5 Lewis Acid Stabilized μ^2-Imido Complex and Molecular Orbitals.

Figure 1.5) with concurrent formation of $(Me_2AlNHDipp)_2$ as a byproduct. While this attempt was unsuccessful in generating a Sm=NDipp moiety, the isolation and structural characterization of a μ^2 bound DAMS ligand greatly facilitated computational analysis on such species. Density functional theory (DFT) studies were completed in order to gain insight into the bonding interactions between the DAMS ligand and the samarium centre.

The HOMO of compound **14** was determined to be a combination of nitrogen's (RN^{2-}) p-orbital (parallel to the aromatic π-system) interacting with an antisymmetric set of 5d samarium orbitals. The HOMO-1 of complex **14** was found to be similar in energy ($\Delta E = 0.017$ au) to the HOMO. The bonding ligand orbital energies are virtually identical.

However, the 5d orbital of each metal in the HOMO is antisymmetric with respect to each other, and symmetric in the HOMO-1.

1.4.4 Language Clarification

The term 'DAMS ligand' was created to provide a clear discussion regarding a variety of ligands which share no common, simple terminology. However, the remainder of this thesis focuses specifically on nitrogenous DAMS ligands. These substituents are known as 'imido' ligands. Herein, the term 'imido' will be used to refer to nitrogenous DAMS ligands (*e.g.* terminal imido = μ^1 bound RN^{2-} DAMS ligand).

1.4.5 Initial Mention of Rare Earth Terminal Imido Complexes

The first instance of a terminal rare earth imido complex mentioned in the literature came in 2003 when Hessen presented a Sc=N bonding motif as a transient intermediate in the decomposition of $L^{Hessen}Sc(CH_2(Me)C=C(Me)CH_2)$, L^{Hessen} = $[CpCH_2CH_2N(Me)_2]$, (**15**, Scheme 1.12) upon exposure to benzonitrile ($PhC{\equiv}N$).[40] The proposed mechanism described benzonitrile inserting into a Sc–CH_2 bond to form the 7-membered metallacycle intermediate $L^{Hessen}Sc(CH_2C(Me)C(Me)CH_2C(Ph)N)$, **15a**. The remaining scandium methylene then attacked the electrophilic imine carbon creating the transient terminal imido intermediate $L^{Hessen}Sc=N(PhCCH_2C(CH_3)C(CH_3)CH_2)$, **15b**, which subsequently dimerizes to give $[L^{Hessen}ScN(CPhC_6H_{10})]_2$ (**16**, Scheme 1.12). It is important to note, however, that complex **15b** was not isolated, nor was any spectroscopic evidence provided to support its formation.

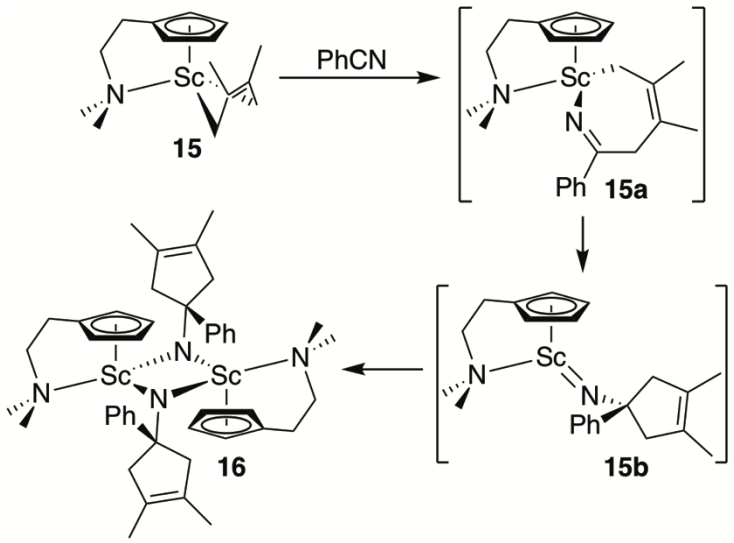

Scheme 1.12 Scandium Terminal Imido Intermediate, **15b**, Proposed by Hessen.

1.4.6 Mechanistic Evidence for the Formation of a Sc=NR Motif

Before their eventual isolation, the formation of terminal rare earth imido functionalities were established through meticulous kinetic studies carried out by Mindiola.[41-42] Similar to the aforementioned experiment reported by Gordon, addition of $L^{Mindiola}Sc(CH_3)(NHDipp)$, $L^{Mindiola}$ = $[2\text{-}P^iPr_2\text{-}4\text{-}Me\text{-}C_6H_3]_2N$, (**17**, Scheme 1.13) to a solution of $Al(Me)_3$ created the structurally characterized Lewis acid stabilized scandium imido complex $L^{Mindiola}ScNDipp(AlMe_3)$ (**17a**, Scheme 1.13). Addition of pyridine (Py) to complex **17a** resulted in activation of the ortho C–H bond across the Sc=N motif, yielding $L^{Mindiola}Sc(NHDipp)(\text{-}\kappa^2\text{-}NC_5H_3)$ (**19**, Scheme 1.13). When pyridine was added directly to complex **17**, conversion to the cyclometalated product **19** was also observed.[41]

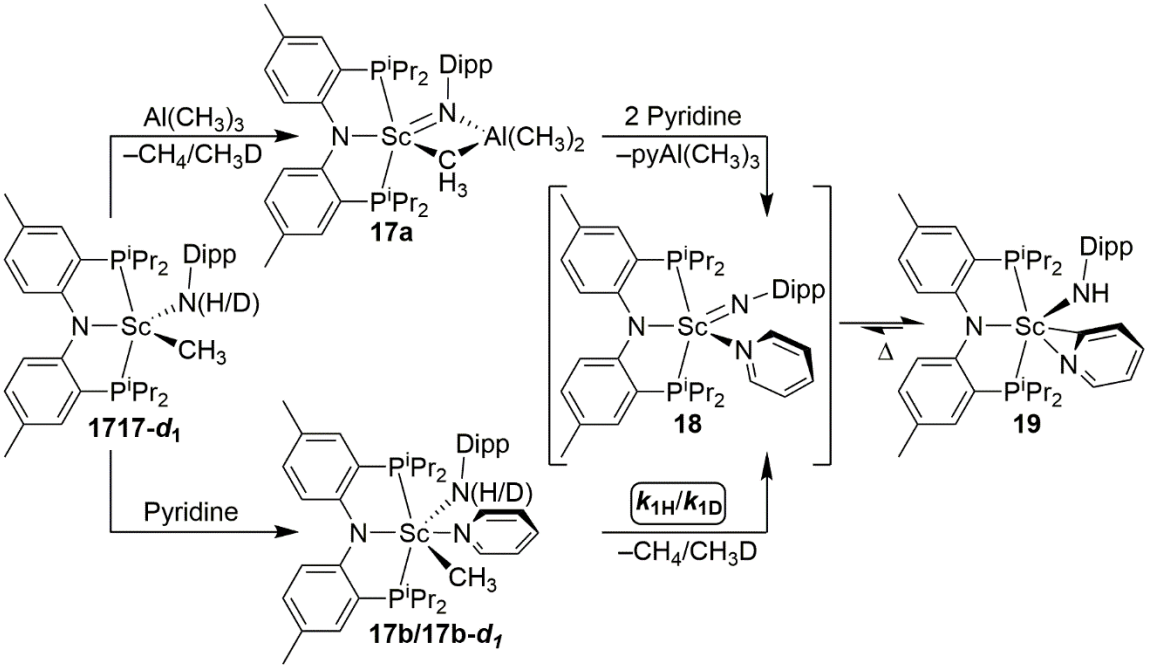

Scheme 1.13 Mechanistic Work Providing Evidence for the Formation of Complex **18**.

In order to provide mechanistic evidence for the formation of the intermediate $L^{Mindiola}Sc{=}NDipp(Py)$ (**18**, Scheme 1.13), an isotopic labeling study utilizing complexes **17** and **17-*d*$_1$** was undertaken. Cleavage of an N–H bond, as opposed to an N–D bond, would be expected to exhibit largely different rate constants (KIE > 1, KIE = Kinetic Isotope Effect). The disappearance of the C–H_3 and N–H/D signals were tracked *via* ^{1}H NMR spectroscopy and the experimentally determined KIE of 5.37(6), was indicative of direct N–(H/D) bond activation as the rate determining step (RDS), lending support for to the formation of intermediate **18**.[42] Additionally, both rate constants were first order with respect to [$L^{Mindiola}Sc(CH_3)(NHDipp)$] (**17**) and [pyridine], indicating the necessity of the Lewis base in the formation of compound **18**.[42]

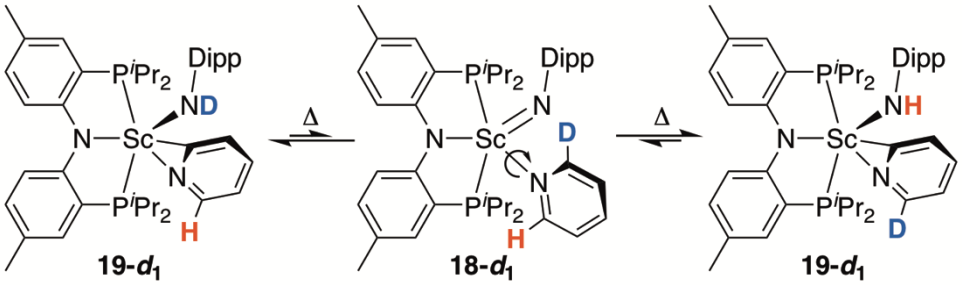

Scheme 1.14 Pyridine Isotope Exchange.

When ortho-d_1-pyridine was utilized the N–H/D exchange of complex **19-*d*$_1$** was monitored by ^{1}H NMR spectroscopy.[42] Shown in Scheme 1.14, free rotation around the Sc–N^{Py} σ-bond in L^{Mindiola}Sc=NDipp(Py-d_1), **18-*d*$_1$**, allowed the C–H/D bond to add across Sc=NDipp. Indeed, a 25% decrease (~1 H to ~0.75 H) was observed in the integration of the N–*H* resonance in the ^{1}H NMR spectrum, lending further evidence to the formation of the Sc=NDipp moiety. Ultimately, these imperative studies revealed that formation of a group 3 terminal imido functionality could be achieved *via* addition of a Lewis base (pyridine) to L^{Mindiola}Sc(CH$_3$)(NHDipp) (**17**), or L^{Mindiola}Sc(NDipp)AlMe$_3$ (**17a**). However, this species were highly unstable and prone to intramolecular C–H bond activation.[41-42]

The dependence of a Lewis base in the formation of a terminal rare earth imido functionality was further emphasised by Piers in 2013.[43] When exposed to heat (60 ºC), L^{Piers}Sc(CH$_3$)(NHDipp), L^{Piers} = (DippNC(^{t}Bu)CHC(^{t}Bu)NDipp), (**20**, Scheme 1.15) experienced intramolecular cyclometalation, yielding (DippNC(^{t}Bu)CHC(^{t}Bu)N(-2-^{i}Pr-6-CHCH$_3$CH$_2$)C$_6$H$_3$)Sc(NHDipp), **20a**.[43-44] Interestingly, addition of 4-dimethylaminopyridine (DMAP) to complex **20** yielded the scandium terminal imido complex L^{Piers}Sc=NDipp (**21**, Scheme 1.15).[43] It is worth noting that while there is significant evidence for the assignment of compound **21** based upon multi-nuclear NMR

spectroscopy and reactivity with unsaturated small molecules, no solid-state structure of complex **21** was obtained.[43]

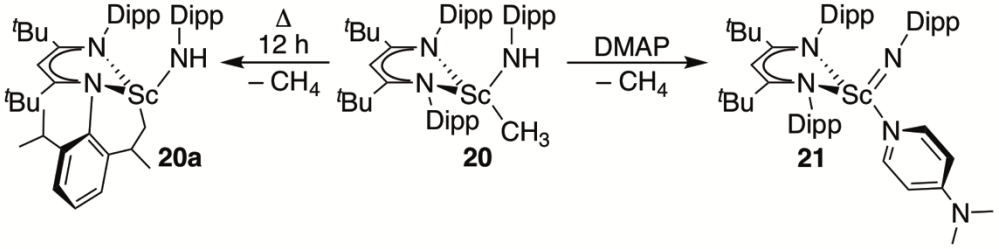

Scheme 1.15 Use of Lewis Base in the Formation of Complex **21**.

1.4.7 Isolation and Reaction Chemistry of the First Structurally Characterized Scandium Terminal Imido Complex

1.4.7.1 Isolation and Characterization

The first example of a structurally characterized complex bearing a terminal rare earth imido functionality came in 2010 from Chen and coworkers.[45] A Nacnac-derived pincer ligand was utilized to stabilize a scandium metal bearing amido and alkyl groups, $L^{Chen2}Sc(CH_3)(NHDipp)$, L^{Chen2} = (DippNC(Me)CHC(Me)$NCH_2CH_2NMe_2$), (**22**, Scheme 1.16). Addition of DMAP to complex **22** promoted N–H bond activation along with concomitant loss of methane affording $L^{Chen2}Sc$=NDipp(DMAP) (**23**, Scheme 1.16). The remarkable stability of this complex allowed for the opportunity to perform X-ray

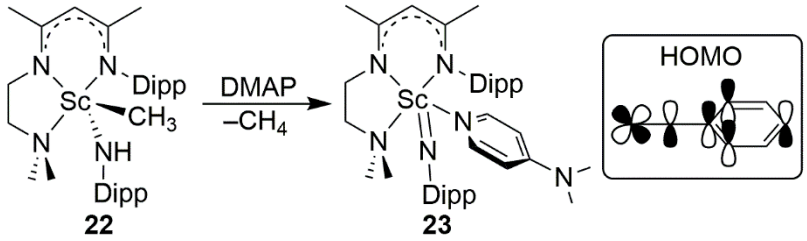

Scheme 1.16 First Example of an Isolated Rare Earth Terminal Imido Complex.

diffraction analysis, which provided the first solid-state structure containing a Sc=N bond. As would be expected for the conversion to a double bond from a single bond, substantial Sc–N contraction (8.1%, 2.047(3) Å (Sc–N) in complex **22** to 1.881(5) Å (Sc=N) in complex **23**) was observed.[45] The solid-state structure also provided suitable geometric parameters for computational structural optimization using DFT (B3LYP/6-311G*/Lanl2DZ). Determination of the Wiberg bond order for the scandium amido (0.66) and imido functionalities (1.32) also supported a significantly stronger interaction between the Sc and N atoms.[45]

1.4.7.2 Reaction Chemistry of L^{Chen2}Sc=NDipp(DMAP)

Preparation of L^{Chen2}Sc=NDipp(DMAP), **23**, opened the door for studying reaction chemistry of the Sc=N bond.[46-48] Addition of CuI to complex **23** afforded L^{Chen2}Sc=NDipp(CuI) (**23a**, Scheme 1.17), wherein the copper atom is coordinated to the lone pair of the N^{imido} atom.[46] Formation of a scandium hydride was achieved by addition of $PhSiH_3$ to complex **23** to give L^{Chen2}ScH(N(SiH_2Ph)Dipp) (**23b**, Scheme 1.17).[47]

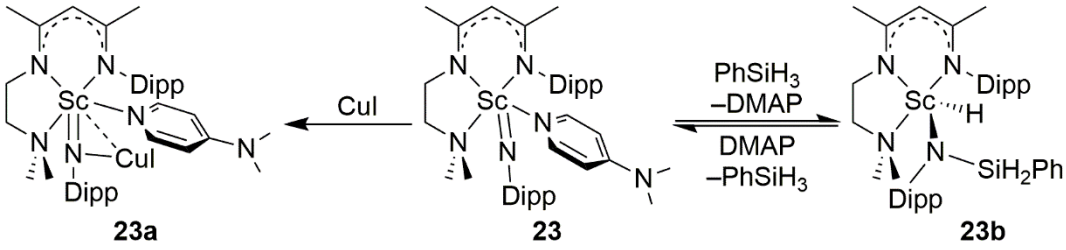

Scheme 1.17 Reactivity of Complex **23** with CuI and $PhSiH_3$.

Reactions involving complex **23** commonly resulted in liberation of free DMAP. Separation of the desired products from DMAP could not be achieved in most cases.[46] In order to bypass this hinderance, removal of the coordinated DMAP in complex **23** was

achieved by addition of 9-borabicyclo[3.3.1]nonane (9-BBN) to afford the Lewis base free complex $L^{Chen2}Sc{=}NDipp$ (**24**, Scheme 1.18). However, complex **24** is thermally unstable at ambient temperature and is prone to C–H bond activation of an N^{ligand}–Dipp methyl group yielding the cyclometalated species $((CH_3)(CH_2)HCNC(Me)CHC(Me)NCH_2CH_2NMe_2)Sc(NHDipp)$ (**24a**, Scheme 1.18).[48]

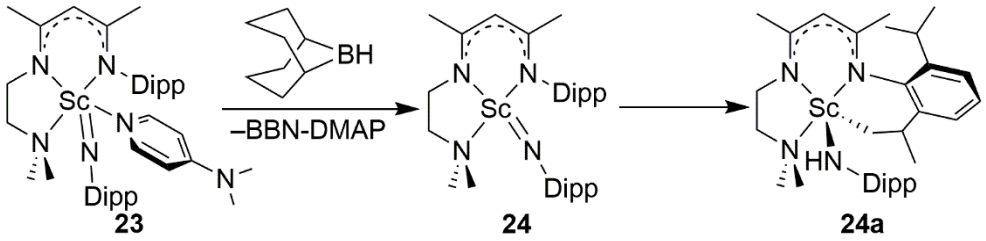

Scheme 1.18 Reactivity of Complex **23** with 9-BBN.

Addition of 2 more equivalents of 9-BBN to complex **23** promoted B–H bond activation across the Sc=N functionality, followed by coordination of the second equivalent of 9-BBN resulting in two 3-centre-2-electron bonds, $L^{Chen2}Sc(N(9\text{-}BBN)Dipp)(H_2\text{-}9\text{-}BBN)$ (**24b**, top left, Scheme 1.19). Cleavage of the C–F bond in fluorocyclohexane was observed when the compound was added to complex **24**, resulting in loss of cyclohexene and generation of the scandium fluoride complex $L^{Chen2}ScF(NHDipp)$ (**24c**, top right, Scheme 1.19). Unsaturated hydrocarbons were also reacted with complex **24**, with an alkene ($H_2C{=}CH^tBu$) undergoing C_{sp2}–H bond activation to afford $L^{Chen2}Sc(NHDipp)(CHCH^tBu)$ (**24d**, bottom left, Scheme 1.19). Interestingly, addition of $PhC{\equiv}CCH_3$ initiated a [2+2] cycloaddition across Sc=N to produce the metalloazacyclobutene complex $L^{Chen2}Sc(\text{-}\kappa^2\text{-}CPhCMeNDipp)$ (**24e**, bottom right, Scheme 1.19).[48]

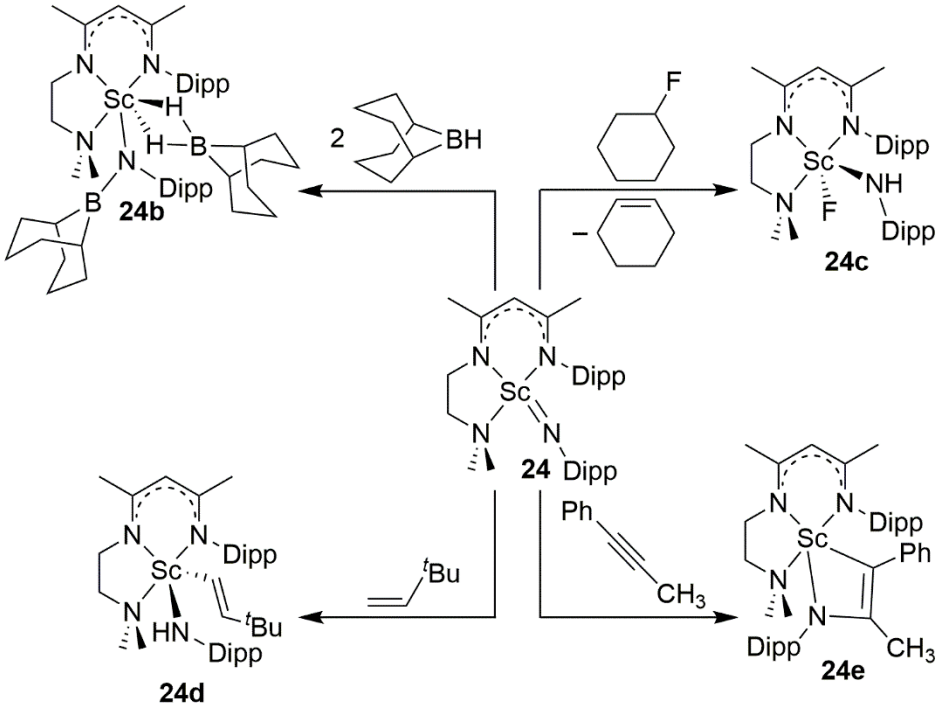

Scheme 1.19 Reaction Chemistry of Complex **24** with Small Molecules.

1.4.8 Internal Lewis Bases for Terminal Scandium Imido Formation

1.4.8.1 Formation and Isolation

Formation of complex **23** ($L^{Chen2}Sc{=}NDipp(DMAP)$) demonstrated that with careful consideration regarding the ancillary ligand, isolation of a scandium imido functionality is indeed feasible. However, the need to remove the coordinated DMAP in order to enhance reaction chemistry proved problematic. Accordingly, Chen prepared a new ligand, HL^{Chen3}, HL^{Chen3} = $DippNC(Me)CHC(Me)NCH_2CH_2NMeCH_2CH_2NMe_2$ (Scheme 1.20) which featured a pendent Lewis base.[49]

Addition of $Sc(CH_2SiMe_3)_3(THF)_2$ to HL^{Chen3} resulted in the loss of $SiMe_4$ and *in situ* formation of $L^{Chen3}Sc(CH_2SiMe_3)_2$. Subsequent addition of $DippNH_2$ promoted a loss of a second equivalent of $SiMe_4$ along with $L^{Chen3}Sc(CH_2SiMe_3)(NHDipp)$ (**25**, Scheme

1.20). Thermolysis of complex **25** promoted coordination of the pendent Lewis base and N–H bond cleavage, resulting in loss of one equivalent of $SiMe_4$ and concomitant formation of $L^{Chen3}Sc{=}NDipp$ (**26**, Scheme 1.20).[46]

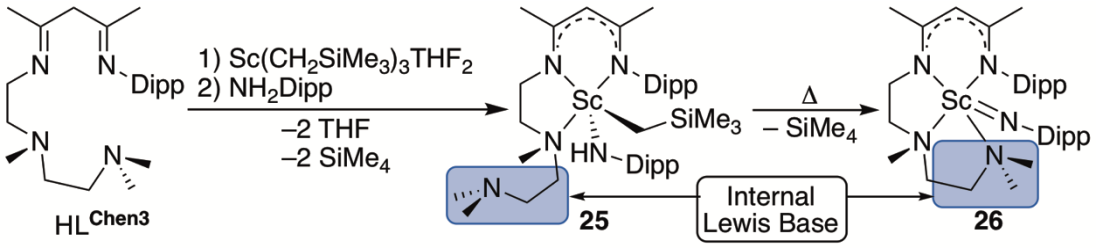

Scheme 1.20 Synthesis of a Scandium Imide Stabilized by a Modified Nacnac Ligand that Features two Pendant Lewis Base Donors.

1.4.8.2 Reaction Chemistry of $L^{Chen3}Sc{=}NDipp$

As compound **26** represented a new class of scandium imido complexes, the activation of small molecules was rigorously investigated. Group 9 dimers ($[M(COD)Cl]_2$, M= Rh, Ir), reacted readily when exposed to 2 equivalents of compound **26.**[47] The reaction afforded $L^{Chen3}Sc{=}NDipp(Cl)\bullet MCOD$ (**26a**, Scheme 1.21) which featured a cationic group 9 metal fragment bound to the $Dipp^{imido}$ substituent in an η^6-fashion and a newly formed Sc–Cl bond. Addition the elemental chalcogen Se to complex **26** led to the formation of a

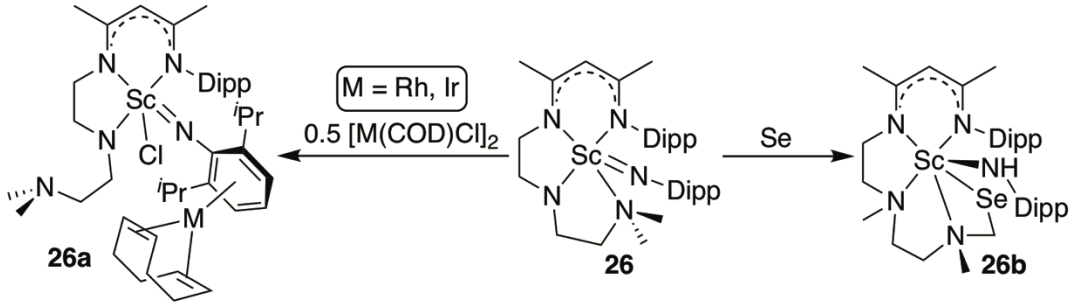

Scheme 1.21 Reactivity of Complex **26** with Transition Metals and Se.

Se–C bond and delivery of an NCH_2–*H* to the imido nitrogen, which generated (DippNC(Me)CHC(Me)$NCH_2CH_2NMeCH_2CH_2NMeCH_2$Se)Sc(NHDipp) (**26b**, Scheme 1.21).

Addition of CO_2 to complex **26** resulted in functionalization of the gas, as two equivalents inserted into the Sc=N bond creating a unique κ^2-$(OOC)_2$NDipp moiety in L^{Chen3}Sc(κ^2-$(OCO)_2$NDipp) (**26c**, top left, Scheme 1.22).[50] Addition of PhN=C=O resulted

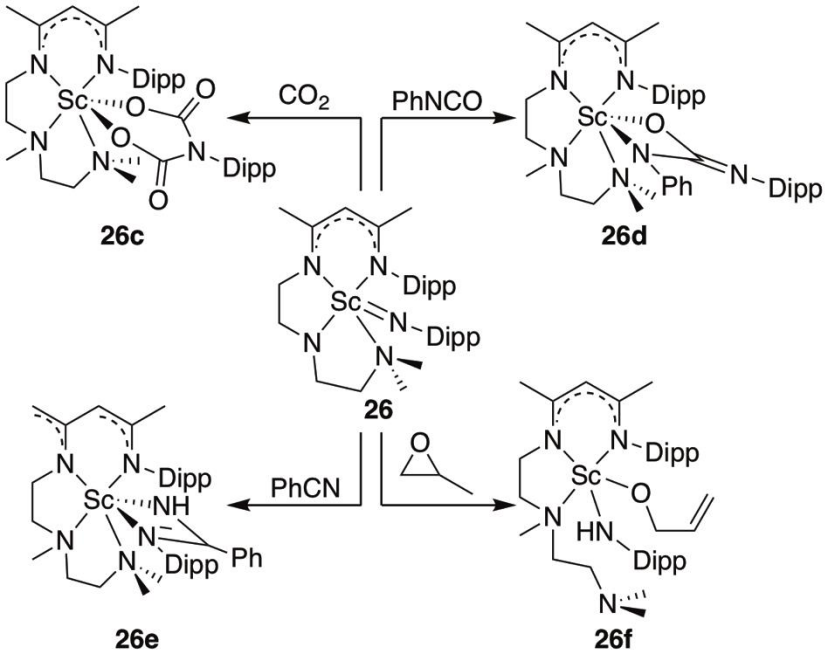

Scheme 1.22 Reactivity of Complex **26** with Unsaturated Small Molecules.

in a [2+2] cycloaddition reaction followed by subsequent isomerization to afford L^{Chen3}Sc(κ^2-(OC=NDippNPh)) (**26d**, Top right, Scheme 1.22). A similar [2+2] cycloaddition reaction occurred with PhC≡N to give L^{Chen3}Sc(κ^2-(NHCPhNDipp)) (**26e**, bottom left, Scheme 1.22) with no evidence of further isomerization. Complex **26** was also shown to promote ring opening of epoxides. Exposure of propylene oxide to compound **26** produced L^{Chen3}Sc(NHDipp)(OCH_2CHCH_2) (**26f**, Scheme 1.22).[50]

1.4.9 Additional Examples in the Literature

While the work of Chen has dominated the field of rare earth imido chemistry, several other compounds have also been reported. For example, Cui and co-workers published the imido complex, $L^{Cui}Sc{=}NDipp(DMAP)_2$, $L^{Cui} = \kappa^3$-((PhN=$PPh_2)_2$N), (**27**,

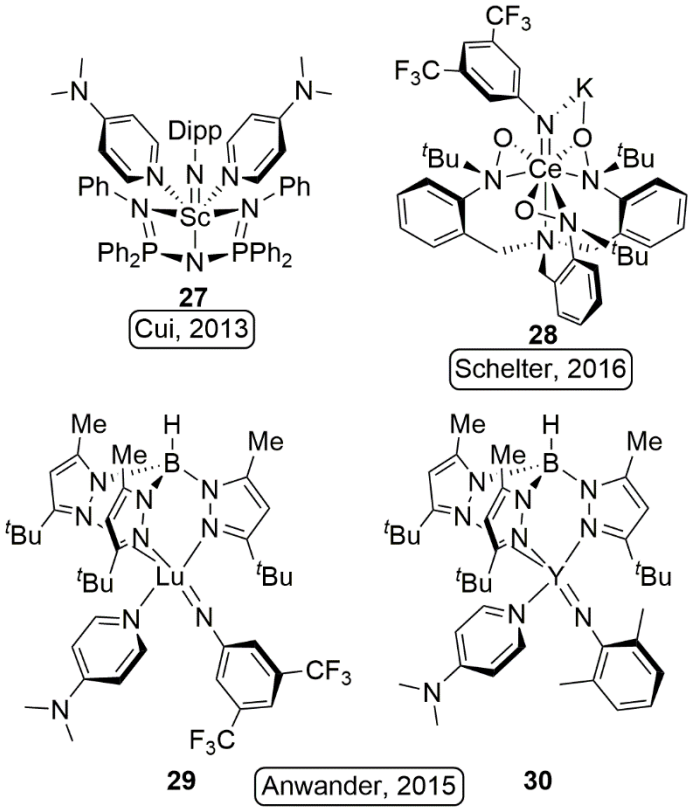

Figure 1.6 Additional Isolated Terminal Rare Earth Imido Complexes.

Figure 1.6) which is supported by an ancillary ligand that bears two phophinimine donors.[51] Similar to the protocol established by Chen, formation of the Sc=N moiety was accomplished by addition of an external Lewis base (DMAP). The Sc=N bond length obtained from an X-ray diffraction analysis (1.853(2) Å) was similar to those reported by Chen (**23** ($L^{Chen2}Sc{=}NDipp(DMAP)$, 1.881(5) Å, and **26** ($L^{Chen3}Sc{=}NDipp$, 1.858(2) Å).

Anwander was the first to synthesize a terminal rare earth imido for a metal other than Sc. Specifically, his team isolated $L^{Anwander}Lu{=}N\text{-}3,5\text{-}C_6H_3(CF_3)_2(DMAP)$ (**29**, Figure 1.6) and $L^{Anwander}Y{=}N\text{-}2,6\text{-}C_6H_3Me_2(DMAP)$ (**30**, Figure 1.5) ($L^{Anwander}$ = HB(-2-Me-4-$^tBuC_3N_2H)_3$).[52] Their formation followed the established protocol in which DMAP invoked alkane loss from an alkylamide metal precursor. As expected, these larger metals exhibited longer RE=N bond lengths (1.993(5) Å (**29**) and 2.024(4) Å (**30**)).[52] Schelter created both the first terminal imido functionality on a paramagnetic rare earth metal, as well as the first anionic example: $L^{Schelter}Ce{=}N\text{-}3,5\text{-}C_6H_3(CF_3)_2K$, $L^{Schelter}$ = N(CH_2-*o*-N(^{t}Bu)O)$_3$, (**28**, Figure 1.6).[53]

Complexes **27**-**30** represent the only other examples of terminal rare earth imido complexes currently in the literature. Unfortunately, no reaction chemistry was reported for complexes **27**-**30**.[51-52, 54]

1.5 Relevant Hayes Literature

1.5.1 Carbazole Based Ligands and Destructive Cyclometalation

Extensive work at establishing several families of modular pincer ligands for stabilizing rare earth complexes has been undertaken within the Hayes group in the past decade.[55-64] Initial ligand designs employed a rigid carbazole backbone upon which two phosphinimine functionalities were installed at the 1 and 8 positions (Scheme 1.23). The design of this ligand facilitated different R-groups to be implemented at the N and P atoms of the phosphinimine substituent (Scheme 1.23). These alterations allow for changes to be made to both the steric bulk and electronic donating properties of the ligand. The Pipp substituent (Pipp = 4-^{i}PrC_6H_4) was commonly employed on the $N^{P=N}$ atom as its presence

greatly increased crystallinity and aided characterization by ^{1}H NMR spectroscopy.[56] In addition, various changes to the P–R_2 groups have been made (*vide infra*) which resulted in multiple families of pincer ligand scaffolds.[55-62, 65] Group 3 metals (primarily Sc and Lu) were chosen as initial targets for metal complexation due to their smaller ionic radii (Sc: 0.745 Å, Lu: 0.848 Å) and diamagnetic electron configurations ($4s^0 3d^0$ (Sc) and $6s^0 5d^0 4f^{14}$ (Lu)), allowing the easy use of multi-nuclear (^{1}H, ^{13}C, ^{31}P) NMR spectroscopy as a characterization technique.

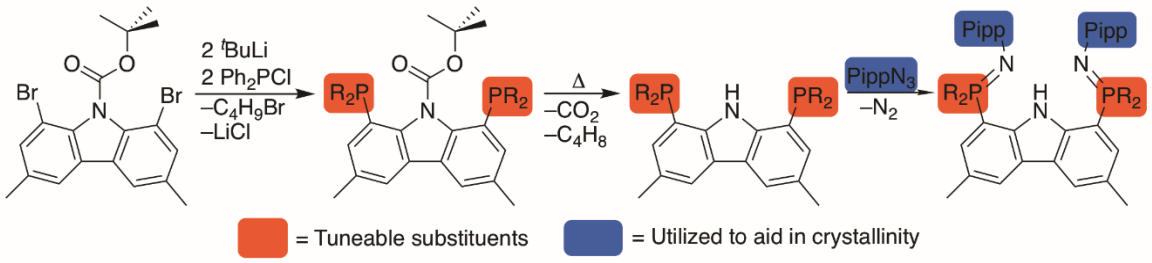

Scheme 1.23 Modular Synthesis of Carbazole Based Ligand.

Preliminary ligand designs utilized P–Ph_2 and N–Pipp substituents on the phosphinimine functionality (HL^{Cz1}, Scheme 1.24).[56] Upon reaction of HL^{Cz1} and $Lu(CH_2SiMe_3)_3(THF)_2$ spontaneous intramolecular C–H bond activation occurred at ambient temperature yielding the cyclometalated complex $L^{Cz1*}Lu(THF)$, L^{Cz1*} = doubly cyclometalated ligand (**31**, Scheme 1.24).

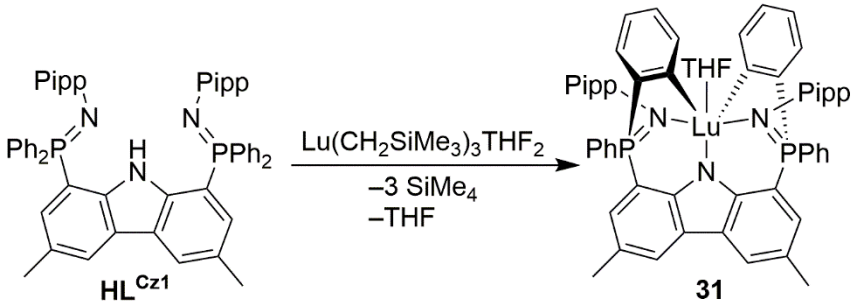

Scheme 1.24 Cyclometalation of HL^{Cz1}.

In an attempt to move the reactive C–H bonds further away from the metal centre phospholane (P–(κ^2-$(CH_2)_4$)) groups were incorporated in HL^{Cz2} (Scheme 1.25).[62] When reacted with $Lu(CH_2SiMe_3)_3(THF)_2$ no activation of the P–(κ^2-$(CH_2)_4$) substituents occurred, rather C–H bond activation of the N–Pipp group was observed, forming $L^{Cz2*}Lu(CH_2SiMe_3)$ (**32**, Scheme 1.25, L^{Cz2*} = N–aryl cyclometalated ligand). When $Sc(CH_2SiMe_3)_3(THF)_2$ was reacted with HL^{Cz2} the putative dialkyl undergoes spontaneous

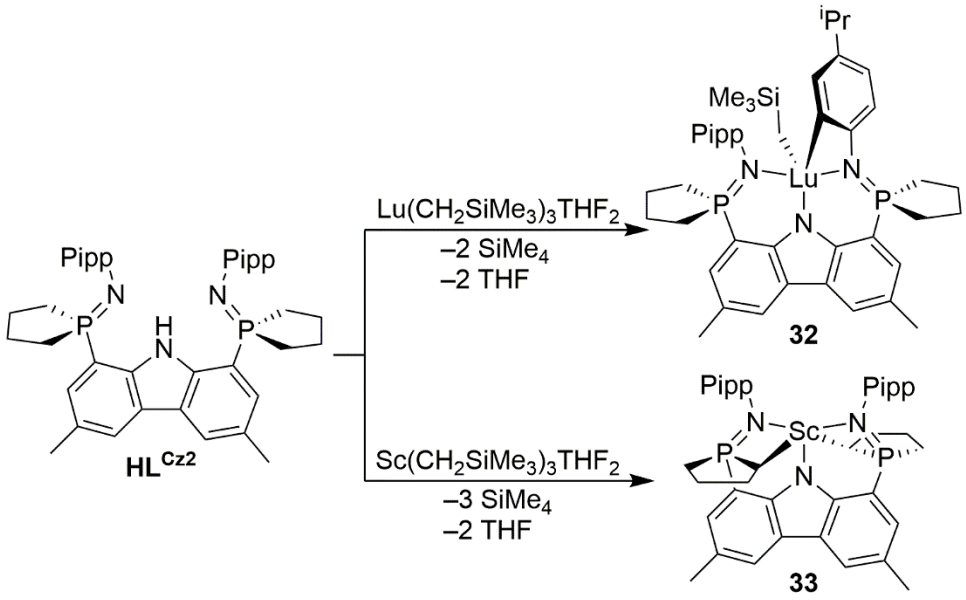

Scheme 1.25 Cyclometalation of HL^{Cz2} with Sc and Lu.

C–H bond activation of the P–(κ^2-$(CH_2)_4$) substituents to give $L^{Cz2**}Sc$ (L^{Cz2**} = doubly cyclometalated ligand, **33**, Scheme 1.25).[62] Interestingly, this result echoes the findings by Diaconesu discussed in section 1.3.2 wherein different rare earth metals supported by a common ligand exhibit different reactivities.[26]

By employing the dioxaphospholane variant (P–(κ^2-(OCH_2CH_2O))) (HL^{Cz3}, Scheme 1.26) the reactive C–H bonds were no longer present.[65] However, upon exposure to $Lu(CH_2SiMe_3)_3(THF)_2$ the short lived dialkyl intermediate $L^{Cz3}Lu(CH_2SiMe_3)_2$ formed,

only to undergo rapid P–O bond cleavage.[65] This decomposition was achieved *via* alkyl migration of the $–CH_2SiMe_3$ substituent from Lu to P, ultimately affording the dinuclear species **34** (Scheme 1.26).

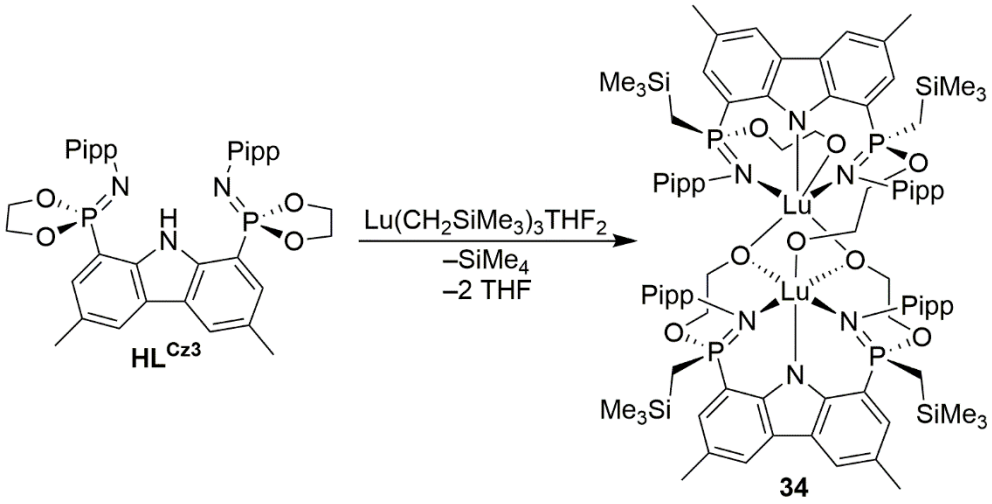

Scheme 1.26 Cyclometalation of HL^{Cz3}.

Attempts to minimize the steric pressure applied by the P–R groups did not prevent C–H bond activation. The reaction between HL^{Cz4} (P–$(CH_3)_2$) and $Lu(CH_2SiMe_3)_3DMAP_2$ released 3 equivalents of $SiMe_4$ and $L^{Cz4*}Lu(DMAP)_2$ (L^{Cz4*} = doubly cyclometalated ligand, **35**, Scheme 1.27).[62] It is likely that the dialkyl complex $L^{Cz4}Lu(CH_2SiMe_3)_2$ formed as a short lived intermediate.

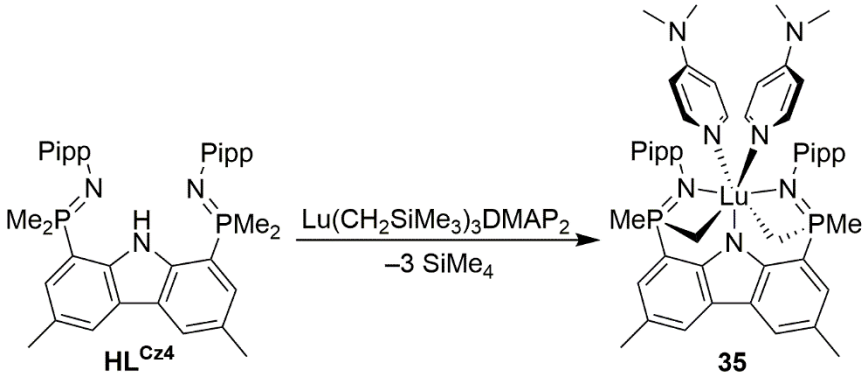

Scheme 1.27 Cyclometalation of HL^{Cz4}.

1.5.2 Pyrrole Based Ligands

With cyclometalation plaguing all rare earth metal complexes supported by carbazole based ligands, the change from a carbazole to pyrrole backbone was made.[55] This modification decreased the steric crowding around the metal centre by reducing the number of atoms in the chelate ring from 6 to 5 (Figure 1.7).

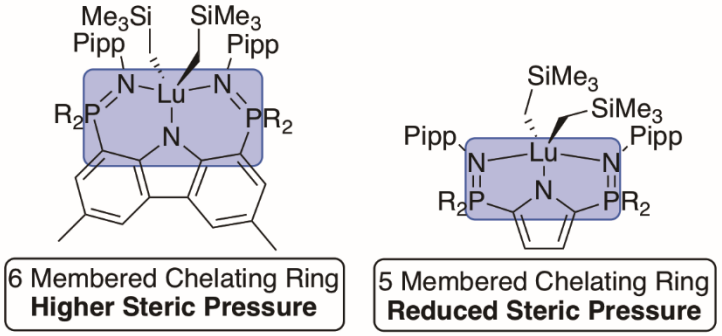

Figure 1.7 Chelate Rings in Carbazole and Pyrrole Based Pincer Ligands.

Synthesis of the pyrrole based ligand HL^{Ph} (HL^{Ph} = 2,5-[PippN=PPh_2]$_2C_4H_2NH$, Scheme 1.28) was achieved through a synthesis similar to its carbazole counterpart.[55] The reactive C–H bonds which were shown to activate with the carbazole based ligands are

pushed further away from the binding pocket of the metal, dramatically increasing the kinetic barrier of unwanted cyclometalation.

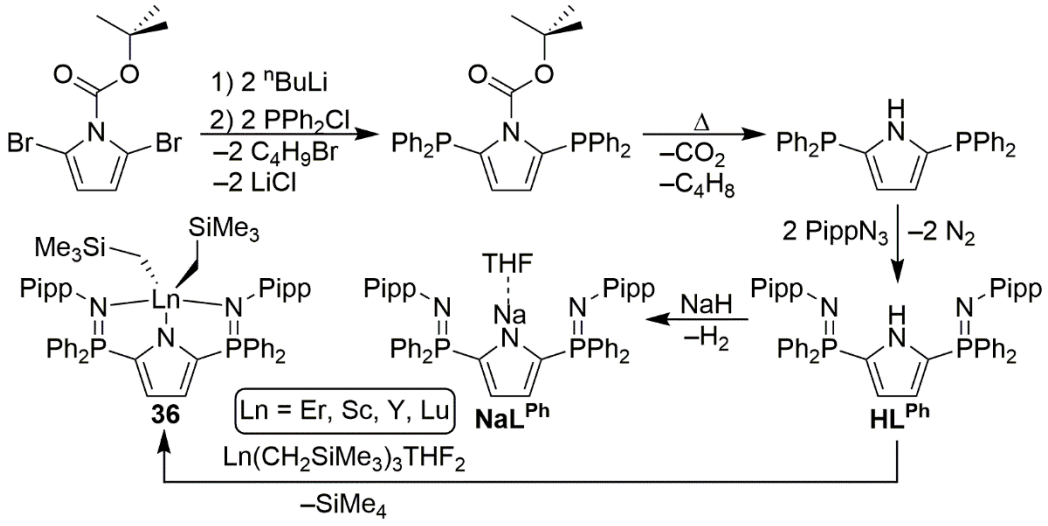

Scheme 1.28 Synthesis of HL^{Ph} and Stable Rare Earth Complexes.

Reaction of HL^{Ph} and $Lu(CH_2SiMe_3)_3(THF)_2$ resulted in the formation of $L^{Ph}Lu(CH_2SiMe_3)_2$ (**36-Lu**, Scheme 1.28); as predicted, the movement to 5 membered chelate rings hindered C–H bond activation.[55] A variety of stable dialkyl complexes (**36-Er**, **36-Sc**, **36-Y**, **36-Lu**, Scheme 1.28) have been supported by this ligand, none of which undergo cyclometalation even after 24 hours in solution at 60 °C.[55, 58] However, when $L^{Ph}Sm(CH_2SiMe_3)_2$ was synthesized spontaneous cleavage of the C^{Ph}–H bond was observed at ambient temperature.[58]

Formation of the sodium salt, NaL^{Ph}, isolated as a THF adduct, can be achieved through the addition of NaH, releasing 1 equivalent of hydrogen gas (Scheme 1.28).[66] This compound opens up avenues for metal complexation through salt metathesis pathways, *vide infra*.

1.6 Project Goals

1.6.1 Chapter 2 Goals

Synthesis of a pincer ligand (L^{Ph}) capable of supporting thermally stable rare earth complexes (**36**, Scheme 1.28) has created a platform from which a group 3 terminal imido complex can be pursued. Notably, all the substituents bound to the nitrogen atom of isolated terminal imido species have thus far been aromatic (Dipp, 3,5-$C_6H_3(CF_3)_2$, 2,6-$C_6H_3Me_2$,).[45, 49, 51-52, 54] This aromaticity can allow for conjugation of the π-bond of the imido group into the aromatic ring of the aforementioned substituent. Currently, no work has been published regarding the effect that delocalization has on the stability of the Sc=N bond in the literature. Thus, use of a non-aromatic substituent (CPh_3) was explored.

Following the synthetic route established by Chen (top, Scheme 1.29), reaction of Ph_3CNH_2 with $L^{Ph}Lu(CH_2SiMe_3)_2$ (**36-Lu**, bottom, Scheme 1.29) was expected to promote

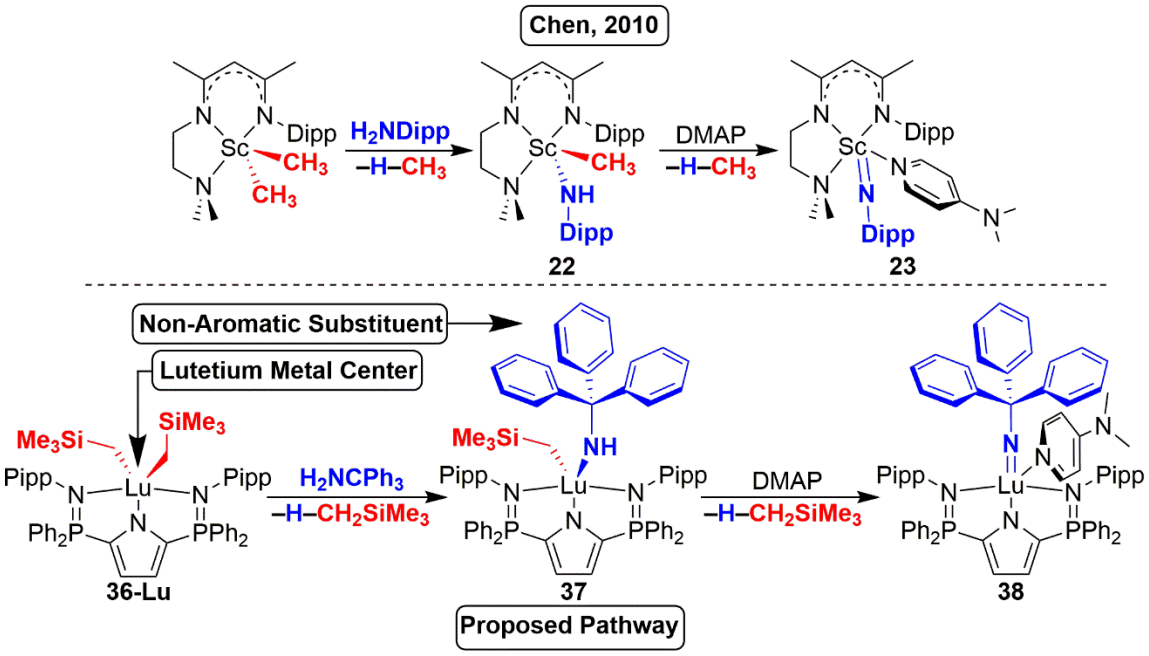

Scheme 1.29 Proposed Synthesis for A Lutetium Rare Earth Imido Complex.

formation of $L^{Ph}Lu(CH_2SiMe_3)(NHCPh_3)$ (**37**, Scheme 1.29). Addition of DMAP to rare earth alkylamido complex has been shown by Chen,[45] Cui,[51] Piers,[43] Mindiola,[41-42] and Anwander (*vide supra*)[52] to assist in N–H bond activation and as such, that route was studied in an attempt to make the lutetium imide $L^{Ph}Lu{=}NCPh_3(DMAP)$ (**38**, Scheme 1.29).

1.6.2 Chapter 3 Goals

Given the decomposition discussed in chapter 2 (*vide infra*), systematic modifications to the ancillary ligand were made with the goal of generating a thermally stable lutetium alkylamide species. Specifically, the electron withdrawing $P–Ph_2$ substituents (HL^{Ph}) were replaced with electron donating $P–^iPr_2$ substituents (HL^{iPr}). The reaction of HL^{iPr} and one equivalent of $RE(CH_2SiMe_3)_3(THF)_2$ (RE = Sc, Lu) was expected to afford the dialkyl complexes $L^{iPr}RE(CH_2SiMe_3)_2$ (**39a** RE = Sc, **39b** RE = Lu, Scheme 1.30). Addition of Ph_3CNH_2 to one equivalent of either complex **39a** or **39b** is expected to generate $L^{iPr}Sc(CH_2SiMe_3)(NHCPh_3)$ (**40a**, Scheme 1.30) or $L^{iPr}Lu(CH_2SiMe_3)(NHCPh_3)$ (**40c**, Scheme 1.30). The thermal stability of complexes **40a** and **40c** can be directly compared to $L^{Ph}Lu(CH_2SiMe_3)(NHCPh_3)$ (**37**). Addition of $DippNH_2$ to complex **39a** or **39b** is predicted form $L^{iPr}Sc(CH_2SiMe_3)(NHDipp)$, **40b**, or $L^{iPr}Lu(CH_2SiMe_3)(NHDipp)$, **40d**, respectively. These complexes represent aromatic analogs of $L^{iPr}Sc(CH_2SiMe_3)(NHCPh_3)$, **40a**, and $L^{iPr}Lu(CH_2SiMe_3)(NHCPh_3)$, **40c**, facilitating direct comparisons regarding the effect the aromaticity has on imido formation. Following the procedure established by Chen (Scheme 1.29), addition of DMAP to complexes **40a-d** is proposed to yield a family of terminal rare earth imido complexes (**41a-d**, bottom, Scheme 1.30).

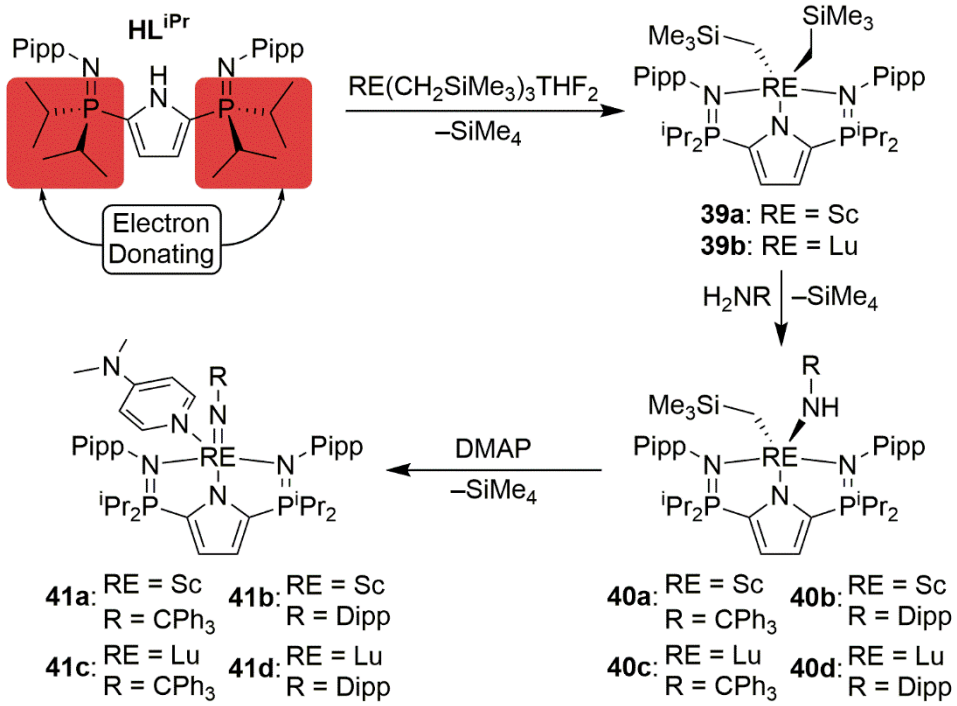

Scheme 1.30 Proposed Work for Chapter 3.

1.6.3 Chapter 4 Goals

Chapters 2 and 3 of this thesis describe the use of alkane elimination strategies focused at generating a rare earth imide complex. However, in order to isolate a rare earth dialkyl complex bearing CH_3 ligands (as opposed to CH_2SiMe_3), salt metathesis strategies must be pursued. Thus, generation of the scandium dihalide complex $L^{iPr}ScCl_2$ is pursued. Addition of two equivalents of MeLi is predicted to afford the desired scandium dialkyl compound $L^{iPr}Sc(CH_3)_2$. To explore the versatility of salt metathesis pathways, preliminary attempts regarding the addition of amide salts $[(THF)LiNHDipp]_2$, $[(THF)LiNHCPh_3]_2$, $(SiMe_3)_2NK$) to $L^{iPr}ScCl_2$ is also conducted.

Given the success Chen experienced by creating a ligand which featured additional Lewis bases (L^{Chen3}, Section 1.4.8), synthesis of a ligand which possesses pyrimidine functionalities bound to the phosphinimine nitrogen is attempted.

Chapter 2 – Insights into the Decomposition Pathway of a Lutetium Alkylamido Complex *via* Intramolecular C–H Bond Activation

2.1 Overview

2.1.1 Previous Work

Since their first isolation in 2010 by Chen,[45] only a handful of rare earth terminal imido complexes have been isolated. Chen has demonstrated that rare earth imido functionalities are capable of reacting with a variety of unsaturated small molecules,[48, 50] main group fragments,[49] and transition metals.[46] The most common synthetic pathway for producing terminal rare earth imido functionalities mimics the procedure outlined by Chen in 2010, wherein a nitrogenous Lewis base (typically DMAP) is added to a rare earth complex bearing an alkyl ligand (*e.g.* CH_3) and an amide ligand (*e.g.* NHDipp) (*e.g.* $L^{Chen2}Sc(CH_3)(NHDipp)$, **22**, Scheme 2.1).[41-43, 45, 49, 51-52, 54] DMAP addition promoted N–

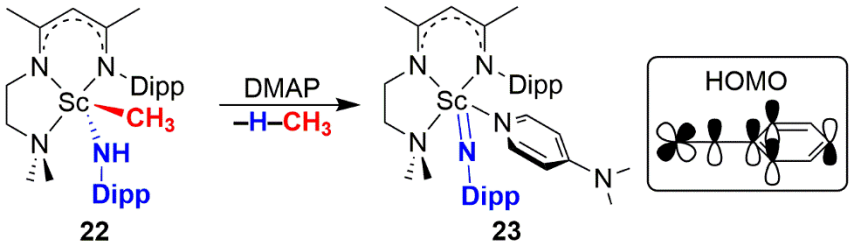

Scheme 2.1 Synthesis and HOMO of Complex **23**.

H bond activation of the alkylamido compound and concomitant alkane elimination giving rise to the terminal imido functionality (*e.g.* L^{Chen2}ScNDipp, **23**, Scheme 2.1).

Every example of an isolated terminal rare earth imido complex has utilized an aromatic substituent bound to the imido-nitrogen atom. In 2010 Chen conducted DFT analysis on complex **23** in order to glean insight into the frontier molecular orbitals. The

HOMO possessed a π-bonding interaction between the d-orbital of scandium and the p-orbital of the imido-nitrogen (Scheme 2.1).[45] However, it was also discovered that the p-orbitals of the aromatic ring were conjugated in this system, thereby delocalizing electron density from the Sc=N bond into the aromatic π-system, and weakening the imide bond.

An attempt at utilizing non-aromatic substituents was reported by Anwander in 2014 when he published the synthesis of $L^{Anwander}Lu(CH_3)(NHAd)$ (**42a**, Scheme 2.2) and $L^{Anwander}Lu(CH_3)(NH^tBu)$ (**42b**, Scheme 2.2).[67] In an effort to generate the lutetium imido

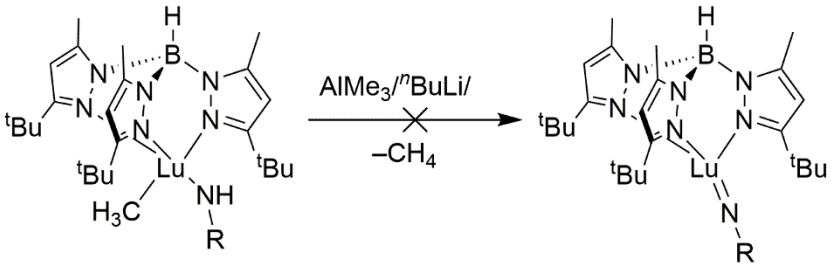

Scheme 2.2 Addition of $AlMe_3$, ^nBuLi, and Heat to Complexes **42a** and **42b**.

complexes $L^{Anwander}Lu{=}NAd$ (**43a**, Scheme 2.2) or $L^{Anwander}Lu{=}N^tBu$ (**43b**, Scheme 2.2), $AlMe_3$, ^nBuLi, or heat was added to complexes **42a** or **42b**, respectively.[67] Unfortunately, no imido complexes were isolated from these reactions. It should be noted, however, that the addition of DMAP (the common synthetic pathway established by Chen) was not explored.

2.1.2 Proposed Work

Previous work regarding the isolation of thermally stable rare earth complexes afforded $L^{Ph}Lu(CH_2SiMe_3)_2$ (**36-Lu**, Scheme 2.3).[55] Complex **36-Lu** provided a rare earth dialkyl complex for which the addition of Ph_3CNH_2, is expected to generate the alkylamido

complex $L^{Ph}Lu(CH_2SiMe_3)(NHCPh_3)$ (**37**, Scheme 2.3). Following the isolation of complex **37**, addition of DMAP was hypothesized to induce N–H bond activation, extrusion of $SiMe_4$, and yield $L^{Ph}Lu{=}NCPh_3(DMAP)$ (**38**, Scheme 2.3). A non-aromatic

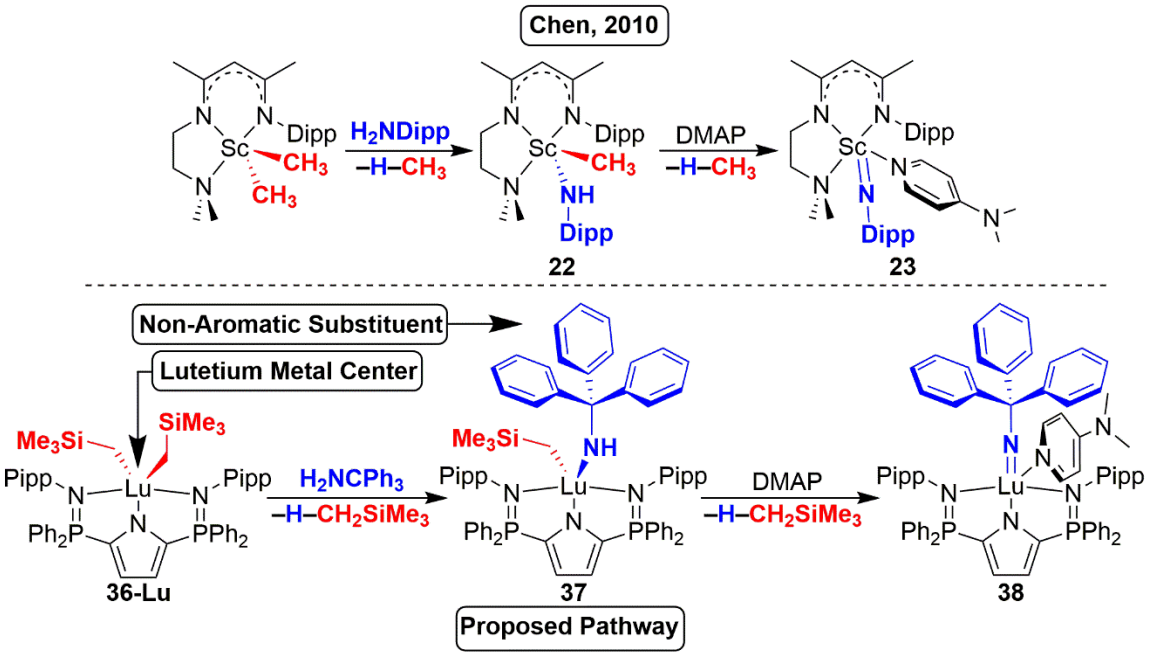

Scheme 2.3 Proposed Pathway to Synthesize Terminal Lutetium Imido Complex.

substituent, CPh_3, was chosen in an attempt to witness any effects the loss of aromaticity had on the resulting lutetium imide complex, **38**.

2.2 Synthesis and Characterization of $L^{Ph}Lu(CH_2SiMe_3)(NHCPh_3)$

Reaction of $L^{Ph}Lu(CH_2SiMe_3)_2$, **36-Lu**, with one equivalent of dry Ph_3CNH_2 was stirred for one hour at ambient temperature in a toluene solution. After this time, all the volatiles were removed *in vacuo* and the desired alkylamido complex $L^{Ph}Lu(CH_2SiMe_3)(NHCPh_3)$, **37**, was isolated as a white powder in 98% yield (Scheme 2.4). This transformation was supported by the appearance of a new signal in the ^{31}P NMR spectrum at δ 23.6, along with concomitant disappearance of the resonance at δ 25.1

corresponding to compound **36-Lu**. Corroborating evidence was also observed in the ^{1}H NMR spectrum as one equivalent of $SiMe_4$ (δ 0.00) emerged in the reaction mixture. In addition, a broad singlet (N–*H*) resonating at δ 2.93, which did not give rise to any cross-peaks in either the ^{1}H–^{1}H COSY or ^{1}H–^{13}C HSQC spectra, gradually appeared over the course of the reaction, eventually integrating for 1 H.

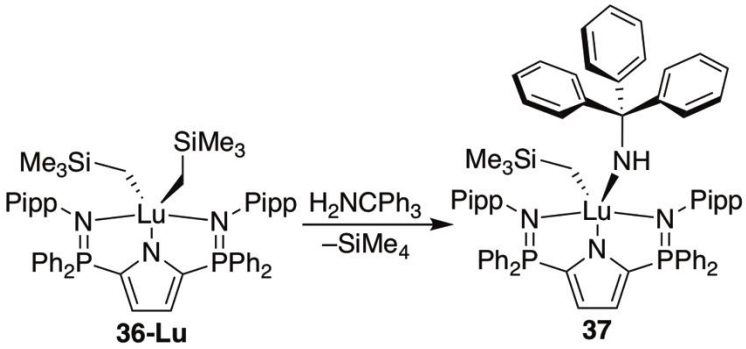

Scheme 2.4 Synthesis of Complex **37**.

2.3 Spontaneous Decomposition of $L^{Ph}Lu(CH_2SiMe_3)(NHCPh_3)$

Although as a dry solid complex **37** is indefinitely stable under an inert atmosphere, it is thermally unstable in solution, even at –35 °C, and steadily decomposed into 0.5 equivalents of $L^{Ph}Lu(NHCPh_3)_2$, **44**, and several unidentified metal containing species (Scheme 2.5). Due to the reactive nature of $L^{Ph}Lu(CH_2SiMe_3)(NHCPh_3)$, **37**, X-ray quality crystals or analytically pure samples were unable to be obtained despite exhaustive efforts. Thermolysis of complex **37** for 24 hours at 80 °C resulted in its complete consumption and generation of one dominant product, compound **44**, which appeared as a singlet at δ 21.7 in the ^{31}P{^{1}H} NMR spectrum. The formation of a signal which integrated to one equivalent of $SiMe_4$ (δ 0.00), and concomitant disappearance of the N–*H* resonance (δ 2.93) of complex **37**, were observed in the ^{1}H NMR spectrum. In addition, a new singlet

which appeared (δ 3.35) and integrated as 2H was assigned as the N–*H* resonance of complex **44**.

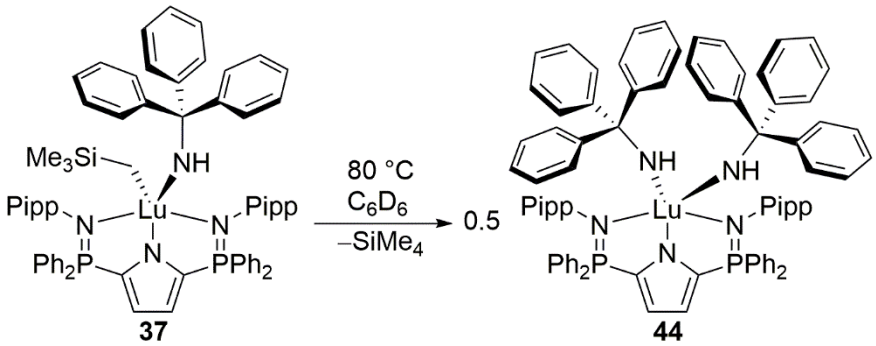

Scheme 2.5 Decomposition of Complex **37**.

2.4 Characterization of Decomposition Intermediate $L^{Ph}Lu(-\kappa^2\text{-}NHCPh_2C_6H_4)$

Intriguingly, careful spectroscopic monitoring of the decomposition of complex **37** revealed the formation of the reaction intermediate $L^{Ph}Lu(-\kappa^2\text{-}NHCPh_2C_6H_4)$, **45**, which resonated at δ 25.0 in the $^{31}P\{^1H\}$ NMR spectrum (Scheme 2.6). Heating to 80 °C produced complex **45** in higher quantity (50% of phosphorus containing material). Complex **45** began converting to $L^{Ph}Lu(NHCPh_3)_2$, **44**, before the alkylamido starting material $L^{Ph}Lu(CH_2SiMe_3)(NHCPh_3)$, **37**, was fully consumed. Thus, despite thorough attempts, complex **45** was not isolated it in high purity.

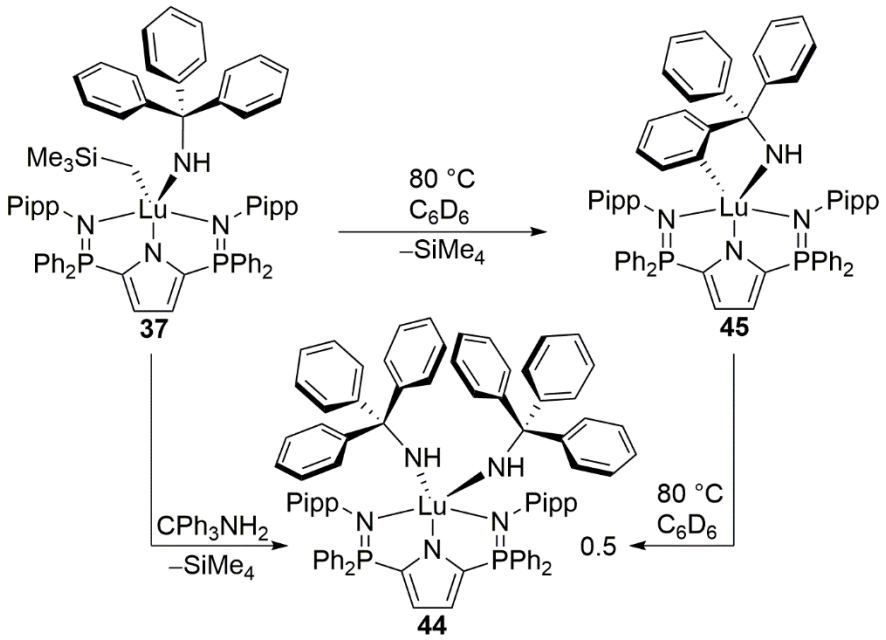

Scheme 2.6 Decomposition of Complex **37** and the Unstable Intermediate, **45**.

In solution, complex **45** exhibits spectral features consistent with C_s symmetry, such as a single resonance in the $^{31}P\{^1H\}$ NMR spectrum. Thus, compound **45** is unlikely to be a metallocycle complex resulting from a single *P*- or *N*-aryl C_{sp2}–H bond activation, as happened with our bis(phosphinimine)carbazole ligand scaffolds (see section 1.5.1).[56-58, 62, 65]

Notably, a new weak, but diagnostic resonance at δ 198.0 was observed in the $^{13}C\{^1H\}$ NMR spectrum, consistent with previously reported C_{sp2} atoms bound to lutetium.[56-57, 68-70] This signal implies, coupled with the C_s symmetry of intermediate **45**, that **37** decomposes *via* ortho-metalation of one of the phenyl rings pertaining to the $NHCPh_3$ ligand to afford the cyclometalated complex **45** (Scheme 2.6).

With the inability to characterize compound **45** as a pure compound *via* 1- and 2-dimensional multi-nuclear NMR spectroscopy, DOSY (diffusion-oriented spectroscopy)

NMR was used to determine if complex **45** was monomeric or dimeric. Due to the similarity of the diffusion coefficient of compound **45** ($4.17(2)x10^{-10}$ m^2s^{-1}), to that of complex **37** ($5.62(2)x10^{-10}$ m^2s^{-1}) and complex **44** ($8.71(2)x10^{-10}$ m^2s^{-1}) the possibility that intermediate **45** existed as a dinuclear species in solution was ruled out.

2.5 Reactivity of $L^{Ph}Lu(CH_2SiMe_3)(NHCPh_3)$ with 4-Dimethylaminopyridine (DMAP)

Since the presence of a Lewis base appears to be a key factor in generating terminal imido species from alkylamido complexes,[41-44] the reaction chemistry of complex **37**, $L^{Ph}Lu(CH_2SiMe_3)(NHCPh_3)$, with varying stoichiometries of DMAP was explored. Over the course of 24 hours at ambient temperature, a slow reaction between complex **37** and 1 equivalent of DMAP led to the formation of 0.5 equivalents of the bisamide complex **44**, $L^{Ph}Lu(NHCPh_3)_2$, as well as unidentified contaminants, similar to the decomposition outlined in section 2.3 (Scheme 2.7). When the experiment was repeated (80 °C for 24 h) using an excess (4 equivalents) of DMAP a slightly broader distribution of unidentified compounds prevailed, but complex **44** remained the predominant product (25 %) after 144 hours. The analogous substoichiometric reaction with 0.5 equivalents of DMAP resulted in complex **44**, which represented 65% of the phosphorus containing material. However, the reaction proceeded at a notably retarded rate. In order to reach completion, the reaction had to be heated to 70 °C for 168 h.

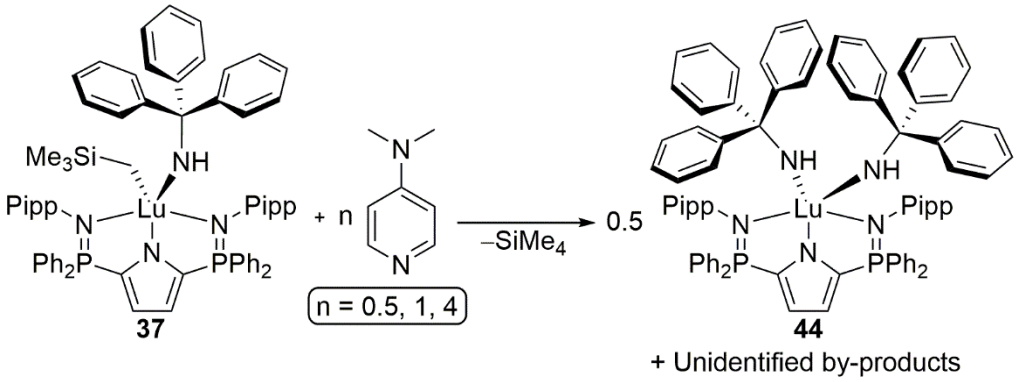

Scheme 2.7 Decomposition of Complex **37** in the Presence of DMAP.

The mechanism for the formation of complex **44** in the presence of DMAP remains unknown. While a ligand redistribution (disproportionation) process may seem plausible, at no point during the reaction was the thermally robust dialkyl species $L^{Ph}Lu(CH_2SiMe_3)_2$, **36-Lu**, observed by ^1H or ^{31}P NMR spectroscopy. Furthermore, there was no spectroscopic evidence for the formation of $L^{Ph}Lu{=}NCPh_3(DMAP)$, **38**. Similarly, no direct support for the formation of $L^{Ph}Lu(\text{-}\kappa^2\text{-}NHCPh_2C_6H_4)$, **45**, was observed throughout the reaction. However, it is conceivable that the orthometalated compound **45**, $L^{Ph}Lu(\text{-}\kappa^2\text{-}NHCPh_2C_6H_4)$, formed only to rapidly decompose into a myriad of products in the presence of DMAP.

2.6 Crystallographic Analysis of $L^{Ph}Lu(NHCPh_3)_2 \bullet C_7H_8$

Complex **44**, $L^{Ph}Lu(NHCPh_3)_2$, was independently synthesized as a white solid in 77% yield by reaction of $L^{Ph}Lu(CH_2SiMe_3)_2$, with 2 equivalents of Ph_3CNH_2 in toluene solution for 22 h at ambient temperature. The product was recrystallized from a 5:3 toluene:heptane mixture at –35 °C which gave colourless X-ray quality needles from which

the solid-state structure was determined. The solid-state structure can be seen in Figure 2.1, with highlighted metrical parameters given in Table 2.1 Complex **44**, which crystallized in

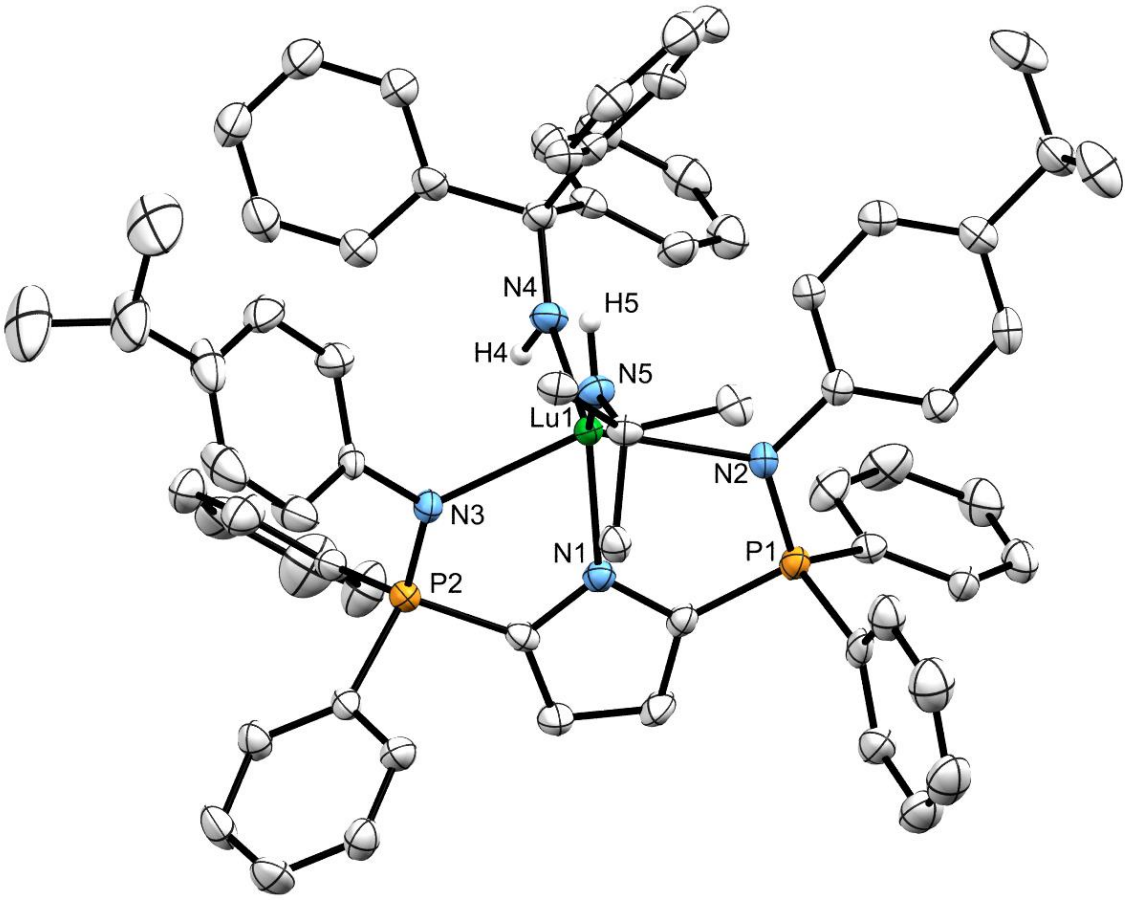

Figure 2.1 X-ray Crystal Structure (30% probability Ellipsoids) of **44•C_7H_8** with Hydrogen Atoms (Except H4 and H5), Isopropyl Groups, and Non-Ipso Carbons of the N5–CPh3 Group are Omitted for Clarity.

the triclinic P–1 space group, exhibits a coordination environment about lutetium that is best described as distorted trigonal bipyramidal (τ^5 = 0.63). The ancillary *NNN*-pincer ligand (L^{Ph}) is coordinated in a planar fashion, occupying both apical positions and one of the equatorial sites. The bulky triphenylmethylamido ligands are located in the remaining equatorial positions. At 2.453(3) Å and 2.397(3) Å the respective Lu–N2 and Lu–N3

distances are slightly longer than the Lu–C bonds found in complex **36-Lu** (2.364(2) Å and 2.332(3) Å).[55] Such elongation is likely a consequence of the sterically demanding $NHCPh_3$ groups. All other geometrical parameters closely match those of **36-Lu**.[10] Interestingly, the Lu–N4 and Lu–N5 bonds lengths of 2.144(4) and 2.143(3) Å, respectively, are slightly shorter than the average solid-state ArHN–Lu bond (Ar = aromatic substituent).[51, 57, 71-74]

Table 2.1 Selected Bond Lengths (Å) and Angles (°) for Complex **44**.

Parameter	Distance (Å)	Parameter	Angle (°)
Lu1–N1	2.293(4)	N2–Lu1–N3	143.7(1)
Lu1–N2	2.453(3)	N1–Lu1–N4	107.0(1)
Lu1–N3	2.397(3)	N4–Lu1–N5	118.3(1)
Lu1–N4	2.144(4)	N1–Lu1–C78	106.8(1)
Lu1–N5	2.143(3)	P1–N2–C17	118.9(3)
P1–N2	1.620(4)	P2–N3–C38	121.3(3)
P2–N3	1.599(4)		

2.7 Deuterium Labelling Study of the Decomposition of $L^{Ph}Lu(CH_2SiMe_3)(NHCPh_3)$

2.7.1 Previous Work

As outlined in section 1.4.6 of this thesis, Mindiola conducted a series of isotopically labeled kinetic studies to determine if a terminal rare earth imido intermediate, **18**, formed during the spontaneous cyclometalation of complex **17b**. Should the C–H bond

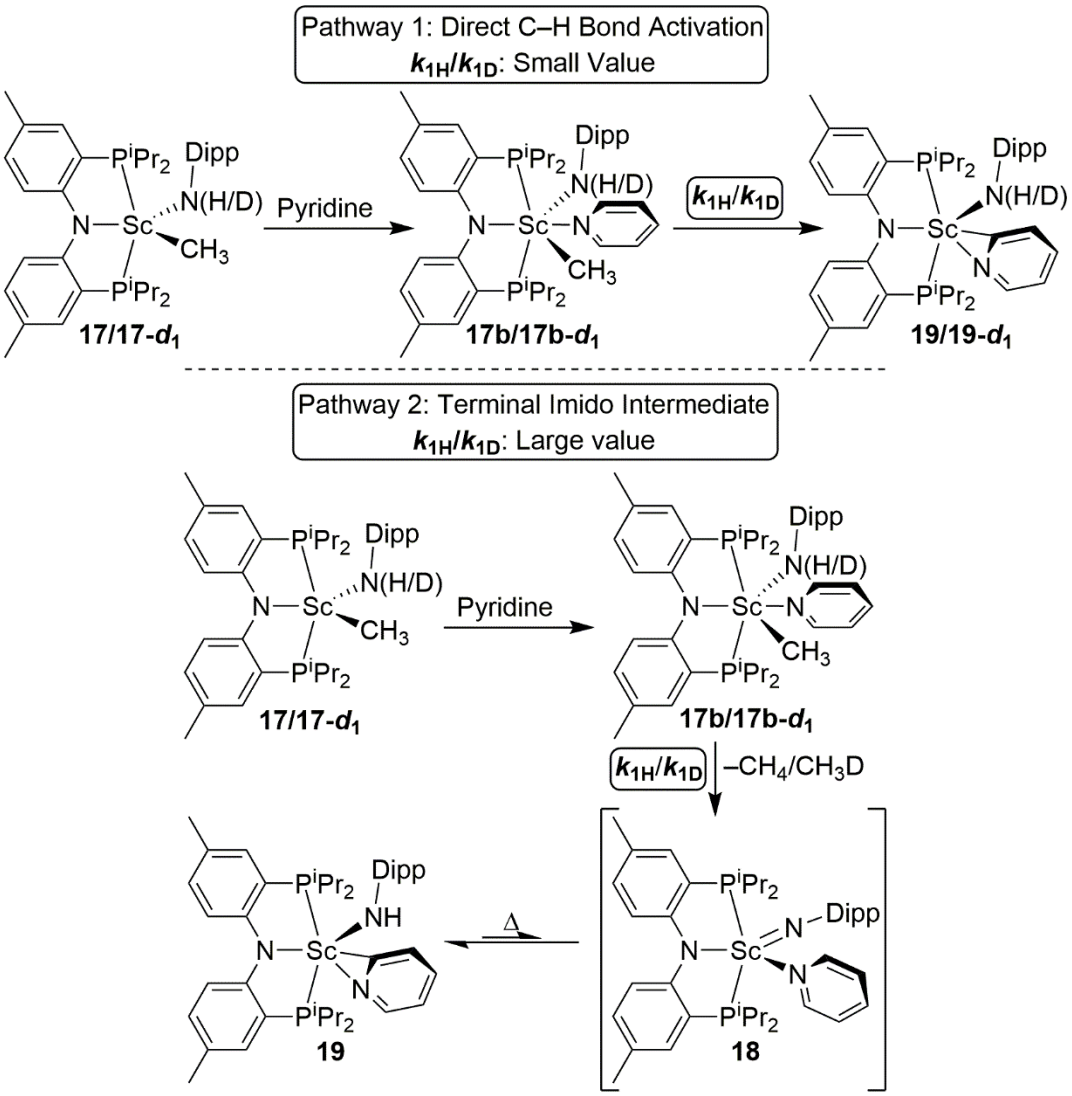

Scheme 2.8 Mechanistic Work Done by Mindiola.

of pyridine have activated directly, the N–H/D bond of compound **17/17-d_1** would have remained intact and gave rise to a small kinetic isotope effect (KIE) value (top, Scheme 2.9). However, if addition of pyridine to complex **17/17-d_1** caused the N–H/D bond to break and form the transient terminal imido intermediate, complex **18**, a large KIE value would be expected (bottom, Scheme 2.9). Indeed, a large KIE value of 5.37(6) was obtained,

indicating the formation of complex **18** in solution. For a more detailed description of this experiment the reader is encouraged to read section 1.4.6 of this thesis.[42]

2.7.2 Objectives of Deuterium Labelling Study

In order to determine if $L^{Ph}Lu(CH_2SiMe_3)(NHCPh_3)$, **37**, formed *via* the short lived imido intermediate, $L^{Ph}Lu{=}NCPh_3$, (**46**, Scheme 2.9) upon decomposition an isotopic labeling experiment, in a similar vein to work carried out by Mindiola, was conducted. Tracking the decomposition of $L^{Ph}Lu(CH_2SiMe_3)(N\mathit{H}CPh_3)$, **37**, and $L^{Ph}Lu(CH_2SiMe_3)(N\mathit{D}CPh_3)$, **37-*d*$_1$**, allowed for the ratio of their respective rate constants to be determined, from which a kinetic isotope effect was calculated. As depicted in Scheme 2.9, the two most plausible pathways that exist for the formation of $L^{Ph}Lu(\text{-}\kappa^2\text{-}NHCPh_2C_6H_4)$, **45**, are:

Pathway 1) Direct C_{sp2}–H bond activation of the $NHCPh_3$ ligand, which would yield a small, secondary KIE as the N–H/D bond remains intact throughout the reaction (top, Scheme 2.9).

Pathway 2) Cleavage of the N–H/D bond occurs, leading to the terminal imido intermediate, **46**, which then undergoes C_{sp2}–H addition across the Lu=N bond, yielding a large, primary KIE (bottom, Scheme 2.9).

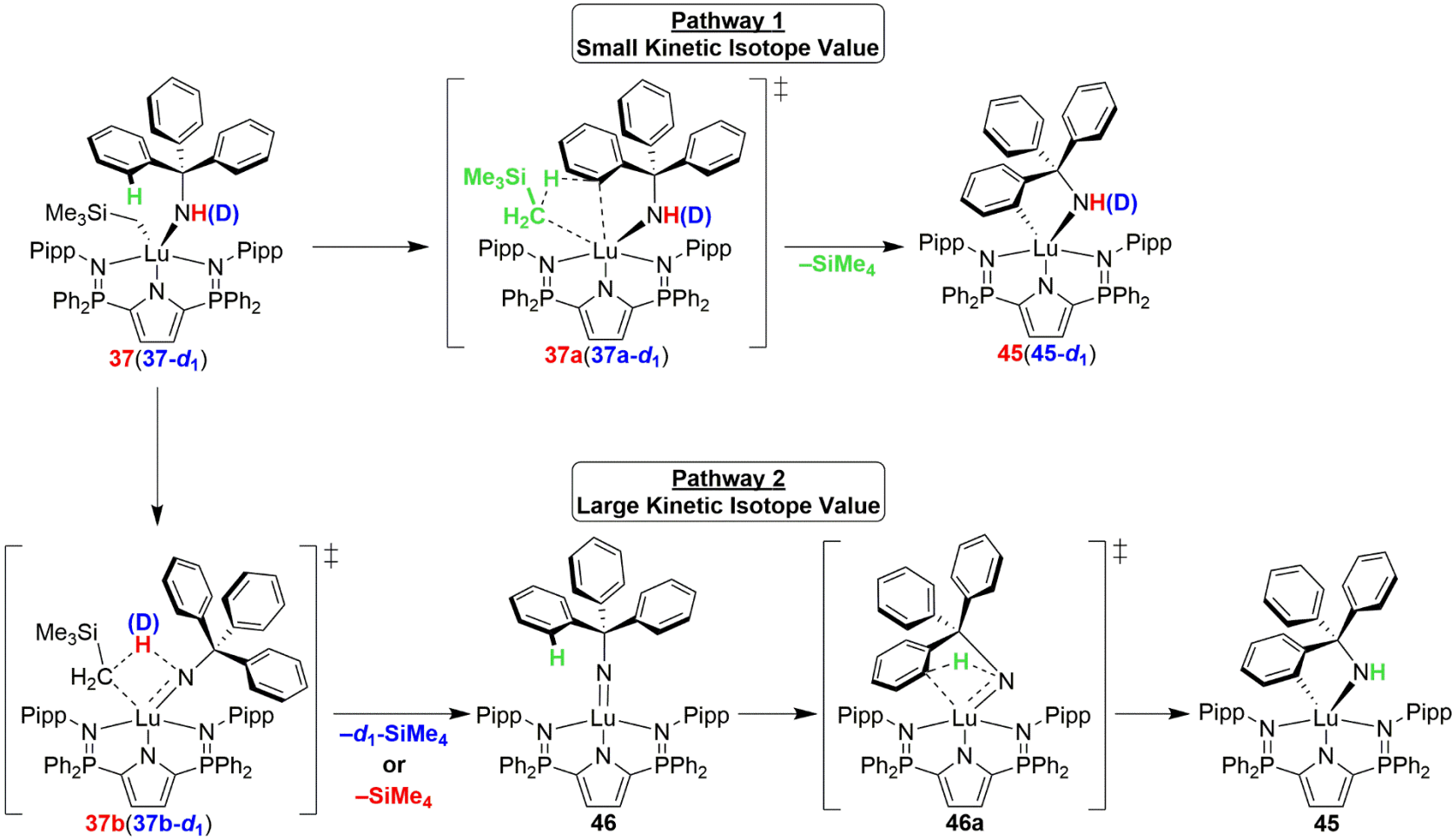

Scheme 2.9 Two Possible Reaction Pathways for the Decomposition of Complex **37**/**37**-d_1.

2.7.3 Formation of Ph_3CND_2 and $L^{Ph}Lu(CH_2SiMe_3)(NDCPh_3)$

Deuteration of the $NHCPh_3$ ligand was achieved by stirring Ph_3CNH_2 with a catalytic amount of 35% DCl in D_2O for 10 minutes at ambient temperature which provided approximately 95% deuterium incorporation, affording Ph_3CND_2. Complex **37-*d*$_1$** was formed by the same synthetic procedure as $L^{Ph}Lu(CH_2SiMe_3)(NHCPh_3)$, **37**, with the exception that a much longer reaction time (24 h vs. 1 h) was required, which is presumably due to a large kinetic isotope effect.

2.7.4 Kinetic Analysis of the Decomposition of $L^{Ph}Lu(CH_2SiMe_3)(NHCPh_3)$ and $L^{Ph}Lu(CH_2SiMe_3)(NDCPh_3)$ and Determination of KIE Value

The thermal decomposition of complexes **37** and **37-*d*$_1$** was quantitatively monitored to three half-lives over a narrow range of temperatures (343 K to 373 K). The reaction was established to be first order in [**37**/**37-*d*$_1$**] with the observed rate constants ranging from $6.84(3)\times10^{-6}$ s^{-1} to $1.38(4)\times10^{-4}$ s^{-1}, for complex **37**, and $7.79(5)\times10^{-6}$ s^{-1} to $1.63(2)\times10^{-4}$ s^{-1}, for complex **37-*d*$_1$**, providing an averaged KIE of 1.3(1) (Table 2.2). This low value is consistent with a secondary KIE and would be expected if **Pathway 1** were operative (Scheme 2.10), as the N–(H/D) bond of **37** and **37-*d*$_1$** remains intact throughout

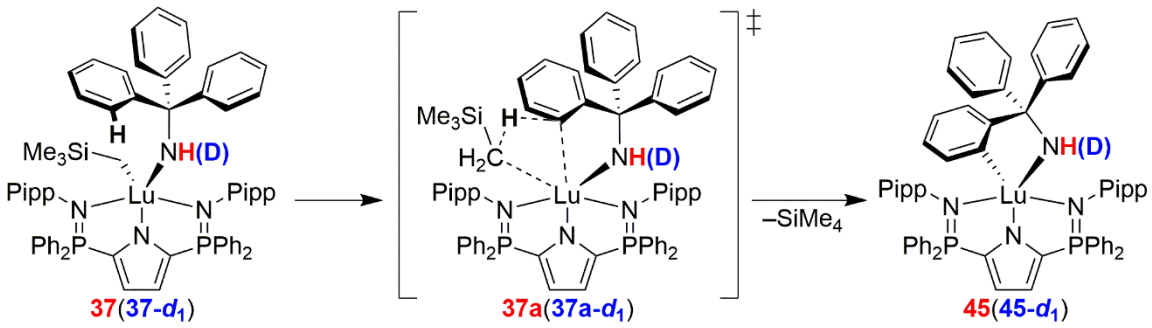

Scheme 2.10 Experimentally Determined Decomposition of Complex **37**/**37-*d*$_1$**.

the entire process. Additionally, no evidence for the formation of d_1-$SiMe_4$, as would be the case had the reaction proceeded according to **Pathway 2**, was observed by either ^1H or ^2H NMR spectroscopy.

Table 2.2 Experimental Rate Constants for the Decomposition of **37** and **37-*d*$_1$**.

T (K)	$\mathbf{k_H(s^{-1})}$ (Figure 2.2)	$\mathbf{k_D(s^{-1})}$ (Figure 2.3)	$\mathbf{k_H/k_D}$
343	$7.79(5)\times10^{-6}$	$6.84(3)\times10^{-6}$	1.2(1)
353	$3.74(4)\times10^{-5}$	$2.32(4)\times10^{-5}$	1.6(2)
363	$6.44(6)\times10^{-5}$	$4.88(3)\times10^{-5}$	1.3(1)
373	$1.63(2)\times10^{-4}$	$1.38(4)\times10^{-4}$	1.2(1)

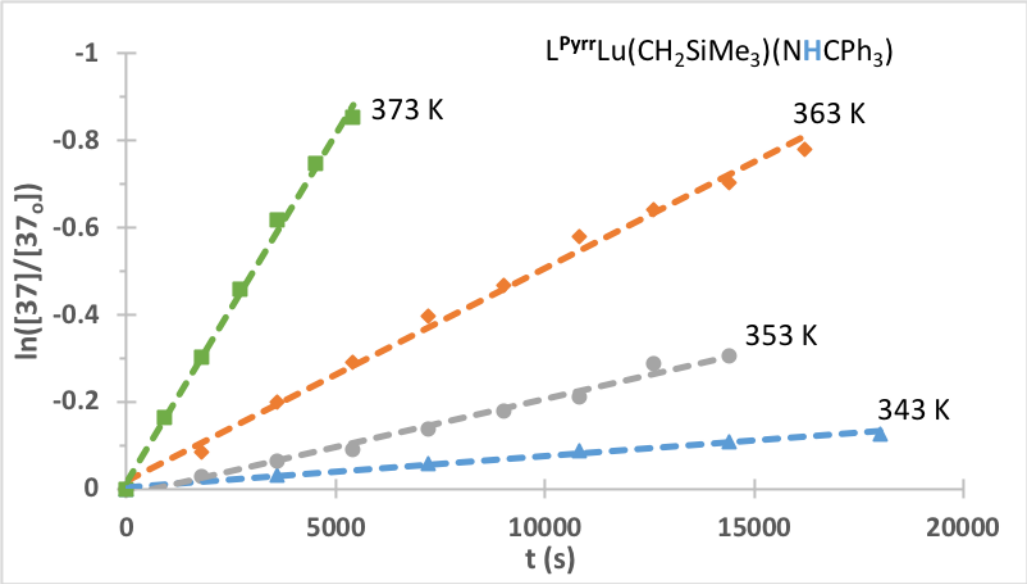

Figure 2.2 First Order Rate Constants for the Decomposition of Complex **37**.

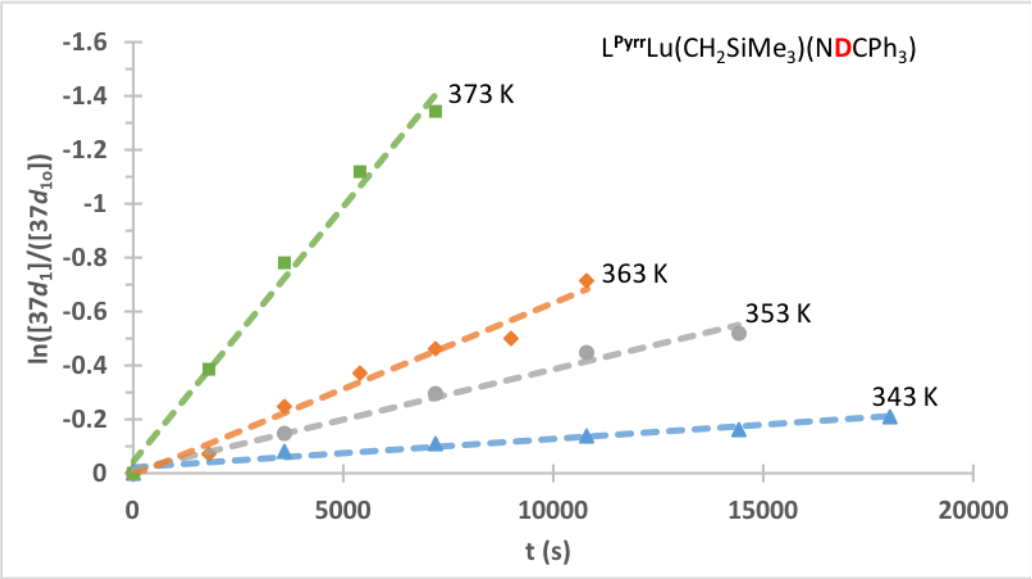

Figure 2.3 First Order Rate Constants for the Decomposition of Complex **37-*d*$_1$**.

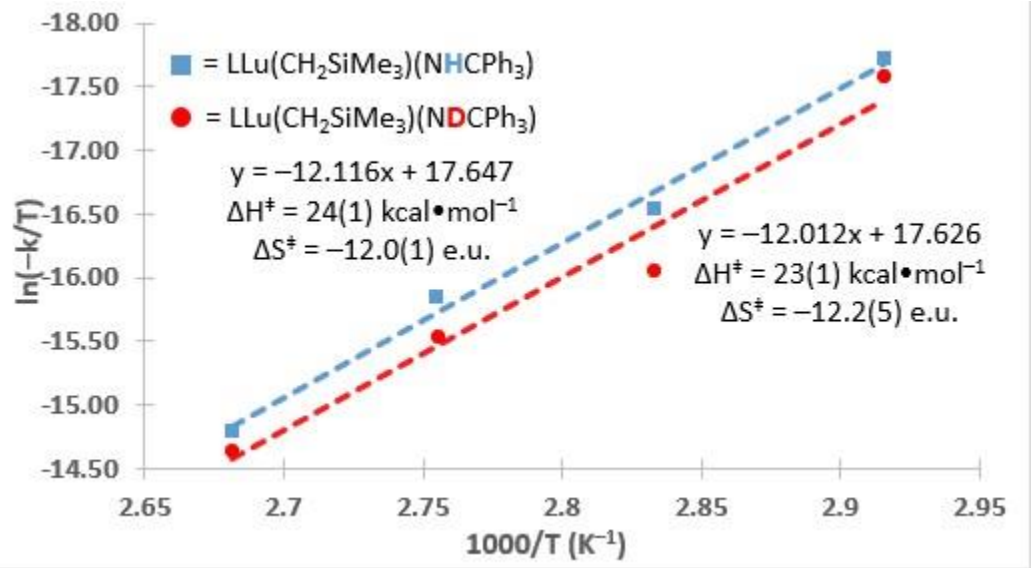

Figure 2.4 Eyring Plot Constructed from the Determined Rate Constants of the Decomposition of Complex **37** and **37-*d*$_1$**.

An Eyring plot was constructed from the obtained rate constants for the decomposition allowing for the extraction of the activation parameters $\Delta H^{\ddagger}$ = 24(1) kcal

mol^{-1} and $\Delta S^{\ddagger}$ = 140 J mol^{-1} (complex **37**), and $\Delta H^{\ddagger}$ = 22(1) kcal mol^{-1} and $\Delta S^{\ddagger}$ = 123 J mol^{-1} (complex **37-*d*$_1$**) for this transformation. Notably, these experimentally determined values closely match those determined computationally, described in section 2.8.4 of this thesis.

2.8 Comparison of Activation Parameters to Computational Analysis

2.8.1 Disclaimer

As mentioned in section 2.4, isolation of intermediate **45**, $L^{Ph}Lu(-\kappa^2\text{-}NHCPh_2C_6H_4)$, as a pure compound could not be achieved. Hence, it seemed prudent to corroborate our experimental data with computational studies. These analyses were performed by Dr. Mikko M. Hänninen, Dr. J. Mikko Rautiainen, and Dr. Heikki M. Tuononen at the University of Jyväskulä. Details of their findings are given here for comparative purposes to our experimental analysis and is used with permission from the authors.

2.8.2 Computational Methods

To alleviate computational demand the modelled system contained methyl substituents *in lieu* of P-phenyl groups. Also, the Pipp (4-^{i}PrC$_6$H$_4$) group was truncated to phenyl. Preliminary mapping of decomposition routes were performed with potential energy surface (PES) scans at the PBE0/SVP/SDD(Lu) level.[75-79] Final transition state and intermediate structures have been calculated at the PBE0/def2-TZVP/SDD(Lu) level of theory.[79-81]

2.8.3 Conformational Determination of $L^{Ph}Lu(CH_2SiMe_3)(NHCPh_3)$

Since a solid-state structure of $L^{Ph}Lu(CH_2SiMe_3)(NHCPh_3)$, **37**, was not available, initial work involved the construction of a conformation based on the solid state geometry of $L^{Ph}Lu(NHCPh_3)_2$, **44**, wherein one of the $NHCPh_3$ ligands was substituted with a CH_2SiMe_3 group. Notably, this procedure yielded two conformers shown in Figure 2.5, **37'**-G1 and **37'**-G2, that can interconvert by rotation of the amido and alkyl groups about the Lu–N and Lu–C bonds, respectively. The distinguishing difference between the two structures is the proximity of the CPh_3 group to the lutetium centre. According to calculations, the shortest distance from a C_{sp2}–H to the CH_2SiMe_3 methylene carbon in **37'**-G1 is only 3.349 Å, whereas in **37'**-G2 the corresponding distance is much longer, 4.491 Å. Hence, it is reasonable to expect that **37'**-G1 would be more prone to C–H bond activation and cyclometalation. Furthermore, the calculations indicate that **37'**-G1 is approximately 4 kcal mol^{-1} lower in energy than **37'**-G2. Given the energies of the **37'** conformations and their structural relationship, **37'**-G1 was used in the following analysis as a starting point for decompositions routes.

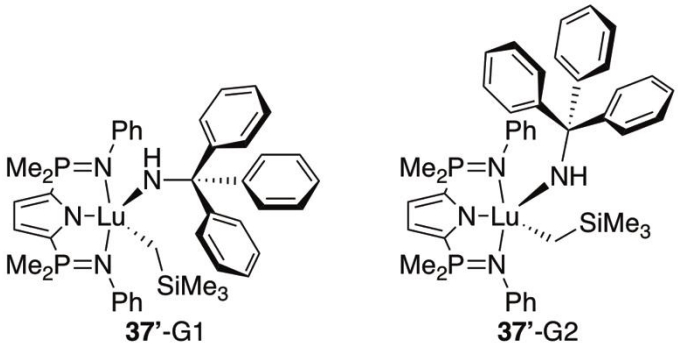

Figure 2.5 Computationally Determined Conformers (PBE0/def2-TZVP/SDD(Lu)) for the Starting Point of Calculations.

2.8.4 Results and Agreement with Experimental Data

Potential Energy Surface (PES) scans of pathway 1 for the formation of **41'**

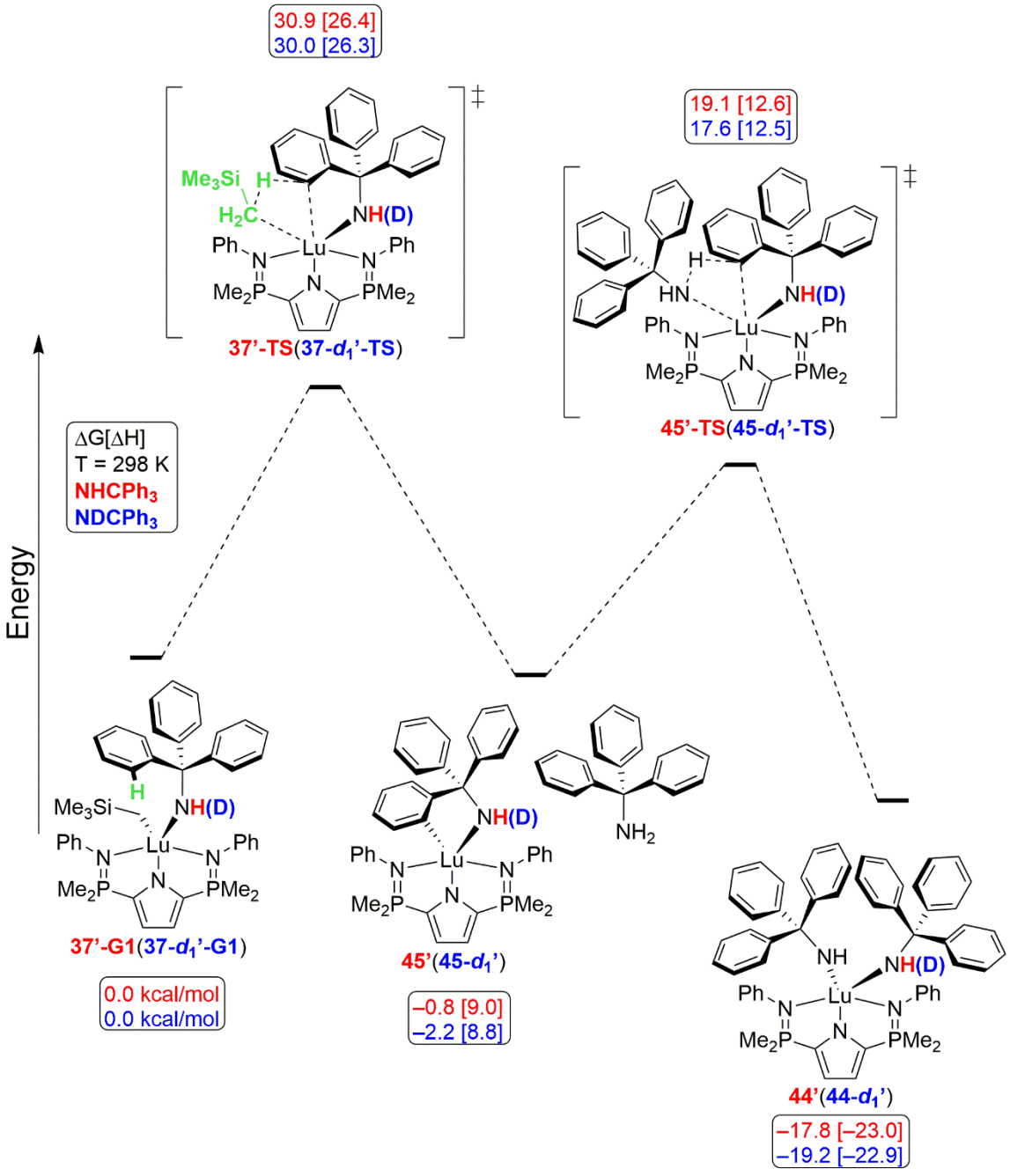

Figure 2.6 Energy Profile (PBE0/SVP/SDD(Lu)) of the Decomposition of Complex **37'**-G1.

($L^{Ph}Lu(NHCPh_3)_2$) from **37'**-G1, and subsequent optimizations, suggested a plausible seven-coordinate stationary point structure corresponding to the transition state **37'**-TS. The identity of the transition state (**37'**-TS) was confirmed by the sole imaginary vibration (–1221 cm^{-1}) corresponding to the proton transfer from an aromatic carbon to the methylene carbon. According to the calculations, the reaction is endothermic (ΔH = 9.0 kcal mol^{-1}) but slightly exergonic (ΔG = –0.8 kcal mol^{-1}) with an activation barrier of $\Delta G^{‡}$ = 30.9 kcal mol^{-1}. These results agree well with the experimental observation that cyclometalation of compound **37** occurs only after a prolonged period (24 hours) at high temperature (80 °C). The insignificant energy difference for the transition state with protio and deuterated amide ligands also supports the small kinetic isotope effect observed experimentally (*vide supra*).

2.9 Conclusions

A new lutetium complex, $L^{Ph}Lu(CH_2SiMe_3)(NHCPh_3)$, **37**, was created and its thermal decomposition into $L^{Ph}Lu(NHCPh_3)_2$, **44**, and reactivity with DMAP were studied. Tracking this reaction by $^{31}P\{^1H\}$ and ^1H NMR spectroscopy revealed the formation of the orthometalated intermediate $L^{Ph}Lu(\text{-}\kappa^2\text{-}NHCPh_2C_6H_4)$, **45**. A kinetic analysis suggested the resulting C_{sp2}–Lu bond was formed *via* direct C_{sp2}–H bond activation of the $NHCPh_3$ ligand, rather than undergoing an initial N–*H* bond cleavage. Further evidence for the N–*H* bond remaining intact was provided by the lack of d_1-$SiMe_4$ produced upon the decomposition of complex **37-*d*$_1$**, ruling out the formation of $L^{Ph}Lu{=}NCPh_3$, **46**, as a reaction intermediate. While the intermediates in this reaction are not isolable in high purity, computations agree with the experimentally suggested structure and mechanism of decomposition. Furthermore, addition of DMAP to a toluene solution of complex **37** does

not promote imido formation. The presence of DMAP induced a decomposition of complex **37** into $L^{Ph}Lu(NHCPh_3)_2$, **44**, and a myriad of unidentified by-products.

Chapter 3 – Lutetium Imido Precursors and Their Reactivity with DMAP (4-dimethylaminopyridine)

3.1 Overview

3.1.1 Previous Work and New Direction

HL^{Ph} was shown to support the thermally stable dialkyl complex $L^{Ph}Lu(CH_2SiMe_3)_2$, **36-Lu**. Protonolysis reactivity between Ph_3CNH_2 and complex **36-Lu** afforded the alkylamido complex $L^{Ph}Lu(CH_2SiMe_3)(NHCPh_3)$, **37**. Unfortunately, spontaneous C–H bond activation of the CPh_3 substituent was observed in solution, yielding a cloudy mixture which contained half an equivalent of the bisamido complex

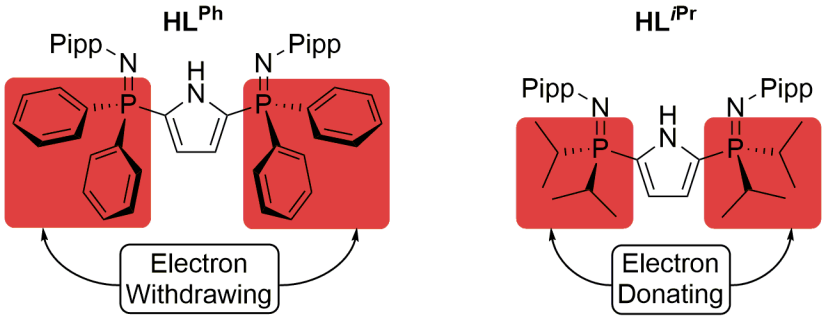

Figure 3.1 Substituent Alterations Made to the Ancillary Ligand.

$L^{Ph}Lu(NHCPh_3)_2$, **44**, and a myriad of unidentified byproducts. Given the thermal instability of complex **37**, alterations to the ancillary ligand were conducted in an attempt at creating thermally stable analogs of $L^{Ph}Lu(CH_2SiMe_3)(NHCPh_3)$. It was hypothesized that replacing the electron withdrawing substituents bound to the $P^{P=N}$ atoms (Ph) for electron donating groups (^{i}Pr) could assist in satiating the harsh electropositive demands of the lutetium metal centre. Thus, work targeting the new ancillary ligand, HL^{iPr} (HL^{iPr} = 2,5-$[P(^{i}Pr)_2N(Pipp)]_2C_4H_2NH$, Figure 3.1), was initiated.

3.1.1.1 Disclaimer

The synthesis of HL^{iPr} is work originally published by Connor S. MacNeil and Kayla E. Glynn.[82] The synthesis and discussion of HL^{iPr} presented in this thesis is given in order to provide full context for the work discussed within Chapter 3 of this thesis. Consent regarding the discussion of HL^{iPr} is given by all contributing authors.

3.1.2 Synthesis of HL^{iPr}

The synthesis of HL^{iPr} largely followed the literature procedure employed for the formation of HL^{Ph}, but PPh_2Cl was substituted by P^iPr_2Cl (Scheme 3.1).[55, 82] Addition of

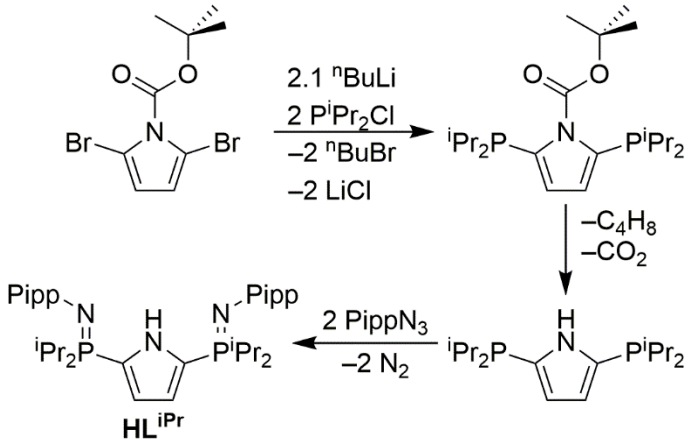

Scheme 3.1 Synthesis of HL^{iPr}.

electron donating substituents on the $P^{P=N}$ atoms resulted in a significant downfield change in the $^{31}P\{^1H\}$ NMR chemical shift of HL^{iPr} (δ 13.5) when compared to that of HL^{Ph} (δ –8.1). The ^1H NMR spectrum of HL^{iPr} revealed that the P–CH(CH_3)$_2$ protons are chemically inequivalent on the NMR timescale, and thus appeared as two distinct resonances with $^3J_{H–H}$ (7.0 Hz) and $^3J_{H–P}$ (13.4 Hz) coupling. A broad singlet (δ 10.4) was also seen in the ^1H NMR spectrum, typical for pyrrole N–H resonances the these pyrrole ligand systems.[55, 82]

3.1.3 X-ray Crystal Structure of HL^{iPr}

A sample of HL^{iPr} dissolved in a minimal amount of warm (50 ºC) heptane, which was allowed to cool to ambient temperature before being placed in a –35 ºC freezer for 18 hours, afforded X-ray quality crystalline material. HL^{iPr} was found to crystallize in the $P2_1/c$ space group, consistent with the previously published solid-state structure.[82] Despite resulting in a large $^{31}P\{^1H\}$ NMR chemical shift change ($\Delta\delta$ = 21.6), the implementation of P–^{i}Pr$_2$ functionalities did not have a dramatic effect on the phosphinimine bond lengths.

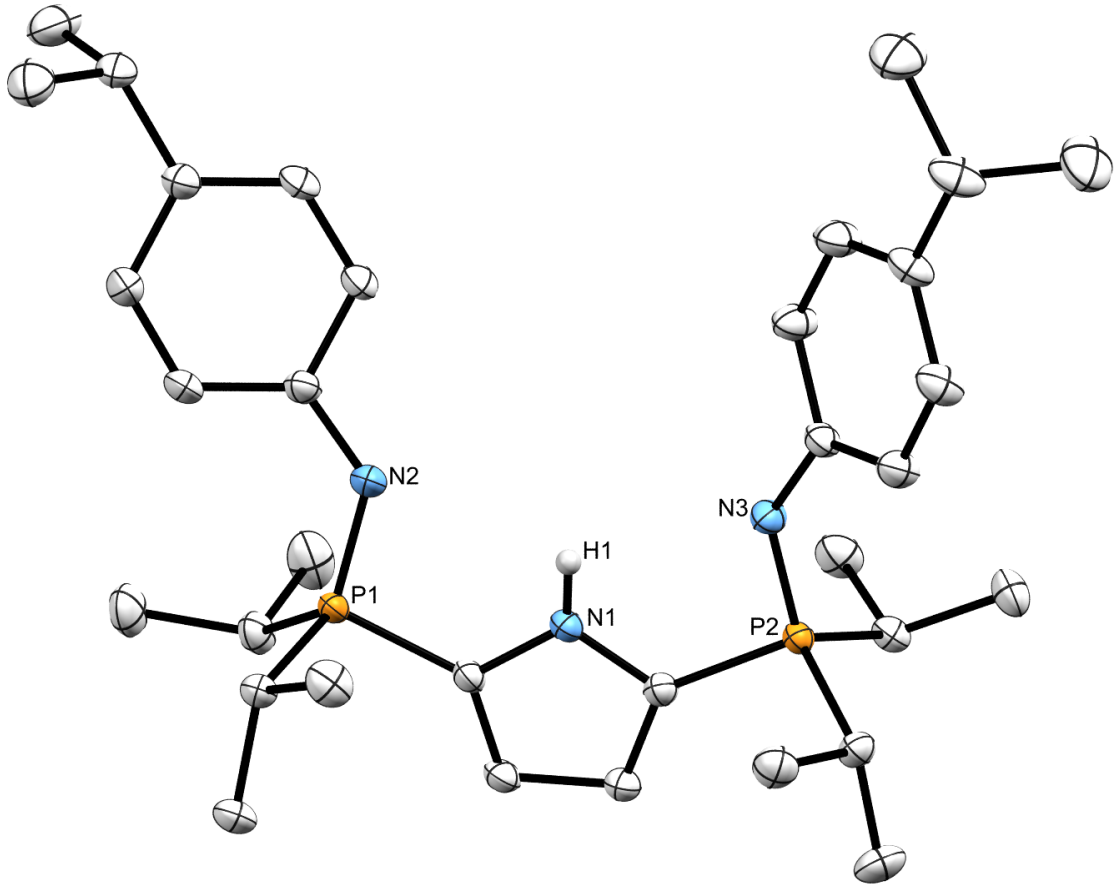

Figure 3.2 X-ray Crystal Structure (50% Probability Ellipsoids) of HL^{iPr}. Hydrogen Atoms (Except H1) are Omitted for Clarity.

Table 3.1 Selected Bond Lengths (Å) and Angles (°) for HL^{iPr} with HL^{Ph} Data Provided for Comparative Purposes.

Parameter	HL^{Ph}	HL^{iPr}
Selected Bond Lengths (Å)		
P1–N2	1.572(2)	1.567(1)
P2–N2	1.572(2)	1.574(1)
N1···N3a	2.851(3)	N/A
Selected Torsion Angles (º)		
N1–C1–P1–N2	23.3(3)	6.8(1)
N1–C4–P2–N3	54.6(3)	–17.7(1)

The P1–N2 and P2–N3 bond lengths in HL^{iPr} (1.567(1) Å and 1.574(1) Å, respectively) match closely to the reported values of HL^{Ph} (Table 3.1). Only a single equivalent of HL^{iPr} is seen in the crystal lattice with the N2 and N3 atoms residing in the same plane as the pyrrole ring (N1–C1–P1–N2: 6.8(1) º, N1–C4–P2–N3: –17.7(1) º). Conversely, only one $N^{P=N}$ atom of HL^{Ph} was found in the plane of the pyrrole ring (N1–C1–P1–N2: 23.3(3) º). The N3 atom was rotated away (N1–C4–P2–N3: 56.6(3) º) from this plane to accommodate the hydrogen bonding interaction observed between the two equivalents of HL^{Ph} found in the lattice.

3.1.4 Proposed Pathway to Rare Earth Terminal Imido Complexes

Reaction of HL^{iPr} with one equivalent of $RE(CH_2SiMe_3)_3(THF)_2$ (RE = Sc, Lu) was expected to yield the dialkyl complexes $L^{iPr}Sc(CH_2SiMe_3)_2$ (**39a**) and $L^{iPr}Lu(CH_2SiMe_3)_2$ (**39b**) (top reaction, Scheme 3.2). Upon their isolation, addition of primary amines to

complexes **39a** and **39b** was expected to create a series of rare earth alkylamido complexes of general formula $L^{iPr}RE(CH_2SiMe_3)(NHR)$ (**40a-d**, **40a**: RE = Sc, R = CPh_3, **40b**: RE = Sc, R = Dipp, **40c**: RE = Lu, R = CPh_3, **40d**: RE = Lu, R = Dipp, right, Scheme 3.2). The decision to utilize Ph_3CNH_2 was made in order to directly probe the effect of installing P–$^iPr_2$ substituents.

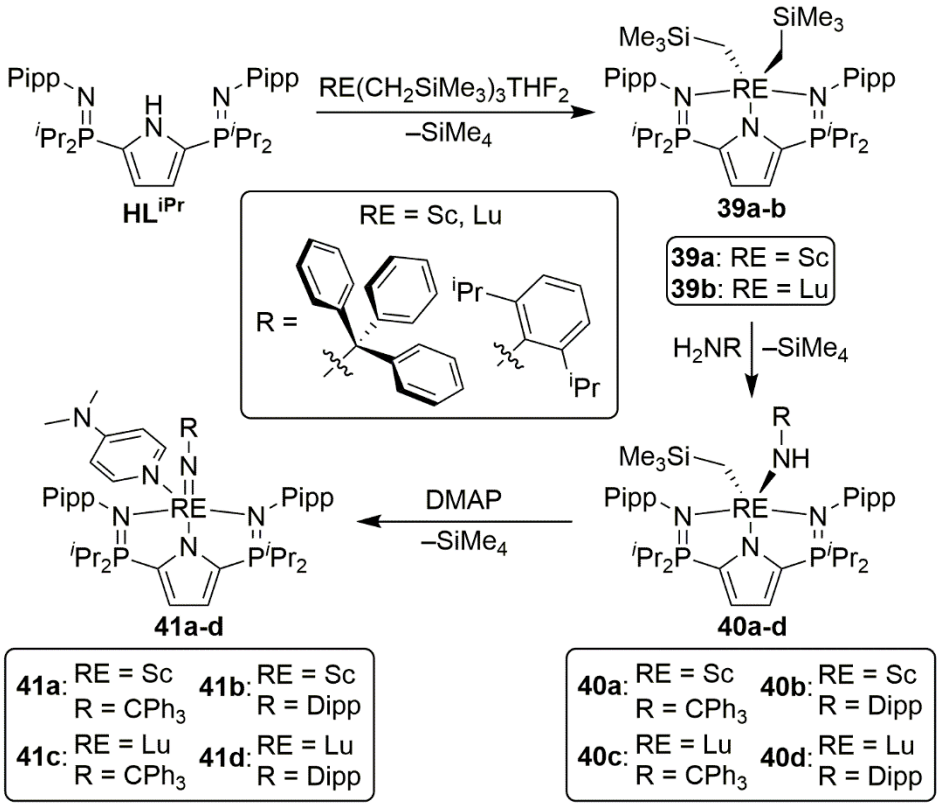

Scheme 3.2 Proposed Synthesis for a Series of Terminal Rare Earth Imido Complexes.

Employing $DippNH_2$ would allow for the synthesis of aromatic analogs of complexes **40a** and **40c**, which would facilitate direct comparisons regarding the effect that aromaticity had on rare earth terminal imido formation. Addition of DMAP to complexes **40a-d** is proposed to yield a family of terminal rare earth imido complexes of general formula $L^{Ph}RE{=}NR(DMAP)$ (**41a-d**, bottom, Scheme 3.2).

3.2 Synthesis of $L^{iPr}Sc(CH_2SiMe_3)_2$ and $L^{iPr}Lu(CH_2SiMe_3)_2$

Isolation of the rare earth dialkyl complexes $L^{iPr}RE(CH_2SiMe_3)_2$ (RE = Sc, Lu), **39a** and **39b**, respectively, was achieved by reaction of HL^{iPr} with $RE(CH_2SiMe_3)_3(THF)_2$ in toluene for 1 hour, followed by removal of all volatiles *in vacuo*. Production of both $L^{iPr}Sc(CH_2SiMe_3)_2$ and $L^{iPr}Lu(CH_2SiMe_3)_2$ were supported by the appearance of 1 equivalent of $SiMe_4$ (δ 0.00) in the ^1H NMR spectra. Additionally, the emergence of a single resonance in the $^{31}P\{^1H\}$ NMR spectra (**39a**: δ 47.98, **39b**: δ 49.29) was observed with simultaneous consumption of the resonance assigned to HL^{iPr} (δ 13.5). Additionally, in the ^1H NMR spectra, complete consumption of the N–*H* resonance (δ 10.4) was observed. As witnessed previously with this ligand,[82] the P–(CH(C*H*$_3$)$_2$)$_2$ (**39a**: δ 0.93, 0.88, **39b**: δ 0.96, 0.85) protons are chemically inequivalent on the NMR time scale. Like the analogous complex supported by our previous generation ligand, $L^{Ph}Lu(CH_2SiMe_3)_2$, no C–H bond activation was observed when compound **39a** or **39b** were heated to 60 °C in C_6D_6 for 48 hours.[55]

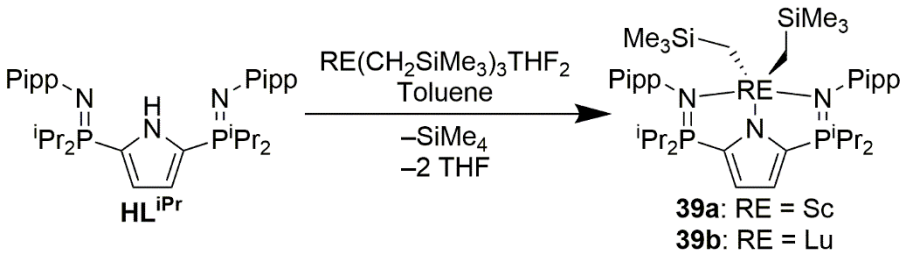

Scheme 3.3 Synthesis of Complexes **39a** and **39b**.

3.2.1 X-ray Crystal Structures of $L^{iPr}Sc(CH_2SiMe_3)_2$ and $L^{iPr}Lu(CH_2SiMe_3)_2$

Single crystals suitable for X-ray diffraction analysis of both complexes **39a** and **39b** were obtained at ambient temperature from a warm (50 °C), saturated heptane solution.

Both complexes **39a** and **39b** crystallized in the $P2_1/n$ space group. The geometry about each metal centre is best described as distorted square pyramidal ($\tau^5 = 0.37$ (**39a**), $\tau^5 = 0.31$ (**39b**)). The solid-state structures revealed that $L^{iPr}Sc(CH_2SiMe_3)_2$ exhibited an average shortening of 0.117 Å in the RE1–C35, RE1–C39, and RE1–N1 bond distances compared to $L^{iPr}Lu(CH_2SiMe_3)_2$, explainable by the difference in ionic radii between the two elements (0.116 Å). Additionally, the phosphinimine bond lengths are identical at the 95% confidence level in both structures (1.619(2) Å, **39a**, 1.611(3) Å, **39b**). Complex **39b** possessed identical (95% confidence level) P=N bond lengths compared to the previously published complexes $L^{Ph}Sc(CH_2SiMe_3)_2$, $L^{Ph}Y(CH_2SiMe_3)_2$, $L^{Ph}Lu(CH_2SiMe_3)_2$, and $L^{Ph}Er(CH_2SiMe_3)_2$, (1.606(4) – 1.610(3) Å).[55, 58, 64]

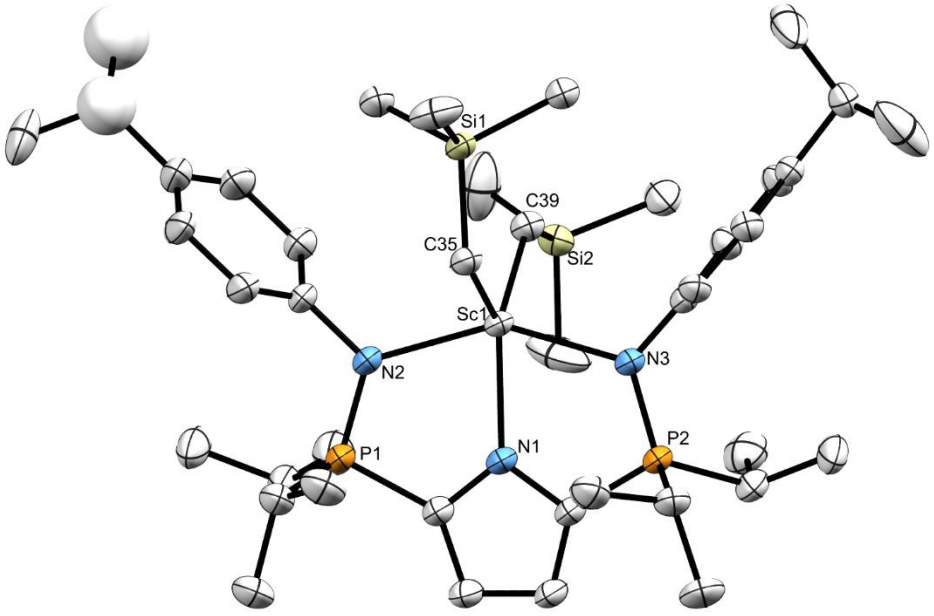

Figure 3.3 X-ray Crystal Structure (50% Probability Ellipsoids) of Complex **39a**. Hydrogen Atoms are Omitted for Clarity.

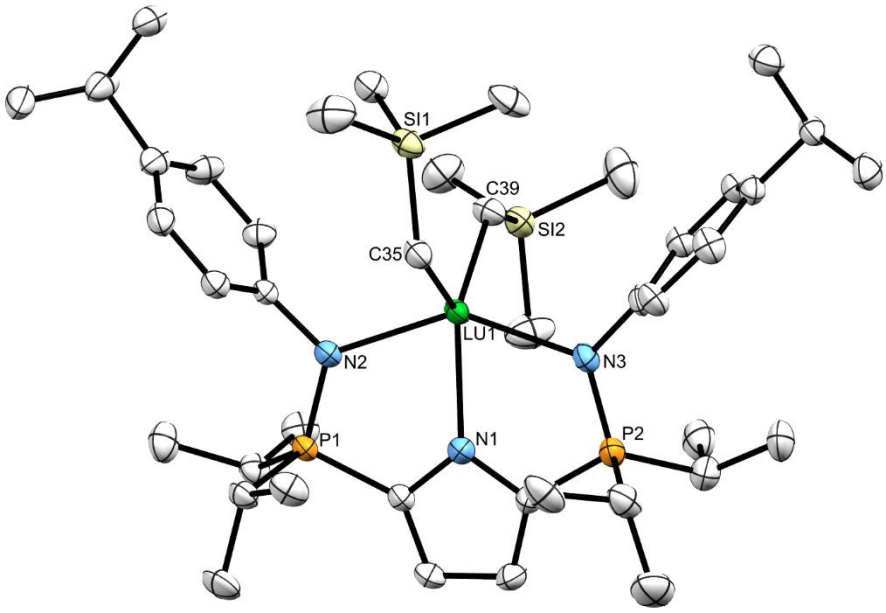

Figure 3.4 X-ray Crystal Structure (50% Probability Ellipsoids) of Complex **39b**.

Hydrogen Atoms are Omitted for Clarity.

Table 3.2 Selected Bond Lengths (Å) and Angles (°) for Complexes **39a** and **39b**.

Parameter	**39a (Sc)**	**39b (Lu)**
Selected Bond Lengths (Å)		
RE1–C35	2.249(2)	2.360(4)
RE1–N1	2.195(2)	2.305(2)
P1–N2	1.619(2)	1.611(3)
Selected Bond Angles (°)		
C35–RE1–C39	109.89(8)	112.1(1)
N2–RE1–N3	149.12(7)	143.79(9)
N1–RE1–C35	123.02(8)	125.0(1)
N1–RE1–C39	127.13(8)	122.9(1)

3.3 Formation of Lutetium Terminal Imido Precursors

3.3.1 Reactivity of $L^{iPr}Sc(CH_2SiMe_3)_2$

3.3.1.1 Reactivity of $L^{iPr}Sc(CH_2SiMe_3)_2$ with Primary Amines

In order to probe the impact the P–$^{i}Pr_2$ substituents have on the these pincer ligands, complex **39a** was exposed to one equivalent of a primary amine (Ph_3CNH_2, $DippNH_2$, $AdNH_2$, or Mes^*NH_2 (Mes* = 2,4,6-$^{t}Bu_3C_6H_2$)). Unfortunately, complex **39a** did not react with neither Ph_3CNH_2, $DippNH_2$, nor Mes^*NH_2 after being heated to 70 ºC for 24 hours.

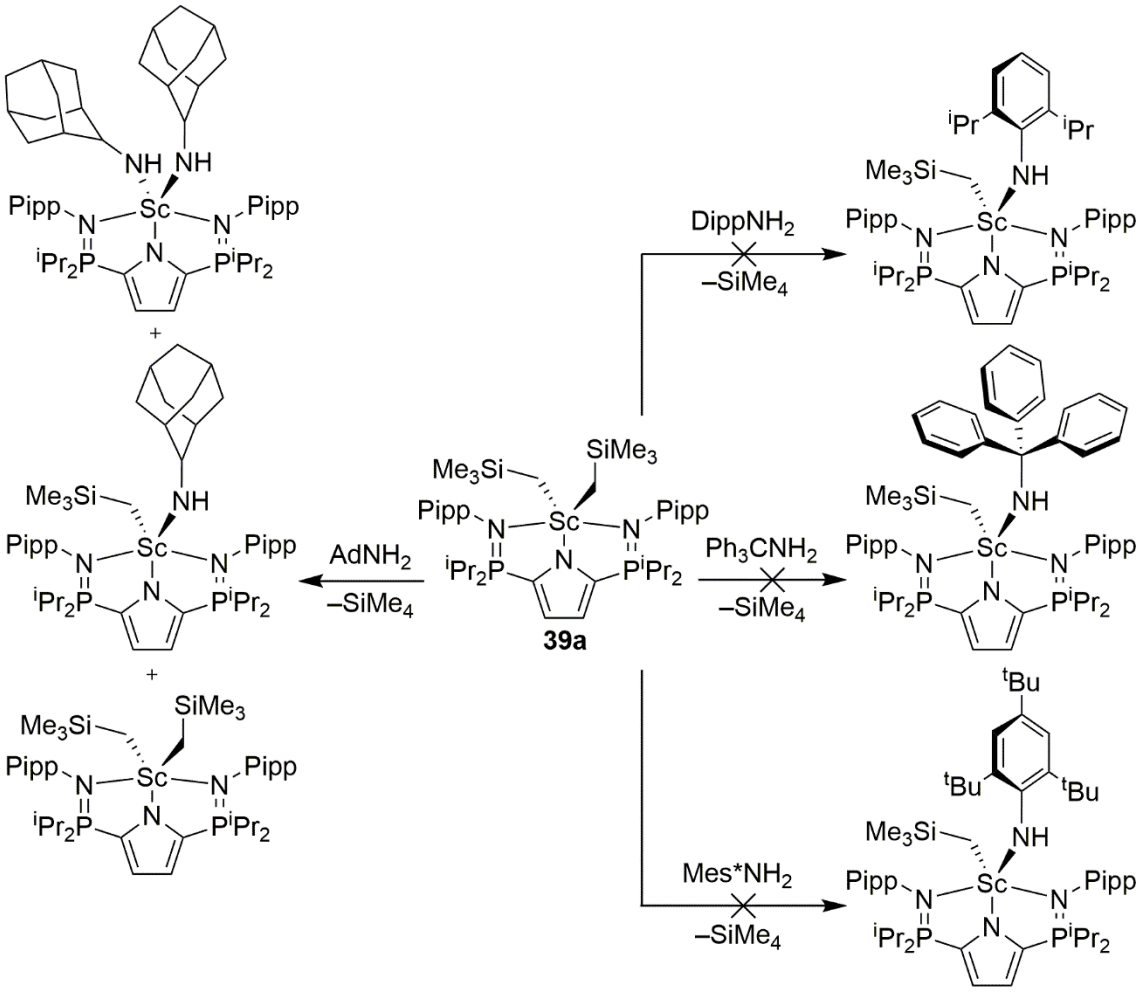

Scheme 3.4 Reactivity of Complex **39a** with Primary Amines.

However, slow, cold addition of 1-adamantylamine ($AdNH_2$) to one equivalent of compound **39a** promoted formation of an inextricable mixture of $L^{iPr}Sc(CH_2SiMe_3)_2$, $L^{iPr}Sc(CH_2SiMe_3)(NHAd)$, and $L^{iPr}Sc(NHAd)_2$ (Scheme 3.4).

3.3.1.2 Reactivity of $L^{iPr}Sc(CH_2SiMe_3)_2$ with $B(C_6F_5)_3$

A cationic scandium complex was created by the addition of $B(C_6F_5)_3$ to complex **39a** in pentane at –35 ºC. The corresponding ion pair immediately precipitated from solution. Filtering the precipitate yielded the product, $[L^{iPr}Sc(CH_2SiMe_2CH_2SiMe_3)][H_3CB(C_6F_5)_3]$ (**47**, Scheme 3.5) as a snow-white solid. A new resonance in the $^{31}P\{^1H\}$ NMR spectrum (δ 55.69), which ultimately comprised 90% of the phosphorus-containing material, emerged with concomitant disappearance of the signal corresponding to complex **39a** (δ 47.96). Evidence of the formation of the $CH_2SiMe_2CH_2SiMe_3$ alkyl group possessed by complex **47** was provided in the ^1H NMR spectrum in which four alkyl resonances (δ 0.07, –0.16, –0.19, –0.32) were present in a 9 : 2 : 6 : 2 ratio. Additional evidence for the abstraction of a CH_3 group is given by the observed B–C*H*$_3$ resonance (δ 1.20). This peak is similar to the chemical shift reported for the free $[H_3CB(C_6F_5)_3]^-$ anion (δ 1.13), indicating a weakly coordinating anion with minor $Sc^{+\cdots}H_3C$–B interactions.[83] Three distinct peaks were observed in the $^{19}F\{^1H\}$ NMR

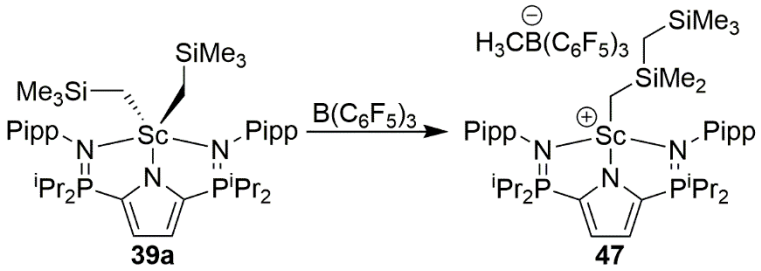

39a **47**

Scheme 3.5 Formation of Complex **47**.

spectrum (δ –130.33, –160.59, –163.37), the Δδ(*m*,*p*-F) of which (2.7 ppm) was also consistent with a weakly coordinating anion.[83] In addition, there was a single resonance in the $^{11}B\{^{1}H\}$ NMR spectrum (δ –14.42). Taken together, this data suggested the formation of a weakly coordinated, four-coordinate borate anion ($H_3CB(C_6F_5)_3$) and the corresponding scandium cation ($L^{iPr}ScCH_2SiMe_2CH_2Me_3$). Unfortunately, exhaustive efforts to crystallize complex **47** were unsuccessful.

3.3.1.3 Possible Formation of $[L^{iPr}Sc(CH_2SiMe_2CH_2SiMe_3)][H_3CB(C_6F_5)_3]$

Abstraction of a CH_3 substituent bound to a rare earth metal *via* addition of $B(C_6F_5)_3$ has been reported in the literature.[25, 84-88] However, only one example of such abstraction resulting in the formation of a $CH_2SiMe_2CH_2SiMe_3$ alkyl group has been

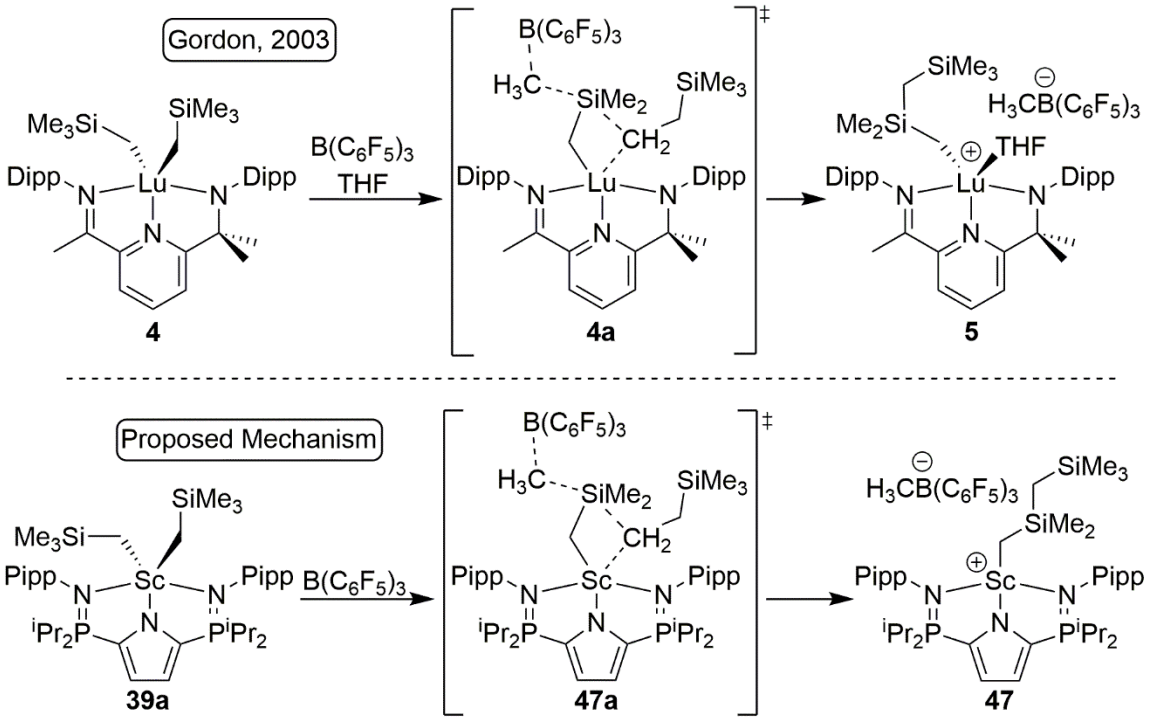

Scheme 3.6 Proposed Intermediate in the Formation of Complex **66**.

reported for a rare earth metal (mentioned in section 1.3.2). In this 2003 report by Gordon, one equivalent of $B(C_6F_5)_3$ was added to $L^{Gordon}Lu(CH_2SiMe_3)_2$, L^{Gordon} = [2-(DippN=CMe)-6-(DippNCMe$_2$)]C_6H_3N, (**4**, Scheme 3.6).[25] While not spectroscopically supported, the CH_3 abstraction is described to go through a concerted intermediate (**4a**, Scheme 3.6) which involved a CH_3 abstraction accompanied with an alkyl migration.[25] As such, it seems reasonable that the reaction of complex **39a** and one equivalent of $B(C_6F_5)_3$ proceeded through a similar intermediate (**47a**, Scheme 3.6).

3.3.2 Reactivity of $L^{iPr}Lu(CH_2SiMe_3)_2$

Addition of either Ph_3CNH_2 or $DippNH_2$ to one equivalent of compound **39b** gave rise to complexes **40c**, $L^{iPr}Lu(CH_2SiMe_3)(NHCPh_3)$, and **40d**, $L^{iPr}Lu(CH_2SiMe_3)(NHDipp)$, respectively (Scheme 3.7). As expected, 1 equivalent of $SiMe_4$ (δ 0.00) was released from both reaction mixtures *via* the ^1H NMR spectra. Furthermore, a sharp singlet integrating for 1 H, which did not give rise to cross peaks in either ^1H–^1H COSY or ^1H–^{13}C HSQC experiments, emerged (δ 2.43 (**40c**), δ 4.14 (**40d**)). This peak was assigned as the N–H resonance. Installation of the $NHCPh_3$/NHDipp ligand resulted in loss of C_{2v} symmetry in complexes **40c** and **40d**, generating two sets of P–

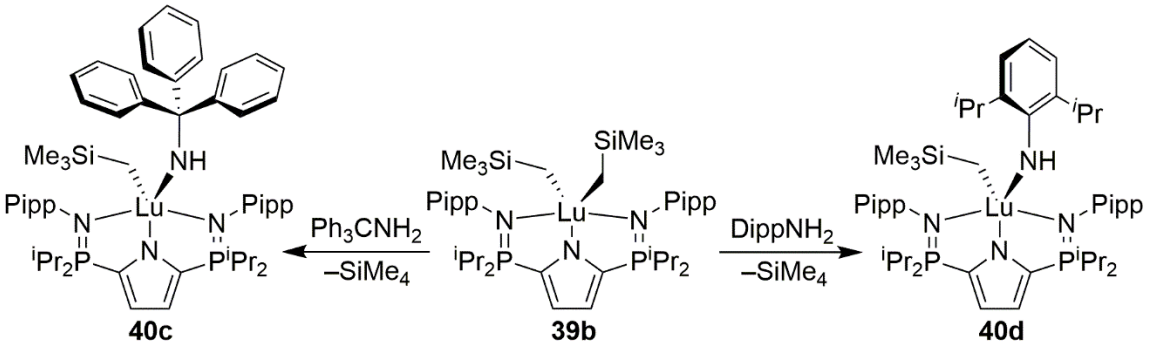

Scheme 3.7 Synthesis of Complexes **40c** and **40d**.

($C\mathit{H}(CH_3)_2)_2$ resonances in the ^{1}H NMR spectrum of compound **40c** (δ 2.16, 1.75) and **40d** (δ 2.26, 1.93). Further evidence for the formation of compounds **40c** and **40d** was provided by the disappearance of the singlet corresponding to complex **39b** in the $^{31}P\{^1H\}$ spectrum (δ 49.29) and the emergence of one new signal (δ 47.85, **40c**, *δ* 48.69, **40d**).

After 24 hours in solution at ambient temperature, no decomposition of either complex **40c** or **40d** was detected by ^{1}H or $^{31}P\{^1H\}$ NMR spectroscopy. To further test the thermal stability of compounds **40c** and **40d**, samples of each were heated to 70 ºC for 72 hours, after which the ^{1}H and ^{31}P NMR spectra were recorded. Remarkably, no decomposition was observed.

3.3.3 X-ray Crystal Structures of $(L^{iPr}Lu(CH_2SiMe_3)(NHCPh_3))_2 \bullet C_7H_{16}$ and $L^{iPr}Lu(CH_2SiMe_3)(NHDipp)$

A minimal amount of warm (50 ºC) heptane was used to produce a saturated solution of either compound **40c** or **40d**. The resulting solution was allowed to cool to ambient temperature before being placed in a –35 ºC freezer for 18 hours, yielding X-ray quality crystalline material. The geometry at the lutetium metal centres in complexes **40c** and **40d** is best described as distorted square (τ^5 = 0.15 (**40c**) τ^5 = 0.12 (**40d**)) with the four nitrogen atoms forming the square base. Compound **40c** crystallized with 2 molecules in the asymmetric unit. The Lu1–C35 bond lengths of complexes **40c** (2.342(3) Å) and **40d** (2.313(5) Å) are marginally shorter than the Lu–C distances observed in $L^{iPr}Lu(CH_2SiMe_3)_2$ (Lu1–C35: 2.360(4) Å, Lu1–C39: 2.366(4) Å). The phosphinimine bond lengths of both complexes **40c** and **40d** displayed no significant change.

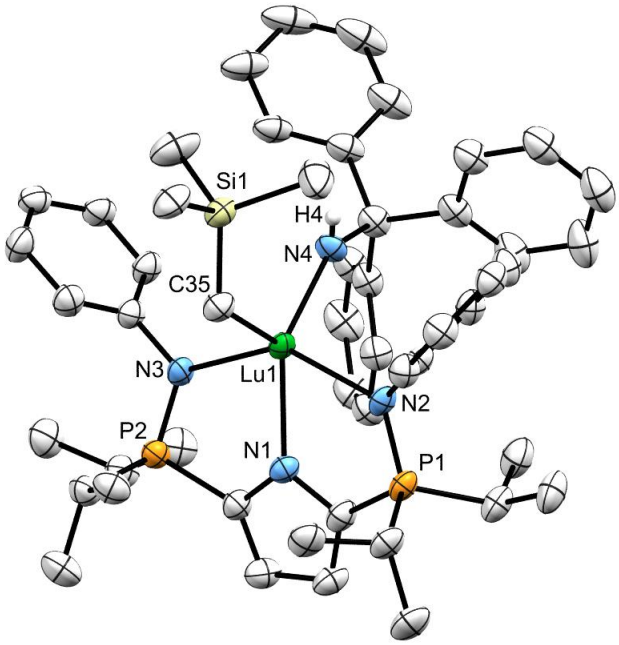

Figure 3.5 X-ray Crystal Structure (50% Probability Ellipsoids) of Complex **(40c)$_2$•C$_7$H$_{16}$**

. Hydrogen (Except H4) and Pipp-^{i}Pr Atoms have been Omitted for Clarity.

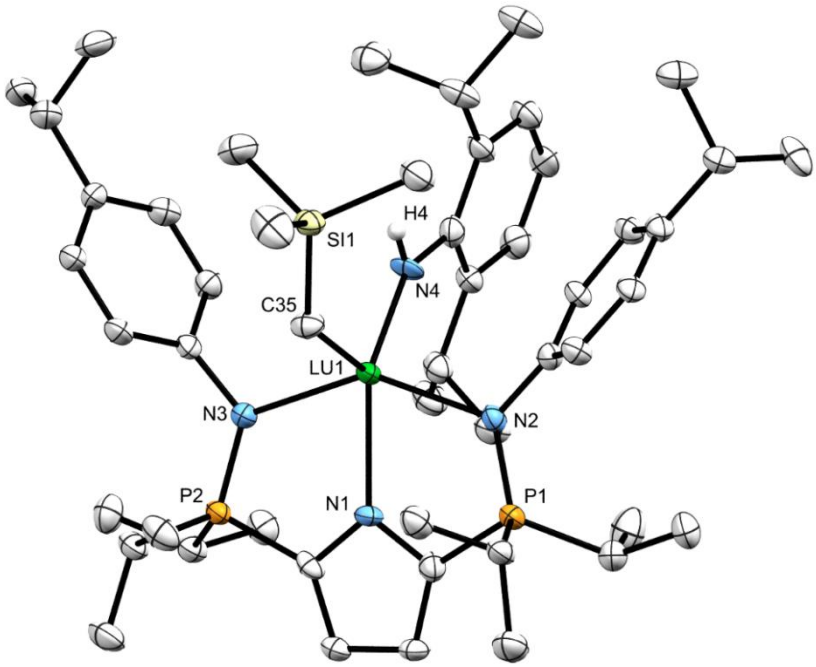

Figure 3.6 X-ray Crystal Structure (50% Probability Ellipsoids) of Complex **40d**.

Hydrogen Atoms (Except H4) have been Omitted for Clarity.

3.3.3.1 Comparisons to Literature Lutetium Alkylamido Compounds

To the best of my knowledge, complexes **42a** ($L^{Anwander}Lu(CH_3)(NHAd)$), **42b** ($L^{Anwander}Lu(CH_3)(NH^tBu)$), and **44** ($L^{Ph}Lu(NHCPh_3)_2$) represent the only reported lutetium complexes characterized by X-ray crystallography that possess an amido ligand bearing a non-aromatic substituent.[52, 64, 67] These Lu–NHR (R = non-aromatic) bond distances range from 2.126(2) Å to 2.144(2) Å.[52, 64, 67] Complex **40c** possesses a comparable Lu–$NHCPh_3$ bond length of 2.154(2) Å. Conversely, numerous examples of lutetium complexes bearing an aromatic amide ligand. [51, 57, 71-74] Thus, a wide range of Lu–NHAr bond lengths (2.144(3) – 2.245(4) Å) are available for comparison.[51, 57, 71-74] The

Table 3.3 Selected Bond Lengths (Å) and Angles (°) for Complexes **40c** and **40d** with Complexes **42a** and **42b** Given for Comparative Purposes.

Parameter	40c	40d	42a	42b
Selected Bond Lengths (Å)				
RE1–C35	2.344(2)	2.313(5)	2.371(2)	2.362(3)
RE1–N4	2.154(2)	2.195(5)	2.128(2)	2.126(2)
P1–N2	1.617(2)	1.625(5)	N/A	N/A
RE1–N1	2.323(2)	2.283(5)	N/A	N/A
Selected Bond Angles (º)				
N2–RE1–N3	142.9(1)	145.3(2)	N/A	N/A
N1–RE1–C35	119.65(2)	111.1(2)	N/A	N/A
N4–RE1–C35	105.3(1)	110.5(2)	92.81(9)	95.19(8)
N1–RE1–N4	135.0(1)	138.4(2)	N/A	N/A

Lu1–N4 distance in complex **40d** (2.195(5) Å) falls in the middle of this range. Notably, the Lu1–N4 contact in complex **40c** is slightly shorter than that of complex **40d** (2.195(5) Å, **40d**, 2.154(2) Å, **40c**) despite the bulky $NHCPh_3$ group.

3.4 Reaction of $L^{iPr}Lu(CH_2SiMe_3)(NHCPh_3)$ and $L^{iPr}Lu(CH_2SiMe_3)(NHDipp)$ with DMAP

3.4.1 Reaction of $L^{iPr}Lu(CH_2SiMe_3)(NHCPh_3)$ with DMAP

Reaction of complex **40c** with 1 equivalent of DMAP promoted slow conversion (12% of compound **40c** consumed in 68 hours) to a new product that exhibited a single resonance in the $^{31}P\{^1H\}$ NMR spectrum (δ 45.3). Another 12 hours at ambient temperature made no significant change to the product distribution. Heating this sample to 60 ºC for 93 hours produced a dark brown, cloudy solution. This mixture contained multiple resonances in the $^{31}P\{^1H\}$ NMR spectrum, with a major new peak (δ 45.3) being formed (47% of phosphorus-containing materials in solution).

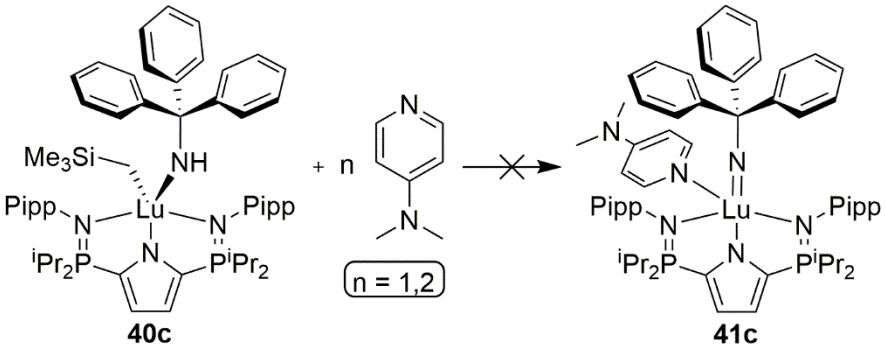

Scheme 3.8 Reactivity of Complex **40c** with DMAP.

Repeating this experiment at 45 °C also resulted in the formation of a similar dark brown, cloudy solution. The $^{31}P\{^1H\}$ NMR spectrum of which revealed multiple

resonances, similar to the distribution witnessed at 60 ºC; the resonance at δ 45.3 was again the major product formed (25% of the phosphorus-containing material in solution).

The reaction between complex **40c** and 2 equivalents of DMAP at 45 ºC resulted in extremely slow consumption of compound **40c** (40% consumed after 4 days), along with concomitant formation of familiar ^{31}P resonance (δ 45.3). A number of other products, consistent with those observed in the equimolar reaction of complex **40c** and DMAP, were also present in the $^{31}P\{^{1}H\}$ NMR spectrum.

3.4.2 Reaction of $L^{iPr}Lu(CH_2SiMe_3)(NHDipp)$ with DMAP

Exposure of complex **40d** to 1 equivalent of DMAP at 45 ºC for 22.5 hours resulted in 20% consumption of compound **40d** and formation of one major product (δ 46.4) in the $^{31}P\{^{1}H\}$ NMR spectrum. Further heating (83.5 hours) resulted in a murky brown solution. The $^{31}P\{^{1}H\}$ NMR spectrum revealed that 60% of compound **40d** had been consumed and the new resonance (δ 46.4) accounted for 25% of the phosphorus-containing materials. A second major resonance, which accounted for 21% of the phosphorus-containing material formed (δ 44.2) as well as a variety of by-products.

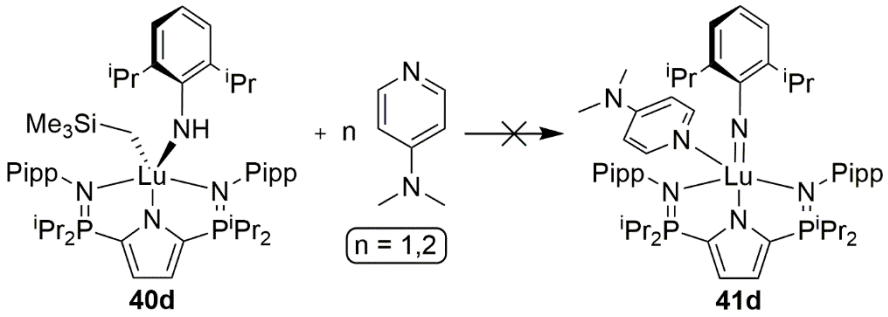

Scheme 3.9 Reactivity of Complex **40d** with DMAP.

Complex **40d** was also reacted with 2 equivalents of DMAP at 45 ºC. After 18 hours the $^{31}P\{^{1}H\}$ NMR spectrum revealed 33% of complex **40d** had been consumed and 1 major product (δ 46.4) accounted for 25% of the material in the $^{31}P\{^{1}H\}$ NMR spectrum. Heating this sample for an additional 145.5 hours left only a small amount of compound **40d** in solution. Similar to the equimolar reaction, the resonance at δ 46.4 was still the dominant product (43% of phosphorus-containing materials).

3.4.3 Comparison of Both Reactions

The ^{1}H NMR spectra of the reaction between either complex **40c** or **40d** with DMAP revealed several commonalities. The chemical shifts of DMAP (δ 8.45, 6.07, 2.21) indicated the Lewis base was not coordinated to the metal centre. Approximately 1 equivalent of $SiMe_4$ was extruded (δ 0.00), and there was no evidence for the retention of any CH_2SiMe_3 groups. The major product in formed in each reaction possessed one P–(C*H*$(CH_3)_2)_2$ resonance. Taken in conjunction with the single $^{31}P\{^{1}H\}$ signal produced (**40c** + DMAP: δ 45.3, **40d** + DMAP: δ 46.4), the major product formed in these reactions was seen to possess C_{2v} symmetry. Furthermore, in each reaction a singlet (**40c** + DMAP: δ 2.26, **40d** + DMAP: δ 4.38) which had no cross-peaks in ^{1}H–^{1}H COSY experiments emerged. Diagnostic aromatic resonances pertaining to the $NHCPh_3$ ligand were retained throughout the reaction of complex **40c** and DMAP, eventually doubling their expected integration value. Similarly, the isopropyl doublet and septet resonances pertaining to the NHDipp ligand were retained throughout the reaction of complex **40d** and DMAP, eventually doubling their original integration values (with respect to DMAP). Taken altogether, the data suggests that the bis-amide complexes, $L^{iPr}Lu(NHCPh_3)_2$ (**48c**) and

$L^{iPr}Lu(NHDipp)_2$ (**48d**) were formed when DMAP was added to complexes **40c** and **40d**, respectively.

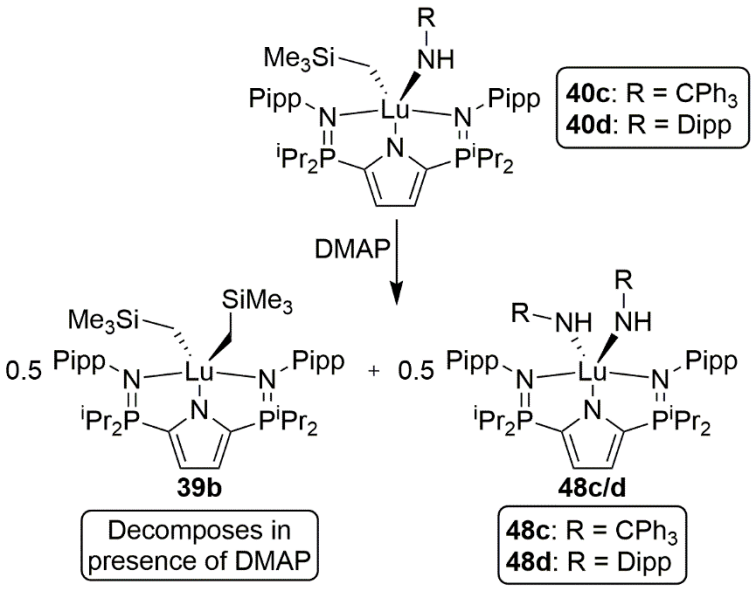

Scheme 3.10 Observed Disproportionation Reaction Between Complexes **40c** and **40d** with DMAP.

In 2004 Piers reported the thermal decomposition of the scandium alkylamido complex $L^{Nacnac}Sc(NH^tBu)(CH_3)$ (L^{Nacnac} = $DippNC(CH_3)CHC(CH_3)NDipp$).[44] Upon being heated to 100 ºC $L^{Nacnac}Sc(NH^tBu)(CH_3)$ underwent a disproportionation reaction yielding half an equivalent of both $L^{Nacnac}Sc(NH^tBu)_2$ and $L^{Nacnac}Sc(CH_3)_2$, the latter of which decomposed upon formation. A Lewis base induced disproportionation reaction also seemed to be a logical pathway for our systems, except no evidence for the formation of $L^{iPr}Lu(CH_2SiMe_3)_2$ was observed in the ^1H or $^{31}P\{^1H\}$ spectra throughout the reactions between complexes **40c** or **40d** and DMAP. However, heating (60 ºC) a sample of $L^{iPr}Lu(CH_2SiMe_3)_2$ (**39b**) and one equivalent of DMAP resulted in decomposition and production of numerous compounds that closely matched the product distribution produced

when DMAP was reacted with either compound **40c** or **40d**. It should be stated that this result was unexpected, as $L^{iPr}Lu(CH_2SiMe_3)_2$ was shown to be stable in solution (section 3.2).

3.5 Independent Synthesis of $L^{iPr}Lu(NHCPh_3)_2$ and $L^{iPr}Lu(NHDipp)_2$

While attempts at isolating $L^{iPr}Lu(NHCPh_3)_2$ (**48c**) and $L^{iPr}Lu(NHDipp)_2$ (**48d**) directly from the crude reaction mixture were unsuccessful, independent synthesis of complexes **48c** and **48d** was achieved by addition of 2 equivalents of Ph_3CNH_2 or $DippNH_2$, respectively, to a stirring toluene solution of $L^{iPr}Lu(CH_2SiMe_3)_2$. Heat (60 ºC), and additional time (69 hours) was required to synthesize compound **48c**, while complex **48d** was prepared in only 24 hours at ambient temperature. Characterization of $L^{iPr}Lu(NHCPh_3)_2$ (**48c**) and $L^{iPr}Lu(NHDipp)_2$ (**48d**) gave ^1H and $^{31}P\{^1H\}$ NMR spectra consistent with the major product formed in the reaction of DMAP with complexes **40c** and **40d**. In order to confirm that compounds **48c** and **48d** were a product in this reaction, and not merely a long-lived intermediate, a sample of $L^{iPr}Lu(NHDipp)_2$ was exposed to 2 equivalents of DMAP at 60 °C; no reaction was observed over 48 hours.

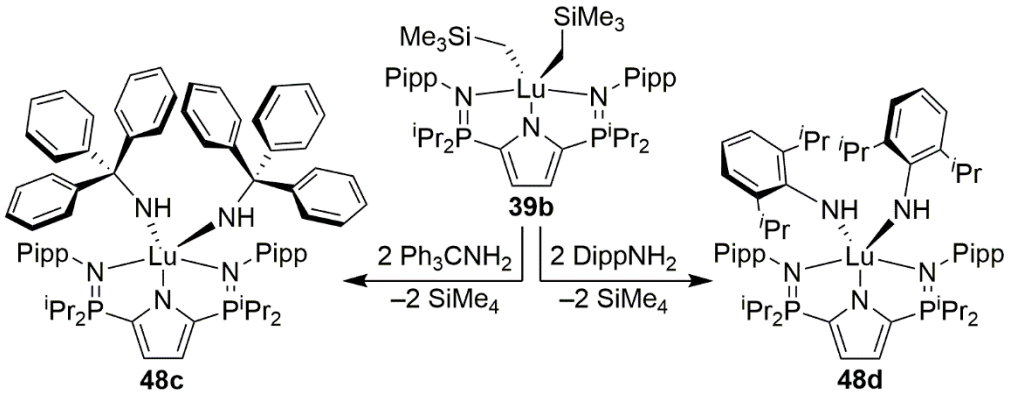

Scheme 3.11 Independent Synthesis of Complexes **48c** and **48d**.

3.5.1 X-ray Crystal Structures of $L^{iPr}Lu(NHCPh_3)_2$ and $L^{iPr}Lu(NHDipp)_2$

X-ray quality crystals of complexes **48c** and **48d** were grown at ambient temperature from a saturated solution of warm (50 ºC) heptane. Like complexes **40c** and **40d**, the geometry of complex **48c** is best described as slightly distorted square planar (τ^5 = 0.19). The square planar geometry of complex **48d,** however, is considerably more distorted (τ^5 = 0.38). This discrepancy in geometry, and the need for heat to promote the formation of **48c**, is likely attributed to the large steric bulk associated with the $NHCPh_3$ ligands.

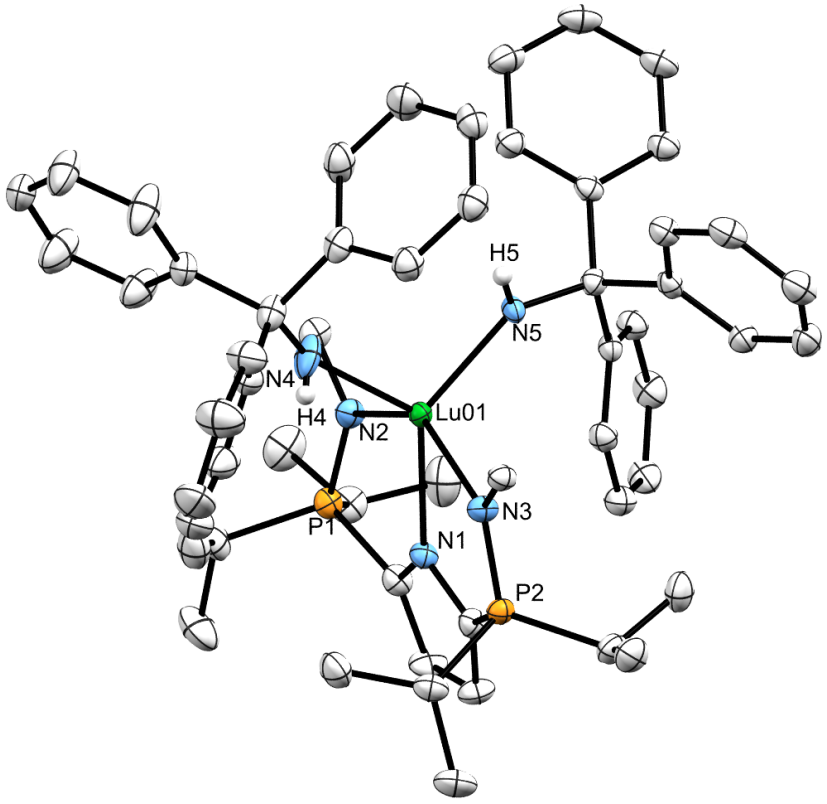

Figure 3.7 X-ray Crystal Structure (50% Probability) of Complex **48c**. Hydrogen (Except H4 and H5) and non-ipso Pipp Carbon Atoms Were Omitted for Clarity.

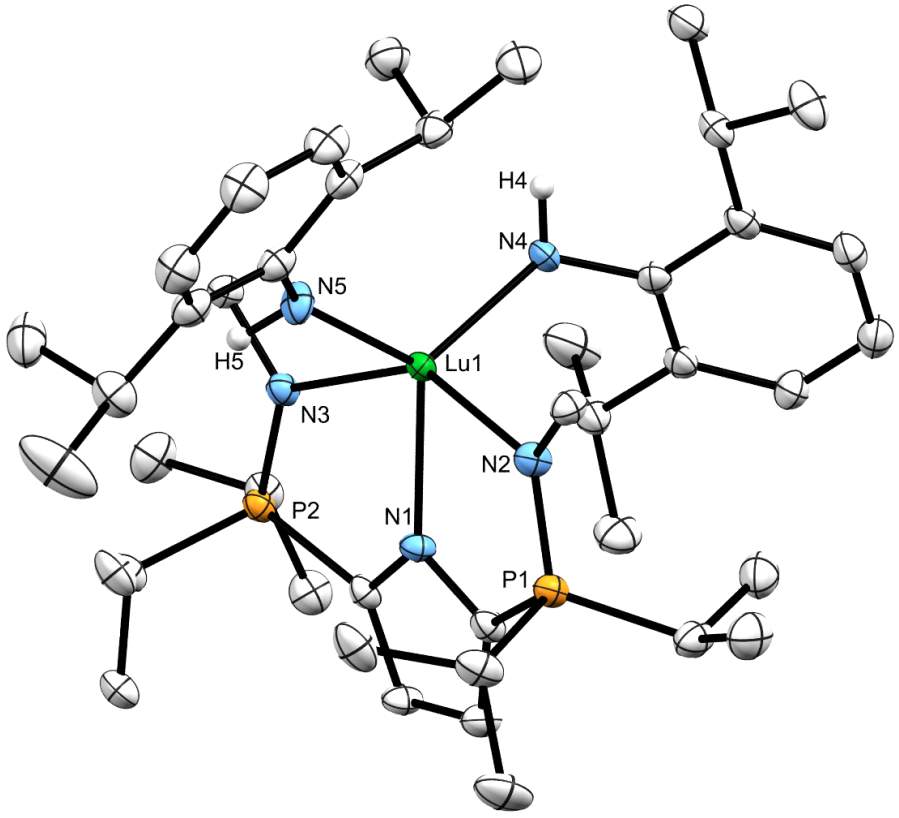

Figure 3.8 X-ray Crystal Structure (50% Probability) of Complex **48d**. Hydrogen (Except H4 and H5) and non-ipso Pipp Carbon Atoms Were Omitted for Clarity.

Table 3.4 Selected Bond Lengths (Å) and Angles (°) for Complexes **48c** and **48d**.

Parameter	**48c**	**48d**
Selected Bond Lengths (Å)		
Lu1–N1	2.327(2)	2.280(2)
P1–N2	1.617(3)	1.615(2)
Lu1–N4	2.153(2)	2.176(2)
Selected Bond Angles (º)		
N2–Lu1–N3	143.59(8)	143.76(7)
N1–Lu1–N4	132.20(8)	119.68(8)

3.6 Conclusions

Complex **37**, $L^{Ph}Lu(CH_2SiMe_3)(NHCPh_3)$, underwent spontaneous C–H bond activation and decomposed into half an equivalent of $L^{Ph}Lu(NHCPh_3)_2$. The full details of this decomposition are presented in Chapter 2 of this thesis. The next-generation pyrrole-based ancillary ligand, HL^{iPr}, was chosen in an attempt to generate thermally stable analogues of complex **37** ($L^{iPr}Lu(CH_2SiMe_3)(NHCPh_3)$ (**40c**) and $L^{iPr}Lu(CH_2SiMe_3)(NHDipp)$ (**40d**)) .

Reaction of HL^{iPr} with 1 equivalent of $RE(CH_2SiMe_3)_3(THF)_2$ (RE = Sc, Lu) proved to be a successful way of synthesizing the rare earth dialkyl complexes $L^{iPr}Sc(CH_2SiMe_3)_2$ (**39a**) and $L^{iPr}Lu(CH_2SiMe_3)_2$ (**39b**) (Scheme 3.12). Regrettably, complex **39a** did not react with Ph_3CNH_2, $DippNH_2$, or Mes^*NH_2 even upon prolonged exposure to heat. Cold, slow addition of $AdNH_2$ to complex **39a** afforded an inextricable

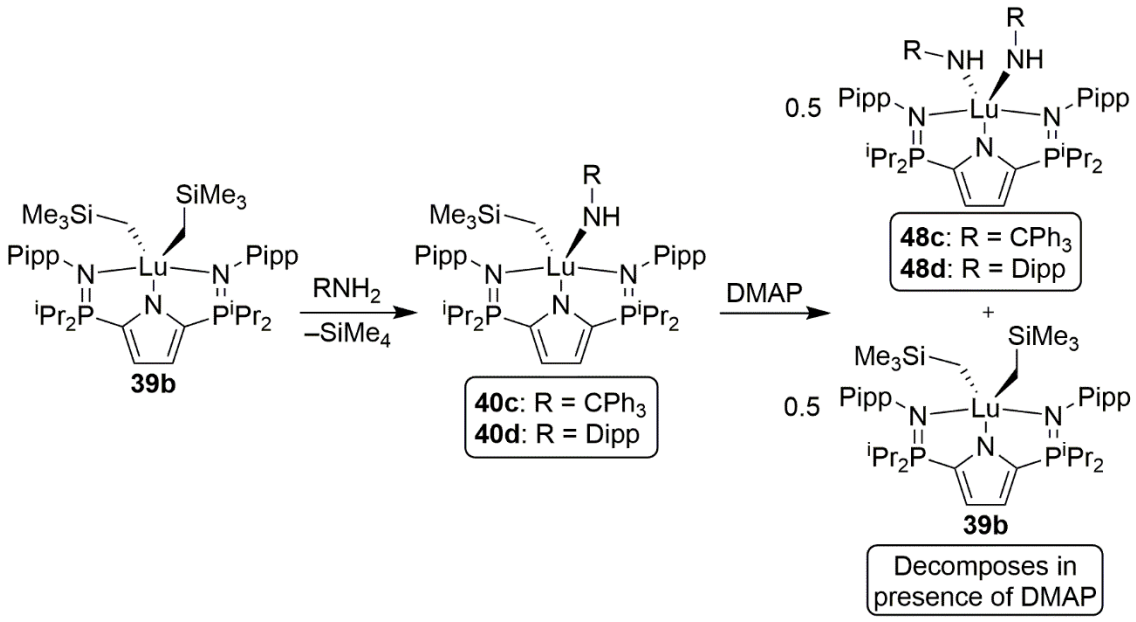

Scheme 3.12 Synthesis of Complexes **40c** and **40d** and Their Reactivity with DMAP.

mixture of $L^{iPr}Sc(CH_2SiMe_3)_2$, $L^{iPr}Sc(CH_2SiMe_3)(NHAd)$, and $L^{iPr}Sc(NHAd)_2$.

Conversely, addition of 1 equivalent of Ph_3CNH_2 or $DippNH_2$ to complex **39b** afforded the expected alkylamido complexes $L^{iPr}Lu(CH_2SiMe_3)(NHCPh_3)$ (**40c**) and $L^{iPr}Lu(CH_2SiMe_3)(NHDipp)$ (**40d**) (Scheme 3.12). Unlike the previous generation lutetium alkylamido complex $L^{Ph}Lu(CH_2SiMe_3)(NHCPh_3)$ (**37**), spontaneous cyclometalation was not observed.[64] Upon addition of DMAP to complex **40c** or **40d** a disproportionation reaction occured, giving half an equivalent of $L^{iPr}Lu(CH_2SiMe_3)_2$ and either $L^{iPr}Lu(NHCPh_3)_2$ (**48**c) or $L^{iPr}Lu(NHDipp)_2$ (**48d**), respectively. In the presence of DMAP $L^{iPr}Lu(CH_2SiMe_3)_2$ decomposed spontaneously upon formation.

Chapter 4 – Alternative Approaches to Forming a Rare Earth Imido Complex – Preliminary Attempts

4.1 Salt Metathesis Strategies

4.1.1 Overview

4.1.1.1 Reasoning for Using CH_3 Ligands

Chapters 2 and 3 of this thesis have focused on the formation of alkyl amido complexes synthesized through alkane elimination pathways which utilize sterically demanding CH_2SiMe_3 ligands (**37**, **40c**, **40d**, top, Scheme 4.1). Addition of a Lewis base (DMAP) to complex **37**, **40c**, or **40d** was predicted to form the terminal rare earth imido complex **38**, **41c**, or **41d**, respectively (top, Scheme 4.1) and one equivalent of $SiMe_4$. However, Chen, Anwander, Piers, and Mindiola all achieved formation of a terminal

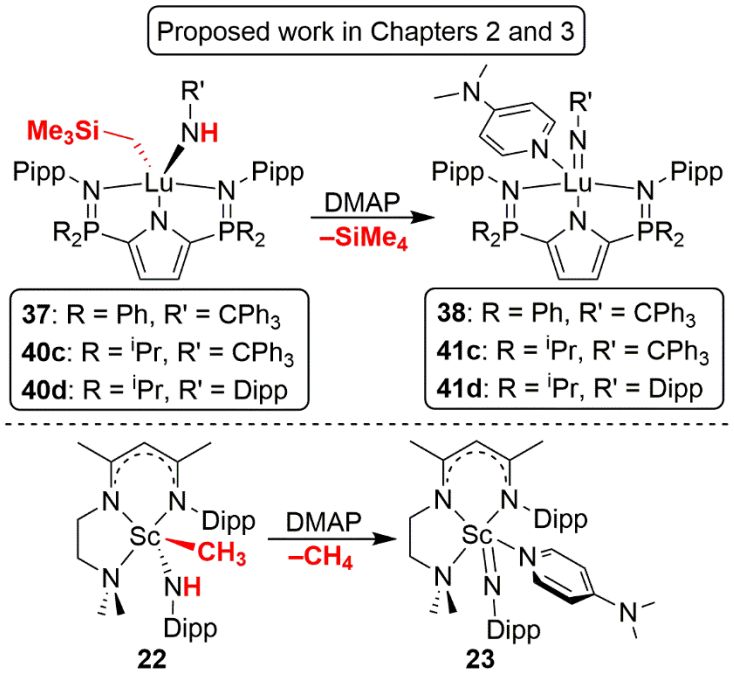

Scheme 4.1 CH_3 vs. CH_2SiMe_3 Ligands.

complex *via* addition of DMAP to an alkyl amido complex which utilized CH_3 ligands ($L^{Chen2}Sc(CH_3)$(NHDipp) is used as a highlighted example, **22**, bottom, Scheme 4.1).[41-43, 45, 52] The implementation of CH_3 substituents was attributed to the formation of a gaseous product upon addition of DMAP (CH_4, bottom, Scheme 4.1).

4.1.1.2 Synthetic Approach to CH_3 Ligands

Large, sterically demanding ligands (*e.g.* CH_2SiMe_3, CH_2Ph) are required to synthesize the homoleptic trialkyl rare earth precursors employed in the alkane elimination pathways utilized in Chapters 2 and 3 of this thesis (top, Scheme 4.2). As such, salt metathesis methodologies are required to coordinate CH_3 ligands to rare earth metals. Chen synthesized $L^{Chen2}Sc(CH_3)_2$ (**22b**, Scheme 4.2) *via* addition of two equivalents of MeLi to the dihalide complex $L^{Chen2}ScCl_2$ (**22a**, bottom, Scheme 4.2). Based on this, the decision to utilize CH_3 ligands was made. In order to pursue this, a scandium dihalide compound (analogous to complex **22a**, Scheme 4.2) supported by our ancillary pincer ligand was needed.

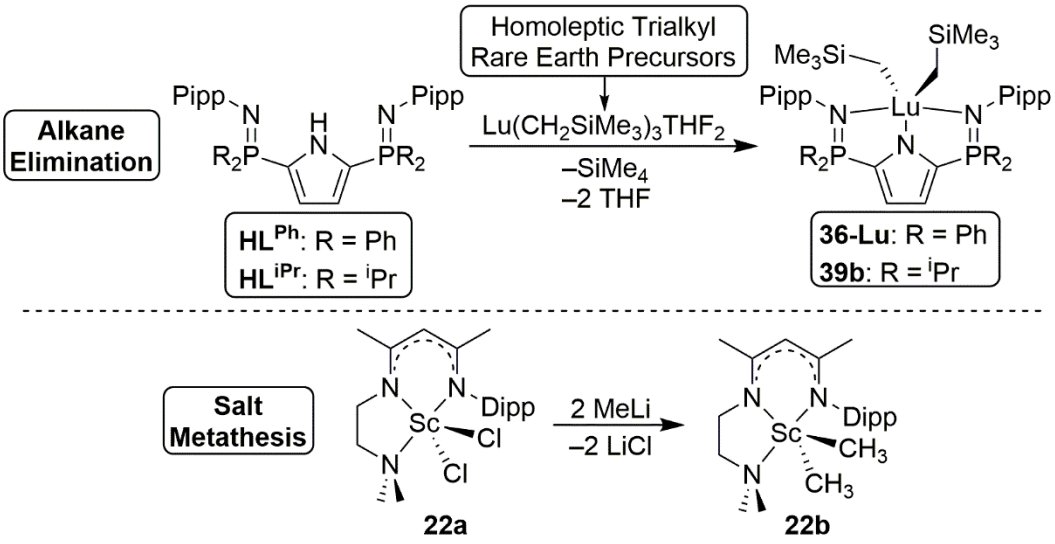

Scheme 4.2 Synthetic Methodology for Implementing CH_3 Ligands.

4.1.2 Previous Hayes Work

Addition of NaH to HL^{Ph} was shown to promote formation of $(THF)NaL^{Ph}$ (Scheme 4.3).[66] Facile production of $L^{Ph}ScCl_2(THF)$ (**49**, Scheme 4.3) was achieved *via* reaction of $(THF)NaL^{Ph}$ and one equivalent of $ScCl_3(THF)_3$.[89] Given the improved stability witnessed when our modified pincer ligand (L^{iPr}) was employed ($L^{iPr}Lu(CH_2SiMe_3)(NHCPh_3)$ vs $L^{Ph}Lu(CH_2SiMe_3)(NHCPh_3)$), the synthesis of $L^{iPr}ScCl_2$ targeted.

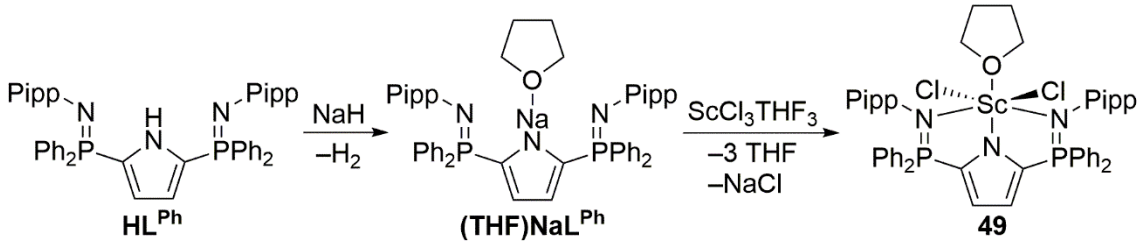

Scheme 4.3 Previous Salt Metathesis Work Done in The Hayes Lab.

4.1.3 Proposed Work

Addition of NaH to HL^{iPr} seemed a logical starting point for the synthesis of NaL^{iPr} (Scheme 4.4). Upon isolation of NaL^{iPr}, addition of $ScCl_3(THF)_3$ was predicted to yield $L^{iPr}ScCl_2$ (**50**, Scheme 4.4). The reaction of two equivalents of MeLi and complex **50** is

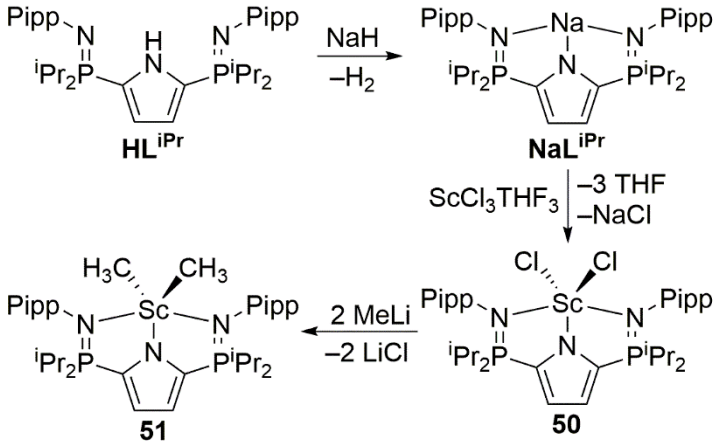

Scheme 4.4 Proposed Formation of Complex **51**.

predicted to promote the formation of the dialkyl complex $L^{iPr}Sc(CH_3)_2$, **51**.

4.1.4 Synthesis of NaL^{iPr} and $L^{iPr}ScCl_2$

Protio ligand HL^{iPr} was reacted with one equivalent of NaH to quantitatively produce NaL^{iPr} (Scheme 4.5). As expected, no N–H resonance was found in the ^1H NMR spectrum (δ 10.4). Additionally, a single resonance was seen in the $^{31}P\{^1H\}$ NMR spectrum (δ 30.70), indicating that C_{2v} symmetry had been preserved.

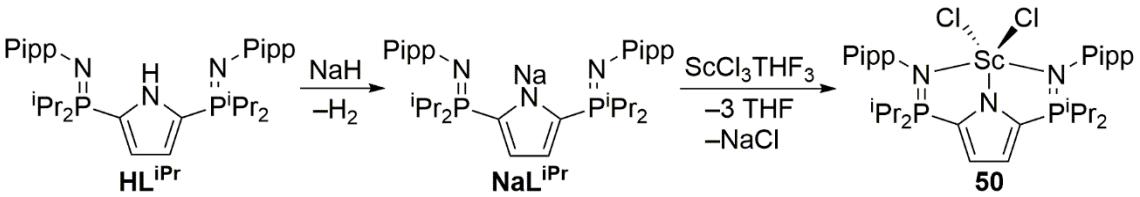

Scheme 4.5 Synthesis of Rare Earth Dihalide **50**.

Facile preparation of $L^{iPr}ScCl_2$ (**50**, Scheme 4.5) was achieved by the reaction of NaL^{iPr} with $ScCl_3(THF)_3$ in THF for 3 hours. Removal of THF *in vacuo* and subsequent reconstitution in toluene afforded NaCl as a white precipitate. After filtration, all volatiles were removed *in vacuo*, which afforded $L^{iPr}ScCl_2$ as a pale yellow solid in 74.7% yield.

4.1.5 X-ray Crystal Structure of $(L^{iPr}ScCl_2)_2 \bullet C_7H_8$

X-ray quality crystals of $L^{iPr}ScCl_2$ (**50**) were grown by dissolving the crude product in a minimal amount of warm (50 ºC) toluene and heptane (1:1). The solid-state structure of complex **50**, shown in Figure 4.1, possesses two equivalents of $L^{iPr}ScCl_2$ in the asymmetric unit. Notably, complex **50** is both monomeric and free of THF, despite its use as a solvent. Both equivalents of $L^{iPr}ScCl_2$ exhibit a five-coordinate geometry about scandium that is best described as heavily distorted square pyramidal (τ^5_{Sc1} = 0.49, τ^5_{Sc2} = 0.43). Sc–N bond lengths (N1–Sc1 = 2.146(6) Å, N4–Sc2 = 2.139(2) Å, N2–Sc1 = 2.198(3)

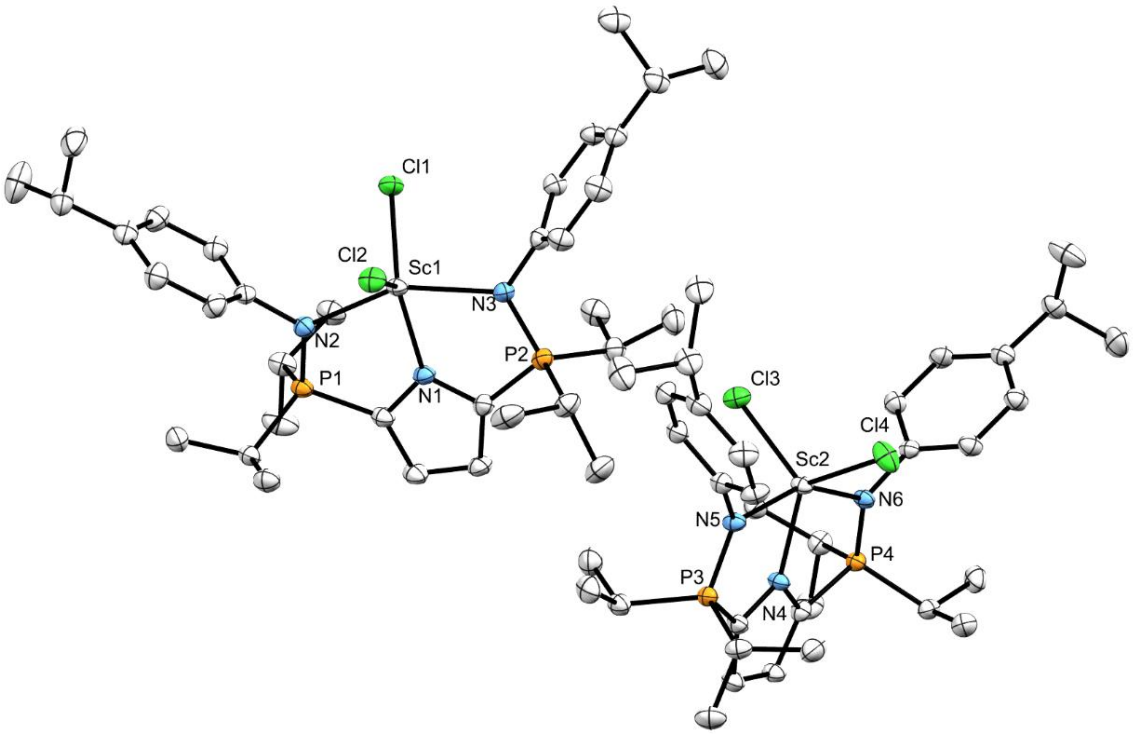

Figure 4.1 X-ray Crystal Structure (50% Probability) of Complex **(50)$_2$•C$_7$H$_8$**. Hydrogen Atoms, one Equivalent of Toluene, and one Equivalent of Distorted Heptane are Omitted for Clarity.

Table 4.1 Selected Bond Lengths (Å) and Angles (º) for Complex **50**.

Parameter	**Distance (Å)**	**Parameter**	**Degree (º)**
Cl1–Sc1	2.3770(8)	N1–Sc1–N2	76.08(8)
Cl2–Sc1	2.3863(6)	N2–Sc1–N3	151.81(8)
N2–Sc1	2.198(3)	Cl1–Sc1–Cl2	114.21(3)
N5–Sc2	2.201(2)	N1–Sc1–Cl2	124.21(6)
N1–Sc1	2.146(2)	N4–Sc2–N6	75.83(8)
N4–Sc2	2.139(2)	N4–Sc1–N6	151.71(8)
P1–N2	1.622(2)	Cl3–Sc2–Cl4	116.68(3)
P3–N5	1.620(2)	N4–Sc2–Cl4	126.13(6)

Å, N5–Sc2 = 2.201(2) Å) closely match with our other scandium complexes bound to pyrrole-based ligands.[55, 62]

4.1.6 Reaction of $L^{iPr}ScCl_2$ and MeLi

Two equivalents of solid MeLi were added to a solution of $L^{iPr}ScCl_2$, **50**, in THF. After stirring for 2 hours at ambient temperature, complex **50** represented 60% of the dissolved phosphorus-containing material, determined *via* $^{31}P\{^1H\}$ NMR spectroscopy. Allowing the reaction to stir for an additional 16 hours resulted in the full consumption of complex **50**. However, the formation of multiple products was observed in the $^{31}P\{^1H\}$ NMR spectrum (δ 47.94, 46.01, 35.41, 33.47, and 28.84). The desired dialkyl complex $L^{iPr}Sc(CH_3)_2$, **51**, could not be isolated as a pure solid from this reaction mixture and thus no spectroscopic assessments could be made. However, independent synthesis of the lithium salt produced in this reaction, $[LiL^{iPr}]_2$ *vide infra*, revealed that resonances at δ 33.47 and 28.84 arose from the production of $[LiL^{iPr}]_2$. The reaction of $L^{iPr}ScCl_2$ with 4 equivalents of MeLi produced a similar mixture of products. Attempts that employed MeLi as a stock 1.6 M solution in diethyl ether were also unsuccessful.

4.1.7 Crystal Structures of $[LiL^{iPr}]_2$ and $(L^{iPr}Sc(CH_3)_2)_2$

Several attempts to crystallize the products from the reaction of complex **50** and MeLi were conducted. Although X-ray quality crystals were obtained, they were not of a scandium containing species, but rather their identity was established to be the lithium salt $[LiL^{iPr}]_2$ (Figure 4.2). This compound, shown in Figure 4.2 with selected metrical parameters given in Table 4.2, was presumably formed by transmetallation. $[LiL^{iPr}]_2$

crystallizes as a dimeric complex in the P–1 space group. Each lithium is bound to a pyrrole nitrogen atom and by a single phosphinimine donor in a κ^2 fashion (N1, N3). In addition,

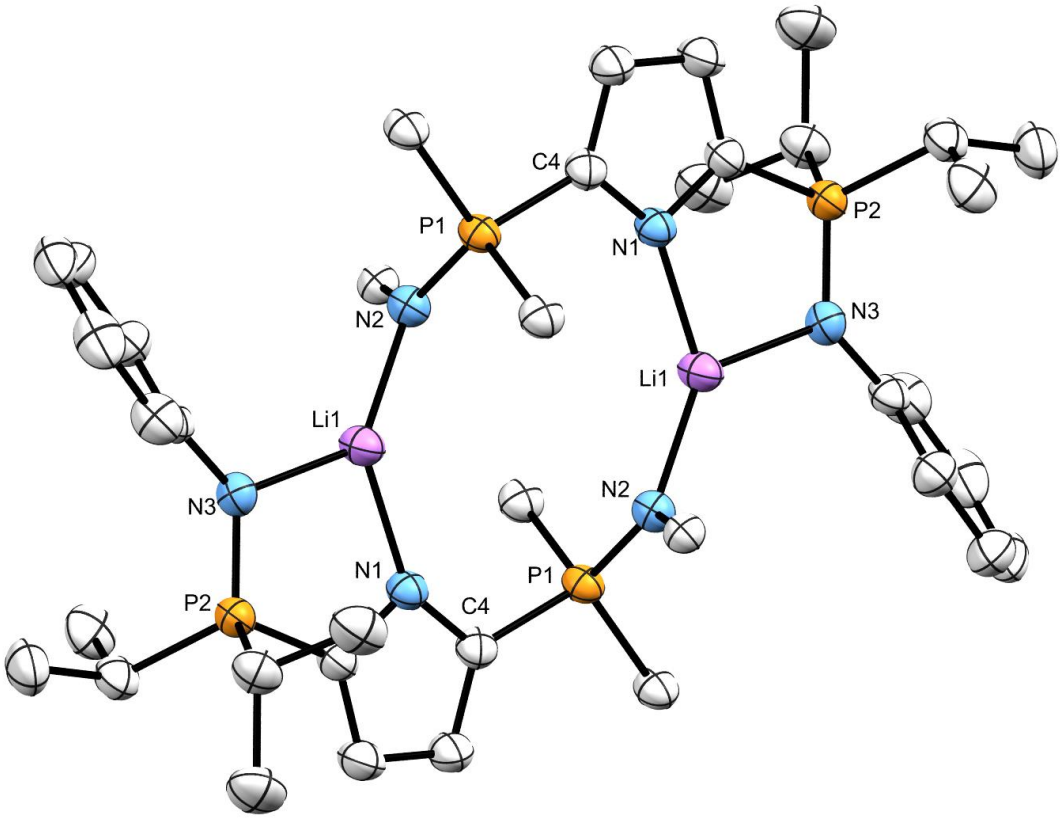

Figure 4.2 X-ray Crystal Structure (50% Probability) of $[LiL^{iPr}]_2$. Hydrogen Atoms and P–^{i}Pr$_2$ CH_3 and non-ipso Pipp Carbon Atoms Within the Metallocycle are Omitted for Clarity.

a phosphinimine belonging to a second ligand (N2) is also coordinated to each lithium atom. This bonding motif created an unusual 10-membered ring (N1–Li1–N2–P1–C4–N1–Li1–N2–P1–C4). As Li1 is almost equidistant from N1 and N3, the C4–N1–Li1 bond angle is 143.63(2) º.

Table 4.2 Selected Bond Lengths (Å) and Angles (º) for $[LiL^{iPr}]_2$.

Parameter	Distance (Å)	Parameter	Degree (º)
N1–Li1	1.996(4)	N1–Li1–N3	92.45(2)
N3–Li1	2.020(5)	N1–Li1–N2	135.14(3)
P1–N2	1.604(3)	P1–N2–Li1a	123.27(2)
P2–N3	1.594(2)	C4–N1–Li1	143.63(2)

After numerous, successive crystallization attempts, an X-ray crystal structure of $L^{iPr}Sc(CH_3)_2$ (**51**) was obtained (Figure 4.3, metrical parameters highlighted in Table 4.3). It should be noted that crystals of complex **51** crystallized simultaneously with $[LiL^{iPr}]_2$. Thus, pure samples of compound **51** could not be obtained. Unfortunately, the quality of the crystals did not afford publishable data. Thus, this structure should be viewed only as a proof of connectivity. The solid-state structure demonstrated that, despite forming an inextricable mixture, $L^{iPr}Sc(CH_3)_2$ formed *via* addition of two equivalents of MeLi to compound **50**.

Table 4.3 Selected Bond Lengths (Å) and Angles (º) for Complex **51**.

Parameter	Distance (Å)	Parameter	Degree (º)
P1–N2	1.59(5)	N2–Sc1–N3	160.2(2)
N1–Sc1	1.90(7)	N5–Sc2–N6	159.7(2)
N4–Sc2	1.94(5)	C71–Sc2–C72	121.8(3)
C71–Sc2	1.96(7)	C35–Sc1–C36	123.6(3)

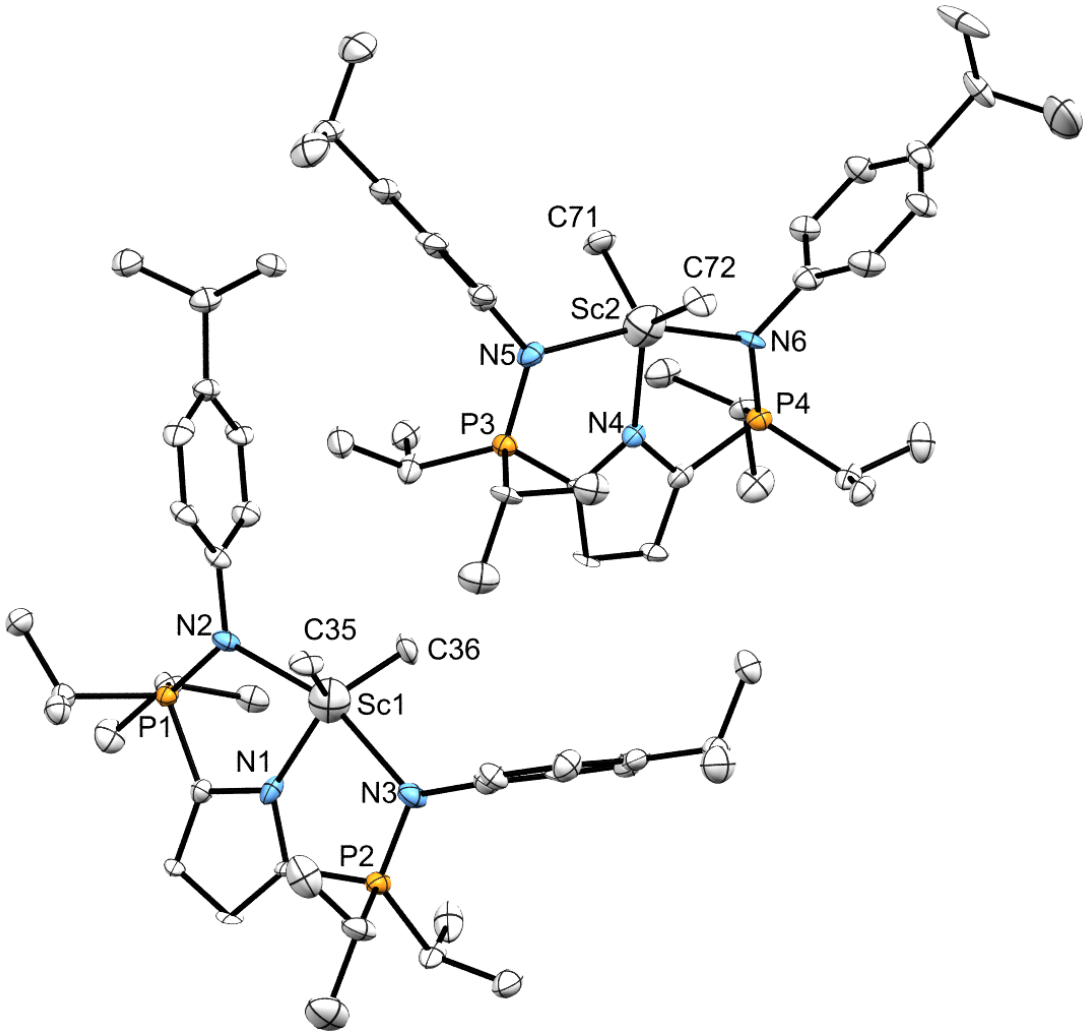

Figure 4.3 X-ray Crystal Structure (50% Probability) of Complex **(51)$_2$**. Hydrogen Atoms are Omitted for Clarity.

4.2 Reactivity of $L^{iPr}ScCl_2$ with Amide Salts

4.2.1 Overview

Given the necessity of an amide ligand (NHR) in the formation of rare earth imido complexes, reactivity of an alkali amide salt with $L^{iPr}ScCl_2$ appeared as a logical pursuit (Scheme 4.6). The reaction of half an equivalent of a sterically demanding amide salt (*e.g.*

[(THF)LiNHCPh$_3$]$_2$, [(THF)LiNHDipp]$_2$) to complex **50** was predicted to replace a single halide ligand and form L^{iPr}ScCl(NHCPh$_3$) (**52**) and L^{iPr}ScCl(NHDipp) (**53**), respectively. Subsequent addition of MeLi to either complex **52** or **53** was hypothesized to yield the alkyl amido species L^{iPr}ScCH$_3$(NHCPh$_3$) (**54**) or L^{iPr}ScCH$_3$(NHDipp) (**55**).

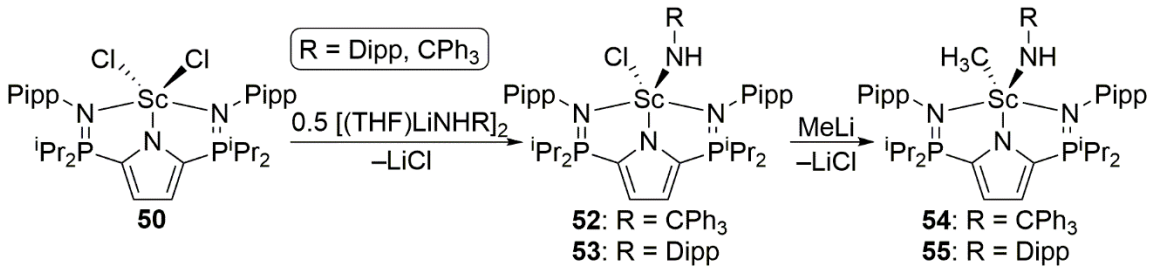

Scheme 4.6 Proposed Reactivity of Complex **50** with Alkali Amide Salts.

4.2.2 Synthesis of [(THF)LiNHDipp]$_2$ and [(THF)LiNHCPh$_3$]$_2$

Samples of [(THF)LiNHDipp]$_2$, **56**, and [(THF)LiNHCPh$_3$]$_2$, **57**, (Scheme 4.7) were prepared by addition of one equivalent of ^{n}BuLi to either DippNH$_2$ or Ph$_3$CNH$_2$ at

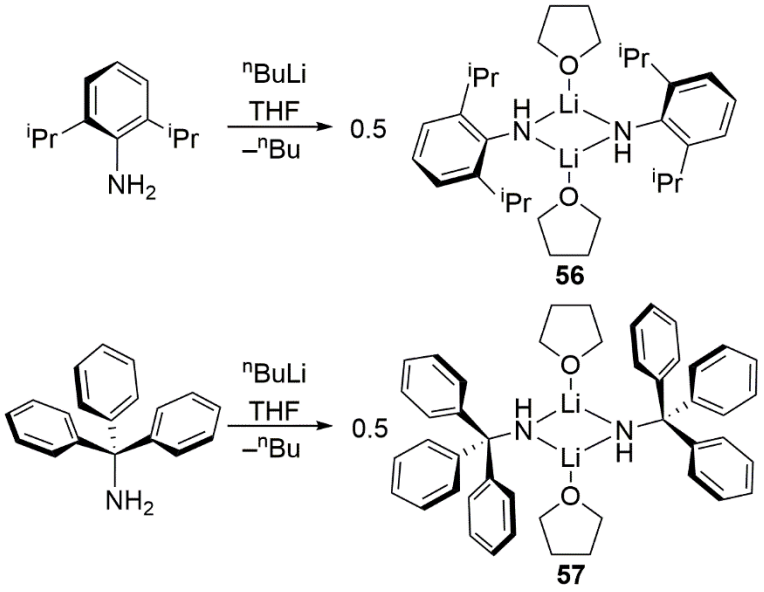

Scheme 4.7 Formation of Compound **56** and **57**.

–35 ºC in THF. Removal of volatiles *in vacuo* afforded the desired products as an off white solid. A N–H proton was observed in the ^{1}H NMR spectrum of the isolated products (δ 2.69, (**56**), δ –0.26 (**57**)) each of which integrated to 1H. Additionally, it was determined that both products retained one equivalent of THF.

4.2.3 Crystal Structure of [(THF)LiNHCPh$_3$]$_2$

X-ray quality crystals of compound **57** were grown by cooling a saturated toluene solution to –35 ºC. The dimeric structure is presented in Figure 4.4; selected metrical parameters are highlighted in Table 4.4. Each nitrogen atom is bound–μ^2 to each lithium

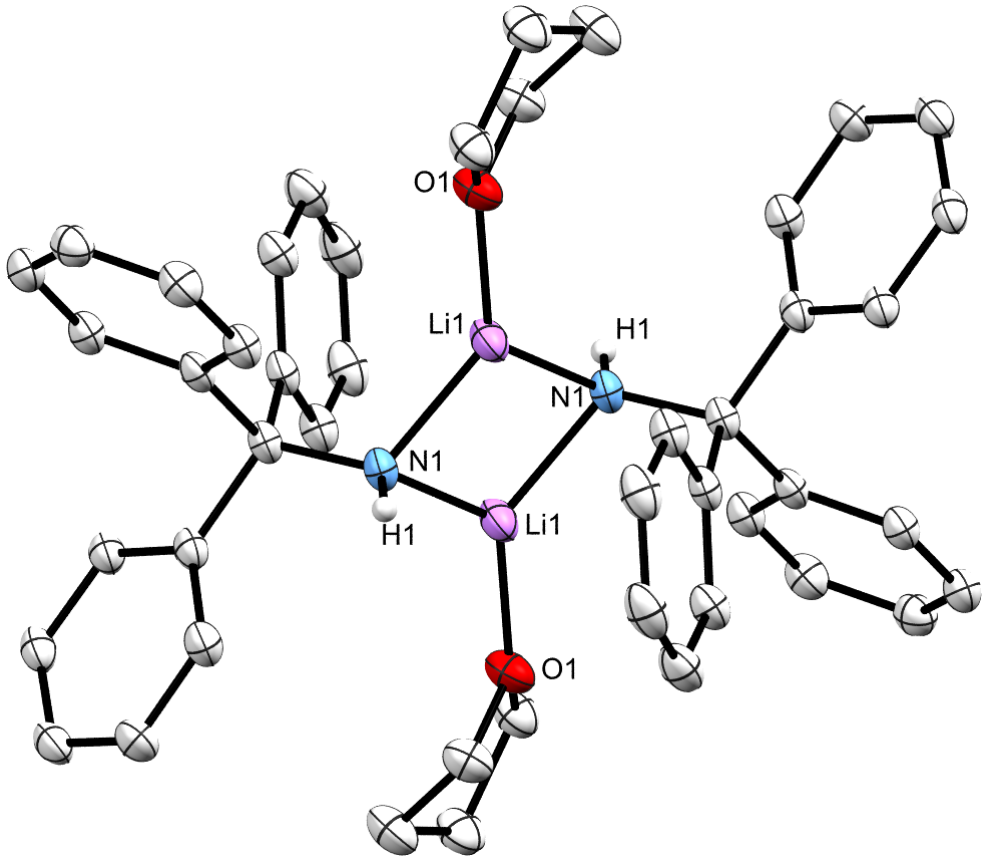

Figure 4.4 X-ray Crystal Structure (50% Probability) for Compound **50**. Hydrogen Atoms (Except H1) are Omitted for Clarity

atom (N1–Li = 1.986 Å). A molecule of THF is also coordinated to each lithium atom.

Table 4.4 Selected Bond Lengths (Å) and Angles (º) for Compound **57**.

Parameter	Distance (Å)	Parameter	Degree (º)
N1–Li1	1.986(2)	N1–Li1–N1A	105.2(1)
N1A–Li1	1.986(2)	Li1–N1–Li1A	74.81(9)
O1-Li1	1.934(2)	O1–Li1–N1	125.0(1)

4.2.4 Reaction of $[(THF)LiNHCPh_3]_2$ and $[(THF)LiNHDipp]_2$ with $L^{iPr}ScCl_2$

$[(THF)LiNHCPh_3]_2$ (**57**) did not react with two equivalents of $L^{iPr}ScCl_2$ (**50**) in toluene even when heated to 60 ºC. However, reaction of half an equivalent of $[(THF)LiNHDipp]_2$ (**56**) and complex **50** resulted in disappearance of the resonance in the $^{31}P\{^1H\}$ NMR spectrum corresponding to $L^{iPr}ScCl_2$ (δ 49.3). A new signal, attributed to the desired product $L^{iPr}ScCl(NHDipp)$ (**53**, Scheme 4.8) was observed (δ 47.93). In the ^1H NMR spectrum, the Dipp and Pipp C–H methine resonances overlapped (δ 2.02) and collectively integrated as 6H (2H (Dipp–C*H*(CH_3)), 4H (P–C*H*(CH_3)$_2$)).

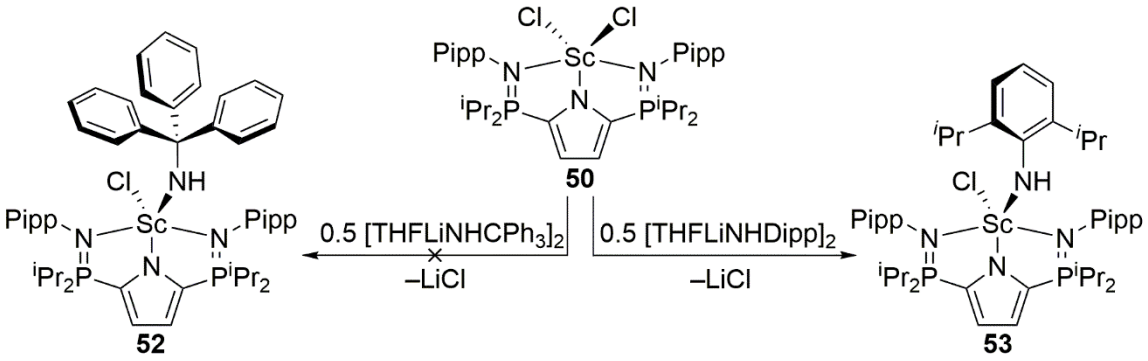

Scheme 4.8 Synthesis of Complex **53**.

4.2.5 Synthesis of $L^{iPr}ScCl(N(SiMe_3)_2)$

One equivalent of $KN(SiMe_3)_2$ was added to a THF solution of $L^{iPr}ScCl_2$ (**50**, Scheme 4.9). Removal of all volatiles *in vacuo* and reconstitution of the crude mixture in toluene afforded KCl as a white precipitate. Filtration and subsequent removal of solvents *in vacuo* afforded $L^{iPr}ScCl(N(SiMe_3)_2)$ (**58**) as a yellow solid (Scheme 4.9). As evidenced by a single peak in the $^{31}P\{^1H\}$ NMR spectrum (δ 48.6) only one phosphorus-containing product was formed. In the ^1H NMR spectrum the $N(SiMe_3)_2$ substituents were observed as two baseline resolved peaks (δ 0.53, –0.10). These resonances integrated in a 9:9 ratio (relative to the two pyrrole protons) which indicated slow rotation about the Sc–$N(SiMe_3)_2$ bond.

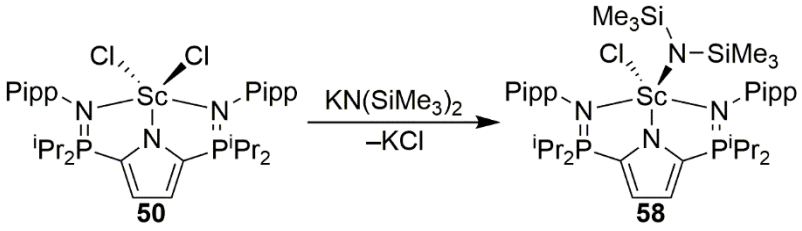

Scheme 4.9 Synthesis of Complex **58**.

4.2.5.1 Thermolysis of $L^{iPr}ScCl(N(SiMe_3)_2)$

In an attempt to generate $ClSiMe_3$ and the lutetium imido complex $L^{iPr}Sc{=}NSiMe_3$,

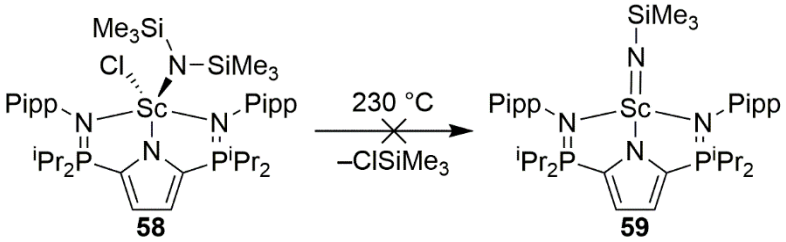

Scheme 4.10 Thermolysis of Complex **59**.

59 (Scheme 4.10), a sample of complex **58** was placed in a *J*-Young NMR tube, dissolved in 500 μL of C_6D_6 and heated to 230 ºC (503.15 K) for 24 hours (Scheme 4.10). Despite the extreme conditions absolutely no reaction was observed by either $^{31}P\{^1H\}$ or ^1H NMR spectroscopy.

4.3 Internal Lewis Bases

4.3.1 Overview

Chen's 2010 terminal imido complex (**23**, Scheme 4.11), and most published examples, are prepared by addition of an external Lewis base (typically DMAP) to an alkyl-amido rare earth complex. This reaction promotes N–H bond activation and alkane loss (top, Scheme 4.11).[45] In 2012 Chen reported the reaction of complex **23** and half an equivalent of $[Rh(COD)Cl]_2$, which produced complex **23f** (top, Scheme 4.11).[46] Despite exhaustive efforts, complex **23f** could not be separated from the equivalent of DMAP

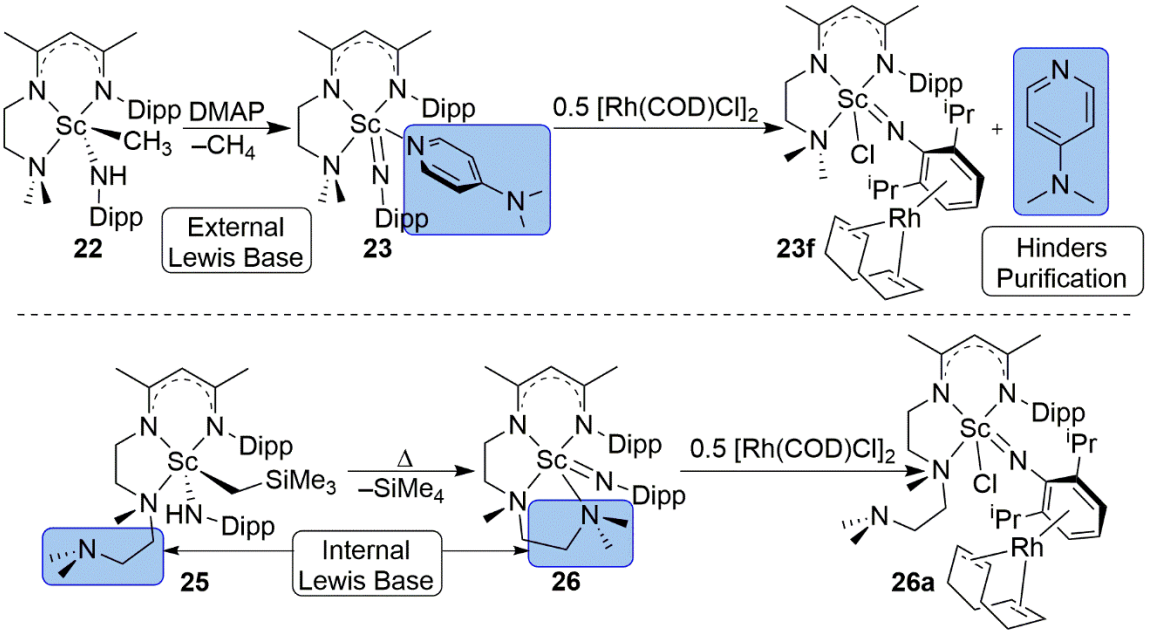

Scheme 4.11 Effect of Implemented Lewis Base on Subsequent Product Isolation.

liberated in this reaction. To combat this issue, Chen designed a similar ligand which contained an additional internal Lewis base.[49] This idea permitted generation of a scandium imido complex that was devoid of DMAP (**26**, Scheme 4.11). As expected, L^{Chen3}Sc=NDipp **26**, reacted cleanly with half an equivalent of $[Rh(COD)Cl]_2$, yielding L^{Chen3}ScCl(NDipp)Rh(COD) (**26a**, bottom, Scheme 4.5).[46] Because the released Lewis base was tethered to the product, **26a**, purification *via* recrystallization proved straightforward. Inspired by this work, a modified ligand system that incorporates an internal Lewis base was targeted.

4.3.2 Previous Work

Previous work in the Hayes lab had aimed at incorporating pyrimidine

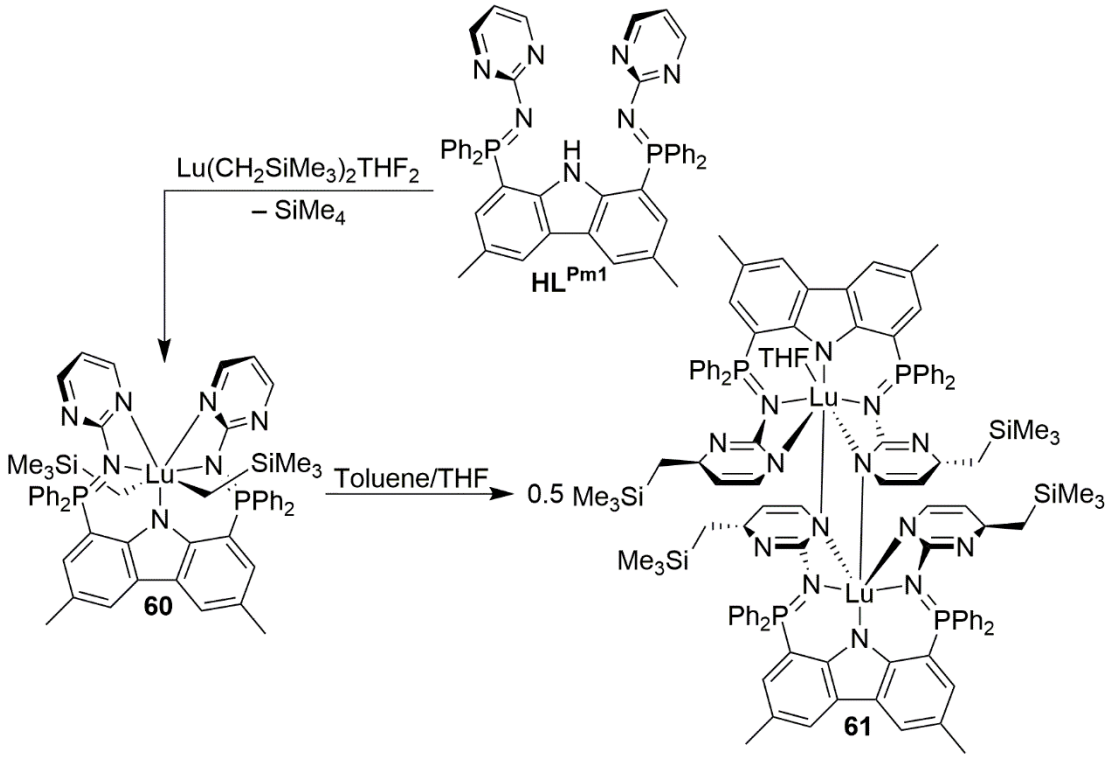

Scheme 4.12 Dearomatization of Pyrimidine Rings in Complex **60** *via* Double Alkyl Migration from Lutetium.

functionalities at the phosphinimine nitrogen (HL^{Pm1}, Scheme 4.12).[60] Complexation of HL^{Pm1} to lutetium was achieved by reaction of HL^{Pm1} with one equivalent of $Lu(CH_2SiMe_3)_3(THF)_2$, which afforded $L^{Pm1}Lu(CH_2SiMe_3)_2$ (**60**, Scheme 4.11) in high yield. Unfortunately, complex **60** decomposed *via* double alkyl-migration of the CH_2SiMe_3 substituents to the pyrimidine non-ipso carbon adjacent to nitrogen. This transformation resulted in dearomatization of the pyrimidine rings and production of the dinuclear complex $[L^{Pm1*}Lu]_2$ (**61**, Scheme 4.12, L^{Pm1*} = dearomatized variant of L^{Pm1}). Because of this unexpected decomposition (only one previous example of similar chemistry had been reported)[90] this ligand scaffold was abandoned. Nonetheless, given the stability of the organometallic complexes supported by HL^{iPr}, it still seemed prudent to explore ligand designs which featured N–pyrimidine substituents.

4.3.3 Internal Lewis Bases in a Pyrrole Based Ligand

4.3.3.1 Synthesis of 5,7-dimethylpyrazolo-1,5a-pyrimidine

Because of the double-alkyl migration experienced by complex **60**, the choice was made to move to 2-azido-4,6-dimethylpyrimidine (**62**, Scheme 4.13), in hopes that the CH_3 groups would to prevent CH_2SiMe_3 migration. The methyl groups also provide a diagnostic resonance for characterization by ^1H NMR spectroscopy. Additionally, the number of pyrimidine CH_3 resonances was expected to provide valuable information regarding compound symmetry and strength of any pyrimidine interactions with the metal centre.

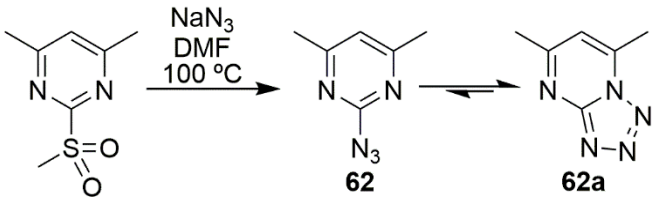

Scheme 4.13 Synthesis of Compound **62/62a**.

Facile production of compound **62** was achieved by the reaction of NaN_3 with 4,6-dimethyl-2-methylsulfonylpyrimidine in hot DMF (100 ºC) for 3 hours (Scheme 4.13). As is common for 2-azidopyrimidine derivatives, compound **62** is susceptible to valence tautomerization with its tetrazole isomer 5,7-dimethylpyrazolo-1,5a-pyrimidine (**62a**, Scheme 4.13).[60, 91-92] Compound **62a** is the predominant structure in this tautomerization, as evidenced by the two separate methyl resonances (*i.e.* the lack of C_2 symmetry) observed in the ^{1}H NMR spectrum (C_6D_6, 22 °C) (δ 2.96 and 2.76).

4.3.3.2 Synthesis of HL^{Pm}

Despite the tetrazole isomer prevailing, compound **62a** participated in a Staudinger reaction with half of an equivalent of 2,5-bis(diisopropylphosphino)-N-H-pyrrole to give the desired ligand HL^{Pm} (Scheme 4.14). It should be noted that due to the equilibrium between compound **62** and **62a**, this reaction required a significantly longer reaction time (18 h) compared to the reaction of $PippN_3$ and 2,5-bis(diisopropylphosphino)-N-H-pyrrole (2 h, section 3.1.2). In the ^{1}H NMR spectrum of HL^{Pm}, only one pyrimidine CH_3 resonance is observed (δ 2.40), which suggested free rotation about the N_{PN}–C_{Pm} σ-bond on the NMR timescale. The C_{2v} symmetry of the ligand was corroborated by the single, sharp resonance (δ 29.63) seen in the $^{31}P\{^1H\}$ NMR spectrum.

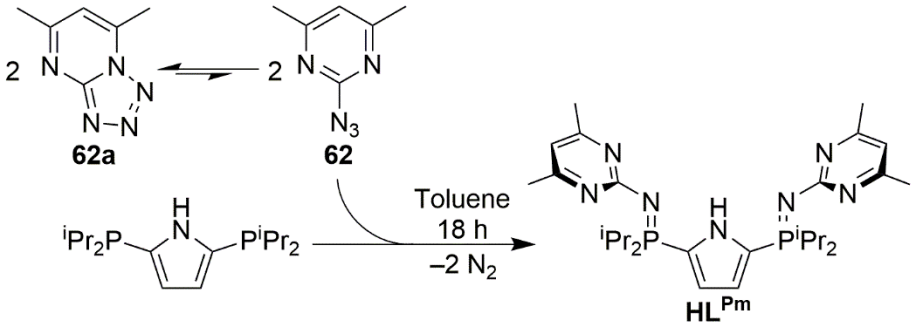

Scheme 4.14 Synthesis of HL^{Pm}.

4.3.4 Crystal Structure of HL^{Pm}

High quality crystals of HL^{Pm}, grown from a saturated toluene/pentane (1:1) solution at –35 °C, permitted an X-ray crystallographic study to be conducted on HL^{Pm}.

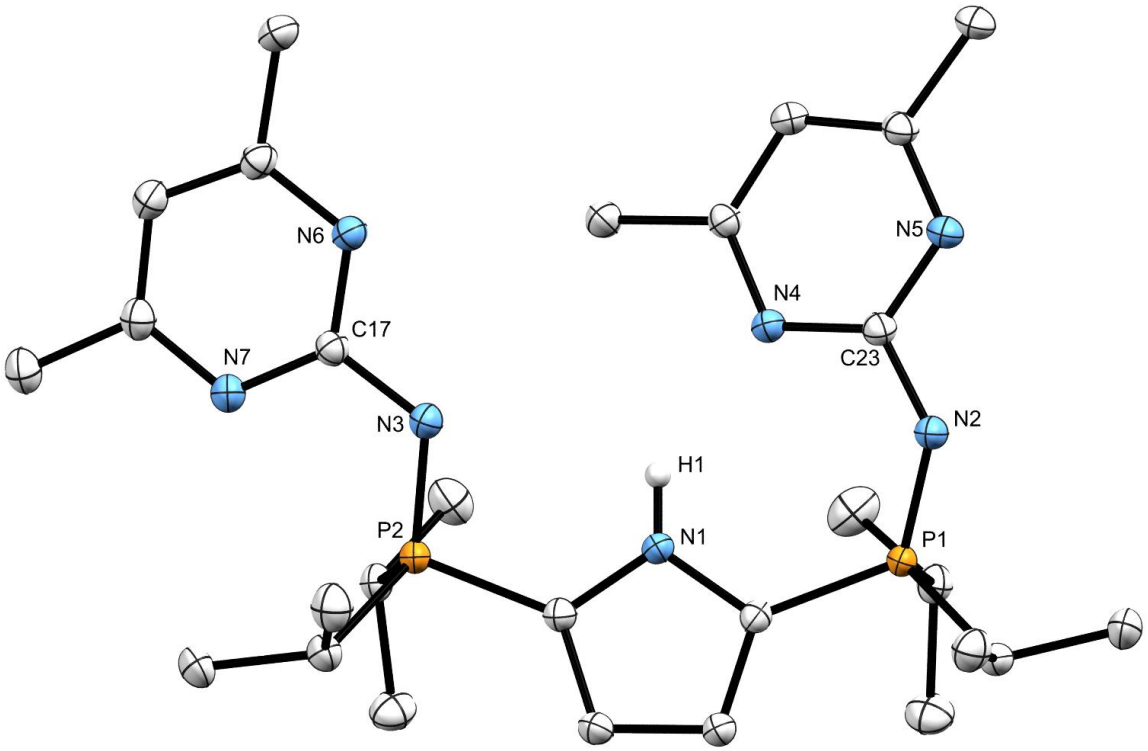

Figure 4.5 X-ray Crystal Structure (50% Probability) of HL^{Pm}. Hydrogen Atoms (Except H1) are Omitted for Clarity.

Table 4.5 Selected Bond Lengths (Å) and Angles (º) for HL^{Pm}.

Parameter	Distance (Å)	Parameter	Angle (º)
N1···N4	2.859(2)	P1–N2–C23	129.3(1)
P1–N2	1.587(1)	P2–N3–C17	119.7(1)
P2–N3	1.609(1)	C4–N1–N4	99.04(9)

Both pyrimidine substituents lie in the same plane as the pyrrole backbone. A pyrimidine nitrogen (N4) appeared to have a long-range interaction with H1 (N4···N1 = 2.859 Å). Both phosphinimine groups were puckered out of the plane of the pyrrole backbone (N1–C1–P1–N2 = 38.9(2) º, N1–C4–P2–N3 = 33.5(1) º) which appears to aid the observed hydrogen bonding while alleviating the steric pressure induced by the pyrimidine-CH_3 substituent.

4.3.5 One Step Imido

4.3.5.1 Overview

In an attempt at reducing the number of synthetic steps needed to generate a rare earth imido complex, $Lu(CH_2SiMe_3)_2(NHMes^*)(THF)_2$ was chosen as the metal starting material. Because this species contains both alkyl and amido groups two reactions can be envisioned upon addition of HL^{Pm} (Scheme 4.15). The first of these, **Reaction A** (top right, Scheme 4.15), would result in a loss of $SiMe_4$ and establish the lutetium alkyl amido complex $L^{Pm}Lu(CH_2SiMe_3)(NHMes^*)$, **64**. However, if amine elimination prevailed, **Reaction B** (top left, Scheme 4.15), the dialkyl lutetium complex $L^{Pm}Lu(CH_2SiMe_3)_2$, **63**, and one equivalent of Mes^*NH_2 would be generated. If **Reaction B** occurred, the free

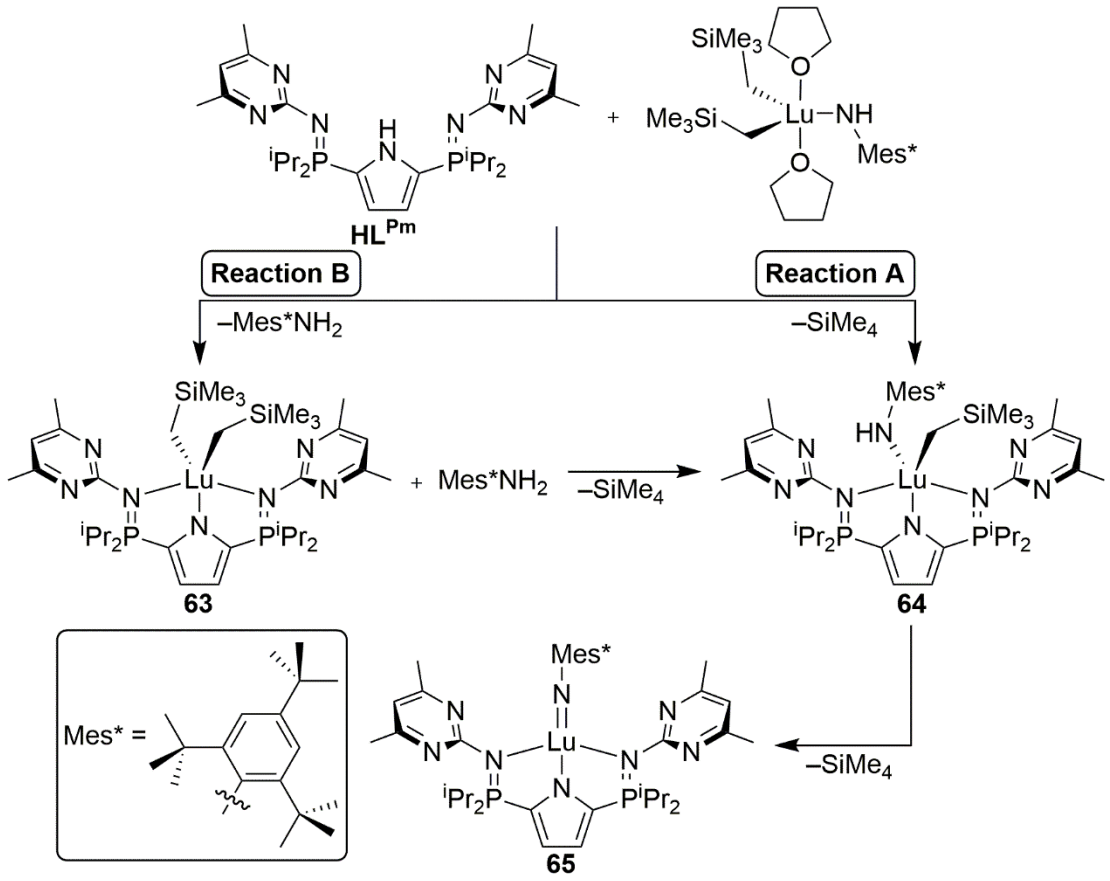

Scheme 4.15 Planned Synthetic Procedure for One-Step Formation a Terminal Rare Earth Imido Complex.

$Mes*NH_2$ might be expected to react with $L^{Pm}Lu(CH_2SiMe_3)_2$, **63**, to afford $L^{Pm}Lu(CH_2SiMe_3)(NHMes*)$, **64**. Should complex **64** be formed, the nitrogen atoms of the pyrimidine substituents could be imagined to promote N–H bond activation and yield the imide complex $L^{Pm}Lu{=}NMes*$ (**65**, Scheme 4.15).

4.3.5.2 Reaction of $Lu(CH_2SiMe_3)_2(NHMes*)(THF)_2$ with HL^{Pm}

Surprisingly, addition of $Lu(CH_2SiMe_3)_2(NHMes*)(THF)_2$ to HL^{Pm} in toluene led to predominant formation of complex **63** (63% *via* $^{31}P\{^1H\}$ NMR spectroscopy, δ 42.4), and $Mes*NH_2$. In addition, an asymmetric impurity was observed in the $^{31}P\{^1H\}$ NMR

spectrum (δ 42.72, 33.09). While this species was not isolated, the possibility of excess $LiCH_2SiMe_3$ in the $Lu(CH_2SiMe_3)_2(NHMes^*)(THF)_2$ sample, and the similarity of the $^{31}P\{^1H\}$ chemical shifts to NaL^{Pm} (*vide infra*), suggested the identity of the unknown to be a lithium salt of the ancillary ligand. Another compound (13.3% by $^{31}P\{^1H\}$ NMR spectroscopy) gave rise to a peak at δ 51.5 in the $^{31}P\{^1H\}$ NMR spectrum. While this resonance was attributed to complex **64**, its low quantity precluded meaningful structural information from being obtained. Attempts to purify this compound by crystallization were unsuccessful. Allowing this reaction mixture to stir in solution at ambient temperature for 2 hours resulted in a 8% increase in the resonance attributed to compound **64** and a 20% decrease in the quantity of $L^{Pm}Lu(CH_2SiMe_3)_2$, **63**. Additionally, a new, unknown product emerged in the $^{31}P\{^1H\}$ NMR spectrum at δ 51.2. Increasing the temperature to 50 ºC for 50 hours resulted in complete consumption of complex **63**, leaving the resonance attributed to compound **63** (δ 51.5) and the unknown product (δ 51.2) in a 1:1 ratio. Further heating did not change the product distribution.

4.3.5.3 Independent Synthesis of $L^{Pm}Lu(CH_2SiMe_3)_2$

To confidently assign the resonances attributed to complex **63** in the ^1H and $^{31}P\{^1H\}$ NMR spectrum of the reaction discussed in section 4.3.5, independent synthesis of $L^{Pm}Lu(CH_2SiMe_3)_2$ (**63**) was pursued. Addition of HL^{Pm} to one equivalent of $Lu(CH_2SiMe_3)_3(THF)_2$ produced the dialkyl complex **63** and one equivalent of $SiMe_4$ (Scheme 4.16). When monitored by multi-nuclear NMR spectroscopy, complex **63** was found to decompose in solution at ambient temperature with 50% of the material being consumed in 18 hours. While numerous complexes formed, the major product formed

resonated at δ 51.2 in the $^{31}P\{^{1}H\}$ spectrum. This result suggests that the unknown product produced in the reaction of $Lu(CH_2SiMe_3)_2(NHMes^*)(THF)_2$ and HL^{Pm} is a decomposition product from complex **63** and not due to the formation of the lutetium imido complex $L^{Pm}Lu{=}NMes^*$ (**65**).

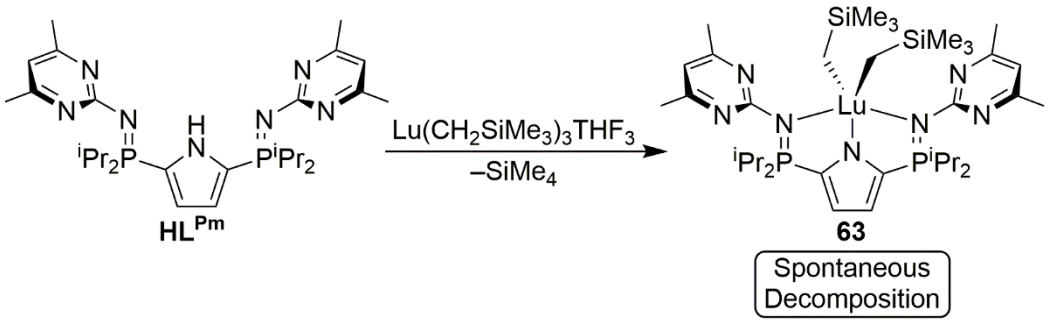

Scheme 4.16 Independent Synthesis of Complex **63**.

4.4 Salt Metathesis with Internal Lewis Bases

4.4.1 Synthesis of NaL^{Pm}

Addition of one equivalent of NaH to HL^{Pm} in toluene produced an orange bubbling solution (presumably from H_2 gas production). After 2 hours all volatiles were removed *in vacuo* leaving NaL^{Pm} as a dark purple solid in quantitative yield (Scheme 4.17). The ^{1}H NMR spectrum revealed the disappearance of the broad N–H resonance (δ 13.21). The CH_3 substituents of NaL^{Pm} resonated as a single peak at δ 2.06 indicating rapid rotation about

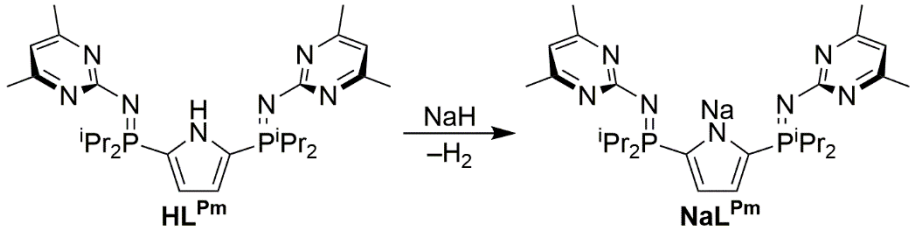

Scheme 4.17 Synthesis of NaL^{Pm}.

the N_{PN}–C_{Pm} bond. A single $^{31}P\{^{1}H\}$ resonance (δ 35.44) is indicative of the C_{2v} symmetry NaL^{Pm} possessed in solution.

4.4.2 Crystal Structure of $NaL^{Pm}\bullet C_7H_{16}$

Dissolving a sample of NaL^{Pm} in a 1:1 mixture of heptane and toluene and placing the saturated solution in a –35 °C freezer for 18 hours proved a successful method for obtaining X-ray quality crystals. In the solid state NaL^{Pm} exists as a dimer. The molecular structure is depicted in Figure 4.6 and highlighted metrical parameters are presented in Table 4.6. Like $[LiL^{iPr}]_2$, the alkali metal is coordinated to one ligand *via* an anionic pyrrole nitrogen (N1–Na1, N8–Na2) and one phosphinimine motif (N3–Na1, N9–Na2). Each sodium is also bound by a phosphinimine and pyrimidine donor of a second ligand.

Table 4.6 Selected Bond Lengths (Å) and Angles (º) for NaL^{Pm}.

Parameter	Distance (Å)	Parameter	Angle (º)
N1–Na1	2.436(1)	N1–Na1–N3	75.17(5)
N3–Na1	2.342(1)	N3–Na1–N6	48.12(5)
N6–Na1	3.044(1)	N6–Na1–N13	78.03(5)
N2–Na2	2.449(2)	N1–Na1–N13	146.39(5)
P1–N2	1.624(2)	P1–N2–Na2	142.52(8)
P3–N9	1.609(1)	N13–Na1–N10	56.23(5)

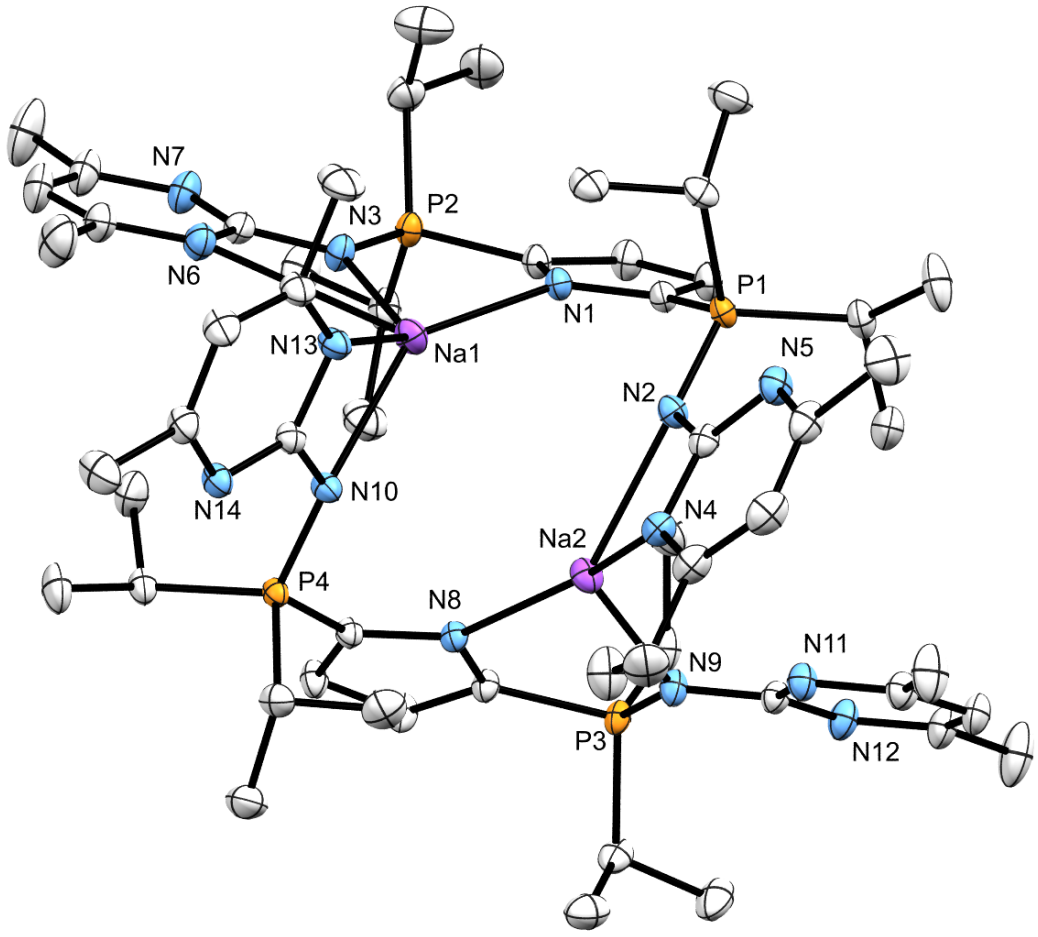

Figure 4.6 X-ray Crystal Structure (50% Probability) of (NaL^{Pm})•C_7H_8. Hydrogen Atoms and One Equivalent of Disordered Heptane are Omitted for Clarity.

4.4.3 Formation of $L^{Pm}ScCl_2$ and $L^{Pm}LuCl_2$

To test the ability of L^{Pm} to support well-defined rare earth halide complexes, NaL^{Pm} was reacted with one equivalent of either $ScCl_3(THF)_3$ or $LuCl_3(THF)_3$ in THF for 3 hours at ambient temperature (Scheme 4.18). Removal of all volatiles *in vacuo* and subsequent reconstitution in toluene afforded NaCl as a white precipitate. After filtration, removal of the volatiles yielded $L^{Pm}ScCl_2$ (**66**) and $L^{Pm}LuCl_2$ (**67**), respectively as a yellow solid (Scheme 4.18). Complexes **66** and **67** maintain the C_{2v} symmetry in solution, evident

by the single peak found in each $^{31}P\{^{1}H\}$ NMR spectrum (δ 53.23 (**66**), δ 52.16 (**67**)). The pyrimidine CH_3 substituents of complexes **66** and **67** appeared as two distinct, sharp peaks each integrating to 6H in the respective ^{1}H NMR spectra (**66**: δ 2.54, 2.28, **67**: δ 2.05, 1.29), suggesting coordination of the pyrimidine substituents to the metal centre.

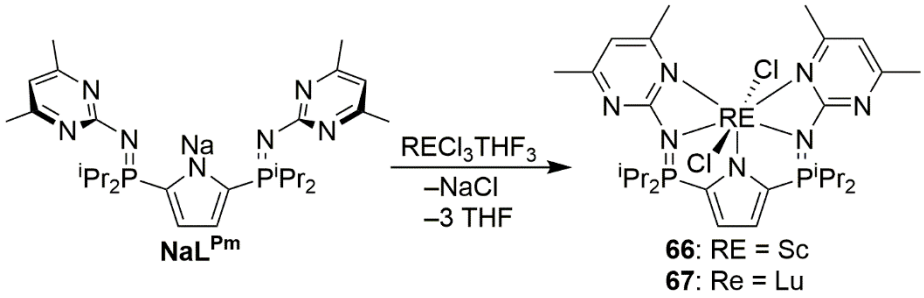

Scheme 4.18 Synthesis of Complexes **66** and **66**.

4.4.4 X-ray Crystal Structures of $L^{Pm}ScCl_2•C_7H_8$ and $L^{Pm}LuCl_2•C_7H_8$

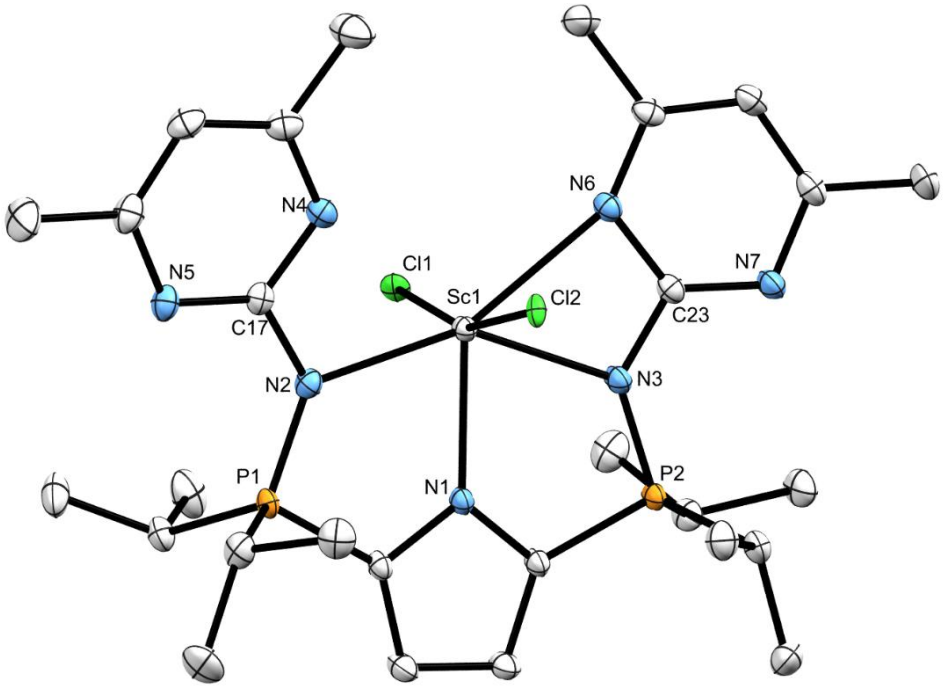

Figure 4.7 X-ray Crystal Structure (50% Probability) of Complex **66•C₇H₈**. Hydrogen Atoms and an Equivalent of Toluene are Omitted for Clarity.

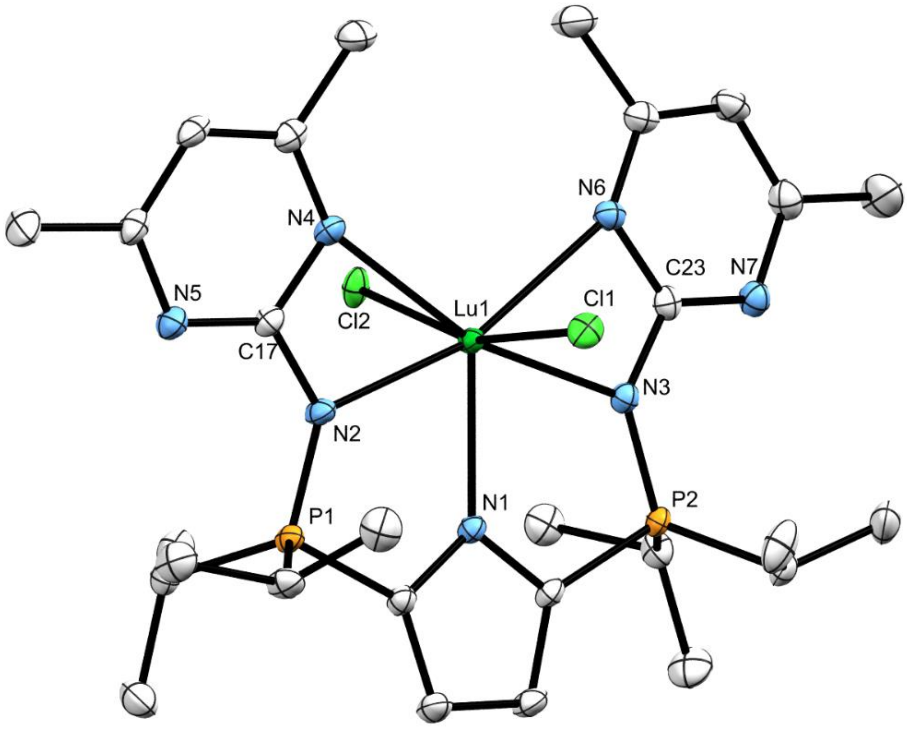

Figure 4.8 X-ray Crystal Structure (50% Probability) of Complex **67•C_7H_8**. Hydrogen Atoms and an Equivalent of Toluene are Omitted for Clarity

Dissolving complex **66** or **67** in a minimal amount of warm (50 ºC) toluene and allowing the saturated solution to slowly cool to –35 ºC over 18 hours afforded X-ray quality crystals of each complex. In the solid-state structures, shown in Figure 4.7 and 4.8, pyrimidine coordination was confirmed. The N4 atom of compound **66** lies 2.81 º further out of the plane of the pyrrole ligand than N6 (P1–N2–C17–N4 torsion angle = 174.3(2) º, P2–N3– C23–N6 torsion angle = 171.46(2) º). The metal centres of complex **66** and **67** both possessed a distorted pentagonal bipyramidal geometry with the five coordinated nitrogen atoms occupying the equatorial sites and the chloride ligands in the axial positions (**66**: Cl1–Sc1–Cl2 = 162.36(3) º, **67**: Cl1–Lu1–Cl2 = 162.48(3) º).

Table 4.7 Selected Bond Lengths (Å) and Angles (º) for Complex **66** and **66**.

Parameter	66 (Sc)	67 (Lu)
Selected Bond Lengths (Å)		
N1–RE1	2.230(2)	2.324(2)
N2–RE1	2.216(2)	2.318(2)
N4–RE1	2.573(2)	2.546(2)
Cl2–RE1	2.4888(8)	2.5808(8)
P1–N2	1.627(2)	1.619(2)
Selected Angles (º)		
Cl1–RE1–Cl2	162.36(3)	162.48(3)
N1–RE1–N2	72.36(7)	69.88(6)
N2–RE1–N4	55.17(7)	54.59(6)
N4–RE2–N6	105.16(6)	111.11(6)

4.4.5 Imide Delivery Agents

4.4.5.1 Overview

Isolation of complex **66** provided a platform for experimentation with magnesium imide salts (MgNR), as they might serve as suitable imide ($^{2-}$NR) transfer agents. Should the desired loss of $MgCl_2$ and concomitant establishment of the RE=NR motif occur, the pendent pyrimidine rings should be readily available to stabilize the resulting complex.

Previous work in the Hayes lab had produced the magnesium amide salts $[MgNC_6H_5(THF)]_6$ and $[MgNC_6F_5]_8(THF)_6$. It was hypothesized that addition of

$[MgNC_6H_5(THF)]_6$ or $[MgNC_6F_5]_8(THF)_6$.to $L^{Pm}ScCl_2$ could form $L^{Pm}Sc(NC_6H_5)$ (**68a**) or $L^{Pm}Sc(NC_6F_5)$ (**68b**), respectively (Scheme 4.19).

4.4.5.2 Addition of $[MgNC_6H_5(THF)]_6$ and $[MgNC_6F_5]_8(THF)_6$ to $L^{Pm}ScCl_2$

Scoping NMR tube reactions were conducted with complex **66** and one sixth of an equivalent of $[MgNC_6H_5(THF)]_6$ in THF-d_8. Upon mixing the two complexes a 7% decrease in the amount of complex **66** was detected by $^{31}P\{^1H\}$ NMR spectroscopy (δ 53.23) and a new resonance appeared at δ 52.07. Tracking the reaction *via* $^{31}P\{^1H\}$ NMR spectroscopy at ambient temperature for an additional 21 hours revealed that approximately 25% of complex **66** was converted into a compound that resonated at δ 52.07. Heating the mixture did not promote further conversion and attempts at recrystallization were unsuccessful.

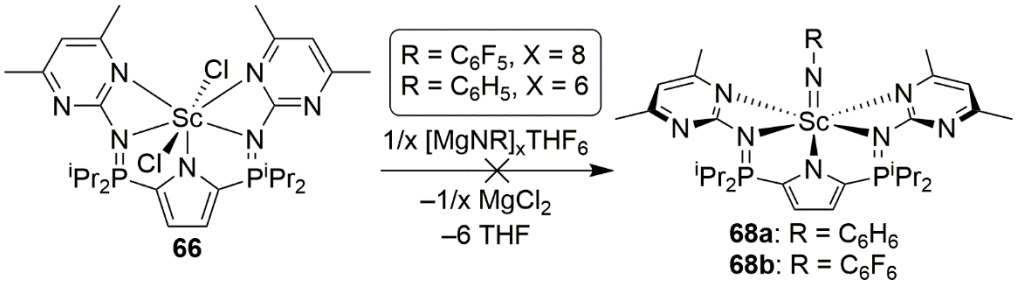

Scheme 4.19 Planned Synthesis for Terminal Imido Bond Formation from Magnesium Imide Salts.

Further attempts were undertaken with $[MgNC_6F_5]_8(THF)_6$ as the imide delivery agent. Replacement of the C_6H_5 group with C_6F_5 allowed for use of $^{19}F\{^1H\}$ NMR spectroscopy. Reaction of one eighth of an equivalent of $[MgNC_6F_5]_8(THF)_6$ with complex **66** at ambient temperature over 21 hours produced one predominant product (52% of the

phosphorus-containing material) which appears at δ 52.97 in the $^{31}P\{^{1}H\}$ NMR spectrum. It should be noted that the product formed in this reaction possessed a very similar $^{31}P\{^{1}H\}$ chemical shift as the product formed in the reaction of complex **66** and $[MgNC_6H_5(THF)]_6$. Increasing the temperature to 60 ºC for 24 hours led to no more conversion. Attempts to isolate this product by recrystallization were unsuccessful. In an attempt to push this reaction towards completion a second attempt which utilized one quarter of an equivalent of $[MgNC_6F_5]_8(THF)_6$ was undertaken. While this yielded a greater amount of product (56% of phosphorus-containing material), purification attempts were unsuccessful. Heating this mixture to 60 ºC for 21 hours resulted in a decrease of the newly formed product (δ 52.97) and the emergence of a new peak in the $^{31}P\{^{1}H\}$ NMR spectrum δ 45.40 which comprised 31% of the phosphorus containing materials.

4.5 Conclusions

Preliminary attempts at investigating alternative pathways at forming a rare earth imido complexes were explored. To explore salt metathesis strategies, $L^{iPr}ScCl_2$, **50**, was synthesized. Addition of 2 equivalents of MeLi led to primary production of the transmetalated species $[LiL^{iPr}]_2$. However, the reaction of $L^{iPr}ScCl_2$ with either half an equivalent of $[(THF)LiNHDipp]_2$ or one equivalent of $KN(SiMe_3)_2$ lead to production of $L^{iPr}ScCl(NHDipp)$, **53**, or $L^{iPr}ScCl(N(SiMe_3)_2)$, **58**.

A new ancillary ligand featuring internal Lewis bases, HL^{Pm}, was synthesized. Formation of the dialkyl complex $L^{Pm}Lu(CH_2SiMe_3)_2$, **63**, resulted in spontaneous decomposition. Efforts to explore salt metathesis reactivities with this ligand afforded the seven-coordinate dihalide complexes $L^{Pm}ScCl_2$, **66**, and $L^{Pm}LuCl_2$, **67**. Reactivity of

complex **66** with magnesium imide salts ($[MgNC_6F_5]_8(THF)_6$ or $[MgNC_6H_5(THF)]_6$) resulted in the formation of a new product, however their identity has not been elucidated.

Chapter 5 – Summary and Future Work

5.1 Summary of Chapters 2 and 3

Chapters 2 and 3 of this thesis described the development of terminal lutetium imido precursors supported by L^{Ph} (Chapter 2) and L^{iPr} (Chapter 3). Facile coordination of the ancillary ligand to the lutetium metal centre was achieved by addition of either HL^{Ph} or HL^{iPr} to $Lu(CH_2SiMe_3)_3(THF)_2$, which yielded the dialkyl complexes $L^{Ph}Lu(CH_2SiMe_3)_2$, **36-Lu**, and $L^{iPr}Lu(CH_2SiMe_3)_2$, **39b**, respectively (Scheme 5.1).

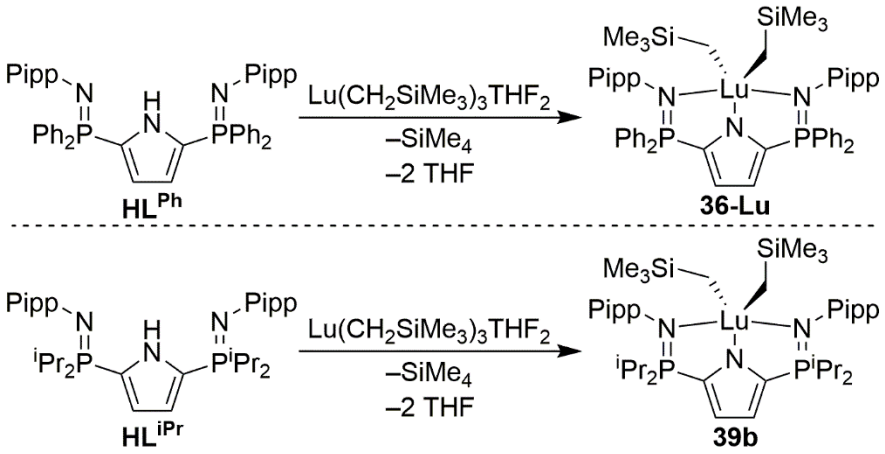

Scheme 5.1 Formation of Complexes **36-Lu** and **39b**.

Addition of Ph_3CNH_2 to complex **36-Lu** was shown to promote formation of $L^{Ph}Lu(CH_2SiMe_3)(NHCPh_3)$, **37**, (Scheme 5.2). Complex **37** underwent spontaneous C–H bond activation of the CPh_3 substituent in solution and produced $L^{Ph}Lu(\text{-}\kappa^2\text{-}NHCPh_2C_6H_4)$, **45**. Further heating resulted in the formation of half an equivalent of $L^{Ph}Lu(NHCPh_3)_2$, **44** (Scheme 5.2). Deuterium labeling (section 2.7.4) suggested that the decomposition of $L^{Ph}Lu(CH_2SiMe_3)(NHCPh_3)$ did not proceed through the lutetium imido intermediate $L^{Ph}Lu{=}NCPh_3$, **46** .

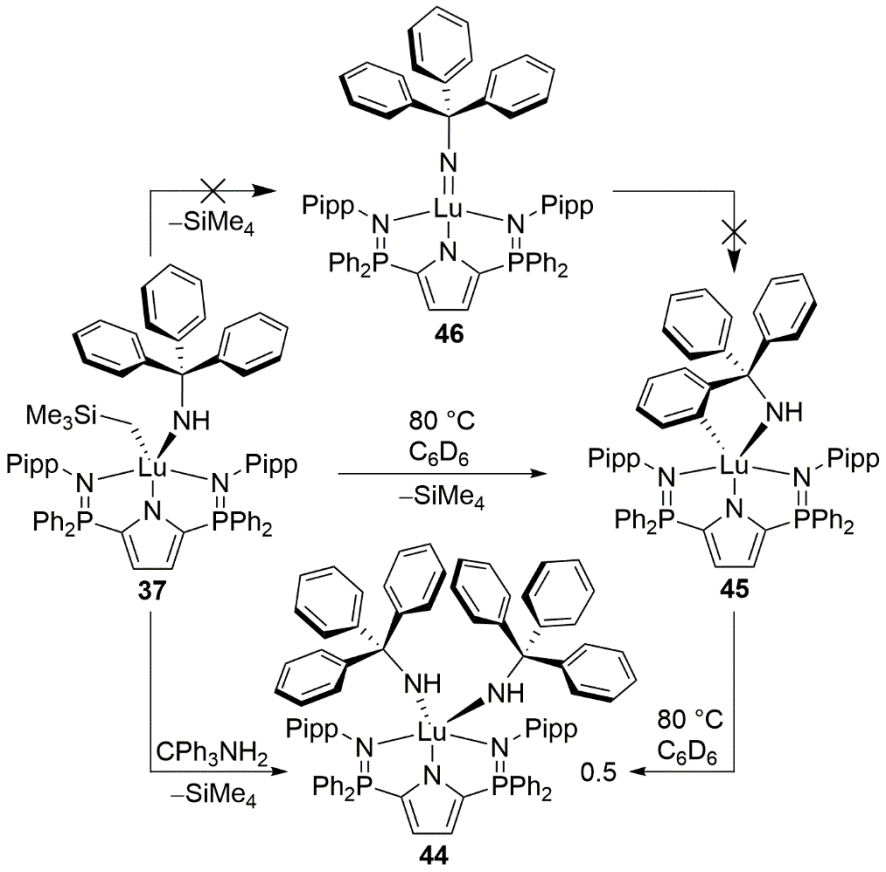

Scheme 5.2 Decomposition of Complex **37**.

Addition of Ph_3CNH_2 or $DippNH_2$ to $L^{iPr}Lu(CH_2SiMe_3)_2$ created the alkyl amido complexes $L^{iPr}Lu(CH_2SiMe_3)(NHCPh_3)$, **40c**, and $L^{iPr}Lu(CH_2SiMe_3)(NHDipp)$, **40d**, respectively (Scheme 5.3). Remarkably, implementation of the electron donating P–$^{i}Pr_2$ substituents resulted in $L^{iPr}Lu(CH_2SiMe_3)(NHCPh_3)$ experiencing no decomposition, even upon prolonged exposure to heat (60 ºC). Similarly, $L^{iPr}Lu(CH_2SiMe_3)(NHDipp)$ underwent no reactivity in solution when heated to 60 ºC. Addition of one or two equivalents of DMAP to complex **40c** induced a disproportionation reaction which formed half and equivalent of both $L^{iPr}Lu(NHCPh_3)_2$, **48c**, and $L^{iPr}Lu(CH_2SiMe_3)_2$, **39b**, which decomposed in the presence of DMAP (Scheme 5.3). An analogous Lewis base induced

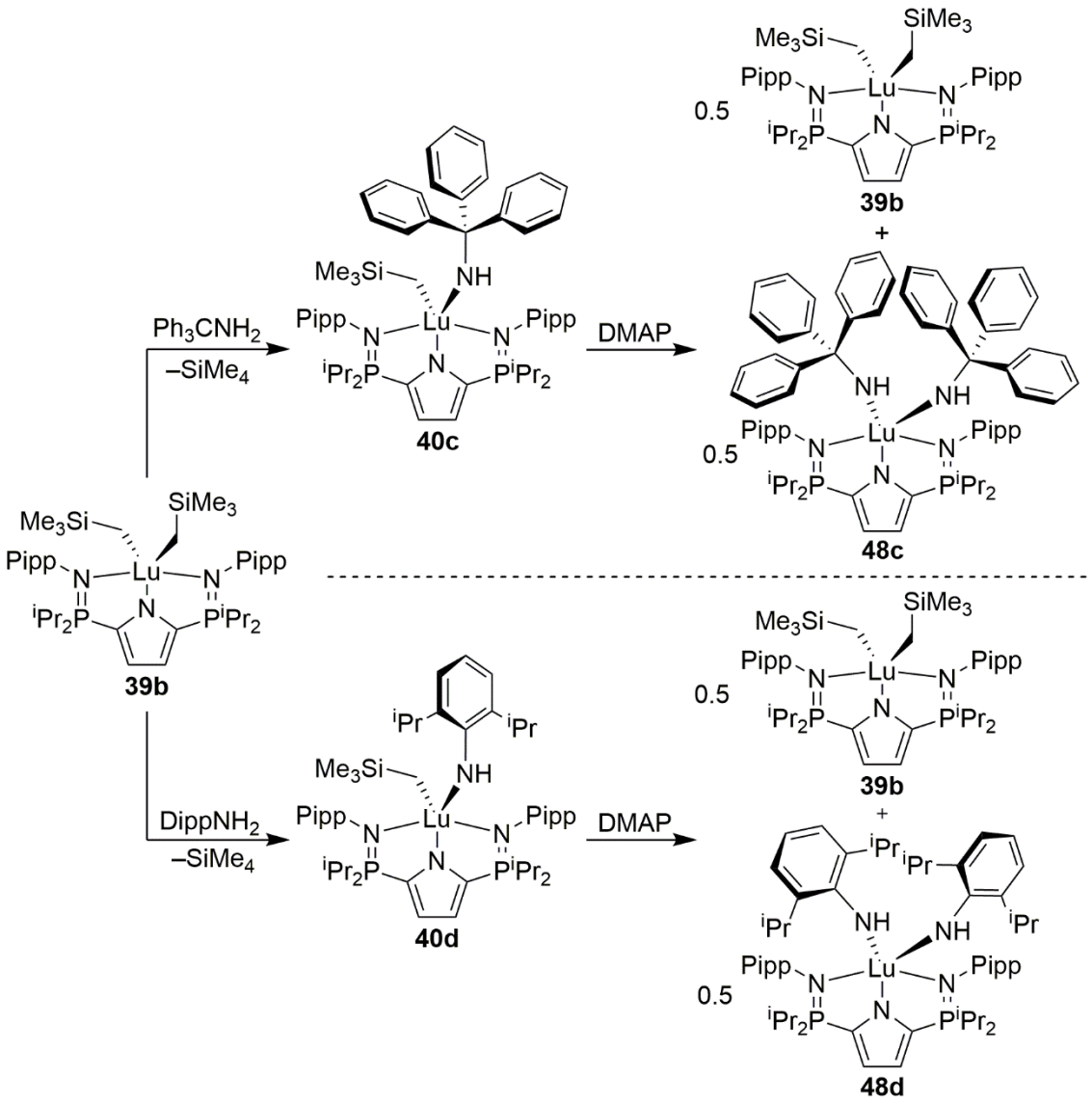

Scheme 5.3 Reactivity of Complex **40c** and **40d** with DMAP.

disproportionation reaction took place when $L^{iPr}Lu(CH_2SiMe_3)(NHDipp)$ was utilized (Scheme 5.3).

5.2 Future Work from Chapter 3

5.2.1 Future Work from Section 3.3.1.2

Formation of the scandium cation $[L^{iPr}Sc(CH_2SiMe_2CH_2SiMe_3)][H_3CB(C_6F_5)_3]$, **47**, was achieved, however time restrictions prevented further studies of this species. Addition of half an equivalent of either $[(THF)LiNHCPh_3]_2$ or $[(THF)LiNHCPh_3]_2$ to complex **47** is hypothesized to generate alkylamido complexes $L^{iPr}Sc(CH_2SiMe_2CH_2SiMe_3)(NHCPh_3)$ (**69a**) and $L^{iPr}Sc(CH_2SiMe_2CH_2SiMe_3)(NHDipp)$ (**69b**) respectively (top, Scheme 5.4). Attempts at generating the analogous cationic lutetium complex, $[L^{iPr}Lu(CH_2SiMe_2CH_2SiMe_3)][H_3CB(C_6F_5)_3]$, **70**, *via* reaction of $B(C_6F_5)_3$ with one equivalent on $L^{iPr}Lu(CH_2SiMe_3)_2$ have not been conducted (bottom,

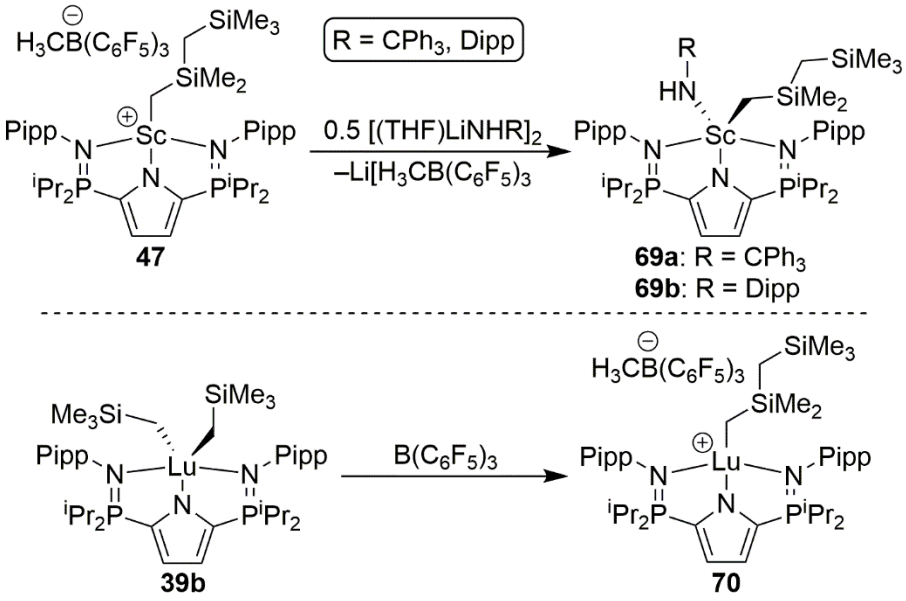

Scheme 5.4 Addition of Amide Salts to Complex **47**, and Formation of Complex **70**.

Scheme 5.4).

5.2.2 Future Work from Section 3.4

In the literature, formation of terminal rare earth imido complexes have been achieved by addition of either DMAP or pyrimidine to an rare earth alkylamido complex.[41-43, 45-46, 51-52] Furthermore, the role the Lewis base plays in this reaction (outside of the fact it is required) has not been explored. Addition of a variety of Lewis bases (*e.g.* THF, pyridine) to complexes $L^{iPr}Lu(CH_2SiMe_3)(NHCPh_3)$, **40c**, and $L^{iPr}Lu(CH_2SiMe_3)(NHDipp)$, **40d**, presents an opportunity to observe whether alternative Lewis bases promote alternative reactivities.

5.3 Summary of Chapter 4

5.3.1 Salt Metathesis Reactivity with L^{iPr}

Protio ligand, HL^{iPr}, was reacted with one equivalent of NaH which formed NaL^{iPr} in quantitative yield. Facile production of $L^{iPr}ScCl_2$, **50**, was achieved through the reaction of NaL^{iPr} to one equivalent of $ScCl_3(THF)_3$ (Scheme 5.5).

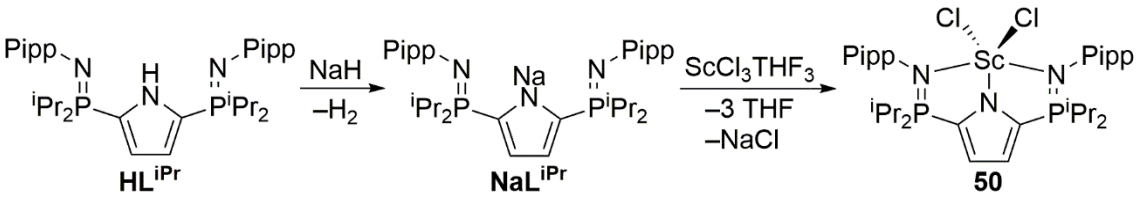

Scheme 5.5 Formation of Complex **50**.

Efforts at derivatizing the halide ligands of complex **50** included the addition of two equivalents of MeLi (Scheme 5.6). While crystals of the desired dialkyl complex $L^{iPr}Sc(CH_3)_2$, **51**, were obtained, the compound was produced in too small a quantity to be isolated, or for definitive spectroscopic assessments to be made. The major product formed

in this reaction was determined to be the lithium salt $[LiL^{iPr}]_2$, presumably formed *via* a transmetalation process.

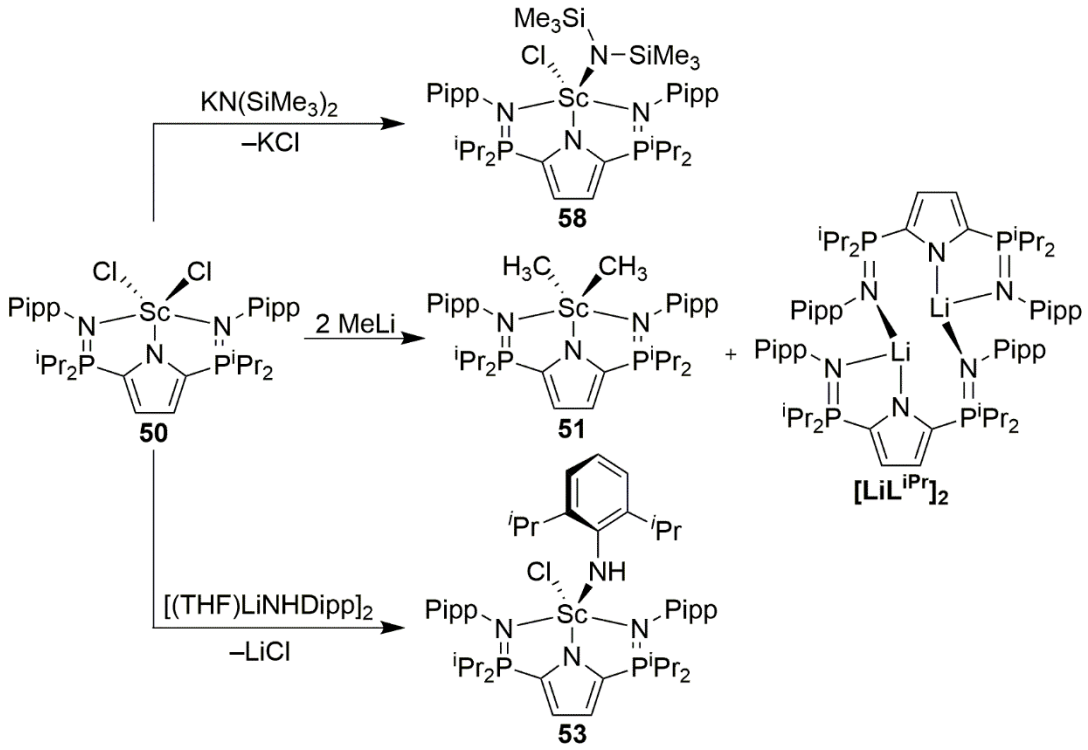

Scheme 5.6 Salt Metathesis Reactivity of Complex **50**.

Reactivity of complex **50** with amide salts was also explored. Addition of half an equivalent of $[(THF)LiNHDipp]_2$ to $L^{iPr}ScCl_2$ promoted formation of $L^{iPr}ScCl(NHDipp)$, **53**, (Scheme 5.6). The analogous reaction between half an equivalent of $[(THF)LiNHCPh_3]_2$ and $L^{iPr}ScCl_2$ did not promote any reactivity. A third amide salt, $KN(SiMe_3)_2$, was reacted with $L^{iPr}ScCl_2$ which led to production of $L^{iPr}ScCl(N(SiMe_3)_2)$, **58**, (Scheme 5.6). In the hope of achieving Si–Cl bond formation and concomitant generation of the lutetium imido complex $L^{iPr}Sc{=}NSiMe_3$, complex **58** was heated to 230 ^oC for 24 hours. Despite these extreme conditions, no reaction was observed.

5.3.2 Internal Lewis Bases

The new ancillary ligand, which featured additional Lewis bases, HL^{Pm}, was synthesized through the reaction of two equivalents of 5,7-dimethylpyrazolo-1,5a-pyrimidine, **62a**, and 2,5-bis(diisopropylphosphino)-N-H-pyrrole (Scheme 5.7). Addition of HL^{Pm} to $Lu(CH_2SiMe_3)_3(THF)_2$ resulted in formation of the lutetium dialkyl complex $L^{Pm}Lu(CH_2SiMe_3)_2$, **63**, (Scheme 5.7). Complex **63** was found to undergo spontaneous reactivity in solution, producing an unknown compound.

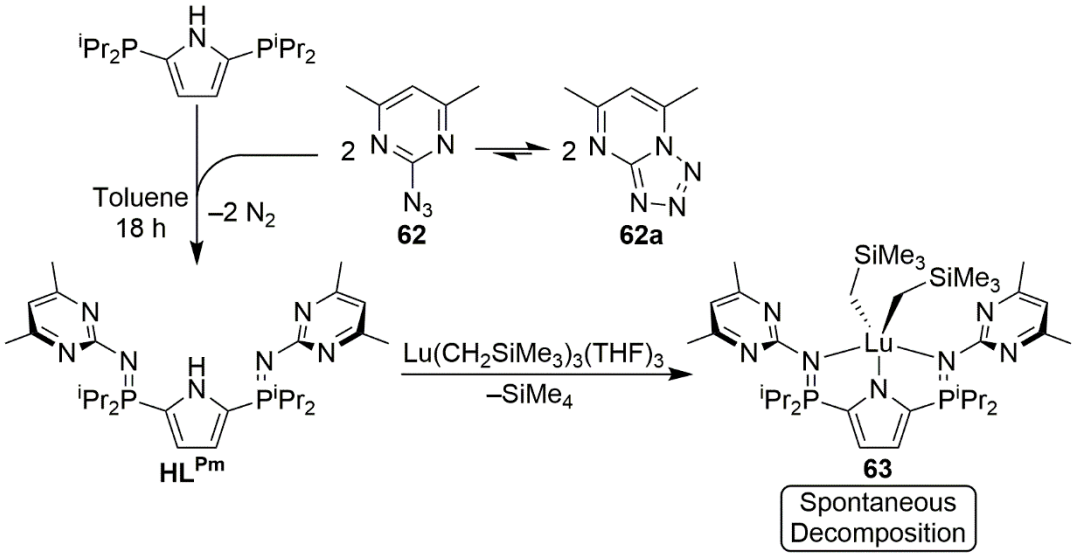

Scheme 5.7 Formation of HL^{Pm} and Complex **63**.

Facile production of NaL^{Pm} was achieved through the reaction of NaH and HL^{Pm}. Addition of $ScCl_3(THF)_3$ or $LuCl_3(THF)_3$ to NaL^{Pm} produced the seven-coordinate dihalide complexes $L^{Pm}ScCl_2$, **66**, or $L^{Pm}LuCl_2$, **67**, respectively (Scheme 5.8).

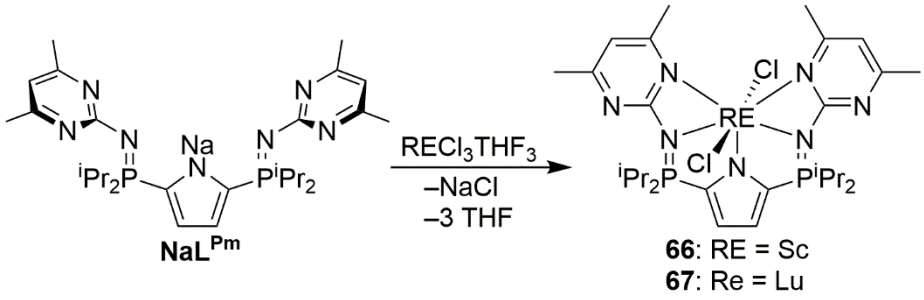

Scheme 5.8 Formation of Complexes **66** and **67**.

5.4 Future Work from Chapter 4

5.4.1 Future Work from Section 4.2

5.4.1.1 Addition of MeLi to L^{iPr}ScCl(NHDipp)

Addition of half and equivalent of [(THF)LiNHDipp]$_2$ to L^{iPr}ScCl$_2$ proved an effective method at generating L^{iPr}ScCl(NHDipp) (**53**, Scheme 5.9). However, time restrictions prevented further reactivity of complex **53**. Addition of MeLi to complex **53** is

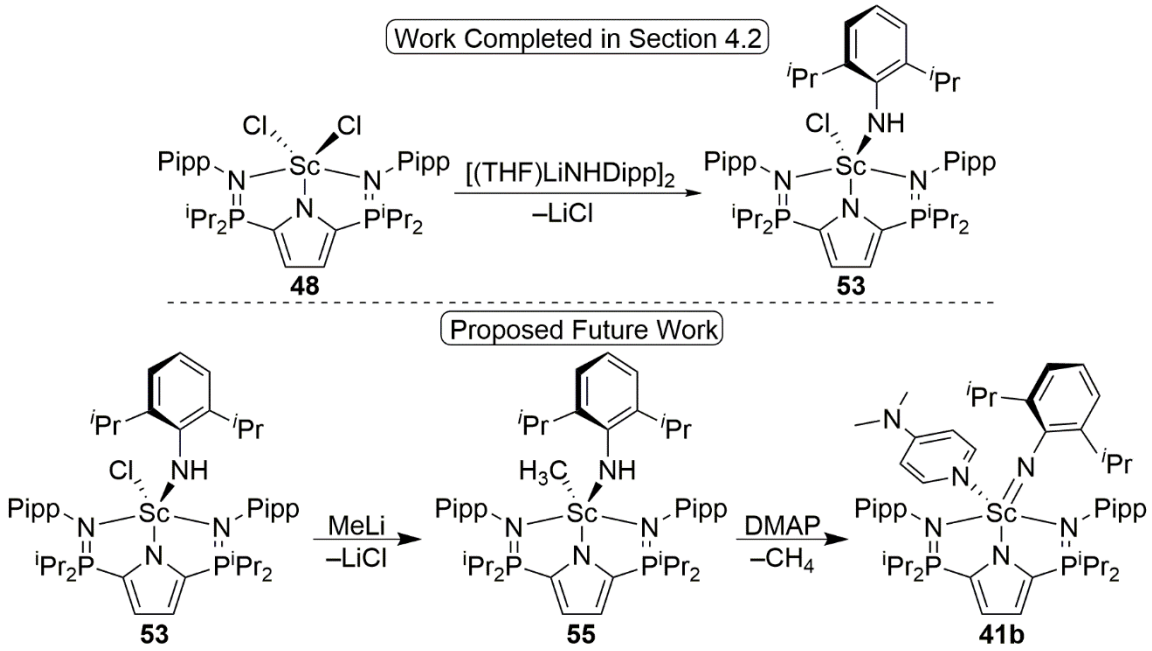

Scheme 5.9 Proposed Future Work from Section 4.2.

predicted to generate the alkyl amido complex $L^{iPr}Sc(CH_3)(NHDipp)$ (**55**, Scheme 5.9). Isolation of complex **59** would allow for the addition of DMAP which is predicted to promote the loss of CH_4 and generate the scandium imido complex $L^{iPr}ScNDipp(DMAP)$ (**41b**, Scheme 5.9).

5.4.1.2 Lutetium Analogs

It should be noted that only scandium containing species were reacted with amide salts. Addition of $LuCl_3(THF)_3$ to NaL^{iPr} is expected to generate the lutetium dihalide species $L^{iPr}LuCl_2$ (**71**, Scheme 5.10). Isolation of $L^{iPr}LuCl_2$ would allow for the propensity for L^{iPr} to undergo transmetalation with MeLi to be further investigated. The reaction of $L^{iPr}LuCl_2$ and two equivalents of MeLi could be envisioned to promote the formation of $[LiL^{iPr}]_2$ (akin to the results presented in section 4.1.7). Conversely, use of the larger, Lu metal centre could result in the production of $L^{iPr}Lu(CH_3)_2$ (**72**, Scheme 5.10).

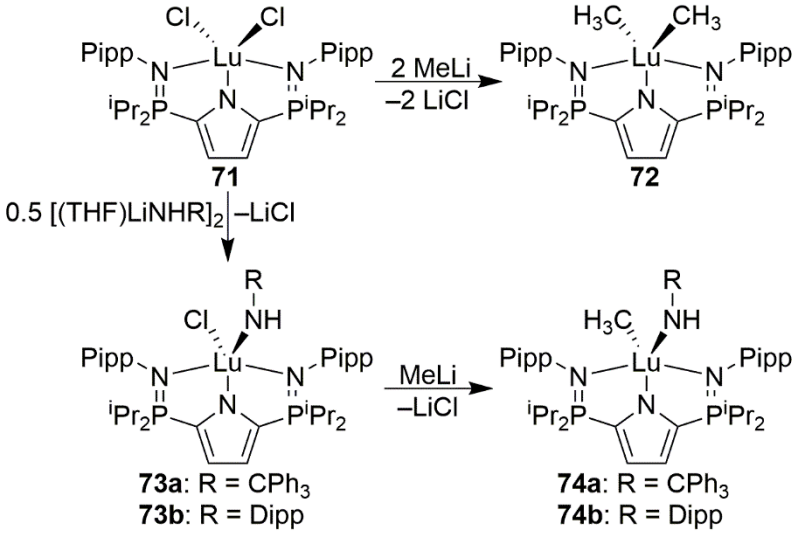

Scheme 5.10 Proposed Synthesis and Reactivity of Complex **71**.

Like the work described in section 4.2.4, the amide salts ($[(THF)LiNHDipp]_2$, $[(THF)LiNHCPh_3]_2$) could be reacted with two equivalents of $L^{iPr}LuCl_2$ to generate,

$L^{iPr}LuCl(NHCPh_3)$ **73a**, and $L^{iPr}LuCl(NHDipp)$, **73b**, respectively (Scheme 5.10). Addition of MeLi to either complex **73a** or **73b** could be envisioned to functionalize the remaining halide ligand and establish the alkyl amido complexes, $L^{iPr}Lu(CH_3)(NHCPh_3)$ **74a**, or $L^{iPr}Lu(CH_3)(NHDipp)$, **74b**, respectively. Formation of complex **74a** and **74b** are of particular interest as they are congeners of the terminal imido precursors investigated in Chapter 3 ($L^{iPr}Lu(CH_2SiMe_3)(NHDipp)$, **40c**, and $L^{iPr}Lu(CH_2SiMe_3)(NHCPh_3)$, **40d**) which differ by a CH_3/CH_2SiMe_3 ligand. Currently, no studies directly comparing the effect differing alkyl ligands have in terminal rare earth imido complex. Addition of DMAP to complexes **74a** or **74b** would allow for a direct comparison to the results presented in section 3.4.

5.4.2 Future Work from Section 4.3.5.3

Production of $L^{Pm}Lu(CH_2SiMe_3)_2$, **63**, was achieved from the addition of HL^{Pm} to $Lu(CH_2SiMe_3)_3(THF)_2$ (Scheme 5.11). However, at ambient temperature complex **63** was found to decompose. Furthermore, $L^{iPr}Lu(CH_2SiMe_3)_2$, **39b**, (which experiences no reactivity upon prolonged exposure to heat) undergoes decomposition when exposed to one equivalent of DMAP. Due to time constraints, minimal efforts focused on elucidating the identity of the product afforded by the decomposition of $L^{Pm}Lu(CH_2SiMe_3)_2$ as well as the reaction of complex **39b** and DMAP have been conducted. The identity of these products are of fundamental interest to our lab.

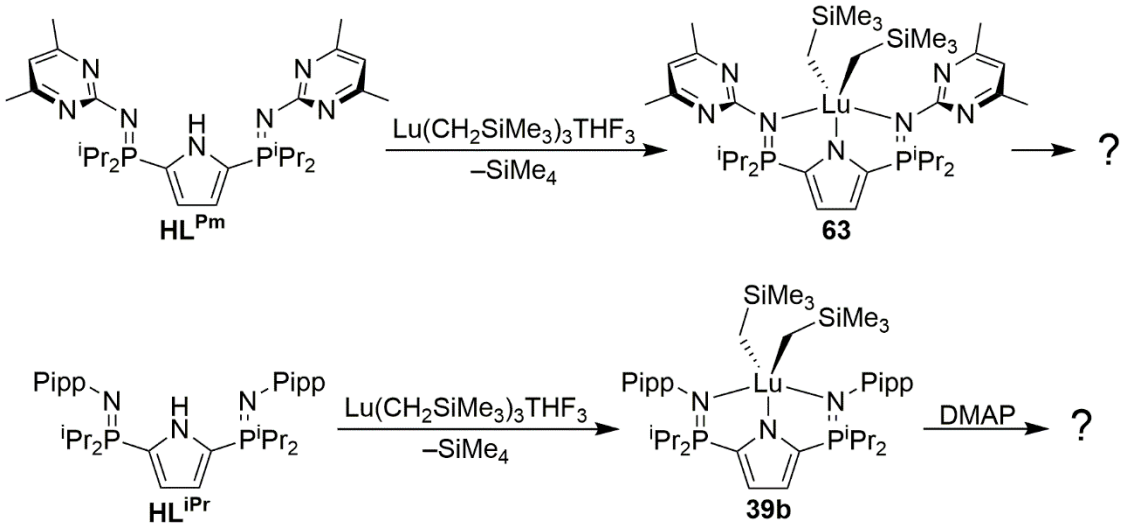

Scheme 5.11 Decomposition of Complex **63** and Reactivity of Complex **39b** and DMAP.

It was hypothesized that the decomposition exhibited by complex **63** could be induced by steric crowding around the metal centre. Addition of $B(C_6F_5)_3$ to $L^{Pm}Lu(CH_2SiMe_3)_2$ is predicted to result in alkide abstraction and produce $[L^{Pm}Lu(CH_2SiMe_2CH_2SiMe_3)][H_3CB(C_6F_5)_3]$ (**75**, Scheme 5.12), akin the reaction between $B(C_6F_5)_3$ and $L^{iPr}Sc(CH_2SiMe_3)_2$ (Section 3.3.1.2). Formation of a cationic species is expected to reduce the steric pressure around the metal centre and could be envisioned to yield a thermally stable species.

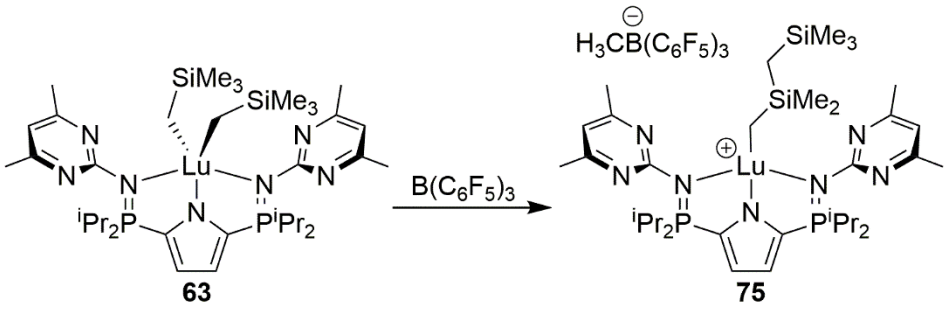

Scheme 5.12 Addition of $B(C_6F_5)_3$ to Complex **63**.

5.4.3 Future Work from Section 4.4.5

Production of $L^{Pm}ScCl_2$, **66**, and $L^{Pm}LuCl_2$, **67**, presents an opportunity to further develop salt metathesis strategies with rare earth metals. However, time restrictions prevented such studies. Formation of rare earth dialkyl complexes bearing two CH_3 ligands remains of interest to the development of rare earth imido complex. As such, addition of two equivalents of MeLi to either complex **66** or **67** to produce the dimethyl complexes $L^{Pm}Sc(CH_3)_2$, **76**, and $L^{Pm}Lu(CH_3)_2$, **77**, respectively, remains a worthwhile pursuit (top, Scheme 5.13). The presence of the pyrimidine substituents, and their coordination to the metal centre could be envisioned to hinder the transmetalation discussed in section 4.1.7. Subsequent addition of Ph_3CNH_2 or $DippNH_2$ would be expected to yield the alkyl amido complexes $L^{Pm}RE(CH_3)(NHCPh_3)$, **78a** (RE = Sc) and **78b** (RE = Lu), and $L^{Pm}RE(CH_3)(NHDipp)$, **78c** (RE = Sc) and **78d** (RE = Lu).

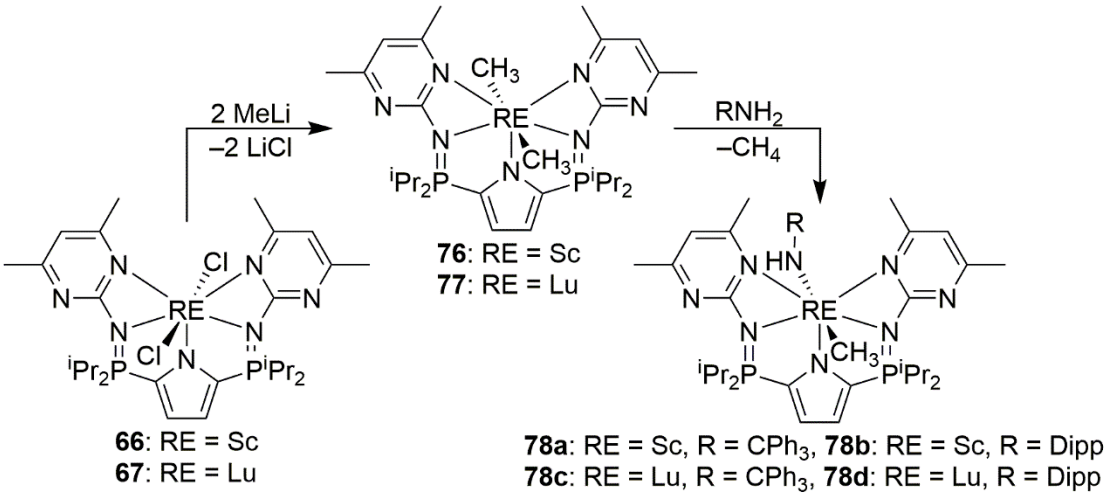

Scheme 5.13 Proposed Future Reactivities for Complexes **66** and **67**.

5.4.4 Future Work from Section 4.4.5

While the reaction of the magnesium imide salts ($[MgNC_6H_5(THF)]_6$ and $[MgNC_6F_5]_8(THF)_6$) with $L^{Pm}ScCl_2$ appeared promising, ultimately, time restrictions prevented further study of these reactions. Given the success that the $NHCPh_3$ and NHDipp ligands have displayed in this thesis, synthesis of the magnesium imide cluster compounds $[MgNCPh_3]_x(THF)_y$, **79**, and $[MgNDipp]_x(THF)_y$, **80**, (x and y ≥ 1, Scheme 5.14) appears as a worthwhile pursuit. Synthesis of $[MgNC_6H_5(THF)]_6$ and $[MgNC_6F_5]_8(THF)_6$ was achieved through addition of $Mg(^nBu)_2$ to $H_5C_6NH_2$ or $F_5C_6NH_2$, respectively. Thus, addition of $Mg(^nBu)_2$ to Ph_3CNH_2 and $DippNH_2$ appears as a logical starting point for the synthesis of $[MgNCPh_3]_x(THF)_y$, **79**, and $[MgNDipp]_x(THF)_y$, **80**, (Scheme 5.14). Addition of compound **79** or **80** to $L^{Pm}ScCl_2$ could be envisioned to generate the scandium imide complexes $L^{Pm}Sc{=}NCPh_3$, **81a**, and $L^{Pm}Sc{=}NCDipp$, **81b** (Scheme 5.14).

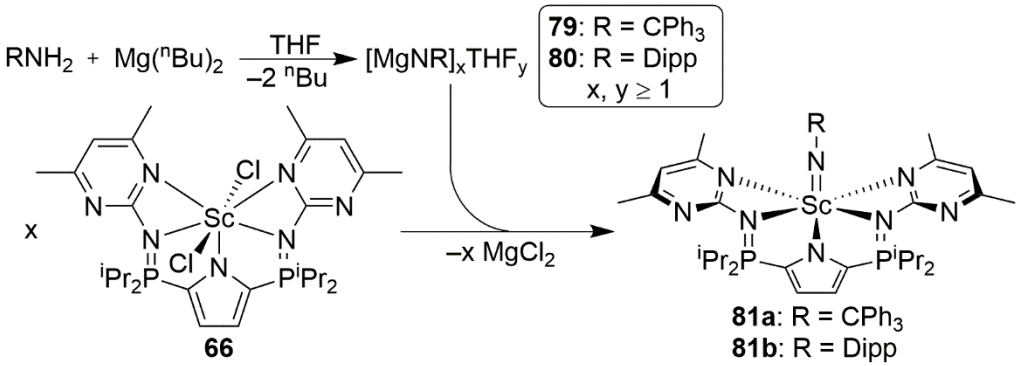

Scheme 5.14 Future Work for Imide Delivery Agents.

Chapter 6 – Experimental Methods

6.1 General Procedures

6.1.1 Laboratory Equipment and Apparati

Unless otherwise specified, all synthetic manipulations were conducted in the absence of air and moisture, under an argon atmosphere using either a double manifold high vacuum line with Kontes valves or an MBraun Labmaster 130 glove box. All vacuum lines and glove box antechambers were evacuated using an Edwards RV12 pump. Specialty glassware designed for this work included swivel frit apparati and thick walled (5 mm) glass bombs, herein referred to as bombs, equipped with Kontes valves.[2] Glass utilized in experimental procedures was stored in a 115 °C oven for a minimum of 12 hours or heated directly *via* a Bunsen burner whereupon the glass was assembled on the vacuum line or placed in the antechamber and evacuated while hot.

6.1.2 Solvents

Solvents utilized in air and moisture sensitive reactions were obtained directly from an MBraun Solvent Purification System (SPS), further degassed and stored over molecular sieves (4 Å) in 500 mL bombs charged with one of titanocene (benzene, toluene, pentane, heptane), CaH_2 (dichloromethane), or Na/benzophenone (THF, diethyl ether) and stored under static vacuum. These solvents were transferred to their receiving flask under reduced pressure and temperature (–78 °C). Solvents used in synthetic procedures that were impervious to air and moisture were acquired from EMD and used with no further purification.

Deuterated solvents used for NMR spectroscopy were dried and stored over either Na/benzopehenone (benzene-d_6, toluene-d_8, THF-d_8) or CaH_2 (chloroform-d_1, bromobenzene-d_5). These solvents were degassed *via* three or more freeze-pump-thaw cycles and distilled under reduced pressure and temperature (–78 °C) into a bomb containing molecular sieves (4 Å).

6.1.3 NMR Spectroscopy

NMR spectra (^{1}H, ^{11}B{^{1}H}, ^{13}C{^{1}H}, ^{19}F{^{1}H}, ^{31}P{^{1}H}, ^{1}H–^{1}H COSY, ^{1}H–^{13}C HSQC, and ^{1}H–^{13}C HMBC) were acquired on a Bruker Avance II 300 MHz spectrometer (^{1}H 300.13 MHz, ^{11}B 96.251 MHz ^{13}C 75.47 MHz, ^{19}F 282.23 MHz, ^{31}P 121.49 MHz). Kinetic and DOSY NMR experiments were performed on a Bruker Avance III HD 700 MHz spectrometer equipped with a gradient controller and a TXO probe with automatic tuning and a shielded z-gradient. The gradient shape was sinusoidal, and its length was 1.8 ms. The gradient strength was increased by 16 increments of 6.2% (2%–95%). The time between the midpoints of these gradients was 99.97 ms. Experiments were performed at 292 K. NMR spectroscopic data is presented in parts per million (ppm) where ^{1}H and ^{13}C{^{1}H} shifts are referenced to $SiMe_4$ through internal ^{1}H and ^{13}C{^{1}H} resonance(s) (respectively) of the corresponding solvent: benzene-d_6 (7.16 ppm and 128.0 ppm), toluene-d_8 (2.09, 6.98, 7.02, 7.09 ppm and 20.4, 125.2, 128.0, 128.9, 137.5 ppm), chloroform-d_1 (7.27 ppm and 77.36 ppm), and bromobenzene-d_5 (7.28, 7.00, 6.93 ppm, and 122.3, 126.1, 129.3, 130.9 ppm). An 85% H_3PO_4 standard with an internal C_6D_6 capillary was used to reference ^{31}P{^{1}H} spectra (0 ppm). ^{11}B spectra were referenced to a boron trifluoride diethyl etherate sample (0 ppm). ^{19}F spectra were referenced to a

trifluorotoluene sample (−63.7 ppm). Unless otherwise stated all NMR samples were prepared and capped in an inert glove-box atmosphere.

^{1}H and $^{19}F\{^{1}H\}$ NMR spectral data is presented in the following manner: chemical shift (ppm), multiplicity, *J* = coupling constant (Hz), number of protons, assignment. $^{13}C\{^{1}H\}$ NMR spectral data is presented in the following manner: chemical shift (ppm), multiplicity, *J* = coupling constant (Hz), assignment. $^{31}P\{^{1}H\}$, $^{11}B\{^{1}H\}$, and $^{19}F\{^{1}H\}$ NMR spectral data is listed by chemical shift.

6.1.4 Kinetics

In regards to the kinetic studies performed on $L^{Ph}Lu(CH_2SiMe_3)(NHCPh_3)$, a consistent amount of compound (0.0185 g, 0.0151 mmol) was placed into an NMR tube charged with a sealed capillary filled with a 1M H_3PO_4 standard. The NMR tube was brought out of the glovebox and chilled to –78 °C. Toluene-d_8 (0.55 mL) was syringed slowly into to the tube. The vessel was shaken vigorously to completely dissolve the compound. The sample was placed into a Bruker Avance III HD 700 MHz NMR spectrometer that was pre-equilibrated to the desired temperature. The sample was allowed to equilibrate to this temperature over the course of shimming the probe (~ 10 min). Rate constants were obtained by monitoring $^{31}P\{^{1}H\}$ resonances referenced to the internal H_3PO_4 standard. $^{31}P\{^{1}H\}$ spectra were recorded at specific time intervals until the reaction had progressed to at least 3 half lives. The extent of reaction at each time interval was determined by integration of the peak intensity relative to that of the H_3PO_4 standard. An appropriately long delay ($> 3T_1$) between scans was utilized to ensure that integration was quantitative and not affected by T_1 relaxation times. The observed rate constant was determined according to the law of mass action.

6.1.5 Computational Analysis

Computational analysis was performed by Dr. Mikko M. Hänninen, Dr. J. Mikko Rautiainen, and Dr. Heikki M. Tuononen at the University of Jyväskylä. The results of these calculations were compiled with our experimental findings and published in a special issue of the *Journal of Organometallic Chemistry* for the occasion of Prof. Gerard Van Koten's 70th birthday.[64] All findings are presented in this thesis to aid in the discussion of experimental findings in Chapter 2 with full permission from the authors.

The geometry optimizations and full vibration analysis of all studied complexes were performed using the Gaussian 09 program package.[75] The PBE1PBE[76] hybrid functional and SVP[78] or def2-TZVP[80-81] basis sets by Ahlrichs *et al.* were used in all optimizations and frequency calculations. For Lu, the small-core SDD pseudopotential by Cao and Dolg was used.[79]

6.1.6 Other Instrumental Analysis

CHNS elemental analyses were performed on an Elementar Americas Vario MicroCube instrument. In cases when carbon percentages were low, vanadium oxide was employed as a combustion agent.

6.1.7 X-ray Crystallography

Crystals grown for X-ray diffraction analysis were coated in Paratone oil and placed on a glass slide. Close visual inspection and selection of the crystals was aided by either a standard microscope or polarizing light microscope. The crystal chosen for diffraction analysis was placed on a MiTeGen Dual Thickness MicroMount attached to the goniometer head. The crystal was centred on a Rigaku SuperNova diffractometer equipped with a

Dectris Pilatus 3R 200K-A detector, Oxford CryoStream 800 cooling system, and molybdenum (NOVA) radiation source (Kα = 0.71073 Å), and copper (MOVA) radiation sources (Kα = 1.5406 Å). Experiments were performed at 100 K to reduce thermal motion of the atoms. CrysAlisPro software was utilized to determine unit cell parameters and SHELXTL software was utilized using least squares methodology for refinement.

6.1.8 Materials

The reagents ^{n}BuLi (1.6 M in hexanes), ^{t}BuLi (1.7 M in hexanes), $LiCH_2SiMe_3$ (1.0 M in pentane), MeLi (1.6 M in diethyl ether), diisopropylchlorophosphine, triphenylmethylamine, 1-adamantylamine, and 2,4,6-tritertbutylanaline were purchased from Sigma Aldrich and used without further purification. Solid samples of $LiCH_2SiMe_3$ and MeLi were prepared by removing the solvent *in vacuo* from a 1.0 M solution of $LiCH_2SiMe_3$ in pentane and 1.6 M solution of MeLi in diethyl ether, respectively. Tris(pentafluorophenylphenyl)borane was purchased from Boulder Scientific purified *via* sublimation. The compound 2,6-diisopropylanaline was purchased from Sigma Aldrich and distilled under reduced pressure into a bomb equipped with a Kontes valve before using. The reagents sodium hydride, 4-dimethylaminopyridine (DMAP), sodium azide, and bis(trimethylsilyl)methylamine were purchased from Alfa Aesar and used without any further purification. Anhydrous lutetium trichloride was purchased from Strem Scientific and utilized without any further purification. Isotopically labeled reagents deuterium oxide and deuterium chloride (35% in D_2O) were purchased from Cambridge Isotopes and used without any further purification. All deuterated solvents and reagents were purchased from Cambridge Isotope Laboratories. The sample of 4,6-dimethyl-2-methylsulfonylpyrimidine used was purchased from Matrix Scientific and used without any further purification.

Samples of 4-isopropylphenylazide,[56] $Sc(CH_2SiMe_3)_3(THF)_2$,[93] $Lu(CH_2SiMe_3)_3(THF)_2$,[94] were prepared according to their literature procedures.

6.2 Preparation of Compounds from Modified Literature Procedures

Synthesis of 2,5-bis(diisopropylphosphino)-N-(tert-butoxycarbonyl)pyrrole

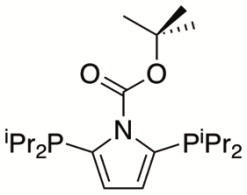

A 2-neck round bottomed flask attached to a swivel frit apparatus was charged with 2,5-dibromo-*N*-(tertbutoxycarbonyl)pyrrole (6.1663 g, 18.973 mmol). THF (250 mL) was vacuum transferred into the flask at –78 °C. The solution was allowed to warm to ambient temperature with stirring in order to dissolve all solids and was subsequently cooled back down to –78 °C. A syringe was used to add ^{n}BuLi (16 mL, 40 mmol) and the resulting mixture was allowed to stir at –78 °C for 1 hour. After this time $^{i}Pr_2PCl$ (6 mL, 37.7 mmol) was added *via* syringe whereupon the cold bath was removed and the solution was allowed to stir while warming to ambient temperature over 18 hours. All volatiles were removed *in vacuo* and pentane (100 mL) was added to the waxy sample. The reaction mixture was filtered, removing insoluble impurities. The pentane was removed *in vacuo* to yield a brown powder (5.9004 g, 77.8%) ^{1}H NMR (benzene-d_6): δ 6.47 (s, 2H, pyrrole-H), 2.02 (m, $^3J_{H–H}$ = 7.0 Hz, $^2J_{H–P}$ = 1.4 Hz, 4H, P–C*H*$(CH_3)_2$), 1.55 (s, 9H, $(CH_3)_3$), 1.10 (dd, $^3J_{H–H}$ = 7.0 Hz, $^3J_{H–P}$ = 1.5 Hz, 12H, P–CH(C*H*$_3$)(CH_3)), 1.06 (dd, $^3J_{H–H}$ = 7.0 Hz, $^3J_{H–P}$ = 1.9 Hz, 12H, P–CH(CH_3)(C*H*$_3$)). ^{13}C{^{1}H} NMR (benzene-d_6): δ 151.4 (s, C=O), 133.9 (d, $^1J_{C–P}$ = 21.4 Hz, ipso-C pyrrole), 118.7 (d, $^2J_{C–P}$ = 1.8 Hz, pyrrole CH), 84.9 (s, O*C*$(CH_3)_3$), 28.4 (s, OC(*C*H$_3$)$_3$), 25.4 (d, $^1J_{C–P}$ = 11.6 Hz, P–*C*H$(CH_3)_2$), 20.4-20.3 (ov m, P–CH(*C*H$_3$)$_2$).

$^{31}P\{^{1}H\}$ NMR (benzene-d_6): δ –10.2. Anal. Calcd. (%) for $C_{21}H_{39}NO_2P_2$: C, 63.14; H, 9.84; N, 3.51. Found: C, 63.21; H, 9.28; N, 4.53.

Synthesis of 2,5-bis(diisopropylphosphino)pyrrole

In an inert atmosphere glove box a sample of 2,5-bis(diisopropylphosphino)-*N*-(tert-butoxycarbonyl)pyrrole (3.1274 g, 7.8185 mmol) was dissolved in toluene (100 mL) and transferred into a glass bomb. The bomb was placed under static vacuum and heated to 155 °C with stirring for 18 hours. The dark brown solution was allowed to cool to room temperature and was cannula transferred into a round bottom flask whereupon all volatiles were removed *in vacuo* yielding a brown solid (1.9900 g, 85.1%). ^{1}H NMR (benzene-d_6): δ 8.42 (br s, 1H, N–H), 6.59 (dd, $^{3}J_{H–P}$ = 2.4 Hz, $^{3}J_{H–H}$ = 2.4 Hz, 2H, pyrrole-H), 1.82 (sp, $^{3}J_{H–H}$ = 7.0 Hz, 4H, P–C*H*$(CH_3)_2$), 1.01 (dd, $^{3}J_{H–P}$ = 15.4 Hz, $^{3}J_{H–H}$ = 7.0 Hz, 6H, CH(C*H*$_3)_2$), 1.03 (dd, $^{3}J_{H–P}$ = 11.2 Hz, $^{3}J_{H–H}$ = 7.0 Hz, 6H, $CH(CH_3)_2$). $^{13}C\{^{1}H\}$ NMR (benzene-d_6): δ 128.4 (d, $^{1}J_{C–P}$ = 23.7 Hz, ipso-C pyrrole), 118.8 (dd, $^{2}J_{C–P}$ = 8.3 Hz, $^{3}J_{C–P}$ = 3.7 Hz, pyrrole CH), 24.2 (d, $^{2}J_{C–P}$ = 8.9 Hz, P–*C*H$(CH_3)_2$), 20.6 (d, $^{1}J_{C–P}$ = 19.4 Hz, P–*C*H(*C*H_3)(CH_3)), 19.5 (d, $^{2}J_{C–P}$ = 8.1 Hz, P–CH(CH_3)(*C*H_3)). $^{31}P\{^{1}H\}$ NMR (benzene-d_6): δ –11.4. Anal. Calcd. (%) for $C_{21}H_{39}NO_2P_2$: C, 64.19; H, 10.44; N, 4.68. Found: C, 63.72; H, 10.87; N, 4.01.

Synthesis of HL^{iPr}

A 2-neck round bottomed flask was charged with 2,5-bis(diisopropylphosphino)-N-H-pyrrole (3.1003 g, 10.356 mmol). Toluene (30 mL) was transferred into the flask at –78 °C *via* vacuum distillation.

The solution was allowed to warm up to ambient temperature and 4-isopropylphenylazide (3.3369 g, 20.700 mmol) was added dropwise over 2 minutes *via* syringe. Bubbles formed immediately upon the addition of the azide and the resulting light brown solution was allowed to stir for 2 hours at room temperature. After this time all volatiles were removed *in vacuo* leaving behind the desired product as a beige powder (5.7401 g, 98.1%). ^{1}H NMR (benzene-d_6): δ 10.4 (br s, 1H, N–H), 7.10 (ov m, 8H, Pipp C–H), 6.40 (s, 2H, pyrrole-H), 2.82 (sp, $^{3}J_{H–H}$ = 7.0 Hz, 2H, Pipp–C*H*$(CH_3)_2$), 2.08 (m, $^{1}J_{H–P}$ = 8.1 Hz $^{3}J_{H–H}$ = 7.0 Hz, 4H, P–C*H*$(CH_3)_2$), 1.26 (d, $^{3}J_{H–H}$ = 7.0 Hz, 12H, Pipp–CH(C*H*$_3)_2$), 1.01 (dd, $^{3}J_{H–P}$ = 13.4 Hz, $^{3}J_{H–H}$ = 7.0 Hz, 12H, P–CH(C*H*$_3$)(CH$_3$)), 0.99 (dd, $^{3}J_{H–P}$ = 13.4 Hz, $^{3}J_{H–H}$ = 7.0 Hz, 12H, P–CH(CH$_3$)(C*H*$_3$)). ^{13}C{^{1}H} NMR (benzene-d_6): δ 149.5 (s, aromatic ipso-C), 138.2 (s, aromatic ipso-C), 127.4 (s, aromatic CH), 124.4 (dd, $^{1}J_{C–P}$ = 108.2 Hz, $^{3}J_{C–P}$ = 5.7 Hz, ipso-C pyrrole), 124.0 (d, $^{3}J_{C–P}$ = 14.2 Hz, aromatic CH), 117.5 (dd, $^{2}J_{C–P}$ = 17.4 Hz, $^{3}J_{C–P}$ = 11.6 Hz, pyrrole CH), 34.2 (s, Pipp–*C*H$(CH_3)_2$), 27.1 (d, $^{1}J_{C–P}$ = 62.7 Hz, P–*C*H$(CH_3)_2$), 25.0 (s, Pipp–CH(*C*H$_3)_2$), 16.9 (s, P–CH(*C*H$_3$)(CH$_3$)), 16.3 (s, P–CH(*C*H$_3$)(*C*H$_3$)). ^{31}P{^{1}H} NMR (benzene-d_6): δ 13.5. Anal. Calcd. (%) for $C_{34}H_{53}N_3P_2$: C, 72.18; H, 9.44; N, 7.43. Found: C, 71.86; H, 9.93; N, 7.88.

Synthesis of NaL^{iPr}

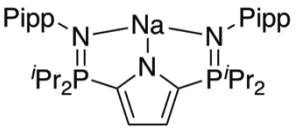

A round bottomed flask was charged with HL^{iPr} (1.0469 g, 1.850 mmol). A second round bottomed flask was charged with NaH (0.0469 g, 1.954 mmol). THF (20 mL) was transferred into each flask at –78 °C *via* vacuum distillation. The flasks were allowed to warm up to ambient temperature with stirring to allow all solid material to dissolve. A syringe was used to transfer the NaH

solution to the stirring HL^{iPr} solution dropwise over the course of 2 minutes. Bubbles began forming immediately upon the addition of NaH. The reaction was allowed to stir at ambient temperature for 2 hours whereupon all volatiles were removed *in vacuo*. Heptane (10 mL) was added to the remaining solid and stirred. The resulting brown solution was filtered, leaving behind the desired product as beige powder (1.0001 g, 93.7%). ^{1}H NMR (benzene-d_6): δ 7.14 (d, $^{3}J_{H–H}$ = 8.2 Hz, 4H, Pipp aromatic C–H), 7.02 (d, $^{3}J_{H–H}$ = 8.2 Hz, 4H, Pipp aromatic C–H), 6.80 (s, 2H, pyrrole-H), 2.77 (sp, $^{3}J_{H–H}$ = 7.0 Hz, 2H, Pipp–C*H*$(CH_3)_2$), 2.19 (br sp, 4H, P–C*H*$(CH_3)_2$), 1.23 (d, $^{3}J_{H–H}$ = 7.0 Hz, 12H, Pipp–CH(C*H*$_3)_2$), 1.00 (ov m, 24H, P–CH(C*H*$_3)_2$). ^{13}C{^{1}H} NMR (benzene-d_6): δ 152.7 (s, aromatic ipso-C), 138.7 (s, aromatic ipso-C), 127.7 (s, aromatic CH), 125.2 (d, $^{3}J_{C–P}$ = 10.9 Hz, aromatic CH), 116.8 (dd, $^{2}J_{C–P}$ = 26.9 Hz, $^{3}J_{C–P}$ = 9.8 Hz, 3,4-pyrrole CH), 34.0 (s, Pipp–*C*H$(CH_3)_2$), 27.2 (d, $^{1}J_{C–P}$ = 60.8 Hz, P–*C*H$(CH_3)_2$), 25.0 (s, P–CH(CH_3)(*C*H$_3$)), 17.6 (s, P–CH(*C*H$_3$)(CH_3)), 16.6 (s, Pipp–CH(C*H*$_3)_2$). One aromatic carbon (2,5-pyrrole C) was not observed. ^{31}P{^{1}H} NMR (benzene-d6): δ 28.0. Anal. Calcd. (%) $C_{34}H_{52}N_3NaP_2$: C, 69.48; H, 8.92; N, 7.15. Found: C, 69.01; H, 8.95; N, 7.26.

Synthesis of 5,7-dimethylpyrazolo-1,5a-pyrimidine

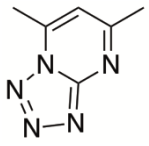

A sample of 4,6-dimethyl-2-methylsulfonylpyrimidine (3.1837 g, 17.096 mmol) was added to a 500 mL Erlenmeyer flask. Three equivalents of NaN_3 (4.1728 g, 64.187 mmol) added to the Erlenmeyer flask containing the pyrimidine. Dimethylformamide (DMF) (30 mL) was added to dissolve the solids. The solution was heated to 100 °C and stirred for 3 hours whereupon the solution was cooled to ambient temperature. The contents of the Erlenmeyer flask were poured into a separatory

funnel and a 6% brine solution (50 mL) was added. The desired product was extracted into $CHCl_3$ (3 × 100 mL). The organic fractions were collected and $MgSO_4$ was added to remove residual water. The mixture was filtered and $CHCl_3$ was removed on a rotary evaporator apparatus. A small amount of DMF remained in the flask and was removed using a high vacuum line leaving behind the crude product as a yellow solid (1.5590 g, 61.1%). X-ray quality crystals were grown by dissolving a portion of the crude product in a minimal amount of xylenes. The solution was placed in a –35 °C freezer for 18 hours and the resulting crystals were isolated by filtration and dried under vacuum. ^{1}H NMR (chloroform-d_1, 22 ºC): δ 6.95 (s, 1H, Ar C–H), 2.96 (s, 3H, CH_3), 2.77 (s, 3H, CH_3). $^{13}C\{^1H\}$ NMR (chloroform-d_1): δ 169.1 (s, ipso *C*–CH_3), 155.2 (s, ipso *C*–N), 144.8 (s, ipso *C*–CH_3), 112.8 (s, aromatic *C*–H), 25.6 (s, CH_3), 17.1 (s, CH_3).

6.3 Preparation of Compounds from Chapter 2

Synthesis of $L^{Ph}Lu(CH_2SiMe_3)(NHCPh_3)$ (37)

In an argon atmosphere glove box, $L^{Ph}Lu(CH_2SiMe_3)_2$ (0.2630 mg, 0.250 mmol) was weighed into a 20 mL scintillation vial and dissolved in 2 mL of benzene. Ph_3CNH_2 (0.0635 mg, 0.245 mmol) was weighed into another vial and dissolved in 3 mL of benzene. The Ph_3CNH_2 solution was added dropwise over 5 min to the benzene solution of $L^{Ph}Lu(CH_2SiMe_3)_2$. The resulting colourless mixture was stirred for 1 h at ambient temperature at which point the benzene solvent was removed *in vacuo* to yield an off-white oily solid. The solid was triturated 3 times with 3 mL of pentane, followed by 3 times with 3 mL of heptane, and dried under reduced pressure to

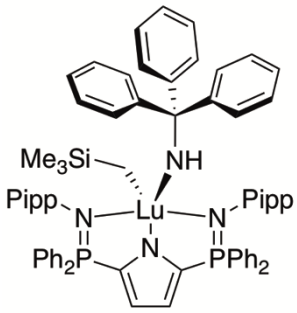

yield a white powder (297.0 mg, 98% (crude)). ^{1}H NMR (benzene-d_6): d 7.55 (ov m, 8H, o-phenyl H), 7.51 (ov m, 4H, m-Pipp H), 6.96–6.94 (ov m, 31 H, *o*-Pipp H (4), *m*- and *p*-phenyl H (12), *m*-, *p*- and *o*-phenyl CPh_3 H (15)), 6.67 (dd, $^{3}J_{H-P}$ = 2.1 Hz, $^{4}J_{H-P}$ = 0.6 Hz, 2H, pyrrole H), 2.93 (s, 1 H, NH), 2.73 (sp, $^{3}J_{H-H}$ = 6.9 Hz, 2H, Pipp–C*H*$(CH_3)_2$), 1.18 (d, $^{3}J_{H-H}$ = 6.9 Hz, 12H, Pipp–CH(C*H*$_3)_2$), 0.16 (s, 9H, Si$(CH_3)_3$), 0.23 (s, 2H, CH_2). ^{13}C{^{1}H} NMR (benzene-d_6): δ 154.7 (s, aromatic ipso-C, CPh_3), 144.1 (d, $^{2}J_{C-P}$ = 4.9 Hz, aromatic ipso-C, Pipp), 143.3 (s, aromatic ipso-C, *p*-Pipp), 133.7 (d, $^{2}J_{C-P}$ = 25.8 Hz, aromatic CH, *o*-Ph), 133.0 (s, $^{1}J_{C-P}$ = 21.3 Hz aromatic ipso-C, pyrrole), 132.6 (s, aromatic CH, *o*-Pipp), 132.2 (s, aromatic CH, *p*-Ph), 131.8 (s, aromatic CH, *m*-Ph), 130.7 (s, $^{1}J_{C-P}$ = 90.8 Hz, aromatic ipso-C, Ph), 129.6 (s, aromatic CH, *o*-Ph CPh_3), 128.0 (s, aromatic CH, *m*-Ph CPh_3), 127.5 (s, aromatic CH, *p*-Ph CPh_3), 126.0 (s, aromatic CH, *m*-Pipp), 119.3 (dd, $^{2}J_{C-P}$ = 29.5 Hz, $^{3}J_{C-P}$ = 11.0 Hz, pyrrole CH), 75.3 (s, Ph_3CNH), 37.0 (s, Lu–CH_2), 34.2 (s, Pipp–*C*H$(CH_3)_2$), 24.7 (s, Pipp–CH(*C*H$_3)_2$), 5.1 (s, Si$(CH_3)_3$). ^{31}P{^{1}H} NMR (benzene-d_6): δ 23.8 (s). Anal. Calcd. (%) for $C_{70}H_{75}LuN_4P_2Si$: C, 67.95; H, 6.11; N, 4.53. Found: C, 66.40; H, 5.12; N, 5.85. Exhaustive attempts to obtain higher quality elemental analyses for this compound were unsuccessful. These data represent the best values obtained to date.

Synthesis of $L^{Ph}Lu(\kappa^{2-N,C}$-$(NHCPh_2(C_6H_4)))$ (45)

In an argon atmosphere glove box, $L^{Ph}Lu(CH_2SiMe_3)(NHCPh_3)$ (25.3 mg, 0.0207 mmol) was weighed into a *J*-Young NMR tube and dissolved in 0.5 mL of benzene-d_6. The resulting solution was heated at 80 °C for 24 h resulting in a pale yellow solution. ^{1}H NMR (benzene-d_6): δ 7.62–

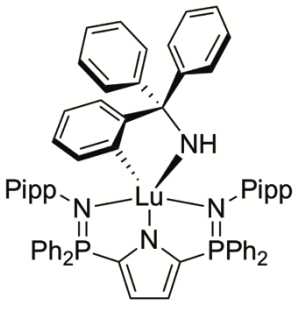

7.46 (ov m, 13H, *o*-phenyl H (8) + *o*-Phenyl CPh_3 H (5)), 7.33 (dd, $^3J_{H–H}$ = 6.6 Hz, $^4J_{H–P}$ = 3.3 Hz, 4H, *o*-Pipp H), 6.98–6.48 (ov m, 25 H, *m*- and *p*-phenyl H (Pipp, PPh_2 and CPh_3) + *m*-Pipp H), 6.61 (d, $^3J_{H–P}$ = 2.1 Hz, 2H, pyrrole H), 3.35 (s, 1 H, NH), 2.73 (sp, $^3J_{H–H}$ = 6.9 Hz, 2H, Pipp–C*H*$(CH_3)_2$), 1.18 (d, $^3J_{H–H}$ = 6.9 Hz, 12H, Pipp–CH(C*H*$_3)_2$). $^{13}C\{^1H\}$ NMR (benzene-d_6): δ 198.0 (s, aromatic C, Lu–C), 154.9 (s, aromatic ipso-C, CPh_3), 154.9 (s, aromatic ipso-C, CPh_3),144.5 (d, $^1J_{C–P}$ = 5.8 Hz, aromatic ipso-C, Pipp), 142.4 (s, aromatic ipso-C, Ph), 134.1 (d, $^2J_{C–P}$ = 10.6 Hz, aromatic CH, *o*-Ph), 133.8 (d, $^2J_{C–P}$ = 11.1 Hz, aromatic CH, *o*-Ph), 132.4 (s, aromatic ipso-C, *p*-Pipp), 130.9 (dd, $^1J_{C–P}$ = 90.7 Hz, $^3J_{C–P}$ = 6.9 Hz, aromatic ipso-C, pyrrole), 129.5 (s, aromatic CH, *o*-Ph CPh_3), 129.0–128.7 (ov m, aromatic CH, *o*-, *p*- and *m*-Ph CPh_3), 128.7 (s, aromatic CH, *m*-Ph CPh_3), 127.2 (s, aromatic CH, *o*-Pipp), 127.1 (s, aromatic CH, *m*-Pipp), 119.2 (dd, $^2J_{C–P}$ = 34.7 Hz, $^3J_{C–P}$ = 10.3 Hz, pyrrole CH), 74.8 (s, Ph_3CNH), 33.9 (s, Pipp–*C*H$(CH_3)_2$), 24.5 (s, Pipp–CH(*C*$H_3)_2$). $^{31}P\{^1H\}$ NMR (benzene-d_6): δ 25.0.

Synthesis of $L^{Ph}Lu(NHCPh_3)_2$ (44)

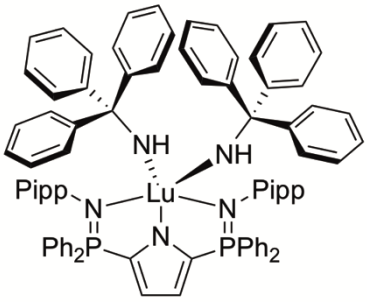

In an argon atmosphere glove box, $L^{Ph}Lu(CH_2SiMe_3)_2$ (50.4 mg, 0.0480 mmol) was weighed into a 20 mL scintillation vial and dissolved in 2 mL of toluene. Ph_3CNH_2 (26.2 mg, 0.101 mmol) was weighed into a separate vial and dissolved in 3 mL of toluene. The Ph_3CNH_2 solution was added dropwise over 5 min to the stirring solution of $L^{Ph}Lu(CH_2SiMe_3)_2$. The resulting colourless mixture was stirred for 22 h at ambient temperature at which point the volatiles were removed *in vacuo* to yield a pale yellow oil.

This oil was triturated 2 times with 3 mL of pentane and dried *in vacuo* to yield a white powder (52.2 mg, 77.0% (crude)). An analytically pure sample was obtained by recrystallization from toluene/heptane (5:3) mixture at 35 °C (6.81 mg, 10%). ^{1}H NMR (benzene-d_6): δ 7.54 (ddd, $^{3}J_{H–P}$ = 20.1 Hz, $^{3}J_{H–H}$ = 7.8 Hz, $^{4}J_{H–H}$ = 1.2 Hz, 8H, *o*-phenyl H), 7.41–7.38 (ov m, 12 H, *m*- and *p*-phenyl H), 7.03–6.91 (30 H, *m*-, *p*- and *o*-phenyl CPh_3 H), 6.78 (dd, $^{3}J_{H–H}$ = 8.4 Hz, $^{4}J_{H–P}$ = 1.8 Hz, 4H, *o*- Pipp H), 6.70 (d, $^{3}J_{H–H}$ = 8.4 Hz, *m*-Pipp H), 6.66 (dd, $^{3}J_{H–P}$ = 2.4 Hz, $^{4}J_{H–P}$ = 1.2 Hz, 2H, pyrrole H), 2.73 (sp, $^{3}J_{H–H}$ = 6.9 Hz, 2H, Pipp–C*H*$(CH_3)_2$), 2.70 (s, 2H, N–H), 1.18 (d, $^{3}J_{H–H}$ = 6.9 Hz, 12H, Pipp–CH(C*H*$_3)_2$). ^{13}C{^{1}H} NMR (benzene-d_6): δ 154.4 (s, aromatic ipso-C, CPh_3), 144.8 (d, $^{2}J_{C–P}$ = 5.5 Hz, aromatic ipso-C, Pipp), 141.9 (s, aromatic ipso-C, Ph), 133.9 (d, $^{2}J_{C–P}$ = 16.2 Hz, aromatic CH, *o*-Ph), 132.6 (s, aromatic ipso-C, *p*-Pipp), 132.2 (s, aromatic CH, *p*-Ph), 131.4 (s, aromatic ipso- C, pyrrole), 129.8 (s, aromatic CH, *o*-Ph, CPh_3), 129.0 (s, aromatic CH, *p*-Ph, CPh_3), 128.7 (s, aromatic CH, *o*-Pipp), 127.9 (s, aromatic CH, *m*- Ph, CPh_3), 126.9 (s, aromatic CH, *m*-Pipp), 125.8 (s, aromatic CH, *m*- Ph), 119.2 (dd, $^{2}J_{C–P}$ = 27.6 Hz, $^{3}J_{C–P}$ = 11.5 Hz, pyrrole C–H), 75.1 (s, Ph_3CNH), 34.0 (s, Pipp–C*H*$(CH_3)_2$), 24.7 (s, Pipp–CH(C*H*$_3)_2$). ^{31}P{^{1}H} NMR (benzene-d_6): δ 21.7 (s). Anal. Calcd. (%) for $C_{85}H_{80}LuN_5P_2$: C, 72.48; H, 5.72; N, 4.97. Found: C, 71.77; H, 5.80; N, 4.54.

6.4 Preparation of Compounds from Chapter 3

Synthesis of $L^{iPr}Sc(CH_2SiMe_3)_2$ (39a)

A 100 mL round bottomed flask was charged with a sample of HL^{iPr} (0.0913 g, 0.161 mmol). Toluene (10 mL) was transferred into this flask *via* vacuum distillation, yielding a

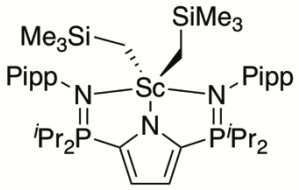

clear, light brown solution. $Sc(CH_2SiMe_3)_3(THF)_2$ (0.0724 g, 0.161 mmol), was added to a 50 mL round bottom flask, and dissolved in toluene (10 mL). The $Sc(CH_2SiMe_3)_3(THF)_2$ solution was added dropwise to the stirring HL^{iPr} solution at ambient temperature dropwise over 3 minutes. The resulting clear, light brown solution was left to stir at ambient temperature for 1 hour upon which all volatiles were removed *in vacuo*. The reaction contraption was brought into an inert atmosphere glove box whereupon heptane (10 mL) was added to the light brown solid and was stirred and heated (50 °C) leaving behind a small amount of a dark, oily solid. This mixture was filtered through a bed of celite which produced a clear, yellow solution. Removal of the heptane *in vacuo* liberating the desired product as a light, pale yellow solid (0.1133 g, 90.0% (crude)). Facile preparation of analytically pure material was achieved through recrystallization from a minimal amount of warm (50 °C) heptane (0.0521 g, 41.37%). ^{1}H NMR (benzene-d_6): δ 7.50 (dd. $^3J_{H–H}$ = 8.4 Hz, $^4J_{H–P}$ = 2.1, 4H, *o*-Pipp–H), 7.23 (d, $^3J_{H–H}$ = 8.1 Hz, 4H, *m*-Pipp–H), 6.51 (d, $^3J_{H–P}$ = 2.1 Hz, 2H, pyrrole–H), 2.80 (sp, $^3J_{H–H}$ = 7.2 Hz, 2H, Pipp–(C*H*$(CH_3)_2$), 2.09 (m, $^3J_{H–H}$ = 6.9 Hz, $^2J_{H–P}$ = 2.7 Hz, 4H, P–(C*H*$(CH_3)_2$), 1.24 (d, $^3J_{H–H}$ = 6.9 Hz, 12 H, Pipp–(CH(C*H*$_3)_2$), 0.93 (dd, $^3J_{H–P}$ = 32.1 Hz, $^3J_{H–H}$ = 7.2 Hz, 12H, P–(CH(CH_3)(C*H*$_3$)), 0.88 (dd, $^3J_{H–P}$ = 31.4 Hz, $^3J_{H–H}$ = 6.9 Hz, 12H, P–(CH(C*H*$_3$)(CH_3)), 0.31 (s, 4H, C*H*$_2$SiMe_3), 0.16 (s, 18H, CH_2Si(C*H*$_3)_3$). ^{13}C{^{1}H} NMR (benzene-d_6): δ 145.54 (s, ipso-Pipp), 144.57 (s, ipso-Pipp), 129.68 (s, *o*-Pipp C–H), 128.41 (d, $^1J_{C–P}$ = 24.1, pyrrole ipso-C) 127.73 (s, *m*-Pipp C–H), 115.90 (dd, $^2J_{C–P}$ = 24.1 Hz, $^3J_{C–P}$ = 10.1 Hz, pyrrole C–H), 40.00 (br s, Sc–CH_2), 34.38 (s, Pipp–*C*H$(CH_3)_2$), 26.30 (d, $^1J_{C–P}$ = 54.0 Hz, P–*C*H(CH_3)(CH_3)), 24.79 (s, Pipp–CH(*C*H$_3)_2$), 16.60 (s, P–(CH(*C*H$_3$)(CH_3)), 16.13 (s, P–(CH(CH_3)(*C*H$_3$)), 4.65 (s, SiMe_3). ^{31}P{^{1}H} NMR (benzene-d_6): δ 47.96.

Synthesis of $L^{iPr}Lu(CH_2SiMe_3)_2$ (39b)

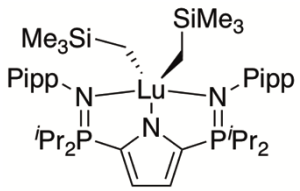

A 100 mL round bottomed flask was charged with a sample of HL^{iPr} (0.1729 g, 0.3040 mmol). Toluene (10 mL) was transferred to this flask *via* vacuum distillation, yielding a clear, light brown solution. $Lu(CH_2SiMe_3)_3(THF)_2$ (0.1766 g, 0.3040 mmol), was added to a 50 mL round bottom flask, and was dissolved in toluene (10 mL). The $Lu(CH_2SiMe_3)_3(THF)_2$ solution was added to the stirring solution at ambient temperature dropwise over 3 minutes. The resulting clear, light brown solution was left to stir at ambient temperature for 1 hour upon which all volatiles were removed *in vacuo*. The reaction contraption was brought into an inert atmosphere glove box whereupon heptane (10 mL) was added to the light brown solid and was stirred and heated (50 °C) leaving behind a small amount of a dark, oily solid. This mixture was filtered through a bed of celite which produced a clear, yellow solution. Removal of the heptane *in vacuo* liberated the desired product as a pale yellow solid (0.2557 g, 92.01%). Facile preparation of analytically pure material was achieved through recrystallization from a minimal amount of warm (50 °C) heptane (0.1218 g, 43.83%). ^{1}H NMR (benzene-d_6): δ 7.43 (dd, $^3J_{H–H}$ = 8.4 Hz, $^4J_{H–P}$ = 1.8 Hz, 4H, 2,5-Pipp C–H), 7.22 (d, $^3J_{H–H}$ = 7.8 Hz, 4H, 3,6-Pipp C–H), 6.50 (d, $^3J_{H–P}$ = 2.1 Hz, 2H, Pyrrole C–H), 2.79 (sp, $^3J_{H–H}$ = 6.6 Hz, 2H, Pipp–(C*H*$(CH_3)_2$), 2.04 (m, $^3J_{H–H}$ = 7.2 Hz, $^1J_{H–P}$ = 2.4 Hz, 4H, P–(C*H*$(CH_3)_2$) 1.22 (d, $^3J_{H–H}$ = 6.9 Hz, 12H, Pipp–(CH(C*H*$_3)_2$) 0.96 (dd, $^3J_{H–H}$ = 6.9 Hz, $^2J_{H–P}$ = 16.2 Hz, 12H, P–(CH(C*H*$_3$)(CH_3), 0.85 (dd, $^3J_{H–H}$ = 6.9 Hz, $^2J_{H–P}$ = 15.5 Hz, 12H, P–(CH(CH_3)(C*H*$_3$), 0.21 (s, 18H, $SiMe_3$), –0.42 (s, 4H, C*H*$_2$$SiMe_3$). ^{13}C{^{1}H} NMR (benzene-d_6): δ 144.32 (dd, $^1J_{C–H}$ = 98.6 Hz, $^4J_{C–H}$ = 24.3 Hz, ipso-pyrrole), 129.12 (d, $^3J_{C–P}$ = 13.2 Hz, 2,5-Pipp–C), 129.11 (d, $^2J_{C–P}$ = 26.4 Hz, ipso-Pipp–C), 127.89 (s, 3,6-Pipp–C), 127.4

(d, $^{2}J_{C-P}$ = 56.1 Hz, ipso-Pipp *C*), 116.51 (dd, $^{2}J_{C-P}$ = 98.6 Hz, $^{3}J_{C-P}$ = 40.2 Hz, Pyrrole–C), 41.30 (s, Lu–*C*H_2), 34.33 (s, Pipp–(*C*H(CH_3)$_2$), 26.42 (d, $^{1}J_{C-P}$ = 54.02 Hz, P–(*C*H(CH_3)$_2$), 24.76 (s, Pipp–(CH(*C*H_3)$_2$), 16.51 (s, P–(CH(*C*H_3)(CH_3), 16.01 (s, P–(CH(*C*H_3)(CH_3), 5.19 (s, Si(*C*H_3)$_3$) $^{31}P\{^{1}H\}$ NMR (benzene-d_6): δ 49.31.

Synthesis of [L^{iPr}Sc(CH$_2$SiMe$_2$CH$_2$SiMe$_3$)][MeB(C$_6$F$_5$)$_3$] (47)

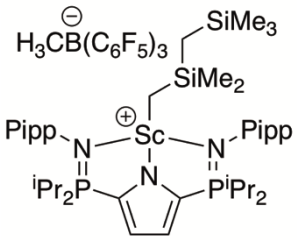

A 50 mL Erlenmeyer flask was charged with L^{iPr}Sc(CH_2SiMe_3)$_2$ (0.2167 g, 0.2764 mmol) and a small stir bar. Pentane (25 mL) was added to the vial and allowed to stir resulting in a slightly cloudy solution. Tris(pentafluorophenyl)borane (0.1396 g, 0.2727 mmol) was weighed into a second 20 mL scintillation vial and dissolved in pentane (12 mL). The tris(pentafluorophenyl)borane solution was pipetted slowly into the stirring L^{iPr}Sc(CH_2SiMe_3)$_2$ solution over 7 minutes. The solution turned a grey-brown colour and formed precipitate immediately upon addition. This mixture was allowed to stir 30 minutes are room temperature before being placed into a –35 ºC freezer overnight. A snow-white precipitate had settled out of the pentane and was filtered over a glass frit. Cold pentane (10 mL) was used to wash the flask and was poured over the filtrate. The filtrate was placed in a scintillation vial and placed under high vacuum for 3 hours to remove all volatiles leaving the desired ion pair as a dry, fluffy, white solid (0.2040 g, 57.7 %). ^{1}H NMR (bromobenzene-d_5): δ 7.06 (s, 8H, aromatic Pipp C–H), 6.57 (s, 2H, Pyrrole C–H), 2.70 (sp, $^{3}J_{H-H}$ = 6.9 Hz, 2H, Pipp–C*H*(CH_3)$_2$), 2.12 (m, $^{3}J_{H-H}$ = 7.2 Hz $^{1}J_{H-P}$ = 8.7 Hz, 4H, P–C*H*(CH_3)$_2$), 1.20 (s, 3H, C*H*$_3$B(C_6F_5)$_3$), 1.11 (d, $^{3}J_{H-H}$ = 6.9 Hz, 12H, Pipp–CH(C*H*$_3$)$_2$), 0.93 (dd, $^{3}J_{H-H}$ = 6.9 Hz $^{3}J_{H-P}$ = 16.8 Hz, 12H, P–CH(C*H*$_3$)$_2$), 0.77 (dd, $^{3}J_{H-H}$ = 6.9 Hz $^{3}J_{H-}$

$_P$ = 16.1 Hz, 12H, P–CH(CH_3)$_2$), 0.07 (s, 9H, SiMe$_3$), –0.16 (s, 2H, CH$_2$), –0.19 (s, 6H, SiMe$_2$), –0.32 (s, 2H, CH$_2$). ^{13}C{^{1}H} (bromobenzene-d_5, C_6F_5 resonances not reported): 150.16 (s, Pipp ipso-C), 148.89 (s, Pipp ipso-C), 130.54 (s, Pipp C–H), 129.95 (s, Pipp C–H), 118.35 (br s, Pyrrole C–H), 67.75 (s, Sc–CH$_2$), 30.81 (s, H$_3$*C*B(C_6F_5), 25.09 (d, $^1J_{C–P}$ = 36.52 Hz, P–C*H*(CH$_3$)(CH$_3$)) 24.82 (s, Pipp–CH(*C*H$_3$)$_2$), 16.35 (s, P–CH(*C*H$_3$)(CH$_3$)), 15.69 (s, P–CH(CH$_3$)(*C*H$_3$)), 4.47 (s, CH$_2$SiMe$_2$CH$_2$Si*Me*$_3$), 2.59 (s, CH$_2$Si*Me*$_2$CH$_2$SiMe$_3$), 2.28 (s, CH$_2$SiMe$_2$*C*H$_2$SiMe$_3$). Pyrrole ipso-C peaks were seen *via* ^{1}H–^{13}C HMBC but were too broad to be accurately identified in the ^{13}C{^{1}H} spectrum. ^{31}P{^{1}H} NMR (bromobenzene-d_5): δ 55.69. ^{19}F NMR (bromobenzene-d_5): δ –130.34 (d, $^3J_{F–F}$ = 23.4 Hz, 2F, ortho C–F), –160.59 (t, $^3J_{F–F}$ = 20.3 Hz, 1F, para C–F), –164.62 (br t, 2F, meta C–F). ^{11}B NMR (bromobenzene-d_5): δ –14.42 (br s, CH$_3$*B*(C_6F_5)$_3$)

Synthesis of L^{iPr}Lu(CH$_2$SiMe$_3$)(NHCPh$_3$) (40c)

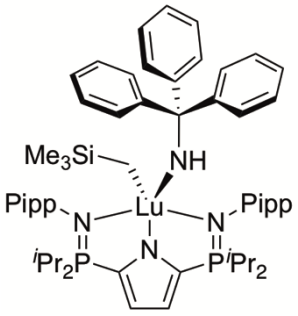

In an inert atmosphere glovebox, sample of L^{iPr}Lu(CH$_2$SiMe$_3$)$_2$ (0.1033 g g, 0.1130 mmol) was weighed into a 20 mL scintillation vial containing a stir bar. The powder was dissolved in toluene (6 mL), yielding a clear yellow solution. One equivalent of Ph$_3$CNH$_2$ (0.0286 g, 0.110 mmol) was added into a 5 mL vial and dissolved using toluene (2 mL). The amine solution was added dropwise over 3 minutes to the stirring yellow solution. After stirring at ambient temperature for 1 hour the reaction mixture was filtered through a bed of celite, eliminating insoluble materials. All volatiles were removed *in vacuo* to yield the desired complex as an off-white solid powder (0.1034 g, 86.4% yield). X-ray quality crystals were grown at ambient

temperature from dissolving the crude powder in a minimal amount of warm heptane (50 °C) (0.0611 g, 51.04% yield). ^{1}H NMR (benzene-d_6): δ 7.53 (m, $^{3}J_{H-H}$ = 3.9 Hz, 6H, *o*-Ph_3), 7.08 (ov m, $^{3}J_{H-H}$ = 3.9 Hz, 13H, *m/p*-Ph_3, aromatic Pipp C–H), 6.96 (d, $^{3}J_{H-H}$ = 6.3 Hz, 4H, aromatic Pipp C–H), 6.54 (d, $^{3}J_{H-P}$ = 1.5 Hz, 2H, Pyrrole), 2.85, (sep, $^{3}J_{H-H}$ = 6.6 Hz, 2H, Pipp–(C*H*(CH_3)$_2$), 2.43 (s, 1H, N–H), 2.16 (m, $^{1}J_{H-P}$ = 9.6 Hz, $^{3}J_{H-H}$ = 6.9 Hz, 2H, P–(C*H*(CH_3)$_2$), 1.75 (m, $^{1}J_{H-P}$ = 9.6 Hz, $^{3}J_{H-H}$ = 7.2 Hz, 2H, P–(C*H*(CH_3)$_2$), 1.32 (d, $^{3}J_{H-H}$ = 6.6 Hz, 6H, Pipp–(CH(C*H*$_3$)(CH_3)), 1.30 (d, $^{3}J_{H-H}$ = 6.9 Hz, 6H, Pipp–(CH(CH_3)(C*H*$_3$)), 0.98 (dd, $^{2}J_{P-H}$ = 6.9 Hz, $^{3}J_{H-H}$ = 7.2 Hz, 6H, P–(CH(CH_3)(C*H*$_3$)), 0.85 (dd, $^{3}J_{P-H}$ = 6.9 Hz, $^{3}J_{H-H}$ = 7.2 Hz, 6H, P–(CH(C*H*$_3$)(CH_3)), 0.77 (dd, $^{2}J_{P-H}$ = 6.9 Hz, $^{3}J_{H-H}$ = 6.9 Hz, 6H, P–(CH(CH_3)(C*H*$_3$)), 0.61 (dd, $^{3}J_{P-H}$ = 6.9 Hz, $^{3}J_{H-H}$ = 7.2 Hz, 6H, P–(CH(C*H*$_3$)(CH_3)), 0.05 (s, 9H, $SiMe_3$), –0.37 (s, 2H, CH_2SiMe_3). ^{13}C{^{1}H} NMR (benzene-d_6): δ 154.67 (s, ipso-CPh_3–C), 144.38 (d, $^{1}J_{C-P}$ = 88.5 Hz, ipso-Pyrrole–C), 129.51 (s, ipso-Pipp–C) 129.6 (s, Pipp–CH), 128.68 (s, Pipp–CH) 128.24 (ipso-Pipp–C) 127.75 (s, CPh_3–CH), 127.69 (s, CPh_3–CH), 125.91 (s, CPh_3–CH), 116.63 (dd, $^{2}J_{P-C}$ = 24.54 Hz, $^{3}J_{P-C}$ = 9.605 Hz, Pyrrole–CH), 75.74 (s, *C*Ph_3), 34.37 (s, *C*H_2SiMe_3), 32.61 (s, Pipp–(*C*H(CH_3)$_2$), 26.83 (d, $^{1}J_{P-C}$ = 54.49 Hz, P–(*C*H(CH_3)$_2$), 26.33 (d, $^{1}J_{P-C}$ = 54.49 Hz, P–(*C*H(CH_3)$_2$), 25.12 (s, Pipp–(CH(*C*H_3)(CH_3)), 24.89 (s, Pipp–(CH(CH_3)(*C*H_3)), 16.49 (ov, P–(CH(*C*H_3)(CH_3) and P–(CH(CH_3)(*C*H_3)), 16.50 (s, P–(CH(CH_3)(*C*H_3)), 16.25 (s, P–(CH(*C*H_3)(CH_3)) 4.61 (s, Si(*C*H_3)$_3$). ^{31}P{^{1}H} NMR (benzene-d_6): δ 47.81.

Synthesis of $L^{iPr}Lu(CH_2SiMe_3)(NHDipp)$ (40d)

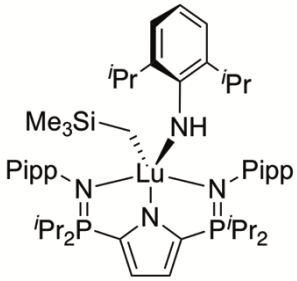

In an inert atmosphere glove box, a sample of $L^{iPr}Lu(CH_2SiMe_3)_2$ (0.1193 g, 0.1305 mmol) was weighed into a 20 mL scintillation vial containing a stir bar. The powder was dissolved in toluene (6 mL), yielding a clear yellow solution. $DippNH_2$ (0.0241 g, 0.136 mmol) was weighed into a syringe and added to a vial containing 5 mL toluene. This amine solution was added dropwise to the stirring solution of $L^{iPr}Lu(CH_2SiMe_3)_2$ dropwise over 5 minutes. The resulting golden yellow solution was left to stir at ambient temperature for 18 hours whereupon all volatiles were removed *in vacuo*. The pale yellow solid was recrystallized in a minimal amount of a warm (50 °C) 1:1 heptane:benzene mixture and placed in a –35 °C freezer for 18 hours. The crsytals were collected by filtration and dried under vacuum (0.0722 g, 55.12% yield). ^{1}H NMR (benzene-d_6): δ 7.33 (d, $^3J_{H–H}$ = 7.5 Hz, 2H, *m*-Dipp C–H), 7.22 (dd, $^3J_{H–H}$ = 8.1 Hz, $^4J_{H–P}$ = 1.8 Hz 4H, *o*-Pipp C–H), 7.01 (d, $^3J_{H–H}$ = 8.1 Hz, 4H, *m*-Pipp C–H), 6.93 (t, $^3J_{H–H}$ = 7.5 Hz, 1H, *p*-Dipp C–H), 6.52 (d, $^3J_{H–P}$ = 2.1 Hz, 2H, pyrrole C–H), 4.14 (s, 1H, N–H), 3.39 (sp, $^3J_{H–H}$ = 6.6 Hz, 2H, Dipp–(C*H*$(CH_3)_2)_2$), 2.73 (sp, $^3J_{H–H}$ = 6.9 Hz, 2H, Pipp–(C*H*$(CH_3)_2$), 2.26 (m, $^2J_{H–P}$ = 6.6 Hz $^3J_{H–H}$ = 6.9 Hz, 2H, P–(C*H*$(CH_3)_2$), 1.93 (m, $^2J_{H–P}$ = 6.6 Hz, $^3J_{H–H}$ = 7.2 Hz, 2H, P–(C*H*$(CH_3)_2$), 1.35 (d, $^3J_{H–H}$ = 6.6 Hz, 2H, Dipp–(CH(C*H*$_3)_2)_2$), 1.20 (d, $^3J_{H–H}$ = 6.9 Hz, 6H, Pipp–(CH(C*H*$_3$)(CH_3)), 1.19 (d, $^3J_{H–H}$ = 6.9 Hz, 6H, Pipp–(CH(CH_3)(C*H*$_3$)), 1.07 (dd, $^3J_{H–H}$ = 6.9 Hz, $^3J_{H–P}$ = 6.9 Hz, 6H, P–(CH(C*H*$_3$)(CH_3)), 0.94 (dd, $^3J_{H–H}$ = 6.9 Hz, $^3J_{H–P}$ = 7.2 Hz, 6H, P–(CH(CH_3)(C*H*$_3$)), 0.80 ((dd, $^3J_{H–H}$ = 6.9 Hz, $^3J_{H–P}$ = 6.9 Hz, 6H, P–(CH(C*H*$_3$)(CH_3)), 0.74 (dd, $^3J_{H–H}$ = 6.9 Hz, $^3J_{H–P}$ = 7.5 Hz, 6H, P–(CH(CH_3)(C*H*$_3$)), 0.03 (s, 9H, $SiMe_3$), -0.44 (s, 2H, CH_2SiMe_3). ^{13}C{^{1}H}

NMR (benzene-d_6): δ 154.70 (s, 2,6-ipso-Dipp), 144.56 (s, ipso-Pipp), 144.08 (s, ipso-Pipp), 133.68 (s, 1-ipso-Dipp), 128.33 (dd, $^1J_{C-P}$ = 135.51 Hz, $^3J_{C-P}$ = 14.34 Hz, ipso-pyrrole), 128.28 (s, Pipp C–H), 127.83 (s, Pipp C–H), 123.08 (s, 3,5-Dipp-C–H), 117.20, (dd, $^2J_{C-P}$ = 15.618 Hz, $^3J_{C-P}$ = 10.110 Hz, pyrrole C–H), 114.56 (s, Dipp–CH), 36.50 (s, *C*H_2SiMe_3), 34.27 (s, Pipp–(*C*H$(CH_3)_2$), 29.29 (s, Dipp–(*C*H$(CH_3)_2$), 27.58 (s, P–(*C*H$(CH_3)_2$), 26.85 (s, P–(*C*H$(CH_3)_2$), 24.77 (s, Dipp–(CH(*C*$H_3)_2$), 24.70 (s, Pipp–(CH(*C*$H_3)_2)_2$), 24.58 (s, Pipp–(CH(*C*$H_3)_2)_2$), 16.84 (s, P–(CH(CH_3)(*C*H_3)), 16.59 (ov s, P–(CH(CH_3)(*C*H_3) and P–(CH(*C*H_3)(CH_3)), 16.38 (s, P–(CH(*C*H_3)(CH_3)), 4.44 (s, CH_2Si*Me*$_3$). $^{31}P\{^1H\}$ NMR (benzene-d_6): δ 47.81.

Synthesis of $L^{iPr}Lu(NHCPh_3)_2$ (48c)

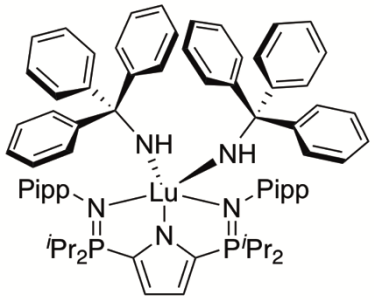

In an inert atmosphere glove box, a 20 mL scintillation vial was charged with $L^{iPr}Lu(CH_2SiMe_3)_2$ (0.0513 g, 0.0561 mmol) and a small stir bar. A second vial was charged with Ph_3CNH_2 (0.0291 g, 0.112 mmol). Toluene (7 mL) was added to each flask to dissolve all materials. The Ph_3CNH_2 solution was transferred into the $L^{iPr}Lu(CH_2SiMe_3)_2$ solution dropwise *via* pasteur pipette. The resulting light brown solution was added to a Kontes-sealed flask, attached to a high vacuum manifold, and allowed to stir at 70 ºC for 69 hours. The flask was allowed to cool to ambient temperature before the contents were transferred to a 50 mL round bottomed flask whereupon all volatiles were removed *in vacuo*. The desired product remained as a light brown solid (0.0544 g, 88.7% (crude)). X-ray quality crystals were grown by dissolving the mixture in a minimal amount of a warm (50 °C) 1:1

mixture of toluene and heptane. The solution was allowed to cool to ambient temperature over 2 hours and was placed in a –35 °C freezer overnight. The resulting crystals were filtered off, rinsed with cold pentane, dried for 8 hours under vacuum. (0.0197 g, 32.1%). ^{1}H NMR (benzene-d_6): δ 7.37 (d, $^{3}J_{H-H}$: 7.7 Hz, 12H, *o*-Ph_3), 7.08 (ov m, 18H, *m*- and *p*-Ph_3), 6.85 (d, $^{3}J_{H-H}$: 8.4 Hz, 4H, 2,6-Pipp C–H), 6.50 (dd, $^{3}J_{H-H}$: 8.4 Hz, $^{4}J_{H-H}$: 1.4 Hz, 3,5-Pipp C–H), 6.55 (d, $^{3}J_{H-P}$: 2.1 Hz, 2H, pyrrole C–H), 2.83 (sep, $^{3}J_{H-H}$: 7.0 Hz, 2H, Pipp–C*H*$(CH_3)_2$), 2.26 (s, 2H, N–*H*), 1.96 (m, $^{2}J_{H-P}$: 6.6 Hz, $^{3}J_{H-H}$: 6.3 Hz, 4H, P–C*H*$(CH_3)(CH_3)$) 1.29 (d, $^{3}J_{H-H}$: 6.3 Hz, 12H, Pipp–CH(C*H*$_3)_2$), 0.81 (dd, $^{3}J_{H-P}$: 16.1 Hz, $^{3}J_{H-H}$: 7.0 Hz, 12H, P–CH(C*H*$_3$)(CH_3)), 0.79 (dd, $^{3}J_{H-P}$: 16.1 Hz, $^{3}J_{H-H}$: 7.0 Hz, 12H, P–CH(C*H*$_3$)(CH_3)). ^{13}C{^{1}H} NMR (benzene-d_6): δ 154.38 (s, Ph_3 ipso-C), 146.04 (s, Pipp ipso-C), 142.74 (s, Pip ipso-C), 129.99 (s, *o*-Ph_3 C), 129.17 (d, $^{3}J_{C-P}$: 7.1 Hz, 2,6-Pipp C), 128.29 (d, $^{1}J_{C-P}$: 125.0 Hz, pyrrole ipso-C), 127.83 (s, *m*-Ph_3 C), 127.36 (s, 3,5-Pipp C), 125.60 (s, *p*-Ph_3 C), 116.88 (dd, $^{2}J_{C-P}$: 22.88 Hz, $^{3}J_{C-P}$: 10.56 Hz, pyrrole CH), 75.41 (s, *C*Ph_3), 34.22 (s, Pipp–*C*H$(CH_3)_2$), 27.03 (d, $^{1}J_{C-P}$: 54.56 Hz, P–*C*H$(CH_3)(CH_3)$), 24.92 (s, Pipp–CH(*C*$H_3)_2$), 16.65 (s, P–CH(*C*H_3)(CH_3)), 16.63 (s, P–CH(CH_3)(*C*H_3)). ^{31}P{^{1}H} NMR (benzene-d_6): 45.27.

Synthesis of L^{iPr}Lu(NHDipp)$_2$ (48d)

In an inert glove box atmosphere, a round bottomed flask was charged with L^{iPr}Lu$(CH_2SiMe_3)_2$ (0.1835 g, 0.2007 mmol) and a small stir bar. A second round bottomed flask was charged with $DippNH_2$ (0.0712 g, 0.402 mmol). Toluene (50 mL) was transferred into each flask at –78 °C. The flask was warmed up to room temperature

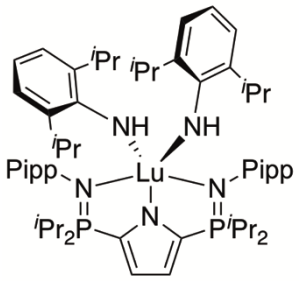

whereupon the $DippNH_2$ solution was transferred into the $L^{iPr}Lu(CH_2SiMe_3)_2$ solution dropwise *via* syringe. The resulting light brown solution was allowed to stir at ambient temperature for 24 hours whereupon all volatiles were removed *in vacuo*. The desired product remained as a light brown solid (0.1844 g, 84.1% (crude)). X-ray quality crystals were grown by dissolving the mixture in a minimal amount of a warm (50 °C) 1:1 mixture of toluene and heptane. The solution was allowed to cool to ambient temperature over 2 hours and was placed in a –35 °C freezer overnight. The resulting crystals were filtered off, rinsed with cold pentane, dried for 8 hours under vacuum. (0.0927 g, 42.3%). ^{1}H NMR (benzene-d_6): δ 7.26 (d, $^3J_{H–H}$ = 7.5 Hz, 4H, 3,5-Dipp C–H), 7.08 (dd, $^3J_{H–H}$ = 8.4 Hz, $^4J_{H–P}$ = 2.1 Hz 4H, 2,6-Pipp C–H), 6.97-6.88 (ov m, 6H, 3,5-Pipp C–H and 6-Dipp C–H), 6.57 (d, 2H, $^3J_{H–P}$ = 2.4 Hz, 3,5–Pyrrole C–H), 4.38 (s, 2H, NH), 3.20 (sp, $^3J_{H–H}$ = 6.9 Hz, 4H, Dipp-C*H*$(CH_3)_2$), 2.67 (sp, 2H, $^3J_{H–H}$ = 6.9 Hz, Pipp C*H*$(CH_3)_2$), 2.08 (m, $^2J_{H–P}$ = 1.8 Hz $^3J_{H–H}$ = 7.2 Hz, 4H, P–C*H*$(CH_3)_2$), 1.28 (d, $^3J_{H–H}$ = 6.9 Hz, 24H, Dipp CH(C*H*$_3)_2$), 1.15 (d, $^3J_{H–H}$ = 7.2 Hz, 12H, Pipp CH(C*H*$_3)_2$), 0.91 (dd, $^3J_{H–H}$ = 7.1 Hz, $^3J_{H–P}$ = 15.7 Hz, 12H, P–CH(C*H*$_3$)(CH_3), 0.79 (dd, $^3J_{H–H}$ = 7.1 Hz, $^3J_{H–P}$ = 15.7 Hz, 12H, P–CH(CH_3)(C*H*$_3$). ^{13}C{^{1}H} NMR (benzene-d_6): δ 154.4 (s, 1-Dipp ipso-C), 144.0 (ov s, 1-Pipp ipso-C and 4-Pipp ipso-C), 134.0 (s, 2,6-Dipp ipso-C), 128.5 (dd, $^1J_{C–P}$ = 134.71 Hz, $^3J_{C–P}$ = 13.72 Hz, Pyrrole ipso-C), 128.4 (d, $^3J_{C–P}$ = 6.4 Hz, 2,6-Pipp C–H), 127.7 (s, 3,5-Pipp C–H), 122.8 (s, 3,5-Dipp C–H), 118.2 (dd, $^2J_{C–P}$ = 17.48 $^3J_{C–P}$ = 9.86 Hz, pyrrole C-H), 114.8 (s, 4-Dipp C–H), 34.2 (s, Pipp *C*H$(CH_3)_2$), 29.9 (s, Dipp *C*H$(CH_3)_2$), 27.5 (d, $^1J_{C–P}$ = 53.57 Hz, P–*C*H$(CH_3)_2$), 24.6 (s, Pipp CH(*C*H$_3)_2$), 24.2 (s, Dipp CH(*C*H$_3)_2$), 17.0 (s, P–CH(*C*H$_3)_2$), 16.9 (s, P–CH(*C*H$_3)_2$). ^{31}P{^{1}H} NMR (benzene-d_6): δ 46.39.

6.5 Preparation of Compounds from Chapter 4

Synthesis of $L^{iPr}ScCl_2$ (50)

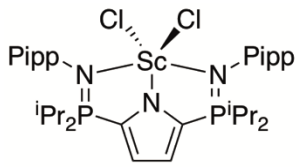

In an inert atmosphere glove box, a 20 mL scintillation vial was charged with NaL^{iPr} (0.3065 g, 0.5314 mmol) and a stir bar. The powder was dissolved in toluene (5 mL) and stirred. $ScCl_3(THF)_3$ (0.1963 g, 0.5340 mmol) was added into a 5 mL vial and dissolved in toluene (5 mL). A pasteur pipette was used to add the $ScCl_3(THF)_3$ to the stirring solution of NaL^{iPr} dropwise over 1 minute. Precipitate began to form immediately upon addition. The mixture was stirred for 1 hour at ambient temperature whereupon the precipitate was removed by filtration. The clear yellow solution was transferred into a clean scintillation vial equipped with a stir bar and all volatiles were removed *in vacuo* leaving behind the desired product as a light yellow solid (0.2700 g, 74.65%). ^{1}H NMR (benzene-d_6): δ 7.77 (dd, $^3J_{H–H}$ = 7.5 Hz, $^4J_{H–P}$ = 1.8 Hz, 4H, 2,6-Pipp C–H), 7.03 (d, $^3J_{H–H}$ = 7.8 Hz, 4H, 3,5-Pipp C–H), 6.61 (d, $^3J_{H–P}$ = 1.8 Hz, 2H, pyrrole C–H), 2.71 (sp, $^3J_{H–H}$ = 6.9 Hz, 2H, Pipp–C*H*$(CH_3)_2$), 2.07 (m, $^3J_{H–H}$ = 7.2 Hz, $^2J_{H–P}$ = 1.8 Hz, 4H, P–C*H*$(CH_3)_2$), 1.13 (ov m, 36H, Pipp–CH(C*H*$_3)_2$ and P–CH(C*H*$_3)_2$). ^{13}C{^{1}H} NMR (benzene-d_6): δ 145.02 (s, Pipp ipso-C), 143.87 (s, Pipp ipso-C), 130.02 (s, Pipp C–H), 129.94 (s, Pipp C–H), 127.13 (d, $^1J_{C–P}$ = 82.62 Hz, pyrrole ipso-C), 115.27 (dd, $^2J_{C–P}$ = 24.82 Hz, $^3J_{C–P}$ = 10.03 Hz, pyrrole C–H), 34.21 (s, Pipp–*C*H$(CH_3)_2$), 27.15 (d, $^1J_{C–P}$ = 54.47 Hz, P–*C*H$(CH_3)_2$), 24.74 (s, Pipp–CH(*C*H$_3)_2$), 16.99 (s, P–CH(*C*H$_3$)(CH$_3$), 16.52 (s, P–CH(CH$_3$)(*C*H$_3$)). ^{31}P{^{1}H} NMR (benzene-d_6): δ 49.34.

Synthesis of [LiL^{iPr}]$_2$

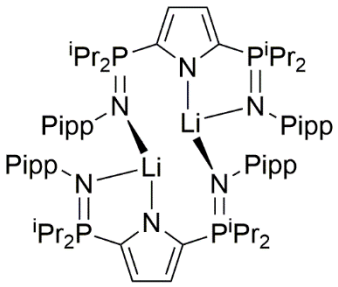

In an inert atmosphere glovebox, a sample of HL^{iPr} (0.0312 g, 0.0551 mmol) was weighed in a 20 mL scintillation vial equipped with a stir bar. Toluene (3 mL) was added to the vial and all material was dissolved while stirring. A sample of trimethylsilylmethyllithium (0.0052 g, 0.055 mmol) was weighed into a 5 mL vial and dissolved in toluene (2 mL). Both vials were placed in a −35 °C freezer for 1 hour. After this time, the vials were removed from the freezer. A pasture pipette was used to add the trimethylsilylmethyllithium solution to the stirring HL^{iPr} soliution dropwise over 1 minute. The reaction mixture was allowed to stir at ambient temperature for 18 hours whereupon all volatiles were removed *in vacuo* yielding a waxy solid. Pentane (4 mL) was added to the solid and stirred at ambient temperature for 5 minutes whereupon all volatiles were removed *in vacuo*, leaving the desired product as a pale brown solid. (0.0297 , 94.3%) ^{1}H NMR (benzene-d_6): δ 7.24 (ov d, $^3J_{H–H}$ = 6.0 Hz, $^3J_{H–H}$ = 6.4 Hz, 8H, Pipp C–H, Pipp C–H), 7.01 (ov d, $^3J_{H–H}$ = 6.0 Hz, $^3J_{H–H}$ = 7.1 Hz Hz, 8H, Pipp C–H, Pipp C–H), 6.88 (t, $^3J_{H–P}$ = 3.2 Hz, 2H, pyrrole C–H), 6.73 (t, $^3J_{H–P}$ = 2.3 Hz, 2H, pyrrole C–H), 2.76 (ov sp, $^3J_{H–H}$ = 6.8 Hz, 4H, Pipp–C*H*$(CH_3)_2$, Pipp–C*H*$(CH_3)_2$), 2.38-2.20 (ov m, 8H, P–C*H*$(CH_3)_2$), 1.30 – 0.97 (ov m, 60 H, Pipp–CH(C*H*$_3)_2$, P–CH(C*H*$_3$)(CH_3), P–CH(CH_3)(C*H*$_3$)), 0.77 – 0.71 (ov m, 12H, P–CH(C*H*$_3$)(CH_3), P–CH(CH_3)(C*H*$_3$)). ^{13}C{^{1}H} NMR (benzene-d_6): δ 152.60 (s, Pipp ipso-C), 150.78 (s, Pipp ipso-C), 140. 49 (s, Pipp ipso-C), 137.67 (s, Pipp ipso-C), 127.18 (s, Pipp C–H), 126.95 (s, Pipp C–H), 123.64 (s, Pipp C–H), 123.45 (s, Pipp C–H), 119.17 (br s, pyrrole C–H), 115.17 (br s, pyrrole C–H), 34.24 (s, Pipp–*C*H$(CH_3)_2$), 34.11 (s, Pipp–*C*H$(CH_3)_2$), 28.71 (d, $^1J_{C–P}$ = 14.3 Hz, P–*C*H$(CH_3)_2$), 27.52 (d, $^1J_{C–P}$ = 12.1

Hz, P–*C*H(CH_3)$_2$), 25.10 (s, Pipp–CH(CH_3)$_2$), 24.96 (s, Pipp–CH(CH_3)$_2$), 19.32 (s, P–CH(*C*H_3)(CH_3)), 17.48 (s, P–CH(CH_3)(*C*H_3)), 16.92 (s, P–CH(*C*H_3)(CH_3)), 16.52 (s, P–CH(CH_3)(*C*H_3)). Both pyrrole ipso carbons were not observed. $^{31}P\{^1H\}$ NMR (benzene-d_6): δ 33.47, 28.84.

Synthesis of L^{iPr}ScCl(NHDipp) (53)

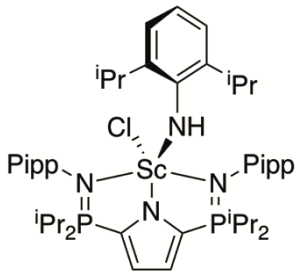

In an inert atmosphere glove box, a sample of L^{iPr}ScCl$_2$ (0.1156 g, 0.1698 mmol) was weighed into a 20 ml scintillation vial equipped with a small stir bar. Toluene (5 mL) and THF (1 mL) were added to dissolve the material. A 5 mL vial was charged with [(THF)LiNHDipp]$_2$ (0.0431 g, 0.0844 mmol) and dissolved in toluene (3 mL). The [(THF)LiNHDipp]$_2$ solution was added to the stirring L^{iPr}ScCl$_2$ solution dropwise over 3 minutes *via* pasteur pipette. Precipitate formed immediately upon addition and the resulting mixture was stirred for 1 hour at ambient temperature. After this time all volatiles were removed *in vacuo* leaving behind an off white solid. Toluene (10 mL) was added to the crude mixture and the precipitate was removed by filtration. The filtrate was placed under high vacuum to remove all volatiles, affording the desired product as a light yellow solid. (0.1007 g, 72.3 %). ^{1}H NMR (benzene-d_6): δ 7.71 (t, $^3J_{H–H}$ = 6.3 Hz, 1H, 4-Dipp C–H), 7.34 (d, $^3J_{H–H}$ = 8.4 Hz, 4H, Pipp C–H), 7.07 (d, $^3J_{H–H}$ = 6.3 Hz, 2H, 3,5-Dipp C–H), 6.93 (d, $^3J_{H–H}$ = 8.4 Hz, 4H, Pipp C–H), 6.54 (d, $^3J_{H–P}$ = 1.8 Hz, 2H, Pyrrole C–H), 5.70 (s, 1H, N–H), 2.66 (sep, $^3J_{H–H}$ = 6.9 Hz, 2H, Pipp–C*H*(CH_3)$_2$), 2.02 (ov sep, 6H, P–C*H*(CH_3)$_2$, Dipp–C*H*(CH_3)$_2$), 1.15 (d, $^3J_{H–H}$ = 6.9 Hz, 12H, CH(C*H*$_3$)$_2$), 1.14 (d, $^3J_{H–H}$ = 6.9

Hz, 12H, CH(CH_3)$_2$), 1.01 (ov m, 24H, P–CH(CH_3)$_2$). ^{31}P{^{1}H} NMR (benzene-d_6): δ 47.93.

Synthesis of L^{iPr}ScCl(N(SiMe$_3$)$_2$) (58)

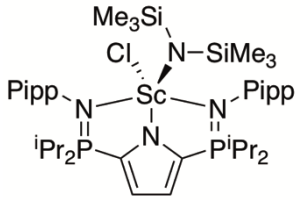

In an inert atmosphere glove box, a sample of L^{iPr}ScCl$_2$ (0.2164 g, 0.3180 mmol) was weighed into a round bottomed flask attached to a swivel frit apparatus. A separate round bottomed flask was charged with KN(SiMe$_3$)$_2$ (0.0551 g, 0.3293 mmol). THF (25 mL) was transferred under reduced pressure and temperature into each flask. The KN(SiMe$_3$)$_2$ solution was added to the stirring L^{iPr}ScCl$_2$ solution dropwise over 3 minutes *via* cannula needle. The solution was allowed to warm up to ambient temperature as it was left to stir for 18 hours. After this time all volatiles were removed *in vacuo* and reconstituted in toluene (25 mL). The swivel frit apparatus was flipped to remove the KCl from the solution. The filtrate was placed under high vacuum to remove all volatiles leaving the desired product as a yellow powder (0.1800 g, 73.2 %). ^{1}H NMR (benzene-d_6): δ 7.79 (d, $^3J_{H–H}$ = 6.9 Hz, 4H, aromatic Pipp C–H), 6.64 (d, $^3J_{H–H}$ = 6.6 Hz, 4H, aromatic Pipp C–H), 6.53 (s, 2H, Pyrrole C–H), 2.78 (sp, $^3J_{H–H}$ = 6.9 Hz, 2H, Pipp–C*H*(CH$_3$)$_2$), 2.31 (m, $^2J_{H–P}$ = 2.6 Hz, $^3J_{H–H}$ = 7.2 Hz, 2H, P–C*H*(CH$_3$)$_2$), 2.00 (m, $^2J_{H–P}$ = 2.6 Hz, $^3J_{H–H}$ = 7.5 Hz, 2H, P–C*H*(CH$_3$)$_2$), 1.22 (d, $^3J_{H–H}$ = 6.9 Hz, 12H, Pipp CH(CH_3)$_2$), 1.12-0.85 (ov m, 24H, P–CH(CH_3)$_2$), 0.53 (s, 9H, SiMe$_3$), –0.10 (s, 9H, SiMe$_3$). ^{31}P{^{1}H} NMR (benzene-d_6): δ 48.57.

Synthesis of HL^{Pm}

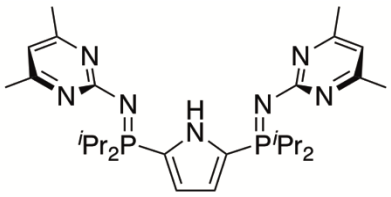

In an inert atmosphere glovebox, a sample of 2,5-bis(diisopropylphosphino)-N-H-pyrrole (0.1090 g, 0.3641 mmol) was weighed into a round bottomed flask. Two equivalents of 3,5-dimethylpyrimidineazide (0.1050 g, 0.7040 mmol) were weighed into a separate round bottomed flask. Toluene (25 mL) was transferred into each flask *via* vacuum distillation at –78 °C. Both solutions were allowed to warm up to ambient temperature while stirring. A cannula was used to add the 3,5-dimethylpyrimidineazide solution to the 2,5-bis(diisopropylphosphino)-N-H-pyrrole solution. Bubbles formed shortly upon the addition of the azide. The solution was left to stir under a constant flow of argon for 18 hours whereupon all volatiles were removed *in vacuo* leaving behind the desired product as a brown solid (0.1729 g, 88.3%). X-ray quality crystals were obtained by dissolving the crude product in a minimal amount of warm (50 °C) heptane. The solution was allowed to cool to ambient temperature before being placed in a –35 °C freezer for 18 hours. The mother-liquor was removed *via* pasteur pipette and cold (–35 °C) pentane (10 mL) was added to the vial to wash the crystals. The pentane was removed *via* pasteur pipette and the crystals were dried *via* vacuum for 2 hours. ^{1}H NMR (benzene-d_6): δ 13.21 (s, 1H, N–H), 6.35 (s, 2H, Pyrrole C–H), 6.08 (s, 2H, Pyrimidine C–H), 2.39 (m, 4H, $^{2}J_{H–P}$ = 2.6 Hz, $^{3}J_{H–H}$ = 7 Hz, P–C*H*$(CH_3)_2$), 2.35 (s, 12H, Pyrimidine CH_3), 1.11 (dd, $^{3}J_{H–H}$ = 6.9 Hz $^{3}J_{H–P}$ = 16.1 Hz, P–CH(C*H*$_3$)(CH_3), 1.02 (dd, $^{3}J_{H–H}$ = 6.9 Hz $^{3}J_{H–P}$ = 16.1 Hz, P–CH(CH_3)(C*H*$_3$)). ^{13}C{^{1}H} NMR (benzene-d_6): δ 168.49 (s, 3,5-Pyrimidine ipso-C), 167.51 (d, $^{2}J_{C–P}$ = 1.5 Hz, 1-Pyrimidine ipso-C), 124.8 (d, $^{1}J_{C–P}$ = 41.5 Hz, Pyrrole ipso-C), 116.91 (br s, 2,4-Pyrrole C–H), 109.14 (s, Pyrimidine C–H), 26.52 (d, $^{1}J_{H–P}$ = 65.9 Hz, P–

*C*H(CH_3)$_2$), 24.54 (s, Pyrimidine CH_3), 17.21 (s, P–CH(*C*H_3)(CH_3), 16.86 (s P–CH(CH_3)(*C*H_3). ^{31}P{^{1}H} NMR (benzene-d_6): δ 29.63.

Synthesis of $L^{Pm}Lu(CH_2SiMe_3)_2$ (63)

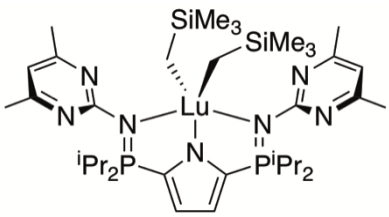

In an inert atmosphere glovebox, a sample of HL^{Pm} (0.0580 g, 0.0999 mmol) was weighed into a 20 mL scintillation vial. A 5 mL vial was charged with $Lu(CH_2SiMe_3)_3(THF)_2$ (0.0552 g, 0.102 mmol). Toluene (3 mL) was added to each vial to dissolve all material. Both solutions were placed in a –35 °C freezer for 1 hour. The $Lu(CH_2SiMe_3)_3(THF)_2$ solution was added to the stirring HL^{Pm} solution dropwise over 1 minute *via* pasteur pipette. The clear yellow solution was left to stir at ambient temperature for 30 minutes whereupon all volatiles were removed *in vacuo*. Pentane (5 mL) was added to the remaining waxy solid and stirred for 5 minutes and subsequently removed *in vacuo* leaving the desired product behind as a pale yellow solid. (0.0737 g, 79.1 %) ^{1}H NMR (benzene-d_6): δ 6.59 (d, $^3J_{H–P}$ = 2.8 Hz, 2H, Pyrrole C–H), 5.98 (s, 2H, Pyrimidine C–H), 2.58 (ov m, 10H, Pyrimidine CH_3 & P–C*H*(CH_3)(CH_3)), 2.01 (s, 6H, Pyrimidine CH_3), 1.19 (dd, $^3J_{H–P}$ = 27.3 Hz, $^3J_{H–H}$ = 7.0 Hz, 12H, P–CH(C*H*$_3$)(CH_3)), 1.00 (dd, $^3J_{H–P}$ = 17.3 Hz, $^3J_{H–H}$ = 7.0 Hz, 12H, P–CH(CH_3)(C*H*$_3$)), 0.02 (s, 18h, $SiMe_3$), –1.17 (s, 4H, Lu–CH_2). ^{13}C{^{1}H} NMR (benzene-d_6): δ 168.57 (s, Pyrimidine ipso-C), 166.08 (s, Pyrimidine ipso-C), 164.64 (s, Pyrimidine ipso-C), 127.91 (Pyrrole ipso-C, determined *via* ^{1}H–^{13}C HSQC), 117.64 (dd, $^2J_{C–P}$ = 17.6 Hz $^3J_{C–P}$ = 10.56 Hz, Pyrrole C–H), 111.48 (s, Pyrimidine C–H), 26.86 (s, CH_2), 26.5 (d, $^1J_{C–P}$ = 53.80 Hz, P–*C*H(CH_3)(CH_3)), 24.36 (br s, endo/exo

Pyrimidine CH_3), 17.50 (s, P–CH(*C*H_3)(CH_3)), 16.57 (s, P–(CH_3)(*C*H_3)), 5.52 (s, $SiMe_3$). $^{31}P\{^1H\}$ NMR (benzene-d_6): δ 42.37.

Synthesis of NaL^{Pm}

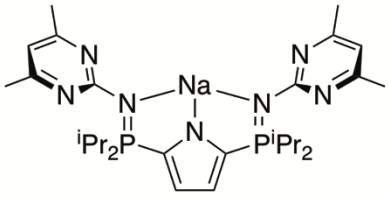

In an inert atmosphere glovebox, a round bottom flask was charged with HL^{Pm} (0.1105 g, 0.1961 mmol) and attached to a high vacuum line. A separate round bottom flask was charged with NaH (0.0048 g, 0.20 mmol). THF (15 mL) was transferred into each flask *via* vacuum distillation at –78 °C. Both vessels were allowed to warm up to ambient temperature while stirring. A cannula was used to transfer the NaH solution into the HL^{Pm} solution dropwise. Bubbles immediately upon the addition of NaH. The reaction was allowed to stir under a constant flow of argon for 2 hours at ambient temperature yielding an orange solution. All volatiles were removed *in vacuo* leaving behind the product as a dark purple solid (0.1046 g, 94.7%). ^1H NMR (benzene-d_6): δ 6.87 (s, 2H, Pyrrole C–H), 5.94 (s, 2H, Pyrimidine C–H), 2.89 (br m, 4H, P–C*H*(CH_3)$_2$), 2.06 (s, 12H, Pyrimidine CH_3), 1.29 (dd, $^3J_{H–H}$ = 6.6 Hz, $^3J_{H–P}$ = 15 Hz, P–CH(C*H*$_3$)(CH_3)), 1.12 (dd, $^3J_{H–H}$ = 6.6 Hz, $^3J_{H–P}$ = 15.6 Hz, P–CH(CH_3)(C*H*$_3$)). $^{13}C\{^1H\}$ NMR (benzene-d_6): δ 168.80 (s, 1-Pyrimidine ipso-C), 166.96 (s, 3,5-Pyrimidine ipso-C), 126.07 (dd, $^1J_{C–P}$ = 146.7 Hz $^3J_{C–P}$ = 20.72 Hz, Pyrrole ipso-C), 116.64 (dd, $^2J_{C–P}$ = 29.01 Hz, $^3J_{C–P}$ = 9.96 Hz, 3,4-Pyrrole C–H), 111.80 (s, Pyrimidine CH), 25.33 (d, $^1J_{C–P}$ = 54.70 Hz, P–*C*H(CH_3)$_2$), 24.27 (s, Pyrimidine CH_3), 17.21 (s, P–CH(*C*H_3)(CH_3)), 16.97 (s, P–CH(CH_3)(*C*H_3)). $^{31}P\{^1H\}$ NMR (benzene-d_6): δ 35.44.

Synthesis of $L^{Pm}ScCl_2$ (66)

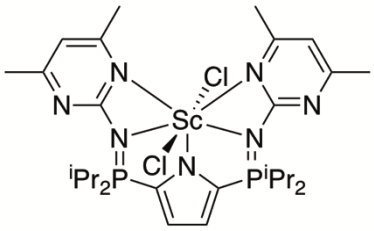

In an inert atmosphere glove box, a 100 mL 2-neck round bottomed flask was charged with NaL^{Pm} (0.2430 g, 0.4311 mmol) and attached to a swivel frit apparatus. A sample of $ScCl_3(THF)_3$ (0.1565 g, 0.4257 mmol) was weighed into a seperate round bottom flask. THF (25 mL) was transferred into each flask at –78 °C. Each flask was allowed to warm up to ambient temperature while stirring. The $ScCl_3(THF)_3$ solution was added dropwise *via* syringe to the stirring NaL^{Pm} solution dropwise over 3 minutes at ambient temperature. The solution was left to stir at ambient temperature for 3 hours whereupon all volatiles were removed *in vacuo* leaving behind a pale yellow solid. Toluene (20 ml) was transferred to the round bottom flask *via* vacuum distillation at –78 °C. The mixture was allowed to warm up to ambient temperature whereupon the swivel frit apparatus was flipped and the NaCl formed in the reaction was filtered away leaving a clear yellow solution in the receiving flask. All volatiles were removed *in vacuo* leaving behind the desired product as a yellow solid (0.2440 g, 86.2%) ^{1}H NMR (benzene-d_6): δ 6.73 (s, 2H, Pyrrole C–H), 6.47 (s, 2H, aromatic Pyrimidine C–H), 2.95 (br m, $^3J_{H–H}$ = 7.2 Hz, 4H, P–C*H*$(CH_3)_2$), 2.54 (s, 6H, Pyrimidine CH_3), 2.28 (s, 6H, Pyrimidine CH_3), 1.32 (dd, $^3J_{H–H}$ = 7.2 Hz, $^3J_{H–H}$ = 15.9 Hz, 12H, P–CH(C*H*$_3$)(CH_3)), 1.26 (dd, $^3J_{H–H}$ = 7.2 Hz, $^3J_{H–H}$ = 15.9 Hz, 12H, P–CH(CH_3)(C*H*$_3$)). ^{13}C{^{1}H} NMR (benzene-d_6): δ 168.05 (s, Pyrimidine ipso-C), 166.33 (s, Pyrimidine ipso-C), 165.31 (s, Pyrimidine ipso-C), 128.4 (dd, $^1J_{C–P}$ = 170.1 Hz $^3J_{C–P}$ = 15.19 Hz, Pyrrole ipso-C), 116.81 (dd, $^2J_{C–P}$ = 23.76 Hz $^3J_{C–P}$ = 12.32 Hz, Pyrrole C–H), 111.57 (s, aromatic Pyrimidine C–H), 26.32 (d, $^1J_{C–P}$ = 27.28 Hz, P–**C**H$(CH_3)_2$), 23.73 (s, Pyrimidine CH_3), 24.13 (s,

Pyrimidine CH_3), 17.40 (s, P–CH(CH_3)(CH_3)), 16.50 (s, P–CH(CH_3)(CH_3)). $^{31}P\{^1H\}$ NMR (benzene-d_6): δ 53.23.

Synthesis of $L^{Pm}LuCl_2$ (67)

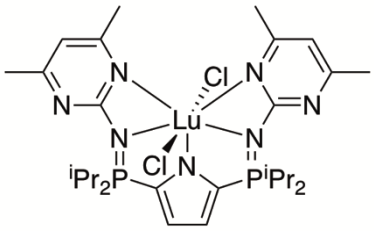

In an inert atmosphere glove box, a 100 mL 2-neck round bottom flask was charged with NaL^{Pm} (0.6903 g, 1.225 mmol) and attached to a swivel frit apparatus. A sample of $LuCl_3(THF)_3$ (0.3486 g, 1.239 mmol) was weighed into a seperate round bottom flask. THF (50 mL) was transferred into each flask *via* vacuum distillation at –78 °C. Each flask was allowed to warm up to ambient temperature while stirring. The $LuCl_3(THF)_3$ solution was added dropwise *via* syringe to the stirring NaL^{Pm} solution dropwise over 5 minutes at ambient temperature. The solution was left to stir at ambient temperature for 3 hours whereupon all volatiles were removed *in vacuo* leaving behind a pale yellow solid. Toluene (50 ml) was transferred to the round bottomed flask *via* vacuum distillation at –78 °C. The solution was allowed to warm up to ambient temperature whereupon the swivel frit apparatus was flipped and the NaCl filtered away leaving a clear yellow solution in the receiving flask. All volatiles were removed *in vacuo* leaving behind the desired product as a pale yellow solid (0.8207 g, 85.2%) ^1H NMR (benzene-d_6): δ 6.68 (d, $^3J_{H–P}$ = 2.4 Hz, 2H, Pyrrole C–H), 5.90 (s, 2H, aromatic Pyrimidine C–H), 2.60 (m, $^3J_{H–H}$ = 7.2 Hz $^2J_{H–P}$ = 2.4 Hz, 4H, P–C*H*(CH_3)$_2$), 2.45 (s, 6H, Pyrimidine CH_3), 2.05 (s, 6H, Pyrimidine CH_3), 1.29 (dd, $^3J_{H–P}$ = 6.9 Hz, $^3J_{H–P}$ = 16.95 Hz, 12H, P–CH(C*H*$_3$)(CH_3)), 1.07 (dd, $^3J_{H–P}$ = 7.2 Hz, $^3J_{H–P}$ = 17.4 Hz, 12H, , P–CH(CH_3)(C*H*$_3$)). $^{13}C\{^1H\}$ NMR (benzene-d_6): δ 168.70 (s, Pyrimidine ipso-C), 166.1 (d, $^2J_{C–P}$ = 5.28 Hz, 2-

Pyrimidine ipso-C), 165.0 (s, Pyrimidine ipso-C), 126.26 (dd, $^{1}J_{C–P}$ = 136.4 Hz $^{3}J_{C–P}$ = 14.63 Hz, Pyrrole ipso-C), 117.68 (dd, $^{2}J_{C–P}$ = 26.03 Hz $^{3}J_{C–P}$ = 10.49 Hz, Pyrrole C–H), 111.64 (s, aromatic Pyrimidine C–H), 26.16 (d, $^{1}J_{C–P}$ = 54.40 Hz, P–*C*H(CH_3)$_2$), 23.48 (s, Pyrimidine CH_3), 21.77 (s, Pyrimidine CH_3), 17.09 (s, P–CH(*C*H_3)(CH_3)), 16.23 (s, P–CH(CH_3)(*C*H_3)). $^{31}P\{^{1}H\}$ NMR (benzene-d_6): δ 52.16.

References

1. Evans, W. *J. Polyhedron* **1987**, *6*, 803.

2. Burger, B. J.; Bercaw, J. E., Vacuum Line Techniques for Handling Air-Sensitive Organometallic Compounds. In *Experimental Organometallic Chemistry*, American Chemical Society: 1987; Vol. 357, pp 79.

3. Wilkinson, G.; Birmingham, J. M. *J. Am. Chem. Soc.* **1954**, *76*, 6210.

4. Bochkarev, M. N.; Fedushkin, I. L.; Dechert, S.; Fagin, A. A.; Schumann, H. *Angew. Chem., Int. Ed.* **2001**, *40*, 3176.

5. Clentsmith, G. K. B.; Cloke, F. G. N.; Green, J. C.; Hanks, J.; Hitchcock, P. B.; Nixon, J. F. *Angew. Chem., Int. Ed.* **2003**, *42*, 1038.

6. Cloke, F. G. N. *Chem. Soc. Rev.* **1993**, *22*, 17.

7. Cloke, F. G. N.; Khan, K.; Perutz, R. N. *J. Chem. Soc., Chem. Commun.* **1991**, 1372.

8. Hitchcock, P. B.; Lappert, M. F.; Maron, L.; Protchenko, A. V. *Angew. Chem., Int. Ed.* **2008**, *47*, 1488.

9. Neculai, A. M.; Neculai, D.; Roesky, H. W.; Magull, J.; Baldus, M.; Andronesi, O.; Jansen, M. *Organometallics* **2002**, *21*, 2590.

10. Gysling, H.; Tsutsui, M., Organolanthanides and Organoactinides. In *Advances in Organometallic Chemistry*, Stone, F. G. A.; West, R., Eds. Academic Press: 1971; Vol. 9, p 361.

11. Waterman, R. *Organometallics* **2013**, *32*, 7249.

12. Thompson, M. E.; Baxter, S. M.; Bulls, R.; Burger, B. J.; Nolan, M. C.; Santarsiero, B. D.; Schaefer, W. P.; Bercaw, J. E. *J. Am. Chem. Soc.* **1987**, *109*, 203.

13. Barisic, D.; Diether, D.; Maichle-Mössmer, C.; Anwander, R. *J. Am. Chem. Soc.* **2019**, *141*, 13931.

14. Johnson, K. R. D.; Hayes, P. G. *Chem. Soc. Rev.* **2013**, *42*, 1947.

15. Evans, W. J.; Davis, B. L. *Chem. Rev.* **2002**, *102*, 2119.

16. Evans, W. J.; DeCoster, D. M.; Greaves, J. *Macromolecules* **1995**, *28*, 7929.

17. Evans, W. J.; Ulibarri, T. A.; Ziller, J. W. *Organometallics* **1991**, *10*, 134.

18. Evans, W. J.; Forrestal, K. J.; Ziller, J. W. *J. Am. Chem. Soc.* **1995**, *117*, 12635.

19. Evans, W. J.; Forrestal, K. J.; Ansari, M. A.; Ziller, J. W. *J. Am. Chem. Soc.* **1998**, *120*, 2180.

20. Evans, W. J.; Forrestal, K. J.; Ziller, J. W. *J. Am. Chem. Soc.* **1998**, *120*, 9273.

21. Evans, W. J.; Drummond, D. K.; Bott, S. G.; Atwood, J. L. *Organometallics* **1986**, *5*, 2389.

22. Evans, W. J.; Drummond, D. K.; Chamberlain, L. R.; Doedens, R. J.; Bott, S. G.; Zhang, H.; Atwood, J. L. *J. Am. Chem. Soc.* **1988**, *110*, 4983.

23. Hänninen, M. M.; Zamora, M. T.; Hayes, P. G., Rare Earth Pincer Complexes: Synthesis, Reaction Chemistry and Catalysis. In *Topics in Organometallic Chemistry*, van Koten, G.; Gossage, R. A., Eds. Springer International Publishing: Cham, 2016; Vol. 54, p 93.

24. Fryzuk, M. D.; Haddad, T. S. *J. Am. Chem. Soc.* **1988**, *110*, 8263.

25. Cameron, T. M.; Gordon, J. C.; Michalczyk, R.; Scott, B. L. *Chem. Commun.* **2003**, 2282.

26. Jie, S.; Diaconesu, P. L. *Organometallics* **2010**, *29*, 1222.

27. Xu, X.; Chen, Y.; Zou, G.; Sun, J. *Dalton Trans.* **2010**, *39*, 3952.

28. Mao, W.; Xiang, L.; Chen, Y. *Coord. Chem. Rev.* **2017**, *346*, 77.

29. Grubbs, R. H. *Angew. Chem., Int. Ed.* **2006**, *45*, 3760.

30. Schrock, R. R. *Angew. Chem., Int. Ed.* **2006**, *45*, 3748.

31. Chauvin, Y. *Angew. Chem., Int. Ed.* **2006**, *45*, 3740.

32. Nicola, T.; Brenner, M.; Donsbach, K.; Kreye, P. *Org. Process Res. Dev.* **2005**, *9*, 513.

33. Kadota, I.; Takamura, H.; Sato, K.; Ohno, A.; Matsuda, K.; Yamamoto, Y. *J. Am. Chem. Soc.* **2003**, *125*, 46.

34. Woodson Jr, C. S.; Grubbs, R. H. Patent No. 6,310,121 B1, October 30, 2001.

35. Woodson Jr, C. S.; Grubbs, R. H. Patent No. 5,939,504, August 17, 1999.

36. Summerscales, O. T.; Gordon, J. C. *RSC Adv.* **2013**, *3*, 6682.

37. Trifonov, A. A.; Bochkarev, M. N.; Schumann, H.; Loebel, J. *Angew. Chem., Int. Ed. Engl.* **1991**, *30*, 1149.

38. Aparna, K.; Ferguson, M.; Cavell, R. G. *J. Am. Chem. Soc.* **2000**, *122*, 726.

39. Masuda, J. D.; Jantunen, K. C.; Ozerov, O. V.; Noonan, K. J. T.; Gates, D. P.; Scott, B. L.; Kiplinger, J. L. *J. Am. Chem. Soc.* **2008**, *130*, 2408.

40. Beetstra, D. J.; Meetsma, A.; Hessen, B.; Teuben, J. H. *Organometallics* **2003**, *22*, 4372.

41. Scott, J.; Basuli, F.; Fout, A. R.; Huffman, J. C.; Mindiola, D. J. *Angew. Chem., Int. Ed.* **2008**, *47*, 8502.

42. Wicker, B. F.; Fan, H. J.; Hickey, A. K.; Crestani, M. G.; Scott, J.; Pink, M.; Mindiola, D. J. *J. Am. Chem. Soc.* **2012**, *134*, 20081.

43. Chu, T.; Piers, W. E.; Dutton, J. L.; Parvez, M. *Organometallics* **2013**, *32*, 1159.

44. Knight, L. K.; Piers, W. E.; Fleurat-Lessard, P.; Parvez, M.; McDonald, R. *Organometallics* **2004**, *23*, 2087.

45. Lu, E. L.; Li, Y. X.; Chen, Y. F. *Chem. Commun.* **2010**, *46*, 4469.

46. Lu, E. L.; Zhou, Q. H.; Li, Y. X.; Chu, J. X.; Chen, Y. F.; Leng, X. B.; Sun, J. *Chem. Commun.* **2012**, *48*, 3403.

47. Chu, J. X.; Lu, E. L.; Chen, Y. F.; Leng, X. B. *Organometallics* **2013**, *32*, 1137.

48. Chu, J. X.; Han, X. H.; Kefalidis, C. E.; Zhou, J. L.; Maron, L.; Leng, X. B.; Chen, Y. F. *J. Am. Chem. Soc.* **2014**, *136*, 10894.

49. Lu, E. L.; Chu, J. X.; Chen, Y. F.; Borzov, M. V.; Li, G. Y. *Chem. Commun.* **2011**, *47*, 743.

50. Chu, J. X.; Lu, E. L.; Liu, Z. X.; Chen, Y. F.; Leng, X. B.; Song, H. B. *Angew. Chem., Int. Ed.* **2011**, *50*, 7677.

51. Rong, W. F.; Cheng, J. H.; Mou, Z. H.; Xie, H. Y.; Cui, D. M. *Organometallics* **2013**, *32*, 5523.

52. Schädle, D.; Meermann-Zimmermann, M.; Schädle, C.; Maichle-Mössmer, C.; Anwander, R. *Eur. J. Inorg. Chem.* **2015**, *2015*, 1334.

53. Solola, L. A.; Zabula, A. V.; Dorfner, W. L.; Manor, B. C.; Carroll, P. J.; Schelter, E. J. *J. Am. Chem. Soc.* **2016**, *138*, 6928.

54. Solola, L. A.; Zabula, A. V.; Dorfner, W. L.; Manor, B. C.; Carroll, P. J.; Schelter, E. J. *J. Am. Chem. Soc.* **2017**, *139*, 2435.

55. Johnson, K. R. D.; Hannon, M. A.; Ritch, J. S.; Hayes, P. G. *Dalton Trans.* **2012**, *41*, 7873.

56. Johnson, K. R. D.; Hayes, P. G. *Organometallics* **2009**, *28*, 6352.

57. Johnson, K. R. D.; Hayes, P. G. *Organometallics* **2011**, *30*, 58.

58. Zamora, M. T.; Johnson, K. R. D.; Hanninen, M. M.; Hayes, P. G. *Dalton Trans.* **2014**, *43*, 10739.

59. Johnson, K. R. D.; Hayes, P. G. *Inorganica Chimica Acta* **2014**, *422*, 209.

60. Johnson, K. R. D.; Hayes, P. G. *Organometallics* **2013**, *32*, 4046.

61. Johnson, K. R. D.; Kamenz, B. L.; Hayes, P. G. *Organometallics* **2014**, *33*, 3005.

62. Johnson, K. R. D.; Kamenz, B. L.; Hayes, P. G. *Can. J. Chem.* **2015**, *94*, 330.

63. Sun, H.; Ritch, J. S.; Hayes, P. G. *Dalton Trans.* **2012**, *41*, 3701.

64. Knott, J. P.; Hänninen, M. M.; Rautiainen, J. M.; Tuononen, H. M.; Hayes, P. G. *J. Organomet. Chem.* **2017**, *845*, 135.

65. Johnson, K. R. D.; Hayes, P. G. *Dalton Trans.* **2014**, *43*, 2448.

66. Hanninen, M. M.; Zamora, M. T.; MacNeil, C. S.; Knott, J. P.; Hayes, P. G. *Chem. Commun.* **2016**, *52*, 586.

67. Schädle, D.; Maichle-Mössmer, C.; Schädle, C.; Anwander, R. *Chem. Eur. J.* **2015**, *21*, 662.

68. Liu, B.; Liu, X.; Cui, D.; Liu, L. *Organometallics* **2009**, *28*, 1453.

69. Petrov, A. P.; Thomas, O.; Harms, K.; Rufanov, K. A.; Sundermeyer, J. *J. Organomet. Chem.* **2010**, *695*, 2738.

70. Hillesheim, Nina S.; Elfferding, M.; Linder, T.; Sundermeyer, J. *Z. Anorg. Allg. Chem.* **2010**, *636*, 1776.

71. Cameron, T. M.; Gordon, J. C.; Scott, B. L. *Organometallics* **2004**, *23*, 2995.

72. Cameron, T. M.; Gordon, J. C.; Scott, B. L.; Tumas, W. *Chem. Commun.* **2004**, 1398.

73. Masuda, J. D.; Jantunen, K. C.; Scott, B. L.; Kiplinger, J. L. *Organometallics* **2008**, *27*, 1299.

74. Thomson, R. K.; Monreal, M. J.; Masuda, J. D.; Scott, B. L.; Kiplinger, J. L. *J. Organomet. Chem.* **2011**, *696*, 3966.

75. Frisch, M. J.; Trucks, G. W.; Schlegel, H. B.; Scuseria, G. E.; Robb, M. A.; Cheeseman, J. R.; Scalmani, G.; Barone, V.; Mennucci, B.; Petersson, G. A.; Nakatsuji, H.; Caricato, M.; Li, X. F.; Hratchian, H. P.; Izmaylov, A. F.; Bloino, J.; Zheng, G.; Sonnenberg, J. L.; Hada, M.; Ehara, M.; Toyota, K.; Fukuda, R.; Hasegawa, J.; Ishida, M.; Nakajima, T.; Honda, Y.; Kitao, O.; Nakai, H.; T., V.; Peralta, J. E.; Ogliaro, F.; Bearpark, M.; Heyd, J. J.; Brothers, E.; Kudin, K. N.; Staroverov, V. N.; Kobayashi, R.; Normad, J.; Raghavachari, K.; Rendell, A.; Burant, J. C.; Iyengar, S. S.; Tomasi, J.; Cossi, M.; Rega, N.; Millam, J. M.; Klene, M.; Knox, J. E.; Cross, J. B.; Bakken, V.; Adamo, C.; Jaramillo, J.; Gomperts, R.; Stratmann, R. E.; Yazyev, O.; Austin, A. J.; Cammi, R.; Pomelli, C.; Ochterski, J. W.; Martin, R. L.; Morokuma, K.; Zakerzewski, V. G.; Voth, G. A.; Salvador, P.; Dannenberg, J. J.; Dapprich, S.; Daniels, A. D.; Frakas; Foresman, J. B.; Ortiz, J. V.; Cioslowski, J.; Fox, D. J. Gaussian 09, Revision D. 01, Gaussian. *Inc.: Wallingford, CT* **2009**.

76. Perdew, J. P.; Burke, K.; Ernzerhof, M. *Phys. Rev. Lett.* **1996**, *77*, 3865.

77. Adamo, C.; Barone, V. *J. Chem. Phys.* **1999**, *110*, 6158.

78. Schäfer, A.; Horn, H.; Ahlrichs, R. *J. Chem. Phys.* **1992**, *97*, 2571.

79. Cao, X.; Dolg, M. *J. Chem. Phys.* **2001**, *115*, 7348.

80. Weigend, F.; Häser, M.; Patzelt, H.; Ahlrichs, R. *Chem. Phys. Lett.* **1998**, *294*, 143.

81. Weigend, F.; Ahlrichs, R. *Phys. Chem. Chem. Phys.* **2005**, *7*, 3297.

82. MacNeil, C. S.; Glynn, K. E.; Hayes, P. G. *Organometallics* **2018**, *37*, 3248.

83. With, J.; van der Linden, A. J.; van de Weg, H.; Horton, A. D. *Organometallics* **1996**.

84. Hayes, P. G.; Parvez, M.; Piers, W. E. *J. Am. Chem. Soc.* **2003**, *125*, 5622.

85. Hayes, P. G.; Parvez, M.; Piers, W. E. *Organometallics* **2005**, *24*, 1173.

86. Lee, L. W. M.; Piers, W. E.; Elsegood, M. R. J.; Clegg, W.; Parvez, M. *Organometallics* **1999**, *18*, 2947.

87. Hayes, P. G.; Welch, G. C.; Emslie, D. J. H.; Noack, C. L.; Parvez, M.; Piers, W. E. *Organometallics* **2003**, 1577.

88. Bambirra, S.; Leusen, D.; Meetsma, A.; Teuben, J. H.; Hessen, B. *Chem. Commun.* **2001**, 637.

89. Knott, J. P.; Hayes, P. G. *Unpublished Results.*

90. Jantunen, K. C.; Scott, B. L.; Hay, P. J.; Gordon, J. C.; Kiplinger, J. L. *J. Am. Chem. Soc.* **2006**, *128*, 6322.

91. Temple, C.; Thorpe, M. C.; Coburn, W. C.; Montgomery, J. A. *J. Org. Chem.* **1966**, *31*, 935.

92. Temple, C.; Montgomery, J. A. *J. Org. Chem.* **1965**, *30*, 826.

93. Estler, F.; Eickerling, G.; Herdtweck, E.; Anwander, R. *Organometallics* **2003**, *22*, 1212.

94. Arndt, A.; Voth, P.; Spaniol, T. P.; Okuda, J. *Organometallics* **2000**, *19*, 4690.

Appendix 1 – Crystallographic Data Tables

Table A1.1 Summary of Crystallography Data Collection and Structure Refinement for Compounds **44**, HL^{iPr}, and **39a**.

	44[a]	**HL^{iPr}**	**39a**
Formula	$C_{84}H_{76}LuN_5P_2C_7H_8$	$C_{34}H_{53}N_3P_2$	$C_{44}H_{70}N_3P_2ScSi_2$
FW/g•mol^{-1}	1484.54	565.73	804.11
Crystal System	Triclinic	Monoclinic	Monoclinic
Space Group	P–1	$P2_1/c$	$P2_1/n$
a (Å)	12.314(2)	13.15650(10)	16.3033(2)
b (Å)	13.648(2)	13.77310(10)	17.2331(2)
c (Å)	23.195(4)	19.58090(10)	17.6226(2)
α (°)	97.8241(18)	90	90
β (°)	99.3181(17)	108.6110(10)	105.8330(10)
γ (°)	106.8141(17)	90	90
Volume (Å^3)	3612.56(10)	3362.63(4)	4763.34(10)
Z	2	4	4
D_{calc} (g•cm^{-3})	1.365	1.117	1.121
μ (mm^{-1})	1.462	1.353	2.664
Crystal Size (mm)	0.2x0.1x0.05	0.1x0.2x0.05	0.05x0.03x0.01
θ range (°)	3.178 to 50	7.09 to 159.708	7.314 to 155.262
K_α (nm)	0.71073	1.54184	1.54184
N	38497	77357	47565
N_{ind}	12722	7317	9885
Data/restraints/parameters	12722/124/903	7317/0/364	9885/0/485
GoF on F^2	1.020	1.026	1.043
R_1 (I>2σ(I))[b]	0.0380	0.0491	0.0587
wR_2 (I>2σ(I))[c]	0.0752	0.1323	0.1750
R_1 (all data)[b]	0.0541	0.0505	0.0641
wR_2 (all data)[c]	0.0818	0.1336	0.1823
$\Delta\rho_{max}$ and $\Delta\rho_{min}$ (e•Å^3)	0.75/–0.73	1.42/–0.63	0.41/–1.25

Notes: [a]Crystallized with one molecule of toluene in the asymmetric unit. [b]$R_1 = \Sigma||F_o|-|F_c||/\Sigma|F_c|$. [c]$wR_2 = \{\Sigma[w(F_o^2-F_c^2)^2]/\Sigma[w(F_o^2)^2]\}^{1/2}$.

Table A1.2 Summary of Crystallography Data Collection and Structure Refinement for Compounds **39b**, **40c**, and **40d**.

	39b	**40c**[a]	**40d**
Formula	$C_{42}H_{74}LuN_3P_2Si_2$	$C_{122}H_{149}Lu_2N_8P_4Si_2$	$C_{50}H_{81}LuN_4P_2Si$
FW/g•mol^{-1}	914.13	2263.49	1003.18
Crystal System	Monoclinic	Triclinic	Monoclinic
Space Group	$P2_1/n$	P–1	$P2_1$
a (Å)	11.2152(3)	12.31417(13)	11.59705(9)
b (Å)	17.6224(5)	21.4332(2)	20.55239(15)
c (Å)	24.0711(6)	24.4686(2)	11.79321(10)
α (°)	90	110.2276(10)	90
β (°)	92.481(2)	104.4073(10)	113.2891(9)
γ (°)	90	92.0411(9)	90
Volume (Å^3)	4752.9(2)	5816.40(11)	2581.85(4)
Z	4	2	2
D_{calc} (g•cm^{-3})	1.277	1.292	1.290
μ (mm^{-1})	2.224	4.262	4.723
Crystal Size (mm)	0.08x0.05x0.01	0.05x0.05x0.03	0.3x0.2x0.1
θ range (°)	6.71 to 61.124	6.984 to 160.818	8.162 to 160.298
K_α (nm)	0.71073	1.54184	1.54184
N	54775	131024	30369
N_{ind}	11880	25332	10423
Data/restraints/parameters	11880/0/503	25332/0/1233	10423/1/553
GoF on F^2	1.038	1.060	1.089
R_1 (I>2σ(I))[b]	0.0372	0.0612	0.0298
$wR2$ (I>2σ(I))[c]	0.0831	0.1672	0.0755
R_1 (all data)[b]	0.0560	0.0669	0.0308
$wR2$ (all data)[c]	0.0899	0.1737	0.0760
$\Delta\rho_{max}$ and $\Delta\rho_{min}$ (e•Å^3)	2.35/–0.74	2.45/–3.25	0.63/–0.70

Notes: [a]Two independent molecules of **40c** and one molecule of heptane crystallized in the asymmetric unit. [b]$R_1 = \Sigma||F_o|-|F_c||/\Sigma|F_c|$. [c]$wR_2 = \{\Sigma[w(F_o^2-F_c^2)^2]/\Sigma[w(F_o^2)^2]\}^{1/2}$.

Table A1.3 Summary of Crystallography Data Collection and Structure Refinement for Compounds **48c**, **48d**, and **50**.

	48c	**48d**	**50**[a]
Formula	$C_{78}H_{96}LuN_5P_2$	$C_{58}H_{88}LuN_5P_2$	$C_{80}H_{112}Cl_4N_6P_4Sc_2$
FW/g•mol^{-1}	1340.5	1092.24	1513.35
Crystal System	Triclinic	Monoclinic	Triclinic
Space Group	P–1	$P2_1/n$	P–1
a (Å)	12.74240(10)	14.96740(10)	13.7447(2)
b (Å)	14.66260(10)	17.02750(10)	15.4431(2)
c (Å)	20.5619(2)	21.66410(10)	21.9581(2)
α (°)	74.4510(10)	90	91.9240(10)
β (°)	89.2780(10)	95.2220(10)	105.5840(10)
γ (°)	71.2670(10)	90	110.9770(10)
Volume (Å^3)	3493.66(6)	5498.34(6)	4148.10(9)
Z	2	4	2
D_{calc} (g•cm^{-3})	1.274	1.319	1.212
μ (mm^{-1})	3.475	4.285	3.654
Crystal Size (mm)	0.1x0.05x0.03	0.3x0.3x0.1	0.01x0.03x0.2
θ range (°)	6.628 to 160.86	6.615 to 160.668	6.976 to 160.054
K_α (nm)	1.51184	1.54184	1.54184
N	79766	64880	52782
N_{ind}	15242	11972	17093
Data/restraints/parameters	15242/0/790	11972/0/623	17093/0/865
GoF on F^2	1.084	1.107	1.010
R_1 (I>2σ(I))[b]	0.0383	0.0297	0.0459
$wR2$ (I>2σ(I))[c]	0.1060	0.0741	0.1205
R_1 (all data)[b]	0.0395	0.0323	0.0595
$wR2$ (all data)[c]	0.1070	0.0752	0.1325
$\Delta\rho_{max}$ and $\Delta\rho_{min}$ (e•Å^3)	2.78/–1.35	0.67/–0.89	0.54/–1.07

Notes: [a]Crystallized with one molecule of toluene in the asymmetric unit. [b]$R_1 = \Sigma||F_o|-|F_c||/\Sigma|F_c|$. [c]$wR_2 = \{\Sigma[w(F_o^2-F_c^2)^2]/\Sigma[w(F_o^2)^2]\}^{1/2}$.

Table A1.4 Summary of Crystallography Data Collection and Structure Refinement for Compounds $[LiL^{iPr}]_2$, **51**, and **57**.

	$[LiL^{iPr}]_2$	**51**[a]	**57**
Formula	$C_{34}H_{48}LiN_3P_2$	$C_{72}H_{116}N_6P_4Sc_2$	$C_{23}H_{24}LiNO$
FW/g•mol^{-1}	571.66	1279.50	337.37
Crystal System	Triclinic	Monoclinic	Monoclinic
Space Group	P–1	$P2_1/n$	$P2_1/c$
a (Å)	11.4013(4)	16.2577(6)	10.0014(2)
b (Å)	12.3987(5)	24.0582(4)	9.8507(2)
c (Å)	12.9181(5)	20.6369(5)	19.0411(3)
α (°)	84.395(3)	90	90
β (°)	74.436(3)	113.021(3)	95.679(2)
γ (°)	70.562(3)	90	90
Volume (Å^3)	1658.82(12)	7428.9(4)	1866.74(6)
Z	2	4	4
D_{calc} (g•cm^{-3})	1.145	1.44	1.200
μ (mm^{-1})	1.372	2.698	0.550
Crystal Size (mm)	0.09x0.02x0.01	0.06x0.05x0.01	0.4x0.2x0.05
θ range (°)	7.104 to 159.272	6.956 to 158.954	8.886 to 160.46
K_α (nm)	1.51184	1.54184	1.54184
N	36211	18	21476
N_{ind}	7155	9968	4069
Data/restraints/parameters	7155/0/372	9968/0/785	4069/0/239
GoF on F^2	1.050	1.549	1.087
R_1 ($I>2\sigma(I)$)[b]	0.0725	0.0928	0.0501
$wR2$ ($I>2\sigma(I)$)[c]	0.2087	0.3077	0.1384
R_1 (all data)[b]	0.0795	0.1088	0.0541
$wR2$ (all data)[c]	0.2150	0.3423	0.1421
$\Delta\rho_{max}$ and $\Delta\rho_{min}$ (e•Å^3)	0.91/–0.59	1.13/–2.64	0.36/–0.28

Notes: [a]Two independent molecules of **51** crystallized in the asymmetric unit. [b]$R_1 = \Sigma||F_o|-|F_c||/\Sigma|F_c|$. [c]$wR_2 = \{\Sigma[w(F_o^2-F_c^2)^2]/\Sigma[w(F_o^2)^2]\}^{1/2}$.

Table A1.5 Summary of Crystallography Data Collection and Structure Refinement for Compounds **HL^{Pm}**, and **NaL^{iPr}**.

	HL^{Pm}	**NaL^{iPr}**[a]
Formula	$C_{28}H_{45}N_7P_2$	$C_{60}H_{88}N_{14}Na_2P_4$
FW/g•mol^{-1}	541.65	1175.30
Crystal System	Monoclinic	Triclinic
Space Group	$P2_1/n$	P–1
a (Å)	11.09120(10)	13.3673(2)
b (Å)	24.3906(2)	13.9702(2)
c (Å)	11.85320(10)	19.7940(4)
α (°)	90	73.259(2)
β (°)	108.5340(10)	86.263(2)
γ (°)	90	70.072(2)
Volume (Å^3)	3040.23(5)	33.25.55(11)
Z	4	2
D_{calc} (g•cm^{-3})	1.183	1.174
μ (mm^{-1})	1.515	0.174
Crystal Size (mm)	1x0.8x0.5	0.03x0.03x0.02
θ range (°)	7.248 to 159.99	6.452 to 61.588
K_α (nm)	1.51184	1.54184
N	33645	79702
N_{ind}	6555	16987
Data/restraints/parameters	6555/0/346	16987/0/725
GoF on F^2	1.075	1.053
R_1 (I>2σ(I))[b]	0.0398	0.0440
$wR2$ (I>2σ(I))[c]	0.1035	0.1155
R_1 (all data)[b]	0.0446	0.0593
$wR2$ (all data)[c]	0.1065	0.1230
$\Delta\rho_{max}$ and $\Delta\rho_{min}$ (e•Å^3)	0.32/–0.39	0.64/–0.78

Notes: [a]One molecule of disordered toluene crystallized in the asymmetric unit. [b]$R_1 = \Sigma||F_o|-|F_c||/\Sigma|F_c|$. [c]$wR_2 = \{\Sigma[w(F_o^2-F_c^2)^2]/\Sigma[w(F_o^2)^2]\}^{1/2}$.

Table A1.6 Summary of Crystallography Data Collection and Structure Refinement for Compounds **66**, and **67**.

	66[a]	**67**[a]
Formula	$C_{35}H_{52}Cl_2N_7P_2Sc$	$C_{35}H_{52}Cl_2LuN_7P_2$
FW/g•mol^{-1}	748.63	878.64
Crystal System	Monoclinic	Monoclinic
Space Group	I2/a	I2/a
a (Å)	19.38530(10)	19.5525(5)
b (Å)	13.28240(10)	13.3420(3)
c (Å)	30.7615(2)	30.8950(7)
α (°)	90	90
β (°)	99.2990(10)	99.413(2)
γ (°)	90	90
Volume (Å^3)	7816.48(9)	79
Z	8	8
D_{calc} (g•cm^{-3})	1.272	1.468
μ (mm^{-1})	3.903	2.732
Crystal Size (mm)	0.7x0.4x0.1	0.7x0.5x0.5
θ range (°)	7.264 to 159.41	6.788 to 61.502
K_α (nm)	0.71073	0.71073
N	43608	48568
N_{ind}	8423	10026
Data/restraints/parameters	8423/0/437	10026/0/437
GoF on F^2	1.061	1.020
R_1 (I>2σ(I))[b]	0.0490	0.0222
wR2 (I>2σ(I))[c]	0.1334	0.0507
R_1 (all data)[b]	0.0490	0.0285
wR2 (all data)[c]	0.1390	0.0526
$\Delta\rho_{max}$ and $\Delta\rho_{min}$ (e•Å^3)	1.41/–0.97	0.92/–0.56

Notes: [a]One molecule of disordered toluene crystallized in the asymmetric unit. [b]$R_1 = \Sigma||F_o|-|F_c||/\Sigma|F_c|$. [c]$wR_2 = \{\Sigma[w(F_o^2-F_c^2)^2]/\Sigma[w(F_o^2)^2]\}^{1/2}$.

Appendix 2 – Publications Arising from this Thesis

Chapter 2 has been published by Jackson Paul Knott. JPK was responsible for all the synthesis of all complexes presented in this publication. Computational analysis was conducted by Dr. Mikko M. Hänninen, Dr. J. Mikko Rautiainen, and Dr. Heikki M. Tuononen at the University of Jyväskulä. Their work is presented in this thesis to provide full context for the experimental work conducted by JPK. Its inclusion in this thesis has been consented to by all contributing authors.

Work which encompasses a large amount of the work presented in this thesis will be submitted *Dalton Transactions* prior to the defence of this thesis. The pending reference of this submission is provided below.

Publications

1. Knott, J. P.; Hänninen, M. M.; Rautiainen J. M.; Tuononen, H. T.; Hayes, P. G. *J. Organomet. Chem.*, **2017**, *845*, 135. *Invited issue for the occasion of Dr. Gerard von Koten's 65th birthday.
2. Knott J. P.; Hayes P. G. *Dalton Trans*, **2019**, to be submitted November 2019.